



The
University
Of
Sheffield.

**The Relationship Between Timber Chemical
Compositions and Mechanical Properties**

Qiushi Peng

A thesis submitted in partial fulfilment of the requirements for the degree of
Doctor of Philosophy

The University of Sheffield

School of Architecture

August 2019

Acknowledgements

Throughout the conducting of the research, I have received a lot of support and assistance. I would like to thank my lead supervisor Dr Wen-Shao Chang, who provide a valuable support for my research by his wealth of knowledge in timber materials, rich experiences of experimentation and patient guidance. I would also like to thank Dr Graham Ormondroyd, Dr Morwenna Spear and Dr Simon Curling, who provided an advanced lab for my research. Their deep understanding and abundant experience supported me and gave me confidence in the experimental period. I would also like to thank Prof Richard Harris, Dr Martin P. Ansell and Mr Gervais Sawyer, who supported my research by their distinctive knowledge in timber industry.

I would like to thank my parents for their unconditional support whilst studying abroad, I could not have finished my PhD without their sympathetic ear and wise advice.

Last but not least, I would like to thank all my friends, Dr Henry Wu, Raymond Shih, Fang-Yu Liin, who shared their research experiences. I would also like to thank my flatmates, Yu-Ting Hung and Yingqi Liu, who supported me all the time in the hardest period.

Abstract

Timber is widely used both in modern and historic construction, with ageing being the most serious risk in the structural mechanical strength. A non-destructive test to predict timber mechanical properties is urgently needed and many studies indicated that chemical compositions have close relationships to the mechanical properties. Hence, this study focusses on the relationships between timber chemical composition and the corresponding mechanical strength, providing contributions to the non-destructive testing of timber mechanical properties. Non-destructive testing has a wide prospect both in evaluation of modern timber construction and historic timber framed building conservation. Heat treatment is a method to cause changes in timber, whilst FTIR is the technique for analysing its chemical compositions. Static and dynamic mechanical properties were tested by a 3-point bending and a dynamic thermal mechanical analysis (DMTA) facility, respectively.

The changes of timber mechanical properties are the results of various combined chemical compositions. In general, condensation and cross-linking reactions play an essential role in timber strength improvement. The static bending mechanical properties, modulus of rupture (MOR) and modulus of elasticity (MOE) increase, whilst in the dynamic mechanical properties and $\text{Tan } \delta$ decrease, which indicates an increase in elasticity and/or decrease of viscosity. Pyrolysis reactions in hemicellulose and lignin, lead to a decrease in the timber static mechanical properties and increase in $\text{Tan } \delta$ of the dynamic ones. Both static bending mechanical properties (MOR and MOE) and dynamic bending mechanical properties (storage modulus, loss modulus and $\text{Tan } \delta$) can be predicted by the peak areas of the normalised FTIR spectrum. The coefficients of determination (R-square) of all the regression models are between 0.62 and 0.9, which indicates that the models are functional.

In studies of timber accelerated ageing, the changes of each peak area during heat treatment are regressed by a model where temperature and treatment period as independent variables. The model shows that new pine can be treated in a two-steps heat treatment, which involves an air and a vacuum step to obtain similar chemical compositions of 580 years old real timber by heat treatment. The R-square of the model is more than 0.7 and thus, shows effective regression.

Contents

ACKNOWLEDGEMENTS.....	I
ABSTRACT	III
LIST OF TABLES.....	IX
LIST OF FIGURES.....	XI
CHAPTER 1 INTRODUCTION	1
1.1 Background and Motivation	1
1.2 Objectives	4
1.3 Outline of the thesis	5
CHAPTER 2 LITERATURE REVIEW.....	7
2.1 Timber composition	8
2.1.1 Timber Cell Composition	10
2.1.2 Relationship between Chemical composition and Mechanical Bonding.....	17
2.1.3 Moisture Content and Environment Temperature	20
2.1.4 Summary	25
2.2 Changes of Timber Chemical Composition.....	26
2.2.1 Chemical Composition Analysis Method	27
2.2.2 Chemical Composition Changes During Natural Ageing.....	37
2.2.3 Chemical Composition Changes from Artificial Treatment	47
2.2.4 Mass Loss and Colour Change during Heat Treatment	55
2.2.5 Summary	60
2.3 Changes in Timber Mechanical Properties.....	64
2.3.1 Static Mechanical Properties of Natural Aged Timber.	64
2.3.2 Static Mechanical Properties of Heat-Treated Timber	67
2.3.2 Dynamic Mechanical Properties of Timber	70
2.3.3 Summary	76
2.4 Conclusions	77
CHAPTER 3 MATERIALS AND EXPERIMENT PLAN	81
3.1 Materials	81
3.2 Experiment Design	85

3.3 Experiment Process and Facility	89
3.3.1 Heat treatment	89
3.3.1 Chemical Analysis	92
3.3.2 Static Mechanical Properties	93
3.3.3 Dynamic Mechanical Properties	93
3.4 Peak Fitting of FTIR	94
CHAPTER 4 CHEMICAL COMPOSITION CHANGES DURING HEAT TREATMENT	99
4.1 Mechanism of Chemical Composition Changes of the Timber Molecule	99
4.2 Chemical Composition Change of the Natural Ageing Process	108
4.3 Equilibrium Moisture Content Change During Heat Treatment	110
4.3.1 EMC Changes of New and Old pine	110
4.3.2 Moisture Content Related to FTIR	114
4.4 Mass Loss of New and Old Timber During Heat Treatment	115
4.5 New Timber Chemical Composition Changes During Heat Treatment	121
4.5.1 New Samples in Vacuum Treatment	121
4.5.2 New Samples in Air Treatment	128
4.5.3 Summary	134
4.6 Old Timber Chemical Composition Changes during Heat Treatment	136
4.6.1 Old Samples in a Vacuum	136
4.6.2 Old Samples in Air Treatment	139
4.6.3 Summary	143
4.7 Peak Interaction Correlation	144
4.8 Discussion and Conclusion	147
CHAPTER 5 MECHANICAL PROPERTY CHANGES DURING HEAT TREATMENT	155
5.1 Moisture Content and Bending Mechanical Properties	157
5.1.1 Static Mechanical Properties and Moisture Content	157
5.1.2 Dynamic Mechanical Properties and Moisture Content	159
5.2 Dynamic Mechanical Difference Between New and Old Pine	165
5.3 Mechanical Property Changes in New Timber	167
5.3.1 Static Bending Mechanical Properties of New Pine	167
5.3.2 Bending Dynamic Mechanical Properties of New Pine	173
5.3.3 Compression Tests Parallel to the Grain of New Pine	175
5.3.4 Summary	181
5.4 Mechanical Property Changes in Old timber	183

5.4.1 Static Bending Mechanical Properties of Old Pine	183
5.4.2 Dynamic Mechanical Properties of Old Pine	187
5.4.3 Summary	189
5.5 Discussion and Conclusion.....	189
CHAPTER 6 CHEMICAL COMPOSITION AND MECHANICAL PROPERTIES	195
6.1 Static Mechanical Properties and Chemical Composition	195
6.1.1 Bending Modulus of Rupture and Chemical Composition	195
6.1.2 Bending Modulus of Elasticity and Chemical Composition	206
6.1.3 Summary	211
6.2 Dynamic Mechanical Properties and Chemical Composition	212
6.2.1 Peak γ of Tan δ	214
6.2.2 Peak β of Tan δ	217
6.2.3 Summary	220
6.3 Discussion and Conclusion.....	221
CHAPTER 7 IMPLEMENTATION	223
7.1 Semi-Destructive Testing on Existing Building Elements.....	223
7.2 Timber Accelerated Ageing.....	224
7.2.1 Regression of Functional Group Changes During Heat Treatment.....	225
7.2.2 Accelerated Ageing Method.....	233
7.3 Summary	239
CHAPTER 8 CONCLUSION.....	241
8.1 Conclusion.....	241
8.2 Further Research	245
BIBLIOGRAPHY	247
APPENDIX I C₁₄ IDENTIFICATION REPORT.....	272
APPENDIX II REGRESSION MODELS	274
Bending MOR Nonlinear Curve Fitting by Origin.....	274
Bending MOR Multiple Regression Analysis by SPSS	280
Bending MOE Multiple Regression Analysis by SPSS.....	282
Storage Moduli of Peak γ Multiple Regression Analysis by SPSS	284
Loss Moduli of Peak γ of Tan δ Multiple Regression Analysis by SPSS	287

Storage Moduli of Peak β of Tan δ Multiple Regression Analysis by SPSS	290
Loss Moduli of Peak β of Tan δ Multiple Regression Analysis by SPSS	292
Temperature of Peak β of Tan δ Multiple Regression Analysis by SPSS	294
Peak area Changes in Air Treatment Multiple Regression Analysis by SPSS	296
Peak area Changes in Vacuum Treatment Multiple Regression Analysis by SPSS	308
Timber Accelerated Ageing Model Origin.....	321

List of Tables

<i>Table 2-1 Cell Types of Timber (Dinwoodie, 1975)</i>	11
<i>Table 2-2 Molecule Content of Timber Cell Walls (Dinwoodie, 1975)</i>	14
<i>Table 2-3 Chemical Functional Group in Timber Molecule</i>	16
<i>Table 2-4 Relationship between Timber Mechanical Property and Moisture Content (Gerhards, 2007)</i>	23
<i>Table 2-5 Relationship between Timber Mechanical Property and Testing Temperature (Gerhards, 2007)</i>	24
<i>Table 2-6 FTIR Wavenumber and Corresponding Chemical Functional Groups</i>	30
<i>Table 2-7 FT-NIR Wavenumber and Corresponding Chemical Bonds</i>	31
<i>Table 2-8 GC/MS Spectrum Peaks and Corresponding Compound (Tamburini et al., 2017)</i>	33
<i>Table 2-9 Wood Samples analysed by Borgin et al. (1975a)</i>	41
<i>Table 3-1 Sample Quantity and Distribution During Heat Treatment</i>	88
<i>Table 3-2 Mass Loss During the Drying Process</i>	91
<i>Table 3-3 FTIR Peak Wavenumber and the Corresponding Chemical Functional Groups</i>	96
<i>Table 4-1 Chemical Functional Group Changes and the Corresponding FTIR</i>	107
<i>Table 4-2 FTIR Peak area of New and Old Pine without Treatment</i>	110
<i>Table 4-3 EMC Change and Standard Deviation of New Pine during Heat-Treatment</i>	112
<i>Table 4-4 EMC Change and Standard Deviation of Old Pine during Heat-Treatment</i>	113
<i>Table 4-5 Mass Loss and Standard Deviation of New Pine During Heat Treatment</i>	117
<i>Table 4-6 Mass Loss and Standard Deviation of Old Pine During Heat Treatment</i>	119
<i>Table 4-7 Correlation of FTIR Peak Area Changes</i>	145
<i>Table 5-1 DMTA of Dry and 10% Moisture Content Samples</i>	161
<i>Table 5-2 Mean MOR (MPa) Changes of New Pine During Heat Treatment</i>	169
<i>Table 5-3 Mean MOE (MPa) Changes of New Pine During Heat Treatment</i>	172
<i>Table 5-4 Dynamic Mechanical Properties of Peak γ of New Pine after 24 Hours Treatment</i>	174
<i>Table 5-5 Dynamic Mechanical Properties of Peak β of New Pine after 24 Hours Treatment</i>	174
<i>Table 5-6 Mass Loss, EMC Change and Static Compression Mechanical Property</i>	181
<i>Table 5-7 MOR (MPa) Changes of Old Pine During Heat Treatment</i>	185
<i>Table 5-8 MOE (MPa) Changes of Old Pine During Heat Treatment</i>	186
<i>Table 5-9 Dynamic Mechanical Properties of Peak γ of Old Pine after 24 Hours Treatment</i>	188
<i>Table 5-10 Dynamic Mechanical Properties of Peak β of Old Pine after 24 Hours Treatment</i>	188
<i>Table 5-11 Coefficient of Variation of MOE and MOR of New Pine During Heat Treatments (20 samples)</i>	191

<i>Table 5-12 Coefficient of Variation of MOE and MOR of Old Pine During Heat Treatments (20 samples)</i>	<i>191</i>
<i>Table 6-1 Pearson Correlation of New Pine Sample between MOR and FTIR Peaks</i>	<i>198</i>
<i>Table 6-2 Pearson Correlation of Old Pine Sample between MOR and FTIR Peaks</i>	<i>199</i>
<i>Table 6-3 MOR Curve Fitting with Different Peaks of the FTIR Spectrum.....</i>	<i>202</i>
<i>Table 6-4 Summary of Multiple Regression Analysis for MOR</i>	<i>205</i>
<i>Table 6-5 Pearson Correlation of All Samples between MOE and Density and FTIR Peaks</i>	<i>208</i>
<i>Table 6-6 Summary of Multiple Regression Analysis for MOE.....</i>	<i>209</i>
<i>Table 6-7 Pearson Correlations between the Storage Modulus of Peak γ and Density and the FTIR Peaks</i>	<i>215</i>
<i>Table 6-8 Pearson Correlations between the Loss Modulus of Peak γ and Density and the FTIR Peaks</i>	<i>216</i>
<i>Table 6-9 Pearson Correlations between the Storage Modulus of Peak β and Density and the FTIR Peaks</i>	<i>218</i>
<i>Table 6-10 Pearson Correlations between the Loss Modulus of Peak β and Density and the FTIR Peaks</i>	<i>218</i>
<i>Table 7-1 Percentage Changes of Each Peak During Heat Treatment.....</i>	<i>225</i>
<i>Table 7-2 MRA Models for Peak 1318, 1456 and 1595 Changes During Heat Treatment.....</i>	<i>230</i>
<i>Table 7-3 New Pine Changing to Old Pine</i>	<i>233</i>
<i>Table 7-4 Results of Simultaneous Equation Systems.....</i>	<i>237</i>
<i>Table 7-5 Model-Predicted and Measured Peak Area of Regression Analysis.....</i>	<i>237</i>

List of Figures

<i>Figure 1-1 Historic Timber Building Distribution in China (National Cultural Heritage Administration)</i>	2
<i>Figure 1-2 Wooden High-Rise Buildings (Confederation of Timber Industries)</i>	2
<i>Figure 1-3 Outline of The Thesis</i>	6
<i>Figure 2-1 Structures of Timber in Different Scale (Hoffmann and Jones, 1990b)</i>	8
<i>Figure 2-2 Structure of Tree Trunk</i>	9
<i>Figure 2-3 Structure of Timber Cell (Huang et al., 2003)</i>	11
<i>Figure 2-4 SEM Image of Timber Cells (Higuchi, 2012)</i>	11
<i>Figure 2-5 Structure of Cellulose (Goring and Timell, 1962)</i>	14
<i>Figure 2-6 Structure of Hemicellulose (Ramage et al., 2017)</i>	14
<i>Figure 2-7 Structure of Lignin (Yang et al., 2007)</i>	15
<i>Figure 2-8 Crystalline Structure of Cellulose (Thygesen et al., 2005)</i>	15
<i>Figure 2-9 Connection of Cellulose, Hemicellulose and Lignin (Ramage et al., 2017)</i>	19
<i>Figure 2-10 Relationship Between Compression Strength and Moisture Content (Dinwoodie, 1975)</i>	21
<i>Figure 2-11 Moisture Between Timber Molecules (Dinwoodie, 2002)</i>	22
<i>Figure 2-12 Relationship between Modulus of Elasticity and Moisture Content (Gerhards, 2007)</i> 23	
<i>Figure 2-13 Relationship between Shear Modulus and Moisture Content (Gerhards, 2007)</i>	24
<i>Figure 2-14 Principle of ATR-FTIR</i>	29
<i>Figure 2-15 GC/MS spectrum (Tamburini et al., 2017)</i>	33
<i>Figure 2-16 Timber Composition Changes during Natural Ageing (Fengel, 1991)</i>	38
<i>Figure 2-17 Timber Molecule Changes during Heat Treatment (Esteves and Pereira, 2008)</i>	50
<i>Figure 2-18 Mass Loss and Treatment Period/Atmosphere (Esteves and Pereira, 2008)</i>	56
<i>Figure 2-19 CIELAB System</i>	57
<i>Figure 2-20 Colour Changes during Natural Aging and Heat Treatment (Matsuo et al., 2010)</i>	59
<i>Figure 2-21 Timber Colour Regression Model (Matsuo et al., 2011)</i>	60
<i>Figure 2-22 Hemicellulose Changes During Heat Treatment (Zhou et al., 2016)</i>	62
<i>Figure 2-23 Oxidation Reaction During Heat Treatment (Liu et al., 2019)</i>	62
<i>Figure 2-24 Hydrolysis Reaction During Heat Treatment (Shevchenko et al., 1999)</i>	63
<i>Figure 2-25 Theory of DMTA Technique</i>	71
<i>Figure 2-26 Relationships between Complex Modulus, Storage Modulus and Loss Modulus</i>	72
<i>Figure 2-27 Tan δ Curve During Temperature Scanning (Havimo, 2009)</i>	72

<i>Figure 2-28 Storage Modulus and Tan δ Curve under Temperature Scanning of Different Species (Birkinshaw et al., 1986)</i>	74
<i>Figure 3-1 Pine Structure Member after Restoration of the Hall of Fusheng</i>	82
<i>Figure 3-2 C14 Radiation of Old Pine</i>	83
<i>Figure 3-3 Cells of Old Pine</i>	83
<i>Figure 3-4 Cells of New Pine</i>	84
<i>Figure 3-5 Resin in Small and Big Samples</i>	84
<i>Figure 3-6 Sample Size and Annual Ring Direction in the Experiment</i>	85
<i>Figure 3-7 Experimental Process</i>	86
<i>Figure 3-8 Oven with Vacuum Pump</i>	89
<i>Figure 3-9 FTIR Spectrum before and after the Drying Process of New Pine</i>	90
<i>Figure 3-10 FTIR Facility used in the Experiment</i>	92
<i>Figure 3-11 3-Point Bending Test Facility</i>	93
<i>Figure 3-12 DMTA Facility</i>	94
<i>Figure 3-13 FTIR Spectrum before and after Pre-Processing</i>	95
<i>Figure 3-14 Peak Fitting of the FTIR Spectrum of Non-treated New Pine</i>	96
<i>Figure 4-1 Mechanism of Hemicellulose Deacetylase</i>	100
<i>Figure 4-2 Mechanism of Hemicellulose Pyrolysis</i>	101
<i>Figure 4-3 Mechanism of Lignin Condensation I</i>	102
<i>Figure 4-4 Mechanism of Lignin Condensation II</i>	102
<i>Figure 4-5 Mechanism of Lignin Cross-Linking</i>	103
<i>Figure 4-6 Mechanism of Lignin-Carbohydrate Complexes formation</i>	104
<i>Figure 4-7 Mechanism of Lignin-Furfural Complexes formation</i>	104
<i>Figure 4-8 Mechanism of Lignin Pyrolysis I</i>	105
<i>Figure 4-9 Mechanism of Lignin Pyrolysis II</i>	106
<i>Figure 4-10 Mechanism of Hydroxyl Group Oxidation</i>	106
<i>Figure 4-11 Mechanism of hydrolysis</i>	107
<i>Figure 4-12 FTIR Spectrum of Non-Treated New and Old Pine</i>	109
<i>Figure 4-13 Equilibrium Moisture Content Change of New Pine during Heat-Treatment</i>	111
<i>Figure 4-14 Equilibrium Moisture Content Variation of New Pine during Heat-Treatment</i>	112
<i>Figure 4-15 Equilibrium Moisture Content Change of Old Pine during Heat-Treatment</i>	113
<i>Figure 4-16 Equilibrium Moisture Content Error of Old Pine during Heat-Treatment</i>	114
<i>Figure 4-17 Relationship between Peak 1642 Area and Moisture Content</i>	115
<i>Figure 4-18 Mass Loss of New Pine During Heat Treatment</i>	117
<i>Figure 4-19 Mass Loss Variation of New Pine During Heat Treatment</i>	118

<i>Figure 4-20 Mass Loss of Old Pine During Heat Treatment.....</i>	<i>119</i>
<i>Figure 4-21 Mass Loss Variation of Old Pine During Heat Treatment.....</i>	<i>120</i>
<i>Figure 4-22 FTIR Spectrum Change of New Pine in 120 °C Vacuum Treatment After 24 hours.....</i>	<i>122</i>
<i>Figure 4-23 FTIR Peak Area Change of New Pine during 120 °C Vacuum Treatment</i>	<i>123</i>
<i>Figure 4-24 FTIR Spectrum Change of New Pine in 200 °C Vacuum Treatment After 24 hours.....</i>	<i>124</i>
<i>Figure 4-25 FTIR Peak Area Change of New Pine During 200 °C Vacuum Treatment.....</i>	<i>125</i>
<i>Figure 4-26 FTIR Spectrum Change of New Pine in 160 °C Vacuum Treatment after 24 hours</i>	<i>127</i>
<i>Figure 4-27 FTIR Peak Area Change of New Pine during 160 °C Vacuum Treatment</i>	<i>127</i>
<i>Figure 4-28 FTIR Spectrum Change of New Pine in 120 °C Air Treatment After 24 hours</i>	<i>129</i>
<i>Figure 4-29 Peak Area Change of New Pine During 120 °C Air Treatment</i>	<i>129</i>
<i>Figure 4-30 FTIR Spectrum Change of New Pine in 160 °C Air Treatment After 24 hours</i>	<i>131</i>
<i>Figure 4-31 Peak Area Change of New Pine during 160 °C Air Treatment</i>	<i>131</i>
<i>Figure 4-32 FTIR Spectrum Change of New Pine in 200 °C Air Treatment After 24 hours</i>	<i>133</i>
<i>Figure 4-33 Peak Area Change of New Pine during 200 °C Air Treatment</i>	<i>133</i>
<i>Figure 4-34 New Pine Chemical Reaction for Different Temperatures, Treatment Period and Atmospheres (air and Vacuum).....</i>	<i>135</i>
<i>Figure 4-35 FTIR Spectrum Change of Old Pine in 120 °C Vacuum Treatment After 24 hours</i>	<i>137</i>
<i>Figure 4-36 Peak Area Change of Old Pine During 120 °C Vacuum Treatment</i>	<i>137</i>
<i>Figure 4-37 FTIR Spectrum Change of Old Pine at 200 °C vacuum Treatment After 24 hours.....</i>	<i>138</i>
<i>Figure 4-38 Peak Area Change of Old Pine During 200 °C Vacuum Treatment</i>	<i>139</i>
<i>Figure 4-39 FTIR Spectrum Change of Old Pine in 120 °C Air Treatment after 24 hours</i>	<i>140</i>
<i>Figure 4-40 Peak Area Change of Old Pine during 120 °C Air Treatment</i>	<i>141</i>
<i>Figure 4-41 FTIR Spectrum Change of Old Pine in 200 °C Air Treatment After 24 hours</i>	<i>142</i>
<i>Figure 4-42 Peak Area Change of Old Pine during 200 °C Air Treatment</i>	<i>142</i>
<i>Figure 4-43 Old Pine Chemical Reaction for Different Temperatures, Treatment Periods and atmosphere</i>	<i>144</i>
<i>Figure 4-44 Peak Area Change of New Pine in Different Treatment</i>	<i>152</i>
<i>Figure 4-45 Peak Area Change of Old Pine in Different Treatment.....</i>	<i>154</i>
<i>Figure 5-1 Schematic Diagram of a 3-Point Bending Test.....</i>	<i>156</i>
<i>Figure 5-2 Stress-Strain Curve of a 3-Point Bending Test</i>	<i>156</i>
<i>Figure 5-3 Relationships Between Dynamic Mechanical Properties</i>	<i>157</i>
<i>Figure 5-4 MOR and Moisture Content of New Pine</i>	<i>158</i>
<i>Figure 5-5 MOE and Moisture Content of New Pine</i>	<i>159</i>

<i>Figure 5-6 Stress-Strain Curve of Dry and 10% Moisture Content Samples.....</i>	<i>159</i>
<i>Figure 5-7 DMTA Storage Modulus of a New Sample in Dry and Moisture Samples</i>	<i>162</i>
<i>Figure 5-8 DMTA Loss Modulus of a New Sample for both Dry and Moisture Samples</i>	<i>162</i>
<i>Figure 5-9 DMTA Tan δ of a New Sample for both Dry and Moisture Samples.....</i>	<i>163</i>
<i>Figure 5-10 DMTA Storage Modulus of an Old Sample for both Dry and Moisture Samples</i>	<i>163</i>
<i>Figure 5-11 DMTA Loss Modulus of an Old Sample for both Dry and Moisture Samples.....</i>	<i>164</i>
<i>Figure 5-12 DMTA Tan δ of an Old Sample for both Dry and Moisture Samples</i>	<i>164</i>
<i>Figure 5-13 DMTA Tan δ of Moisturised New and Old Pine</i>	<i>166</i>
<i>Figure 5-14 DMTA Tan δ of Dry New and Old Pine.....</i>	<i>166</i>
<i>Figure 5-15 Changes in the Mean MOR of New Pine During Heat Treatment</i>	<i>168</i>
<i>Figure 5-16 Change in the MOR Variation of New Pine During Heat Treatment</i>	<i>169</i>
<i>Figure 5-17 Mean MOE Changes of New Pine During Heat Treatment.....</i>	<i>171</i>
<i>Figure 5-18 MOE Variation Changes of New Pine During Heat Treatment</i>	<i>172</i>
<i>Figure 5-19 DMTA Mean Tan δ of New Pine Samples after Heat Treatment.....</i>	<i>173</i>
<i>Figure 5-20 Mass loss of Compression Test Samples During Heat Treatment</i>	<i>176</i>
<i>Figure 5-21 Mass loss Variation of Compression Test Samples During Heat Treatment.....</i>	<i>176</i>
<i>Figure 5-22 EMC Change of Compression Test Samples During Heat Treatment</i>	<i>177</i>
<i>Figure 5-23 EMC Error Change of Compression Test Samples During Heat Treatment.....</i>	<i>177</i>
<i>Figure 5-24 Compression MOE Parallel to the Grain of New Pine.....</i>	<i>179</i>
<i>Figure 5-25 Compression MOE Variation Parallel to the Grain of New Pine</i>	<i>179</i>
<i>Figure 5-26 Compression MOR Parallel to the Grain of New Pine.....</i>	<i>180</i>
<i>Figure 5-27 Compression MOR Variation Parallel to the Grain of New Pine.....</i>	<i>180</i>
<i>Figure 5-28 Scanning Electron Microscope (SEM) of Timber Cells.....</i>	<i>183</i>
<i>Figure 5-29 MOR of Old Pine Changes During Heat Treatment</i>	<i>184</i>
<i>Figure 5-30 MOR Variation Changes of Old Pine During Heat Treatment</i>	<i>184</i>
<i>Figure 5-31 MOE Changes of Old Pine During Heat Treatment.....</i>	<i>186</i>
<i>Figure 5-32 MOE Variation Changes of Old Pine During Heat Treatment.....</i>	<i>186</i>
<i>Figure 5-33 DMTA Mean Tan δ of Old Pine Samples after Heat Treatment.....</i>	<i>187</i>
<i>Figure 6-1 MOR & Peak 1318 / Peak 1730 of New Pine</i>	<i>199</i>
<i>Figure 6-2 MOR & Peak 1318 / Peak 1730 of Old Pine</i>	<i>200</i>
<i>Figure 6-3 Relationship between Predicted MOR and Measured MOR by Curve Fitting.....</i>	<i>203</i>
<i>Figure 6-4 Relationship between Predicted MOR and Measured MOR by MRA</i>	<i>205</i>
<i>Figure 6-5 Relationship between Predicted MOE and Measured MOE by MRA.....</i>	<i>210</i>
<i>Figure 6-6 Relationship between Predicted MOE and Measured MOE by RR</i>	<i>211</i>
<i>Figure 6-7 Relationships of Two Peaks Storage Modulus.....</i>	<i>213</i>

<i>Figure 6-8 Relationships of Two Peaks Loss Modulus</i>	<i>214</i>
<i>Figure 6-9 Predicted and Measured Storage and Loss Moduli of Peak γ</i>	<i>216</i>
<i>Figure 6-10 Predicted and Measured $\tan \delta$ at Peak γ.....</i>	<i>217</i>
<i>Figure 6-11 Predicted and Measured Storage and Loss Moduli of Peak β.....</i>	<i>219</i>
<i>Figure 6-12 Predicted and Measured $\tan \delta$ at Peak β</i>	<i>220</i>
<i>Figure 7-1 A Protective Layer after 100 hours UV Exposure.....</i>	<i>224</i>
<i>Figure 7-2 Predicted and Measured Peak Area Changes of Regression Model.....</i>	<i>233</i>
<i>Figure 7-3 Model-Predicted and Measured Peak Area of the Air Treatment Method</i>	<i>238</i>
<i>Figure 7-4 Model-Predicted and Measured Peak Area of the Vacuum Treatment Method.....</i>	<i>238</i>
<i>Figure 7-5 Model-Predicted and Measured Peak Area of the Combined Treatment Method.....</i>	<i>239</i>

Chapter 1 Introduction

1.1 Background and Motivation

Timber ageing causes a series of problems in all historic timber buildings, which affect the mechanical properties significantly and slowly reduce structural stability. Historic timber buildings are distributed across all nations, because timber was the earliest material used in architecture in human civilisation. In china, historic timber buildings can be found in all human activity areas (Figure 1-1). Chinese architects have 4,000 years' experience of timber construction, but the oldest existing timber structure is the Nan-Chan temple approximately 1,200 years old. Most buildings collapsed due to the ageing effects, which cause construction failure during natural disasters such as earthquakes, typhoons and flooding. Timber is still an important building material in modern construction. Owing to deep understanding with regards to timber material and easy assembly, tall frame constructions can be built by cross laminated timber (CLT) and more such buildings are planned (Figure 1-2). It can be foreseen that ageing will cause structural problems in all these proposed timber buildings as well. As a result of the ageing process, in particular the effects on mechanical properties, it is an important to study timber structures. However, the mechanical strength of each member of a timber structure cannot be evaluated easily and quickly due to the fact that they cannot be disassembled. Hence, non-destructive or less-destructive testing methods are needed. In fact, many studies have reported good relationships between timber mechanical properties and wood colour (Matsuo et al., 2010; Matsuo et al., 2011; Bekhta and Niemz, 2003) or stress waves (Dackermann et al., 2014; Wang et al., 2004; Ross et al., 1999). However, the former is also affected by timber extractives (Burtin et al., 1998; Gierlinger et al., 2004), while the latter sometimes conflict

with the properties evaluated by real mechanical testing (Attar-Hassan, 1976). Hence, a more effective non-destructive method needs to be developed.

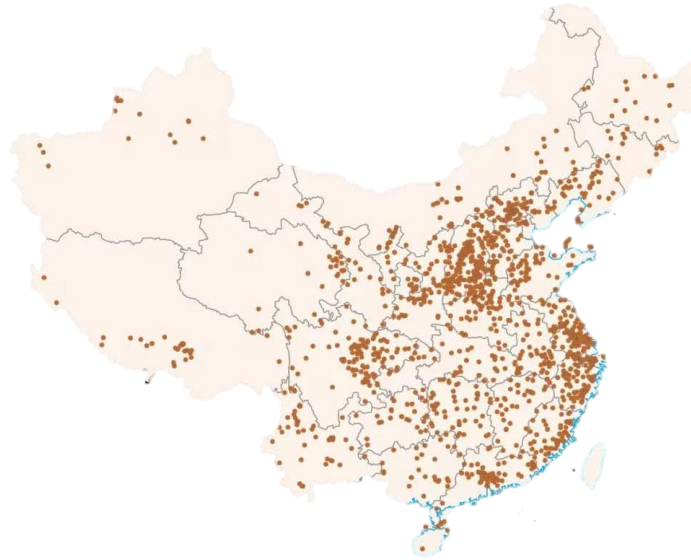


Figure 1-1 Historic Timber Building Distribution in China (National Cultural Heritage Administration)

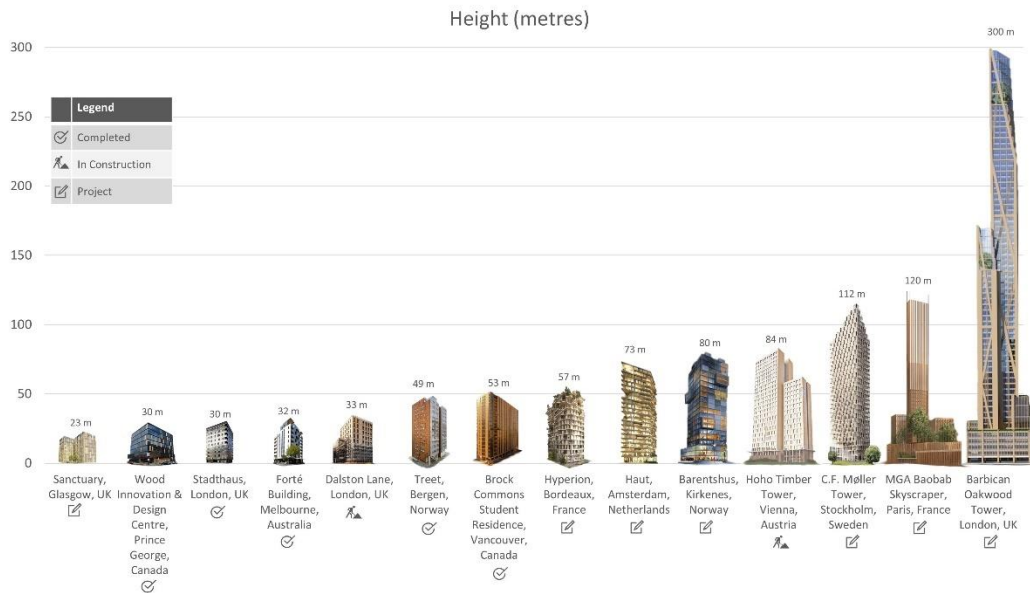


Figure 1-2 Wooden High-Rise Buildings (Confederation of Timber Industries)

Fengel (1991) pointed out that the chemical compositions of timber during ageing has different changes in different environments. Cavalli et al. (2016) also reported that mechanical properties vary during the natural ageing process and the changes are based on distinctive environments. The findings of these two comprehensive studies imply that timber's chemical composition has close relationships with its mechanical properties. These relationships have been uncovered through experiments, which involved rupturing covalent bonds and detecting the corresponding mechanical strength (Illston et al., 1979; Winandy and Rowell, 1984), but the regression mathematic models were not discussed in these studies. Hence, timber chemical composition analysis can be a non-destructive testing method to predict mechanical properties. However, due to conservation philosophies, natural aged timber samples are restricted for destructive testing. Another method that can cause changes both in the chemical composition and mechanical properties of timber is needed for research purposes. Donetzhuber and Swan (1965) reported that timber ageing can be accelerated by temperature, which led to an important timber industry: heat treatment.

Nowadays, timber heat treatment is a mature industry and various treatment methods are implemented. Esteves and Pereira (2008) identified several common heat-treatment methods, including Thermowood in Finland, Plato Wood in the Netherlands, OHT-Oil treatment wood in Germany, the Bois Perdure and Rectification method in France, WTT in Denmark and Huber Holz in Austria. All the treatments can cause distinctive changes in timber molecules' chemical composition and mechanical strength. Specifically, heat treatments at certain temperatures, for particular periods and in distinct atmospheres can lead to changes in both timber molecule composition and mechanical strength. Hence, this

makes them a suitable method for studying the relationships between chemical composition and mechanical properties of timber.

In sum, timber's chemical composition is highly related to its mechanical properties and non-destructive testing of the latter can provide valuable data about this relationship. In this study, the overall aim is to simulate timber mechanical properties by chemical composition and to accelerate ageing of timber by modifying chemical compositions. Both are investigated by heat treatment. The objectives of the research are provided in the following section.

1.2 Objectives

As above mentioned, this research is focused on the relationship between the chemical composition of timber and its mechanical properties. Changes in timber are accelerated by temperature and detected by specific testing facilities, both chemical and mechanical. The objectives of the research are as follows:

- Find the relationship between the chemical composition of timber and the corresponding mechanical properties during heat treatment. The chemical composition is detected by the FTIR technique, which illustrates the functional groups of timber molecules by their corresponding peaks on the FTIR spectrum. The mechanical properties are detected by static 3-point bending and dynamic mechanical thermal analysis (DMTA) facilities.
- Create regression models to predict mechanical properties by the peaks of the FTIR spectrum, which provide fundamental data for the non-destructive testing of timber mechanical properties. Non-destructive testing can be exploited in mechanical evaluation both for historic timber structure conservation and new timber structures.

- Define the chemical composition changes during different heat treatments. Theoretically, the changes of the FTIR peaks, corresponding to functional groups of timber molecule can be predicted by these three independent variables. The aim is to provide a regression model for controlling chemical changes in timber molecules during heat treatment.
- Produce a mathematic regression model to accelerate chemical changes of timber molecule by heat treatment to a certain composition. A piece of 580 year old pine is utilised in this study, such that the regression model could provide a method for changing the chemical compositions of new timber to old.

1.3 Outline of the thesis

The literature is reviewed in chapter 2. Timber cell structure, the chemical composition of cell walls, the changes in molecule composition as well as the mechanical properties during natural ageing and artificial modifications are discussed in the chapter. A detailed experiment plan is provided in chapter 3, which introduces the experimental materials used, heat treatments applied, detecting method for the timber chemical and mechanical properties, and the data analysis methods. Timber chemical composition and mechanical properties changes are analysed in detail in chapter 4 and chapter 5, respectively. The effects of moisture content on these phenomena are also discussed in the two chapters. Mathematic models are regressed in chapter 6 and chapter 7. Chapter 6 considers timber mechanical properties according to the function groups of its molecules, which are detected by FTIR techniques. Chapter 7 simulates the changes in the FTIR peaks during heat treatment and builds a method for accelerating pine samples to 580 years old by specific temperatures, time periods and specific treatment atmospheres. A comprehensive

presentation of the contributions of the study and a conclusion is provided in chapter 8.

Figure 1-3 shows the structure of this thesis.

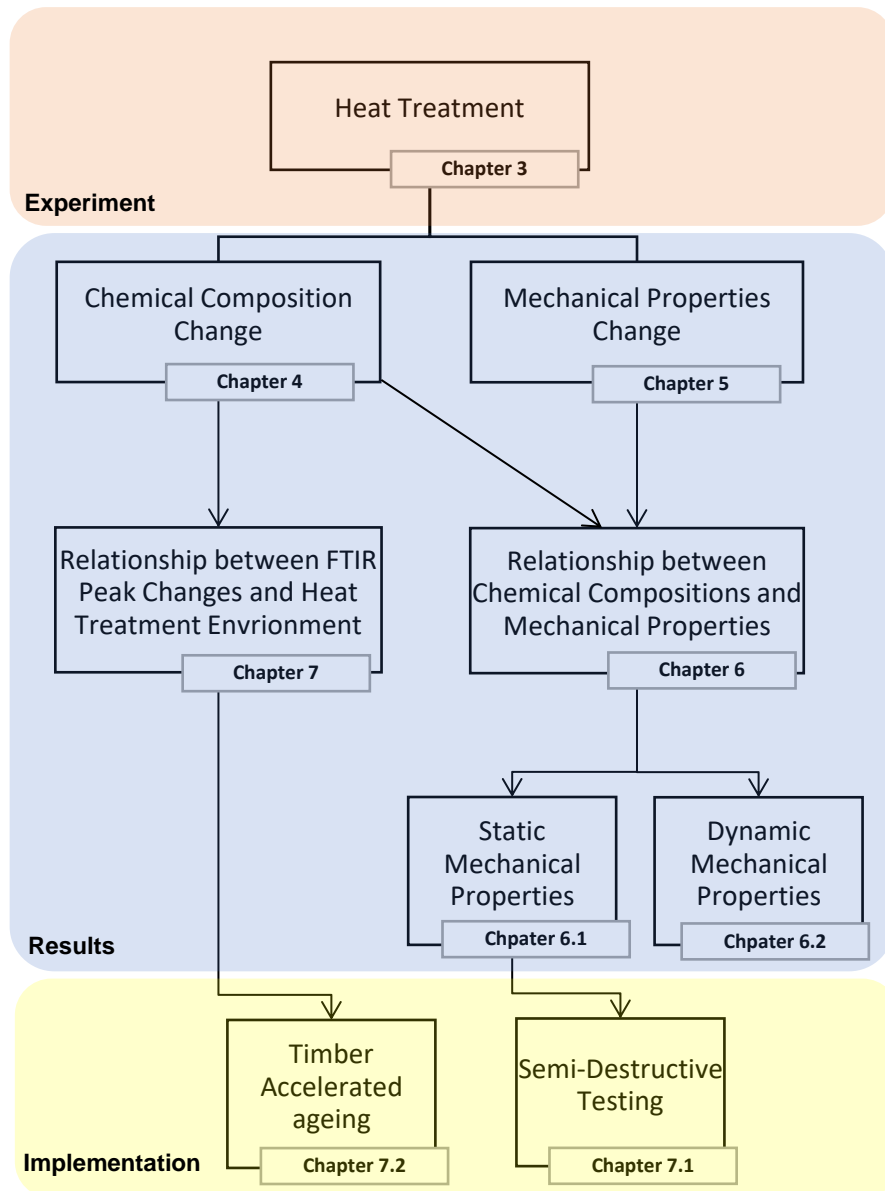


Figure 1-3 Outline of The Thesis

Chapter 2 Literature Review

Illston et al. (1979) described timber as a kind of “low-density, cellular, polymeric” composite, which could be treated as a new material category. Timber mechanical performance is the same as an elastic material under low stress and short periods, but it can be treated as a linear orthotropic viscoelastic material under high level stress and long periods. Hence, timber’s distinctive composition structure is worthy of study. In addition, many studies focusing on timber ageing, hold that mechanical improvements or durability can cause a few changes chemically and mechanically and these are reviewed in this chapter. Moreover, several mechanical and chemical composition test methods are also discussed.

In this chapter, timber composition from cell level to molecular level and the relationship between chemical composition and mechanical property are introduced in section 2.1. The changes of chemical composition and mechanical properties in different atmospheres are discussed in the following two sections, 2.2 and 2.3. This chapter is divided into the following four sections:

- Timber composition and its relationship to its mechanical properties
- Natural and artificial timber chemical composition change
- Natural and artificial timber mechanical change
- Conclusions.

2.1 Timber composition

Timber structure is complex, and in each level, from the trunk to the molecular, it has its own distinctive features (Figure 2-1). Trees need to resist gravity and lateral force, such as wind, during their entire growing life, which is achieved by timber cell division. On a section of a tree trunk, differentiated areas due to cell division are easily observed by the colour (Figure 2-2). From spring to late summer, with appropriate temperature, cells divide quickly to expand the trunk and produce a layer with a light colour. In the colder seasons, the tree goes dormant, but the cells still grow, showing a dark layer. The light layer is named as earlywood or springwood, while the dark one is latewood or autumnwood. The cell walls of latewood are thick and strong, providing most of the mechanical strength. The earlywood is porous and has the function of delivering moisture and nutrients to keep the tree alive. Cell wall composition has a strong relationship with mechanical behaviour, which will be discussed in detail in the following subsection 2.1.1.

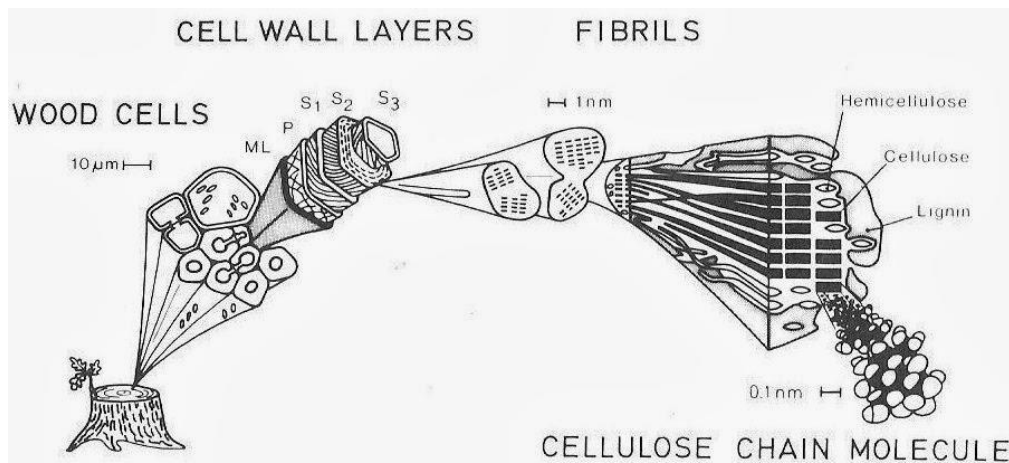


Figure 2-1 Structures of Timber in Different Scale (Hoffmann and Jones, 1990b)

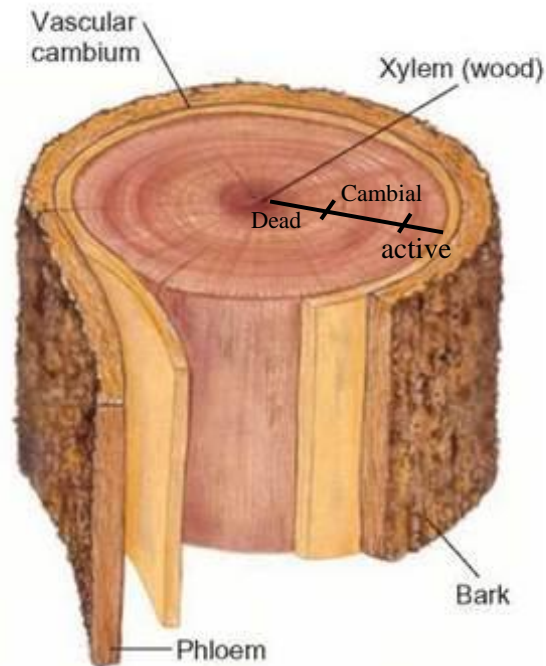


Figure 2-2 Structure of Tree Trunk

With a tree trunk widening layer by layer, cells differentiate into phloem and xylem parts. Phloem is a layer of living cells with the function of cell division, delivering polysaccharide produced by photosynthesis and storage. Moreover, phloem is a thin layer with low mechanical strength, which will be removed when the timber is used for construction. Hence, in this part of the literature review, phloem is not studied further, and the following reviews of the literature are focused on xylem.

Xylem contains three layers, these being active xylem, the cambial zone and dead xylem, from outside to inside (Bertaud and Holmbom, 2004) (Figure 2-2). Active xylem, also named sapwood, is living cells including tracheids, vessels and fibres with the function of storage and delivery. When trees widen to a certain size, active xylem cells undergo a series of changes, turning into a strength enhanced status through the following steps: cell expansion → thickening of the secondary cell wall → lignification → death and becoming heartwood. The cell wall is thickened by producing cellulose, hemicellulose and a small

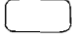
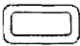
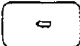

amount of lignin after cell expansion. It becomes strengthened in the lignification period by an ill-defined phenolic polymer of lignin depositing on an extracellular polysaccharidic matrix (Barceló, 1997). Finally, the cells die and turn into heartwood, which is the strongest part of a trees providing mechanical performance for timber structures.

The general situation regarding timber is that the cell walls of sapwood are responsible for growth, while heartwood supports the tree. Sapwood turns into heartwood at a certain trunk width. However, a tree is able to adjust size ratio of heartwood and sapwood by itself due to external factors, according to Berthier et al. (2001), who studied the trunk of the maritime pine (*Pinus pinaster Ait*). They found that the heartwood area develops radially and longitudinally more on the compressed side of the tree, which is caused by wind or obliqueness to resist external force. In addition, 12 52-year old trees with obliqueness of 0° to 22° were investigated to prove that a tree can maintain the optimal proportion of sapwood in the trunk to help its growth. Similar results on heartwood were elicited by Bamber (1976).

2.1.1 Timber Cell Composition

The cell is the fundamental unit for understanding timber. There are four types of cell in xylem, which are parenchyma, tracheids, fibres and vessels with the functions of storage, support and conduction, respectively (Table 2-1) (Huang et al., 2003). Trees have various species, but generally divide into softwood and hardwood, as distinguished by cell type. Softwoods do not have vessel and fibre cells such as gymnosperms. Hardwoods (normally dicotyledon) contain all four kinds of cells (Pandey, 1999).

Table 2-1 Cell Types of Timber (Dinwoodie, 1975)

Cell	Softwood	Hardwood	Function	Wall thickness
Parenchyma	√	√	Storage	
Trocheids	√	√	Support conduction	
Fibres		√	Support	
Vessels (pores)		√	Conduction	

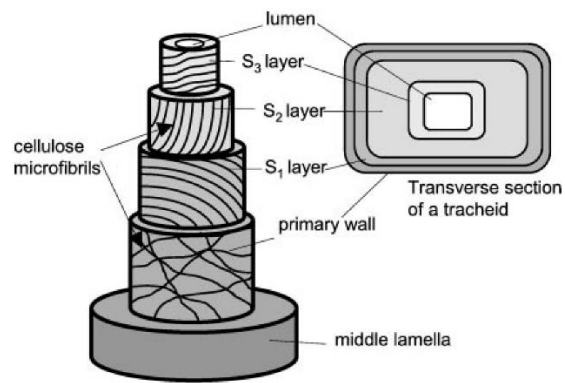


Figure 2-3 Structure of Timber Cell (Huang et al., 2003)

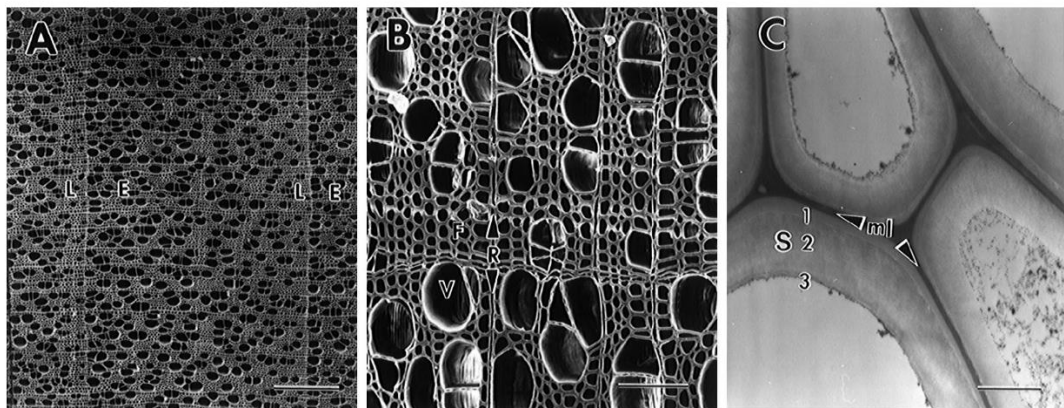


Figure 2-4 SEM Image of Timber Cells (Higuchi, 2012)

Polysaccharides (cellulose and hemicellulose) and lignin with other substances, including minor solubles (stilbenes, flavonoids tannins and terpenoids) insolubles (pectin and cell wall proteins) and Trace elements comprise the chemical composition in the cell wall. However, polysaccharides and lignin only appear on the cell wall starting from its secondary formation (Higuchi, 2012).

A wood cell wall consists of several layers, which appear in different periods of growing (Figure 2-3 and Figure 2-4). The middle lamella contains abundant pectic substances and differentiate to primary wall as the first step of cell wall division. When new the cell reaches a mature size, a new secondary cell wall with three layers, S1, S2 and S3, is composed inside the primary wall. The secondary cell wall is composed of cellulose microfibrils with a certain direction, with their direction in S1, S2 and S3 being different. Lignin and hemicellulose are produced later in the three layers. S1 is the thinnest layer, which only contributes 5% to 10% to the cell wall thickness and the cellulose microfibrils angle is 60° to 80° to the cell axis. S2 is the thickest layer and occupies 75% to 85 % of the total thickness, thus contributing much of the cell's mechanical strength. Its cellulose microfibrils' angle is between 5° and 30° to the cell axis. This angel of S2 plays a decisive role in physical and mechanical performance. Timber rigid and modulus of elasticity in the longitudinal direction is affected by the S2 cellulose microfibrils' angles to cell axis, (Plomion et al., 2001). The cellulose microfibrils in S3 are 60° to 90° to the cell axis, but the arrangement is not strict as for the S1 and S2 layers. According to Dinwoodie (2000), the S2 layer is mainly responsible for the mechanical property of timber cell wall, while S1 and S3 have significant influence on the mechanical property of the transverse direction.

Chemical and ultrastructure

Table 2-2 shows that cellulose, hemicellulose, lignin and extractives are the main molecule forming cell walls (Dinwoodie, 1975). In fact, 45-50% of cell wall composition is cellulose (Figure 2-5), which is a long slender chain including 8000-10,000 cellobiose units, $(C_6H_{10}O_5)_n$, bonded by β -1-4 linkage (Goring and Timell, 1962). Cellulose molecules in the cell wall are arranged in a certain order and create a relatively stable structure, which is crystalline (Figure 2-8). According to Thygesen et al. (2005), who studied the crystallinity of cellulose by chromatographic measurement of monomers after hydrolysing samples, plant-based materials contain 90% to 100% cellulose crystallinity, whilst wood-based ones have 60% to 70%. Hemicellulose is soluble non-cellulosic polysaccharides that occupy approximately 25% of the content of dry wood (Figure 2-6). They have a shorter chain than cellulose and take various forms. Heteropolymers (glucomannan, galactoglucomannan, arabinogalactan and xylan) and homopolymers (galactan, arabinan and β -1, 3-glucan) are two typical kinds of hemicellulose (Keegstra and Raikhel, 2001). Hemicellulose content is different across wood species, with softwoods containing more glucomannans than hardwoods, whilst the latter contain more xylans. Lignin, comprising 25% to 35% cell wall content, is a kind of phenolic polymer developed from hydroxycinnamoyl alcohols (a kind of monolignol) including ρ -coumaryl, coniferyl and sinapyl alcohols. Lignin has three types, namely Hydroxyphenyl, Guaiacyl and Syringyl, the difference between them being the level of methoxylation. Structurally, the lignin molecule is much shorter than that of cellulose and it contains many branch chains (Figure 2-7).

Table 2-2 Molecule Content of Timber Cell Walls (Dinwoodie, 1975)

Molecule	Content (%)	Polymeric state	Molecular derivatives	Function
Cellulose	45-50	Crystalline, highly orientated large molecules	Glucose	Fibre
Hemicellulose	20-25	Semi-crystalline, small molecules	Non-cellulosic polysaccharides	Matrix
Lignin	25-30	Amorphous, large 3D molecules	Phenol propane	
Extractives	0-10	Non-polymeric		Extraneous

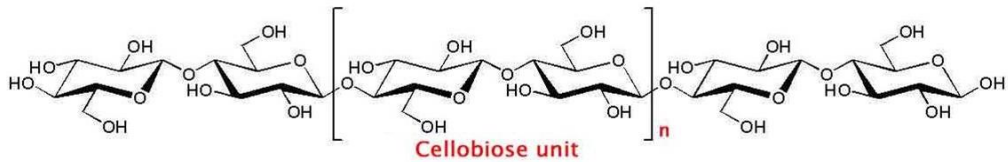


Figure 2-5 Structure of Cellulose (Goring and Timell, 1962)

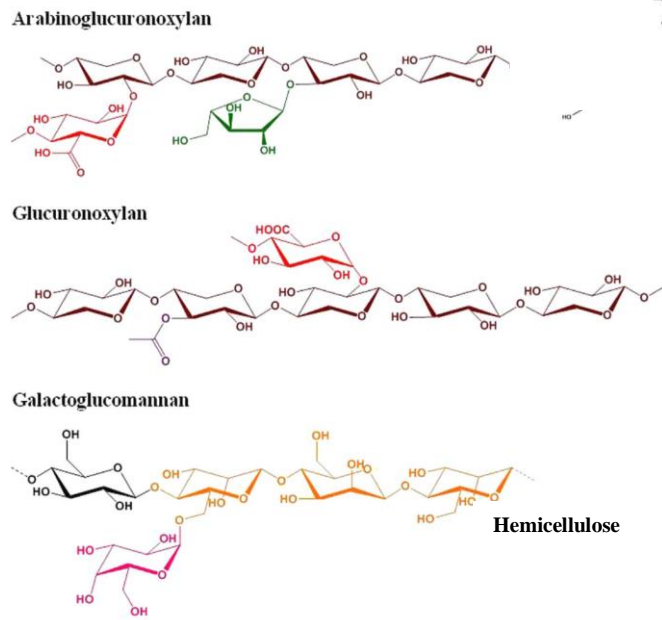


Figure 2-6 Structure of Hemicellulose (Ramage et al., 2017)

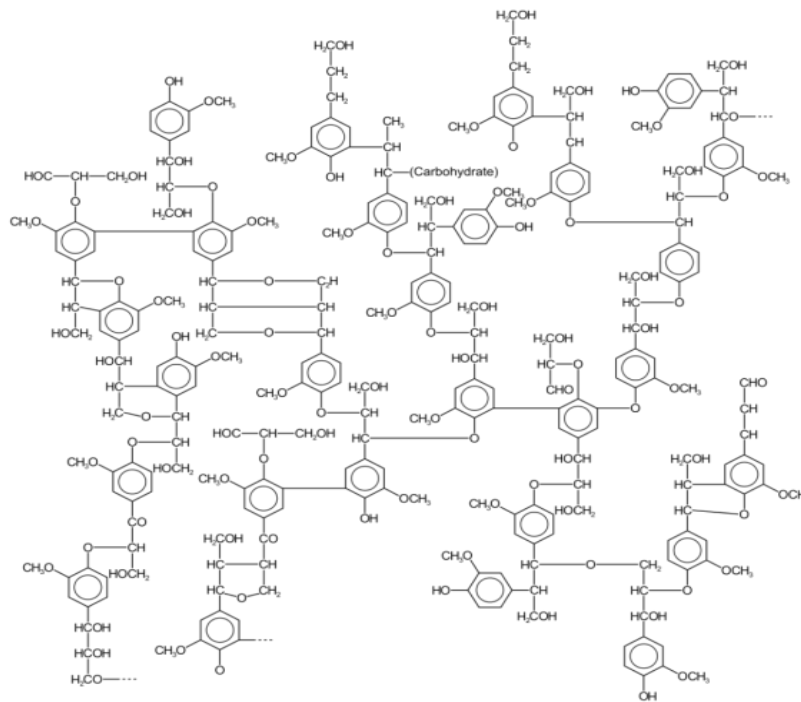


Figure 2-7 Structure of Lignin (Yang et al., 2007)

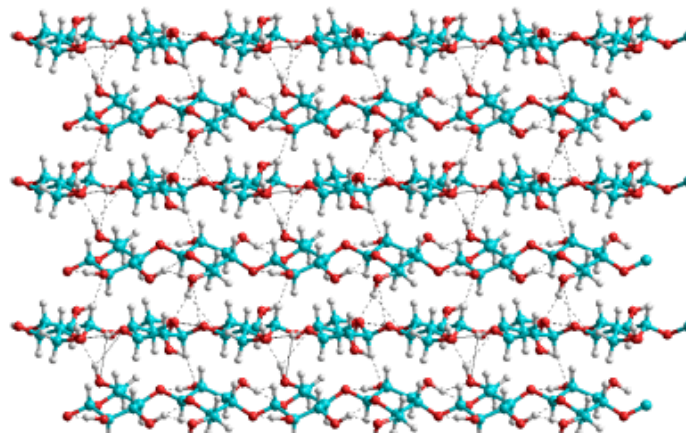


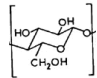
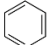
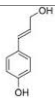
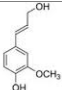
Figure 2-8 Crystalline Structure of Cellulose (Thygesen et al., 2005)

All the three molecules, cellulose, hemicellulose and lignin consist of carbon, oxygen, hydrogen and nitrogen, which are 49-50%, 45-50%, 6% and 0.1-1% content, respectively, in timber molecule composition. In addition, there are a few trace elements such as calcium, potassium, magnesium, sodium, manganese, iron, phosphorus, sulphur and silica in timber, but the total content is less than 0.1%. Timber molecules contain many repeated specific

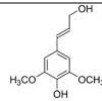
group, called functional groups (Table 2-3) and timber molecule chemical compositions changes are based on the activity of these groups.

To sum up, timber cells as fundamental units provide mechanical properties for the tree to resist external force, while the mechanical strength of cell wall is obtained by the distinctive function of cellulose, hemicellulose and lignin. Cellulose with a crystalline structure supports the wall, while hemicellulose and lignin, with many branch chains, compact all the molecules of cell wall closely. Hence, theoretically, the status of the timber molecule has a close relationship to its mechanical property, which is discussed in the following subsection.

Table 2-3 Chemical Functional Group in Timber Molecule

Functional groups name	Chemical composition	Location
Microfibrils		Cellulose
Hydroxyl	$\text{R}-\text{O}-\text{H}$	Cellulose, hemicellulose and lignin
Methylene groups	$\begin{array}{c} \text{H} \\ \\ -\text{C}-\text{H} \\ \\ \text{H} \end{array}$	Cellulose, hemicellulose and lignin
Carbonyl group	$\begin{array}{c} \text{O} \\ \\ \text{R}'-\text{C}-\text{R}' \end{array}$	Cellulose, hemicellulose and lignin
Ether linkage	$\text{R}-\text{O}-\text{R}'$	Cellulose, hemicellulose and lignin
Aromatic skeletal		Lignin
Hydroxyphenyl ring		Lignin
Guaiacyl ring		Lignin

Syringyl ring



Lignin

2.1.2 Relationship between Chemical composition and Mechanical Bonding

Atoms may share electrons with one another to form an attractive force, which gives fundamental strength to single molecules. Different lengths or matrices lead to distinctive mechanical behaviours of high weight molecules, such that in polymer materials, molecule status has a close relationship with mechanical properties. Generally, the molecules of high weight solid polymers have two types of arrangement (Ward and Sweeney, 2012):

1. Single chain with a rotational isomerism structure without connection to its neighbour;
2. Molecular bundle neighbouring molecules.

A timber molecular arrangement may contain both of these (Ramage et al., 2017). Cellulose is arranged parallel to the cell axis while and hemicellulose bundle cellulose to enhance connections of cellulose microfibrils (Figure 2-9). Lignin, with many branch chains, binds all cellulose and hemicellulose in the cell wall. Hence, cellulose with the supporting function, hemicellulose and lignin with a connection function create the structure system to provide mechanical strength. However, whilst the arrangement of the timber molecule is the same, different molecule content and density contribute to variant mechanical properties of timber. Generally, as a polymer, the mechanical properties of timber are affected by the following aspects (Landel and Nielsen, 1993; Tobolsky and Eyring, 1943):

1. Molecular weight (length);
2. Crossing link and branch chain;

3. Molecular orientation;
4. Crystallinity;
5. Copolymerisation;
6. Plasticisation;
7. Fillers;
8. Blending;
9. Phase separation and orientation in blocks, grafts and blends.

Moreover, polymer molecular structure stability is affected by environmental effects significantly, including:

- Temperature;
- Time, frequency, rate of straining or stressing;
- Pressure;
- Type of deformation (shear, tensile);
- Heat treatment;
- Moisture content.

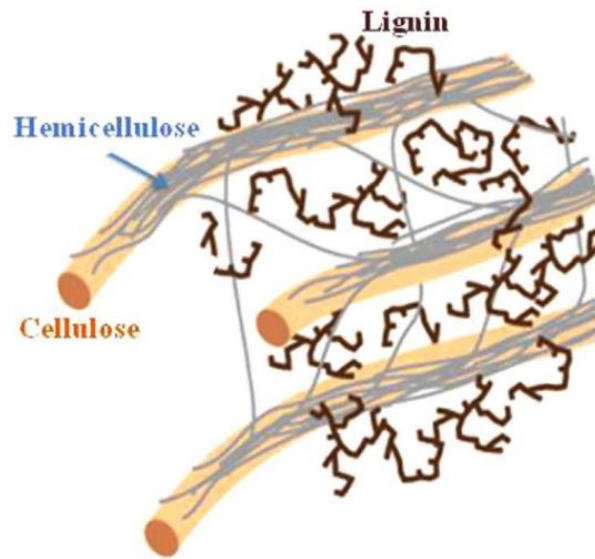


Figure 2-9 Connection of Cellulose, Hemicellulose and Lignin (Ramage et al., 2017)

Not just theoretically, for many studies have proven empirically that the chemical composition of wood has a close relationship with its mechanical properties. Illston et al. (1979) ruptured the covalent bonding of the timber molecule by gamma irradiation, which led to bond quantity reducing from 5000 to 200, i.e. the tensile strength decreased significantly. A similar result was reported by Winandy and Rowell (1984) who demonstrated that the mechanical properties of timber comprise covalent and hydrogen interpolymer bonds of cellulose, hemicellulose and lignin. Boonstra et al. (2007b) compared previous literature with his results and claimed that tensile strength is affected by amorphous cellulose and that hemicellulose and lignin might be involved also. Longitudinal compressive strength and shear strength are affected by crystallisation and lignin cross-linking, respectively (Boonstra et al., 2007b). Timber bending strength decreases due to degradation of hemicellulose, but it is enhanced by lignin cross-linking. In fact, cellulose and glucomannan play an important role in the strength parallel to cell axis (Åkerholm and Salmén, 2001). Lignin plays a mechanical role in all directions and it also affects viscoelastic behaviour (Åkerholm and Salmén, 2003). Winandy and Lebow (2001) created a three-parameter model and link chemical composition to bending strength

though Klason lignin, glucose, mannose, xylose, arabinose and galactose of timber molecule by a previous published report (Winandy and Lebow, 1996). Even though this research only provided a preliminary model, it predicted bending strength well with, $R^2 \geq 0.75$ on a straight-grained pine. Brittleness also has a high relationship with the degradation of amorphous polysaccharides, according to Shida and Saito (2007).

In addition, timber molecules have thermoplastic features especially on hemicellulose and lignin. In a specific temperature range, hemicellulose (127°C to 235°C) and lignin (167°C to 217°C) change into softened status and then connect to cellulose by secondary intermolecular bonding. The molecules become rigid again after heat treatment, which led to two converse results on the timber strength properties, enhancing and decreasing. (Hillis and Rozsa, 1978; Hillis, 1984).

In conclusion to this subsection, the changes in the timber molecule, especially hemicellulose and lignin, can have positive or negative influence on mechanical behaviours. Hence, the relationships need to be studied in more depth.

2.1.3 Moisture Content and Environment Temperature

Not only does the chemical composition of timber affect mechanical behaviour, for moisture content and temperature also play significant roles (Gerhards, 2007).

Moisture content

Water is from the environment and trees use it well for growing and improving mechanical strength. Free water and bond water are two existing types in the cell wall. Free water exists in cell lumen, whereas bonding water penetrates between the timber molecular chain and connects to the timber molecules by hydrogen bonding. The moisture content at the point where there is only bond water in the cell wall, i.e. no free water, is named the fibre

saturation point (FSP). Figure 2-10 shows the relationship between compression strength and moisture content (Dinwoodie, 1975). Timber loses strength when the moisture content increases but is not affected by this when the content is beyond the FSP. Moreover, tensile stress parallel- and perpendicular to the grain are stronger at a moisture content of between 7% and 13% (Kretschmann and Green, 2007). Becker and Noack (1968) explained moisture behaviour (more than 12%) in wood molecules by a torsional viscoelasticity experiment. High moisture content leads to relaxation of timber molecules. Bond water is attracted by timber molecular chains by hydrogen bonding. The hydrogen bond is secondary bond as it exists between water and timber molecules. Hence, hydrogen atoms of bond water bonding to timber molecules (cellulose, hemicellulose and lignin) provides extra elasticity between the molecules (Steiner, 2002).

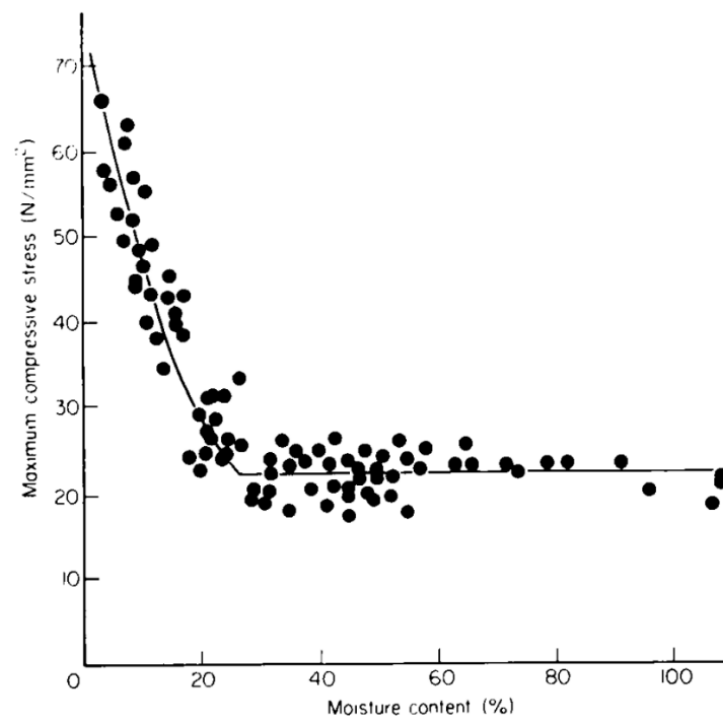


Figure 2-10 Relationship Between Compression Strength and Moisture Content (Dinwoodie, 1975)

If a large members of water molecules penetrate the gaps between timber molecules, the timber will swell, but if none exists, it will shrink. Figure 2-11 shows different amounts of water molecules existing between timber. Moisture content is changeable, being affected by different humidity and temperature (Dinwoodie, 1975; Dinwoodie, 2002). In many studies, equilibrium moisture content (EMC) is usually measured at 20°C with 65% humidity.

Basic of Shrinkage and Swelling

- ❑ Water forms H- bond with OH- group of cellulose microfibrils
- ❑ -OH group of cellulose molecules are responsible for hygroscopicity of wood
- ❑ With increase of temperature and humidity wood shrink by losing water molecules from micro-fibrils

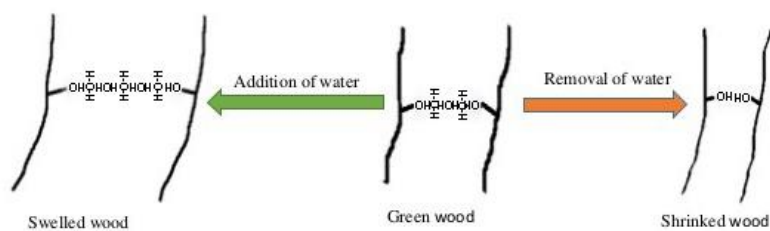


Figure 2-11 Moisture Between Timber Molecules (Dinwoodie, 2002)

For many studies, a close relationship between moisture content and the mechanical strength of timber has been found. As early as Lavers (1967), was discovered that a moisture content above 20% can reduce the mechanical properties in all respects. Gerhards (2007) reviewed more than 10 previous works and produced a table about the mechanical properties relating to moisture content at 20°C (Table 2-4, Figure 2-11 and Figure 2-13), finding that timber with 6% moisture content has the best strength in all directions. That is, this decreases when moisture content increase to 12% and drops significantly with 20% moisture content. The moisture content is affected by the quantity of hydroxyl groups in same environment humidity according to Jämsä and Viitaniemi (2001), who demonstrated that moisture content reducing is accompanied by hydroxyl groups decreasing. Boonstra and Tjeerdsma (2006) also reported that hydroxyl groups decrease due to cellulose

crystallisation and lignin polycondensation during heat treatment, leading to a reduction of moisture content.

Table 2-4 Relationship between Timber Mechanical Property and Moisture Content (Gerhards, 2007)

Timber property	Relative change in property from 12% MC	
	At 6% MC (%)	At 20% MC (%)
Modulus of elasticity, parallel to the grain	+9	-13
Modulus of rupture, perpendicular to the grain	+20	-23
Shear modulus	+20	-20
Bending strength	+30	-25
Tension strength, parallel to the grain	+8	-15
Compression strength, parallel to the grain	+35	-35
Shear strength, parallel to the grain	+18	-18
Tension strength, perpendicular to the grain	+12	-20
Compression strength, perpendicular to the grain at the proportional limit	+30	-30

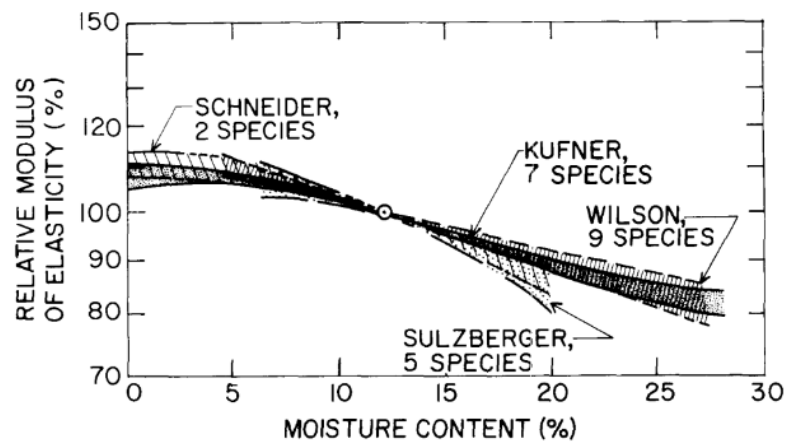


Figure 2-12 Relationship between Modulus of Elasticity and Moisture Content (Gerhards, 2007)

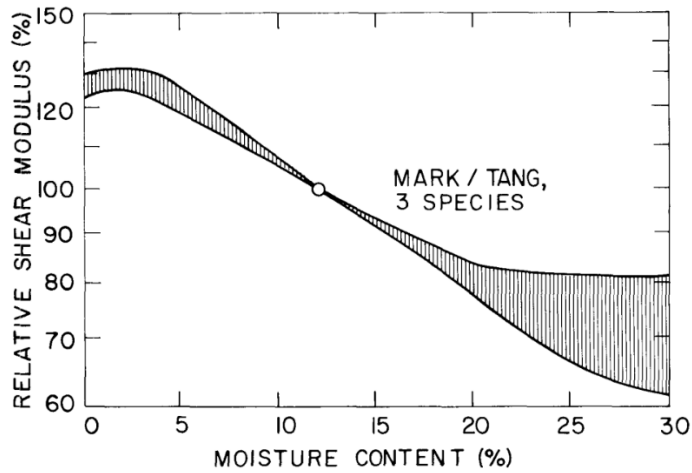


Figure 2-13 Relationship between Shear Modulus and Moisture Content (Gerhards, 2007)

Temperature

Long term temperature causes many changes to the chemical composition of timber and, affect the mechanical properties. Short term temperature can affect the latter due to molecular activity. High temperatures improve molecules relative motion, thereby impacting on the mechanical properties of polymers (Tager, 1972).

The mechanical properties of timber can be tested by various methods in a lab, according to a review by Gerhards (2007) (Table 2-5), who studied timber mechanical properties from -50°C, 20°C and 50°C, timber is strong at a low temperature but loses strength as temperature rises.

Table 2-5 Relationship between Timber Mechanical Property and Testing Temperature (Gerhards, 2007)

Timber property	Moisture content (%)	Relative change in property from 20°C (%)	
		At -50°C	At +50°C
	0	+11	-6
Modulus of elasticity, parallel to the grain	12	+17	-7
	>FSP	+50	-

Modulus of rupture, perpendicular to the grain	6	-	-20
	12	-	-35
	≥ 20	-	-38
Shear modulus	>FSP	-	-25
Bending strength	≤ 4	+18	-10
	11-15	+35	-20
	18-20	+60	-25
	\geq FSP	+110	-25
Tension strength, parallel to the grain	0-12	-	-4
Compression strength, parallel to the grain	0	+20	-10
	12-45	+50	-25
Shear strength, parallel to the grain	>FSP	-	-25
Tension strength, perpendicular to the grain	4-6	-	-10
	11-16	-	-20
	≥ 18	-	-30
Compression strength, perpendicular to the grain at the proportional limit	0-6	-	-20
	≥ 10	-	-35

Hence, from the above moisture content and environmental temperature affect the mechanical properties significantly. Accordingly, experiments on these properties should record moisture content and testing temperature, which kept constant when designing mechanical strength comparison investigations.

2.1.4 Summary

As a kind of building material, the heartwood of tree trunk commonly appears in timber structures, because the cell walls are mechanically enhanced by lignification. These consist of cellulose, hemicellulose and lignin after lignification. Cellulose has long slender chain and a crystalline structure, which supports the cell wall. Hemicellulose and lignin are

shorter, but with a lot of branch chains to bind all the molecules firmly and to form a matrix structure, respectively. The three molecules work together and contribute to the unique mechanical behaviour of timber. However, timber molecular composition can be modified due to activity of chemical functional groups, thus affecting the mechanical strength.

Moisture and temperature can affect mechanical properties significantly. A certain content of moisture provides extra elasticity for the cell walls, but excessive water swells molecules and leads to loss of molecular connection, thus marring the mechanical properties of the timber. Timber strength decreases with temperature rising, so the mechanical properties are affected by different temperatures, whilst the chemical composition and moisture content remain the same regardless of the temperature in a short-term period.

To sum up, the chemical composition of timber, moisture content and temperature are the three main factors affecting mechanical behaviour.

2.2 Changes of Timber Chemical Composition

Timber chemical composition can change in any kind of natural environment and is unstoppable. It changes slowly in the natural environment and this process is called ageing. Many studies related to timber natural ageing have provided valuable information about timber chemical changes during this process. In particular, temperature can accelerate the rate of chemical change (Donetzhuber and Swan, 1965). The timber heat treatment industry uses this feature to improve the mechanical properties of timber by modifying the chemical composition of the timber molecule. Chemically, if the changes affect the molecular length or matrix, the mechanical behaviours will also be significantly changed (Tobolsky and Mark, 1971). Hence, for all chemical composition discussed in this section, the focus is on the changes affecting molecule physical status.

In this section, first, the chemical analysis methods are reviewed. Regarding polymer chemical analysis, each method has its own advantages and disadvantages. Chemical changes of natural ageing and artificial processes are discussed in the second and third subsections. A few factors, such as mass loss and colour change due to chemical composition change, are subsequently discussed and then, conclusions are drawn.

2.2.1 Chemical Composition Analysis Method

Generally, classic wet chemical analysis, pyrolysis, and spectroscopy are the three common methods for detecting the chemical composition of timber. Classic wet chemical analysis has a long history and involves analysing chemical composition by chemical reagents, with most analysis being conducted in the liquid phase. For the pyrolysis method, chemical composition of timber decomposed to liquids or gaseous phase with a certain rate of temperature rising. The liquid and gases are examined to predict original molecule composition. Chemical bonds of all substances can absorb a specific frequency light wave, which is the principle underpinning the spectroscopy method.

Classic Wet Chemical Analysis

Wet chemical analysis is a series of chemical tests in liquid that is based on the specific characteristics of the three timber molecules, cellulose, hemicellulose and lignin. Lignin structure is stable due to condensation structure, but few acids can break glycosidic linkages on cellulose and hemicellulose into individual sugar which can dissolve in water, so the residue is lignin. During the wet chemical analysis process, first, timber is milled into powders and treated in 72% H₂SO₄ for two hours then, in a dilute H₂SO₄ concentration of 3%, finally being boiled for four hours. Carbohydrates (cellulose and hemicellulose) dissolve in the liquid and lignin residue floats in the liquid. Lignin content is measured after filtering, washing and weighting. The residue is named Klason lignin and the method is the

standard lignin detecting analysis method (TAPPI T222). The content of holo-cellulose (cellulose and hemicellulose) and lignin is measured as the timber chemical composition. In addition, the ratio H/L (holo-cellulose/lignin) is normally treated as a reference to describe wood chemical composition change. However, Wacek and Schroth (1950) indicated that a certain percentage of lignin is soluble in acid. Regarding which, recent research has shown that a very small amount (less than 5%) of softwood lignin dissolves in acid, but higher amount (greater than 5%) does so for hardwoods and grasses during wet chemical analysis process. Since lignin can absorb UV light, but sugar cannot, the filtrate after the TAPPI T222 method further investigated by UV absorbance to detect lignin, which is known as acid soluble lignin. However, the quantity of this cannot be defined and, thus the wet chemical method of detecting lignin has approximately a 5% variation.

In fact, holocellulose can be measured directly by the chlorite method, which involves putting wood meal into glacial acetic acid and sodium chlorite liquid between 70°C and 80°C for three or four hours. Lignin is soluble in the liquid and the residue is full of holocellulose. Moreover, cellulose can be isolated by a mixture liquid of acetylacetone, 1,4-dioxane and hydrochloric acid (Seifert, 1960). However, according to Tamburini et al. (2017), a certain percentage of lignin is also extracted by this method, which leads to unreliable results.

Hence, a wet chemical analysis report contains Klason lignin, acid soluble lignin, the ratio of H/L (holo-cellulose/lignin) as well as the content of hemicellulose and cellulose as basic data to illustrate timber chemical composition.

Spectroscopy (FTIR/FT-NIR)

The IR (infrared spectroscopy) technique is considered a quick method for detecting timber composition. Light with a specific frequency is absorbed by specific chemical functional

groups or bonds and a transformed light scan obtains a spectrum. There are many peaks on the spectrum, each corresponding to a specific composition. Chemical composition is studied by functional group changes.

Two similar techniques FTIR (Fourier transform infrared) and FT-NIR (Fourier transform near-Infrared) spectroscopy with different spectrum of light being scanned, which are commonly deployed for analysing chemical functional groups. Mid-infrared lights are absorbed by chemical functional groups while near-infrared lights are affected by the bonds between atoms.

A device emits light with a wide range of frequencies to the samples and a few specific frequencies are absorbed by it. The rest of the light penetrates or is reflected by the sample and then, received by the device. The received light signal is analysed on a computer by Fourier transformation. Many studies (Rana et al., 2010; Chen et al., 2010; Colom et al., 2003; Kotilainen et al., 2000; Schultz et al., 1985; Horikawa et al., 2019) reported chemical compound and its corresponding wavenumber on FTIR spectrum (Table 2-6). The FT-NIR spectrum compound and corresponding wavenumber (Table 2-7) have been studied by Tsuchikawa and Siesler (2003); Yonenobu and Tsuchikawa (2003); Siesler et al. (2008); Osborne et al. (1993); Schwanninger et al. (2004). An advanced FTIR accessory is attenuated total reflectance (ATR) FTIR/FT-NIR which test samples more quickly (Figure 2-14) (Yamauchi et al., 2004).

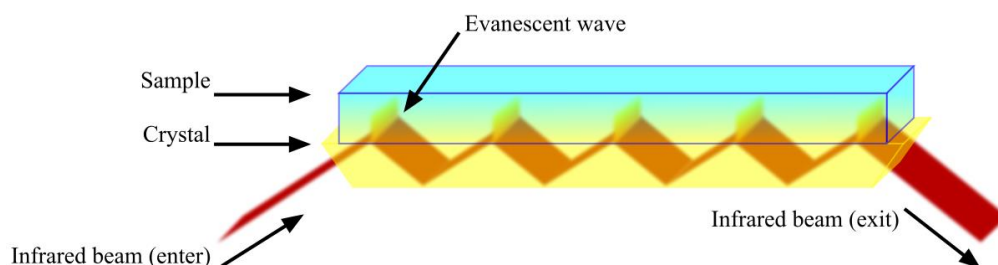


Figure 2-14 Principle of ATR-FTIR

Table 2-6 FTIR Wavenumber and Corresponding Chemical Functional Groups

No.	wavenumber	Compound	Reference
1	3336	O-H Stretch	Kondo (1997)
2	2938	CH- stretch in methyl- and methylene groups	Kotilainen et al. (2000)
	2882	CH- Stretch in methyl- and methylene groups	
-	2103	Absorption caused by the ATR crystal	
	1990	Absorption caused by the ATR crystal	
3	1730	C=O stretching in unconjugated ketone,	Harrington et al. (1964)
		carbonyl, aliphatic and ester groups (frequently of carbohydrate origin)	Barker and Owen (1999) Chow (1971)
4	1642	-OH bending, affected by water absorption	Marchessault (1962)
			Fengel and Wegener (1984)
5	1595	C=C stretching; COO ⁻ stretching	Faix (1991)
			Harrington et al. (1964)
6	1507	Aromatic skeletal vibration	Faix (1991)
			Harrington et al. (1964) Marchessault (1962)
7	1456	C-H deformation stretching in CH ₂ and CH ₃ ,	Kotilainen et al. (2000)
		aromatic skeletal vibrations	Harrington et al. (1964)
8	1421	O-H in aromatic skeletal; C-H deformation stretching in CH ₂ and CH ₃	Harrington et al. (1964)
9	1366	C-H bending	Liang and Marchessault (1959)
10	1335	Phenol group, -OH bond to aromatic	Sarkanen and Ludwig (1971)
		hydrocarbon group	Marchessault and Liang (1962)
11	1318	Condensation of guaiacyl unit and syringyl	Evans et al. (1992)
		unit, syringyl unit and CH ₂ bending stretching	Kotilainen et al. (2000)
12	1262	C-O stretching (lignin)	Harrington et al. (1964)
			Marchessault (1962)
13	1226	C-C, C-O-C (lignin)	Faix (1991)
14	1204	C-O-C or O-H in -plane bending	Parker (1983)

15	1154	bridge C–O–C stretching	Müller et al. (2009) Marchessault (1962)
16	1110	C-OH stretching	Müller et al. (2009) Higgins et al. (1961)
17	1054	C–C, C–O stretching	Müller et al. (2009) Higgins et al. (1961)
18	1025	C–H in-plane deformation, C-O stretching	Kotilainen et al. (2000) Higgins et al. (1961)
19	895	Aromatic vibration at β -glycosidic linkage	Müller et al. (2009) Evans et al. (1992)

Table 2-7 FT-NIR Wavenumber and Corresponding Chemical Bonds

wavenumber	Compound
7000	-OH in amorphous regions in cellulose
6718	-OH in Semi-crystalline regions in cellulose
6450	-OH in crystalline regions in cellulose
6287	-OH in crystalline regions in cellulose
5980	-CH in aromatic skeletal in lignin
5800	-CH in furanose/pyranose in hemicellulose
5587	-CH in semi- or crystalline regions in cellulose
5464	-OH and -CO in semi- or crystalline regions in cellulose
5219	-OH in water
4890-4620	-OH and -CH in cellulose
4820	-CH in semi- or crystalline regions in cellulose
4198	-CH in holo-cellulose

Pyrolysis GC/MS analysis

Pyrolysis-gas chromatography-mass spectrometry (Pyrolysis GC/MS) analysis is a combined method. In the GC part, the sample is heated in nitrogen from low to high

temperature, by which the molecules are pyrolysed, thus becoming shorter, normally as a gas or volatile substance. Depending on the sample's pyrolysis behaviour, two different heating methods are available: keeping at a certain temperature or rising to higher temperature at a certain rate. Timber consists of complex high-weight molecules with various pyrolysis behaviours, so the rising heating method is commonly used for timber sample analysis. The pyrolysis products are examined by a gas chromatography column. Gas are brought into the tube, termed a column, by an inert gas (nitrogen or helium). Column wall is coated with specific substance which can hold the gas. However, the ability to hold specific chemical compounds is different due to adsorption capacity of column, such that pure chemical components leave the column one by one over time. A computer receives all the signals and produce a component-time spectrum. The decomposition products of wood can be deducted and compared with reference chromatograms to speculate about the original molecular composition (Yang et al., 2007). Table 2-8 and Figure 2-15 shows the GC/MS spectrum and components of *Ficus sycomorus* wood pyrolysis (Tamburini et al., 2017).

Łucejko et al. (2012) compared wet chemical analysis and pyrolysis analysis, reporting that the results of two methods similar on aged wood, but show a large deviation on new wood on the ratio of Hemicellulose / Lignin. Non-bounded or non-lignin aromatic molecules on new timber might be the reason of the difference.

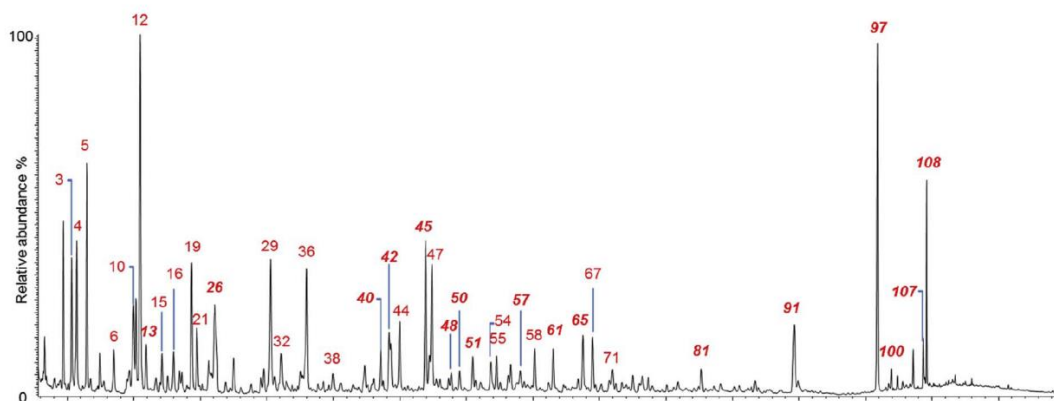


Figure 2-15 GC/MS spectrum (Tamburini et al., 2017)

Table 2-8 GC/MS Spectrum Peaks and Corresponding Compound (Tamburini et al., 2017)

number	compound	origin
1	1,2-dihydroxyethane (2TMS)	Holo-cellulose/Lignin
2	2-hydroxymethylfuran (TMS)	Holo-cellulose
3	Phenol (TMS)	Lignin
4	2-hydroxypropanoic acid (2TMS)	Holo-cellulose/Lignin
5	2-hydroxyacetic acid (2TMS)	Holo-cellulose/Lignin
6	1-hydroxy-1-cyclopenten-3-one (TMS)	Holo-cellulose
7	3-hydroxymethylfuran (TMS)	Holo-cellulose
8	o-cresol (TMS)	Lignin
9	2-furancarboxylic acid (TMS)	Holo-cellulose
10	Unknown holocellulose I	Holo-cellulose
11	m-cresol (TMS)	Lignin
12	2-hydroxy-1-cyclopenten-3-one (TMS)	Holo-cellulose
13	p-cresol (TMS)	Lignin
14	3-hydroxy-(2H)-pyran-2-one (TMS)	Holo-cellulose

15	Unknown holocellulose II	Holo-cellulose
16	Unknown holocellulose III	Holo-cellulose
17	Z-2,3-dihydroxycyclopent-2-enone (TMS)	Holo-cellulose
18	E-2,3-dihydroxycyclopent-2-enone (TMS)	Holo-cellulose
19	1,2-dihydroxybenzene (TMS)	Holo-cellulose
20	3-hydroxy-(4H)-pyran-4-one (TMS)	Holo-cellulose
21	5-hydroxy-(2H)-pyran-4(3H)-one (TMS)	Holo-cellulose
22	2-hydroxymethyl-3-methyl-2-cyclopentenone (TMS)	Holo-cellulose
23	1-hydroxy-2-methyl-1-cyclopenten-3-one (TMS)	Holo-cellulose
24	1-methyl-2-hydroxy-1-cyclopenten-3-one (TMS)	Holo-cellulose
25	1,3-dihydroxyacetone (2TMS)	Holo-cellulose
26	Guaiacol (TMS)	Guaiacyl lignin
27	Unknown holocellulose IV	Holo-cellulose
28	3-hydroxy-6-methyl-(2H)-pyran-2-one (TMS)	Holo-cellulose
29	Unknown holocellulose V	Holo-cellulose
30	2-methyl-3-hydroxy-(4H)-pyran-4-one (TMS)	Holo-cellulose
31	2-methyl-3-hydroxymethyl-2-cyclopentenone (TMS)	Holo-cellulose
32	2,3-dihydrofuran-2,3-diol (2TMS)	Holo-cellulose
33	2-furylhydroxymethylketone (TMS)	Holo-cellulose
34	5-hydroxymethyl-2-furaldehyde (TMS)	Holo-cellulose
35	4-methylguaiacol (TMS)	Guaiacyl lignin
36	1,2-dihydroxybenzene (2TMS)	Holo-cellulose
37	2-hydroxymethyl-2,3-dihydropyran-4-one (TMS)	Holo-cellulose
38	1,4:3,6-dianhydro- α -D-glucopyranose (TMS)	Holo-cellulose
39	Z-2,3-dihydroxycyclopent-2-enone (2TMS)	Holo-cellulose
40	4-methylcatechol (2TMS)	Guaiacyl lignin
41	4-ethylguaiacol (TMS)	Guaiacyl lignin
42	Syringol (TMS)	Syringyl lignin
43	1,4-dihydroxybenzene (2TMS)	Holo-cellulose
44	Arabinofuranose (4TMS)	Holo-cellulose

45	4-vinylguaiacol (TMS)	Guaiacyl lignin
46	3-hydroxy-2-hydroxymethyl-2-cyclopentenone (2TMS)	Holo-cellulose
47	E-2,3-dihydroxycyclopent-2-enone (2TMS)	Holo-cellulose
48	4-ethylcatechol (2TMS)	Guaiacyl lignin
49	3-hydroxy-2-(hydroxymethyl) cyclopenta-2,4-dienone (2TMS)	Holo-cellulose
50	Eugenol (TMS)	Guaiacyl lignin
51	4-methylsyringol (TMS)	Syringyl lignin
52	3-methoxy-1,2-benzenediol (2TMS)	Syringyl lignin
53	3,5-dihydroxy-2-methyl-(4H)-pyran-4-one (2TMS)	Holo-cellulose
54	1,6-anhydro- β -D-glucopyranose (TMS at position 4)	Holo-cellulose
55	1,6-anhydro- β -D-glucopyranose (TMS at position 2)	Holo-cellulose
56	Z-4-isoeugenol (TMS)	Guaiacyl lignin
57	Vanillin (TMS)	Guaiacyl lignin
58	1,2,3-trihydroxybenzene (3TMS)	Holo-cellulose
59	5-methyl-3-methoxy-1,2-benzenediol (2TMS)	Syringyl lignin
60	4-ethylsyringol (TMS)	Syringyl lignin
61	E-4-isoeugenol (TMS)	Guaiacyl lignin
62	1,4-anhydro-D-galactopyranose (2TMS)	Holo-cellulose
63	1,6-anhydro-D-galactopyranose (2TMS)	Holo-cellulose
64	2-hydroxymethyl-5-hydroxy-2,3-dihydro-(4H)-pyran-4-one (2TMS)	Holo-cellulose
65	4-vinylsyringol (TMS)	Syringyl lignin
66	1,4-anhydro-D-glucopyranose (2TMS at position 2 and 4) 306 73	Holo-cellulose
67	1,2,4-trihydroxybenzene (3TMS)	Holo-cellulose
68	Acetovanillone (TMS)	Guaiacyl lignin
69	4-hydroxybenzoic acid (2TMS)	Lignin
70	4-propenylsyringol (TMS)	Syringyl lignin
71	1,6-anhydro- β -D-glucopyranose (2TMS at position 2 and 4)	Holo-cellulose
72	Vanillic acid methyl ester (TMS)	Guaiacyl lignin
73	5-vinyl-3-methoxy-1,2-benzenediol (2TMS)	Syringyl lignin

74	Z-4-isopropenylsyringol	Syringyl lignin
75	1,4-anhydro-D-galactopyranose (3TMS)	Holo-cellulose
76	Unknown lignin I	Lignin
77	Syringaldehyde (TMS)	Syringyl lignin
78	2,3,5-trihydroxy-4H-pyran-4-one (3TMS)	Holo-cellulose
79	1,6-anhydro- β -D-glucopyranose (3TMS)	Holo-cellulose
80	1,4-anhydro-D-glucopyranose (3TMS)	Holo-cellulose
81	E-4-isopropenylsyringol (TMS)	Syringyl lignin
82	1,6-anhydro- β -D-glucofuranose (3TMS)	Holo-cellulose
83	Unknown lignin II	Lignin
84	Unknown lignin III	Lignin
85	Vanillic acid (2TMS)	Guaiacyl lignin
86	Acetosyringone (TMS)	Syringyl lignin
87	5-propyl-3-methoxy-1,2-benzenediol (2TMS)	Syringyl lignin
88	Coumaryl alcohol (2 TMS)	Guaiacyl lignin
89	syringic acid methyl ester (TMS)	Syringyl lignin
90	Vanillylpropanol (2TMS)	Guaiacyl lignin
91	Z-coniferyl alcohol (2 TMS)	Guaiacyl lignin
92	4-hydroxy-3,5-dimethoxycinnamic acid methyl ester (TMS)	Syringyl lignin
93	Coniferylaldehyde (TMS)	Guaiacyl lignin
94	Trihydroxycinnamyl alcohol (3TMS) 398 73	Syringyl lignin
95	Syringic acid (2TMS)	Syringyl lignin
96	Unknown lignin IV	Lignin
97	E-coniferyl alcohol (2 TMS)	Guaiacyl lignin
98	3,4-dihydroxy-5-methoxybenzoic acid (3TMS)	Syringyl lignin
99	Syringylpropanol (2TMS)	Syringyl lignin
100	Z-sinapyl alcohol (2TMS)	Syringyl lignin
101	Unknown lignin V	Lignin
102	3,4-dihydroxycinnamyl alcohol (3TMS)	Guaiacyl lignin
103	Trihydroxycinnamyl alcohol I (3TMS)	Syringyl lignin

104	Sinapylaldehyde (TMS)	Syringyl lignin
105	Trihydroxycinnamyl alcohol II (3TMS)	Syringyl lignin
106	Z-2-methoxy-3,4-dihydroxycinnamyl alcohol (3TMS)	Syringyl lignin
107	Sinapyl alcohol (TMS)	Syringyl lignin
108	E-sinapyl alcohol (2TMS)	Syringyl lignin
109	E-2-methoxy-3,4-dihydroxycinnamyl alcohol (3TMS)	Syringyl lignin
110	Unknown lignin VI	Lignin
111	Unknown anhydrosugar I (dimer)	Holo-cellulose
112	Unknown anhydrosugar II (dimer)	Holo-cellulose
113	Unknown anhydrosugar III (dimer)	Holo-cellulose
114	Unknown anhydrosugar IV (dimer)	Holo-cellulose
115	Unknown anhydrosugar V (dimer)	Holo-cellulose
116	Unknown anhydrosugar VI (dimer)	Holo-cellulose
117	Unknown anhydrosugar VII (dimer)	Holo-cellulose

2.2.2 Chemical Composition Changes During Natural Ageing

Chemical composition changes in timber are inevitable. The process of organic substances transforming back to inorganic ones, such as carbon dioxide, water and ammonia, is a natural cycle, but timber ageing is not (Fengel, 1991). It is a series of slow changes to timber molecules, which is affected by the environment. Oxygen content, water storage and temperature are the most essential factors affecting the natural ageing process. Fengel (1991) studied the chemical composition changes of natural aged woods for various species and storage environments, concluding that hemicellulose and polyose content decrease quicker than cellulose for the first one thousand years. Whilst cellulose content starts to dramatically decrease after 10^7 years. The content of non-hydrolysable residue, including crystallised cellulose and cross-linked lignin increase gradually (Figure 2-16). Hence, the timber ageing process can be treated as one where the molecular composition turns into having a stable status. A similar conclusion was also reported by Ando et al. (2006), who

elicited that a 270 year old Japanese red pine (*Pinus densiflora* Sieb. et Zucc.) was much more stable than new wood after carrying out an acoustic emission test on the microscopic fracturing process.

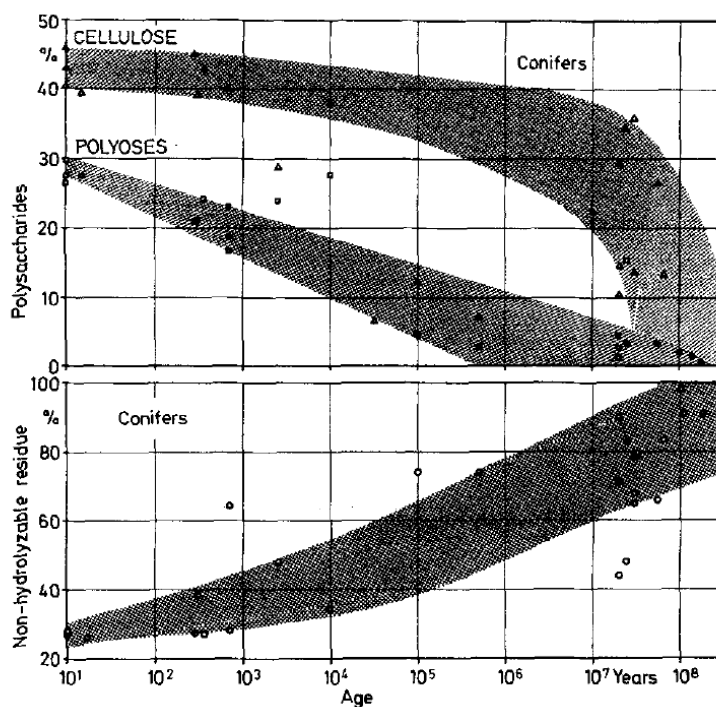


Figure 2-16 Timber Composition Changes during Natural Ageing (Fengel, 1991)

The next part of the literature reviews is divided into two categories: aerobic environment (in air) and anaerobic environment (in water or mud). The timber chemical changes in the former condition are much more complex than those in the latter. Tamburini et al. (2017) investigated different wood species samples (*Faidherbia albida*, *Ficus sycomorus*, *Taxus baccata*, *Pinus sylvestris* and *Tamarix sp.*) from Egypt for different times (230 years old, from 1787AD, 2,000 years old, from 332 BC to 395AD and 3,800 years old, from 1760 BC). Whilst both the wet chemical method and FTIR indicated that lignin and holocellulose (cellulose and lignin) of the sample had been reduced by degradation, the chemical changes

were different even for the same species in the same environment. Thus, the factors affecting timber natural ageing are more complex.

Tamburini et al. (2017) also evaluated the wet chemical analysis method and pointed out that the ratio of holocellulose/lignin (H/L), which normally illustrates wood's chemical composition change, is not suitable for degradation evaluation in air. However, a few accessorial methods, such as FTIR and pyrolysis analysis, can provide comprehensive information. In addition, microbials attacking natural aged timber in air lead to more complex results regarding the chemical composition, according to Naumann et al. (2005), Genestar and Palou (2006), Blanchette (2000), Blanchette et al. (1991) and Blanchette et al. (1994).

In air

The chemical composition of timber may change anytime and anywhere, in particular, it starts to age after harvesting. The first stage of timber change after harvest, is a decrease in moisture content and oxygen invasion into the cells (Fengel, 1991). Sapwood is still alive 180 days after cutting, with sugar still decomposing to provide energy for living cells in it, as was found for Japanese Katsura (*Cercidiphyllum japonicum*) and cedar (*Cryptomeria japonica*) (Ohashi et al., 1988). Lignin is oxidised immediately after harvesting according to Fischer and Schmidt (1983). Fengel and Stöcklhuber (1985) compared fresh and 15 years naturally drying pine, concluding that lignin is significantly oxidised both in sapwood and heartwood in the latter case, but the acid soluble lignin does not show any variation.

Fengel (1991) introduced an unpublished work after studying pieces of 290 year old spruce and 365 year old pine from a roof structure and found that cellulose content had not changed significantly when compared with recent dry wood, but polyoses (hemicellulose) had

decreased a lot. Acid insoluble lignin was tested by a wet chemical method and showed the same content as new timber (ibid).

108-390 years fir samples (*Abies Alba*) belonging to a historic building were studied by Kačík et al. (2014) using a wet chemical method. Cellulose content increased 13% on the 390 year old sample than new samples due to hemicellulose degradation. However, cellulose molecular structure was stable with no significant change. Moreover, hemicellulose decreased by approximately 24% due to degradation. In terms of hemicellulose degradation, arabinoglucuronoxylan degraded more than galactoglucomannan. Lignin content was reduced 4%, whereas condensation and cross-linking reactions are observed.

Tsuchikawa et al. (2005) reported that cellulose does not show any degradations in crystalline areas but does degrade greatly in non-crystalline ones regarding hemicellulose and lignin when studying a piece of 1,300 year old hinoki cypress (*Chamaecyparis obtusa*) from a pillar of the Todaiji temple in Japan.

A piece of 1,800 year old teak (*Tectona grandis*) from a Buddhist temple in India was found by Narayanamurti et al. (1958) and chemical analysis showed that the cellulose and lignin content had decreased by approximately 2% when compared with new teak. However, considering the experiment data variation, 2% was not a significant figure to define decreasing. Moreover, soluble lignin extracted by ethanol benzene increased by approximately 14 times for the same comparison (ibid).

Borgin et al. (1975a) studied seven old wood samples with IR spectroscopy (Table 2-9). Specifically, ship components samples were stored in a moist soil environment, while others were stored in dry air. He demonstrated that the lignin of the wood samples stored in dry air had oxidised dramatically due to increasing of the carbonyl groups especially on

two species: *Pinus pinea* and *Juniperus phoenicea*. Borgin et al. (1975b) also investigated these samples using electron microscopy (SEM) and a polarised light microscope. He reported that the cell walls of the old samples were no different to new wood (ibid). Cell wall structure was also well preserved in 2,000 to 4,000 years old thorn wood (*Acacia sp.*, *Tamarix spec.*), according to Nilsson and Daniel (1990).

Table 2-9 Wood Samples analysed by Borgin et al. (1975a)

Timber	Scientific name	Age	Location
Pine	<i>Pinus sylvestris</i>	900 years	Oseberg Viking ship in Norway
Oak	<i>Quercus robur</i>	1100 years	Klastad Viking ship in Norway
Oak	<i>Quercus robur</i>	1100 years	Oseberg Viking ship in Norway
Pine	<i>Pinus sylvestris</i>	2200 years	Buried wooden implements in Norway
Juniper	<i>Juniperus phoenicea</i>	4100 years	Pyramid of Sneferu in Egypt
Pine	<i>Pinus pinea</i>	4300 years	Pyramid of Teti in Egypt
Thorn	<i>Acacia nilotica</i>	4400 years	Pyramid of Neferirkare in Egypt

Eight 3,000 years old oak samples (*Quercus sp.*) which contained both heartwood and sapwood, were studied by the classic wet chemical method by Tamburini et al. (2015). The samples belonged to a pavement of the ancient living area in Biskupin in Poland. Polysaccharides (mainly hemicellulose) were found to have degraded significantly in all the samples, which had led to the lignin content increasing from 32.5% to 62.1%. In addition, wood from the outside layer had degraded significantly, whereas the inside layer was well preserved. In analytical pyrolysis coupled with gas chromatography and mass spectrometry (Py-GC/MS) analysis, lignin monomers (sinapyl and coniferyl alcohols) content was greater in well preserved specimens, whilst guaiacyl and syringyl units with short side chains emerged as being common in the degraded samples (ibid).

Grosser et al. (1974) studied a piece of 4,500 year old juniper (*Juniperus drupacea*) from Chattuscha in Asia Minor (1900-1200BC) in a dry atmosphere by FTIR. Carbohydrate content was only 5.1%, including 4.7% cellulose. They also compared milled sample lignin with new juniper and found a guaiacyl (peak at 1,270 cm^{-1}) increase, but syringyl vibration (peak at 1,220 cm^{-1} and 1,320 cm^{-1}) and phenolic OH group (peak at 1,365 cm^{-1} , hydroxyl) had decreased, which indicated lignin condensation.

Fengel (1991) introduced another unpublished work on a 5,000 year boat component sample (*Acacia nilotica* and *Tamarix spec*) from an Egyptian tomb chamber. Chemical analysis illustrated that the cellulose content is 55.2% and the polyoses (mainly hemicellulose) content decreased largely to 5.2% compared to new sample. Hydrogen/carbon ratio was 1.2 whilst the oxygen/carbon ratio was much higher than recent wood, which means that lignin is oxidised during the natural ageing process. It was also reported that the cell wall colour became dark (ibid). Similar chemical composition was reported by Nilsson and Rowell (2012), who found 10,000 years old timber in a Chinese tomb with a dry environment.

Chowdhury et al. (1967) studied four India wood samples that were 2,000 year old *Shorea robusta*, 2,200 year old *Tectona grandis*, 7,500 year old *Lagerstroemia speciosa* and 47,000 year old *Mesua ferrea*, reporting that crystallised cellulose was well preserved in the first three samples. However, in the oldest sample all the cellulose was non-crystallised, which indicate that crystallised cellulose can transit to amorphous cellulose over an extremely long period.

In water and soil

Even though biological degradation causes distinctive chemical composition changes in timber stored in water or soil and decreases its mechanical strength (Huisman et al., 2008),

many studies have demonstrated that the condition of a waterlogged sample is better than one from an air environment. Moreover, softwood resists decay in a water atmosphere more than hardwood for at least 3,000 years (Zoia et al., 2015). Similar results were also reported by Capretti et al. (2008), who studied three shipwrecks dating back to the first to second century AD from near Naples in Italy. The wet chemical method showed that softwood cypress (*Cupressus sempervirens L.*) changes less than hardwood beech (*Fagus sylvatica L.*) or oak (*Quercus caducifolia*) and walnut (*Juglans regia L.*). Christensen et al. (2006) investigated 1,400 to 1,800 year old pine and ash wood of an arrow and found that lignin was better preserved in a softwood (ash sample) than in hardwood (pine sample). In addition, Iiyama et al. (1988) compared three samples buried in soil of softwood torreyia (*Torreya spp.*, 6,000 years old), hardwood ash (*Fraxinus spp.*, 12,000 years old) and chestnut (*Castanea spp.*, 6,000 years old) with new wood. The lignin content of the softwood was less than 45%, which is same as the content of new wood, but the hardwood lignin content increased to 80% and 81%, respectively, for the hardwoods due to hemicellulose degradation. A few 2,600 year old samples stored in seawater, including two hardwoods oak, and alder (*Quercus spp. subgenus Leucobalanus* and *Alnus rubra*) and one softwood spruce (*Picea sitchensis*) were studied by Hedges et al. (1985). They reported that the spruce experienced a slight change in the seawater, but the oak and alder degraded dramatically that 90% of the polysaccharides and 15-25% lignin disappeared. Hence, it was evidenced that softwoods resist decay in this water better than hardwoods. This study also reported the stability of hardwood molecule components in seawater according to the following order: vanillyl and ρ -hydroxyl lignin structural > syringyl lignin structural > pectin > α -cellulose > hemicellulose (ibid).

Cellulose and hemicellulose degrade slightly for the first 400 years. A 5 year comparison experiment was conducted by Komorowicz et al. (2018), who immersed English oak

heartwood (*Quercus robur L.*) in the Baltic Sea. Both cellulose and pentosans (hemicellulose) decreased 5%. Fengel and Wegener (1988) studied spruce after water storage for 17 years and found that the cellulose and polyoses (mainly hemicellulose) kept the original content. However, the authors also reported that the deviation of the wet chemical method was higher. Zoia et al. (2015) examined the chemical composition on an approximately 400 year old softwood (*Abies alba*) and hardwood (*Quercus robur*) shipwreck by the wet chemical method and reported no significant difference from new wood regarding holocellulose.

However, hemicellulose content decreased significantly after 400 years mainly due to a hydrolysis reaction. Five pieces of pedunculate oak (*Quercus robur L.*) that were 700, 1,000 (two pieces), 1,700 and 2,700 years old were found in water storage in Poland by Sandak et al. (2010). Both wet chemical and FT-IR analysis demonstrated that the carbohydrates (hemicellulose) had degraded significantly, but the cellulose content did not show a clear change. Łucejko et al. (2012) analysed seven samples by the pyrolysis method, including alder (*Alnus glutinosa*), oak (*Quercus roburs*) and beech (*Fagus sylvatica*) between 900 and 1,200 years, reporting that the old timber sample contained fewer pyrolysis products of polysaccharide thus the hemicellulose was largely degraded. Van Bergen et al. (2000) studied 6,000 year old oak samples (*Quercus sp.*) and found a reduction in hydrogen and oxygen elemental content. The reason is that carbohydrates had decomposed, mainly because of hydrolysis in a water environment, which led to an increase in Klason lignin from 28.77% to 67.35%. Passialis (1997) studied several waterlogged samples (*Picea abies*, *Pinus silvestris* and *Quercus sp.*), ranging from 300 to 100,000 years old found in anaerobic areas, including glaciers, burial grounds, housing settlements and shipwrecks, by wet chemical analysis. Hemicellulose is largely degraded. Similar results were elicited by Van Bergen et al. (2000), who studied four oak samples (*Quercus sp.*)

stored in water (two at a 6,000BP site on the south coast of England and natural aged samples: one was first century AD from a well and another from a cathedral's portal dating to the sixteenth century, using pyrolysis-gas chromatography/mass spectrometry. They demonstrated that the polysaccharide content of natural aged wood was the same as new wood, but this decreased dramatically in water stored wood. Hence, it was concluded that hemicellulose greatly disappears in water storage.

The crystalline structure protects cellulose molecules even in a 100,000 year old sample (*Picea abies*) stored in water (Passialis, 1997). However, the amorphous region of cellulose exhibits degradation for a 6,000 year old waterlogged sample, according to Van Bergen et al. (2000). That is, the FTIR technique deployed showed that amorphous cellulose is largely degraded due to a decrease in β -glycosidic linkages (peak at 894 cm^{-1}). Oxidation reaction on lignin was also observed on the FTIR spectrum. Moreover, it emerged that cellulose cannot resist to microorganism attack (ibid). Iiyama et al. (1988) reported that cellulose degradation is greater than hemi-cellulose a 6,000 to 12,000 year old small sample. Higher protein content indicated that microorganisms are responsible for cellulose decrease. Kim et al. (1990) also observed higher degradation in cellulose than hemicellulose due to microorganisms for 700 year old pine wood (*Pinus massoniana*) stored in seawater. Hence, microorganisms consume cellulose as food.

Lignin in an anaerobic environment, especially in water, is well preserved (Zoia et al., 2015). Komorowicz et al. (2018) immersed a five year old wood in seawater and reported that the lignin content increased 7% due to the degradation of pentosans (hemicellulose). Borgin et al. (1975a) found two pieces of old ship components wood samples aged 900 and 1,100 years stored in moist soil. Lignin content increased slightly due to a reduction in carbohydrate content on *Quercus robur*. Łucejko et al. (2012) also reported stable lignin for 900 to 1,200 year old samples by wet chemical analysis, but lignin content increases

due to hemicellulose degradation. Similar results were reported by Sandak et al. (2010), where lignin content was found to be increased due to degradation of carbohydrates, but the total quantity had not changed when investigating five pieces of pedunculate oak samples from 700 to 2,700 years. Lignin content increases from 1.3 to 3.6 times more than new wood, according to Passialis (1997), who studied some waterlogged samples (*Picea abies*, *Pinus silvestris* and *Quercus sp.*) by wet chemical analysis. These, samples ranged from 300 to 100,000 years old, being found in anaerobic area including glaciers, burial grounds, housing settlements and shipwrecks.

However, lignin chemical structure might become changed according to Xia et al. (2018), who comprehensively investigated the lignin of a piece of 1,700 to 2,100 year old waterlogged pine wood. They reported that part of the lignin molecular weight had reduced due to depolymerization, especially for the β -O-4 and β -5 linkage. NMR analysis also illustrated a demethoxylation reaction on the syringyl lignin of waterlogged oak samples (Van Bergen et al., 2000). Both guaiacyl and syringyl lignin content of a 6,600 year old *Bischofia polycarpa* stored in a river decreased according to Pan et al. (1990). Lignin molecules showed O-demethylation, acidcatalysed hydrolysis and a condensation reaction on aromatic methoxy groups, α -aryl bonds and aromatic rings, respectively. o-acetyl groups on xylan (hemicellulose) were found to hydrolyse to acetic acid, which promoted hydrolysis and condensation reactions in carbohydrates and lignin, respectively.

As mentioned above, internal wood chemical changes are lesser than for the outer layer, probably due to latter protecting the former. Łucejko et al. (2012) studied 900 to 1,200 year old oak samples and reported that holo-cellulose drops dramatically in sapwood but remains in heartwood.

Extractives changes vary because of tree species. Extractives of both softwood and hardwood are hydrolysed after one year storage in water, according to Assarsson and Akerlund (1967), but resin is much more stable during such storage. In addition, soluble extractives were found to have disappeared from 6,600 years old sample (Pan et al., 1990). Moreover, Fengel and Wegener (1988) studied spruce in water storage for 17 years and reported that extractives only had a slight reduction.

A 32,000 to 45,000 years old pine was found by Staccioli and Tamburini (1988), with the wood illustrating fossilisation. It emerged that cellulose had dramatically degraded; only 10% remained when compared to new wood. Fossilisation is a lengthy process, where mineral elements (normally silicon) replace the carbon of the timber molecule. However, timber chemical composition and mechanical property of this status are not structural materials, so timber in fossilisation is discussed no further in this research.

2.2.3 Chemical Composition Changes from Artificial Treatment

Engineers concerned about the durability of timber structures have devised several artificial treatments for accelerating chemical composition changes, which have provided valuable information in this respect. Generally, fungi and rot attack and UV exposure cause many distinctive chemical composition changes in timber. Heat treatment can improve durability, dimensional stability and the mechanical strength of timber. Hence, the timber heat treatment industry has become a mature and important part of the timber trade. Timber chemical changes are frequently accelerated by human intervention to study decay or improve mechanical properties. UV light, biological attack and temperature are the three main tools utilised for composition change.

In fact, chemical modifications and glued laminated timber can improve mechanical strength significantly (Follrich et al., 2006; Gaspar et al., 2010; Rowell et al., 2009; Sernek et al., 2008), but this will not be discussed in the chapter.

UV Light

UV light with specific frequency can rupture chemical bonds directly in a short time. However, this light only affects the surface since the molecules are degraded to a firm layer that acts as a protective layer (Croll and Skaja, 2003; Forsthuber and Gröll, 2010; Jelle, 2012; Stark and Matuana, 2004; Sudiyani et al., 2003). Thus, all studies discussing the chemical composition changes caused by just UV light refer to the sample surface.

Lignin is most affected and quickly degrades due to the ratio of lignin/carbohydrate reduction. That is, this diminished dramatically after 50 hours exposure, according to Pandey (2005), who detected the chemical composition changes of pine (*Pinus roxburghii*) and rubber wood (*Hevea brasiliensis*) by FTIR after 1000W UV light exposure from 0 to 700 hours. Moreover, it emerged that degradation is higher in the latter than the former. Pandey and Vuorinen (2008) reported that lignin aromatic structures degrade to o- and p-quinone structures by UV-vis reflectance, UVTT spectra and FTIR-PAS. They also reported that syringyl lignin degrades higher than guaiacyl lignin for both pine and rubber wood. Similar results were reported by Colom et al. (2003), who exploited a xenon test chamber to induce photodegradation on hardwood aspen (*Populus tremula*) and softwood buxus (*Buxus sempervirens*). It was found that all lignin feature bands containing 1595 cm^{-1} , 1510 cm^{-1} and 1465 cm^{-1} of FTIR decreased quickly and even disappeared after 24 weeks exposure. Macleod et al. (1995) obtained the FTIR spectrum of a red cedar panel after 50 weeks outdoor exposure and discovered that the bond peaks relating to lignin were at 1510 cm^{-1} and 1265 cm^{-1} was decreased.

Biological Attack

Both beetles and fungi usually cause decay in timber structures, but in lab environments the latter is most commonly researched in this context. Weiland and Guyonnet (2003) exploited brown rot (*poria placenta*) to attack maritime pine (*Pinus pinaster*) and beech (*Fagus sylvatica*), detecting the changes by FTIR. The lignin content increases due to cellulose and hemicellulose consumed by microorganisms. Hence, it is clear that fungi consume the polysaccharides (mainly hemicellulose and cellulose) of the cell wall, which results in high lignin content in the residue. Humar et al. (2006) found similar results from brown rot (*Antrodia vaillantii* and *Gloeophyllum trabeum*) decay in Norway spruce (*Picea abies*). They also reported MOE decreases and mass loss for the samples. Lignin increase was also observed by Pandey and Pitman (2003), who studied Scots pine (*Pinus sylvestris* L.) and beech (*Fagus sylvatica* L.) attacked by brown rot (*Coniophora puteana*) for 12 weeks.

White rot (*Phanerochaete chrysosporium* and *Coriolus versicolor*) causes different changes to lignin than brown rot, according to Faix et al. (1991). Both lignin and carbohydrate reduce by the same amount in the former case. White rot also causes the appearance of a new peak on the FTIR spectrum, as reported by Mohebbi (2005), who studied its influence (*Trametes versicolor*) on beech wood (*Fagus sylvatica*) for 84 days. New peaks on the FTIR spectrum appeared after 28 days exposure due to the chemical bond breaking for the hemicellulose (FTIR spectrum 1,650-1,800 cm^{-1}) and the aromatic derivatives of lignin (FTIR 1,500-1,550 cm^{-1}). Not only does the FTIR technique prove that white rot consumes lignin more than brown rot, for this has also been shown to be the case through by wet chemical analysis. Ferraz et al. (2000) evaluated pine (*Pinus radiata*) and blue gum (*Eucalyptus globulus*) attacked by six white rot (*Merulius tremellosus*, *Poria medulla-panis*, *Trametes versicolor*, *Punctularia artropurpurascens*, *Ceriporiopsis*

subvermispora and *Ganoderma aplanatum*) and two brown rot (*Poria cocos* and *Laetiporus sulfureus*) form for a period from 30 days to one year. Chemical changes were detected by both wet chemical analysis and FTIR. The study showed that the total lignin content of pine samples was reduced from 28.1% to 23.3%-27% by white rot attacking but increased to 28%-29.3% from the brown rot attack.

Heat treatment

Timber heat treatment has a long history of improving timber mechanical properties by causing specific chemical composition changes. Durability and stability are also improved through this process (Kamdern et al., 2002; Sandberg et al., 2013). Mechanical property changes during heat treatment will be discussed in the following chapter, in subsection 2.3.2, so this part only focuses on chemical composition changes. Generally, such changes on timber molecules during heat treatment are crystallisation, degradation/decomposition, condensation and cross-linking (Figure 2-17).

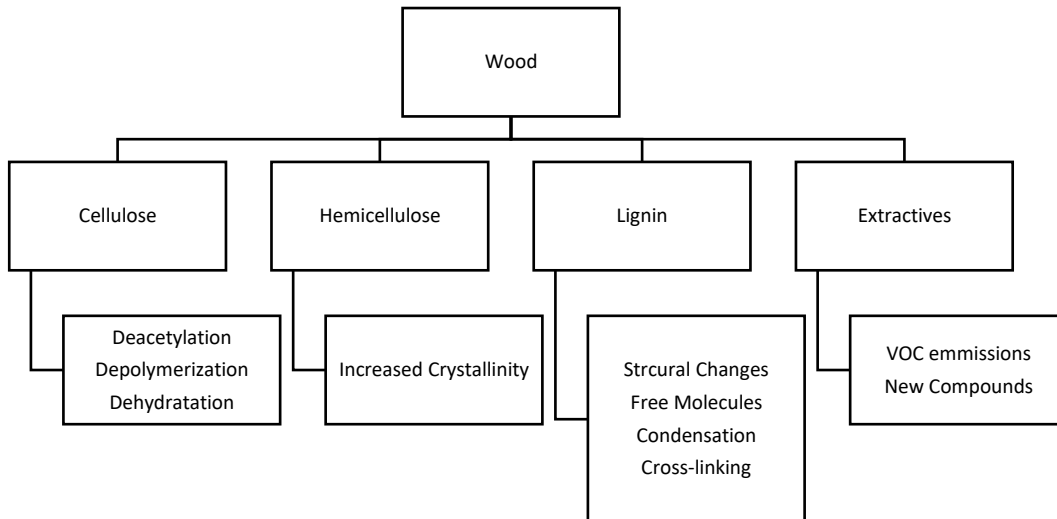


Figure 2-17 Timber Molecule Changes during Heat Treatment (Esteves and Pereira, 2008)

The earliest literature relating to timber heat-treatment is that of Tiemann (1920), who dried timber at a high temperature and found significant enhancement in dimensional stability, but the equilibrium moisture content had decreased. Esteves and Pereira (2008) concluded that regarding chemical changes during heat treatment under 150°C, loss of moisture from free to bond water is the main characteristic. At the temperature between 180°C and 250°C, chemical changes in wood are various and affected by treatment atmosphere significantly. Above 250°C, timber is carbonised and degraded, releasing various gases. Chemical changes in sapwood are more serious than heartwood, in particular, the hydrolysis reaction, according to Metsa-Kortelainen et al. (2006), who heated the sapwood and heartwood of Norway spruce (*Picea abies*) at 170°C, 190°C, 210°C and 230°C with different humidity.

Cellulose is the most stable molecule in timber due to its crystalline structure. Bourgois and Guyonnet (1988) found that heat treatment on sawdust of maritime pine at 260°C did not affect the cellulose structure significantly in an environment without oxygen. Yildiz et al. (2006) heated spruce wood (*Picea orientalis*) at 130°C, 150°C, 180°C, and 200°C for 2, 6 and 10 hours in air, eliciting that apart from the sample at 200°C for 10 hours, the quantity of cellulose was little affected. Esteves et al. (2008) studied eucalyptus wood (*Eucalyptus globulus Labill*) by heat treatment in an oven with air and in an autoclave with steam at 170°C-200°C and 190°C-210°C, respectively, finding that the cellulose as little affected. Hence, cellulose is relatively stable in environments of air, anaerobic and steam under 250°C.

Heat treatment can cause crystallisation in molecules, which improves the molecular structure as well as making them aligned and solid. Wikberg and Maunu (2004) reported crystallinity of cellulose increased in spruce, birch and aspen for 195°C steam treatment as well and on oak at 160°C with steam treatment. However, the carbohydrates in hemicellulose and amorphous cellulose molecule were substantially degraded. Similar

results were reported by Nakao et al. (1989) and Stamm (1956). Boonstra and Tjeerdsma (2006) elicited the same findings by a different heat treatment method with a two-stage treatment named “hydro-thermolysis”. This method involves treating samples at 165°C to 185°C for 30 minutes, then 170°C to 180°C for 4 hours and inserting a drying process at 50°C to 60°C between the two stage. Sivonen et al. (2002) heated a pine sample (*Pinus sylvestris*) at 180°C and 230°C for 4 hours and detected changes in the NMR spectrum peak at 89 ppm, which relates to cellulose. Though this study, they observed an increase in cellulose crystallinity with rising temperature. Pétrissans et al. (2003) also studied heat treatment according to NMR spectrum on pine (*Pinus sylvestris*), spruce (*Picea karst*), beech (*Fagus sylvatica*) and poplar (*Populus nigra*) for 8 hours at 240°C in an inert environment. The increase of the peak at 89 ppm and 85 ppm of the spectrum provided proof of a clear crystallisation change after heat treatment. In addition, an X-ray technique can also illustrate crystallisation increase during heat treatment. Bhuiyan et al. (2000) studied up to 5 days heat-treatment of cellulose powder, spruce (*Picea sitchensis*) and buna (*Fagus crenata*) in different humidity from 180°C to 220°C. There was crystallisation increase with temperature for spruce and buna, with there being no significant changes in pure cellulose. The crystallinity of timber increases in a high humidity environment (Bhuiyan and Hirai, 2005). Hence, heat treatment increases the crystallinity of cellulose under 250°C and moisture content is also an important factor.

Hemicellulose is easily affected by heating and starts to change even at low temperature (Zhou et al., 2016). Kocaefe et al. (2008) studied birch (*Betula papyrifera*) and aspen (*Populus tremuloides*) heated in a rising temperature from 100°C to 230°C in an inert atmosphere, with 80% nitrogen and 20% carbon dioxide. The FTIR spectrum showed that birch with a higher hemicellulose content changes dramatically. Due to the various molecular structures of hemicellulose, it pyrolyzes to various shorter chains according to

Alen et al. (2002), who heated Norway spruce (*Picea abies*) in a steam environment at 180°C to 225°C for 2 to 8 hours. Sivonen et al. (2002) and Weiland and Guyonnet (2003) studied hemicellulose behaviour by both NMR and FTIR, finding that it degrades to acetic acid at 180°C treatment. Sivonen et al. (2002) also observed that the methyl and carboxylic carbons of acetyl groups decrease in hemicellulose which indicates deacetylation. Tjeerdsma et al. (1998) studied acetic acid degraded by hemicellulose in beech (*Fagus sylvatica L.*) and scots pine (*Pinus sylvestris L.*) by NMR, providing that acetic acid has a catalysing function of degrading polysaccharide to formaldehyde, furfural and other aldehydes. Nuopponen et al. (2005) probed chemical composition by FTIR and UVR spectroscopy, eliciting that furfural is degraded from pentosans. In addition, hemicellulose dehydration reaction was observed during heat treatment in nitrogen at temperatures of 230°C to 260°C on maritime pine (*Pinus pinaster*) and beech (*Fagus sylvatica*) (Weiland and Guyonnet, 2003). Many studies have proved that gas and liquid are released from timber during heat treatment due to hemicellulose decomposition. Bourgois and Guyonnet (1988) reported that acetic acid, formic acid and furfural are from thermolysis of xylose, glucuronic chains and dehydration of xyloses, respectively. In terms of liquid release, 21.5% water, 7.5% acetic acid, 5% formic acid, 3.5% methanol and a small amount of furfural are measured by Dirol and Guyonnet (1993), who heated spruce, poplar and fir at 200°C to 260°C. To sum up, hemicellulose is affected in all atmosphere heat treatments, including air, steam and inert gas. Degradation is the main chemical reaction to hemicellulose, which leads to the release of gas and liquid.

Lignin changes during heat treatment have registered varying results, which have not been consistent. Bourgois and Guyonnet (1988) extracted sawdust of maritime pine lignin by the sulfuric acid method (ASTM, D1106-56) and reported that lignin increases in an inert atmosphere at 260°C treatment from an untreated 28% to 37%, 41%, 51%, 54% and 84%

for 20 minutes, 30 minutes, 1 hour, 1.2 hours and 4 hours, respectively. Similar results were reported by Zaman et al. (2000), who heated scots pine (*Pinus sylvestris*) and silver birch (*Betula pendula*) in steam at 200°C to 230°C for 4 hours to 8 hours. Esteves et al. (2008) compared oven treatment (in air) with autoclave treatment (saturated steam) at 190°C to 200°C and demonstrated that the lignin content increased from 24.7% to 33.5% for 24 hours with the former treatment and 31.8% for 12 hours with the latter, respectively. In a steam atmosphere, lignin shows a hydrolysis reaction, especially for softwood, according to Shevchenko et al. (1999), who studied this for fir (*Pseudotsuga menziesii*) by the NMR technique. However, a few researchers (Esteves et al., 2008; Boonstra and Tjeerdsma, 2006; Tjeerdsma and Militz, 2005) have demonstrated that lignin detection method is affected by a condensation reaction, whereby the lignin quantity might not have increased, but rather, been condensed. Cross-linking during heat treatment is an important change for lignin. Kotilainen et al. (2000), Tjeerdsma and Militz (2005) detected chemical changes by FTIR, observing a clear increase in methylene bridges (-CH₂-) is the products after lignin cross-linking. Similar results were reported by Nuopponen et al. (2005), who explained the lignin cross-linking reaction process: ether linkages (β -O-4) breaks to phenolic hydroxyl groups, α - and β -carbonyl groups firstly, the bond vacancy re-link to methylene bridge by crosslinking.

However, a few studies have shown that lignin is degraded at the beginning of heat treatment. Windeisen et al. (2007) detected lignin and non-hydrolysable residue on beech wood after heat treatment from 453k Joule heat to 493k Joules. If wood absorbing 473k Joule heat, thioacidolysis products are more than non-hydrolysable residue. Since lignin condensation products are a kind of non-hydrolysable residue, its degradation rate is much higher than condensation in this stage. However, when wood absorbs 493k Joule heat, non-hydrolysable residues increase significantly faster than thioacidolysis products, which

indicate that a lignin condensation reaction is the main change in this stage. Similar results have been found with GC (Gas chromatography). Hence, lignin degradation and condensation happen together during heat treatment, but the degradation mainly happens at the beginning, while condensation can occur in any atmosphere under 260°C.

Extractives evaporate along axial parenchyma cells to the outside during heat treatment, according to Nuopponen et al. (2003), who implemented heat treatment on Scots pine from 100°C to 240°C. Moreover, it was found that these extractives disappear when heated above 180°C. This study also indicated that resin acids evaporate from the heart of the samples to the edge and disappeared above 200°C. Similar results were reported by Kamdem et al. (2000).

2.2.4 Mass Loss and Colour Change during Heat Treatment

Temperatures accelerate chemical changes in timber molecules (Bourgois et al., 1989). It also causes changes in the density and colour of the timber due to decomposition and oxidation, respectively.

Mass loss during heat treatment leads to a decrease in density, which reduces mechanical strength (Reiterer et al., 2002). Esteves and Pereira (2008) reviewed many studies of heat treatment and concluded that mass loss generally depends on the tree species, temperature and treatment period (Figure 2-18). Zaman et al. (2000) reported that the mass loss of pine (*Pinus sylvestris*) at 205°C and 230°C treatment for 8 hours is less than for birch (*Betula pendula*). Mburu et al. (2008) observed the mass loss of first hour treatment at 250°C in nitrogen is 15% which is largely higher 30% after 24 hours treatment. Bourgois and Guyonnet (1988) reported that the mass loss of maritime pine is 18.5% after 15 minutes treatment and reaches 30% after an hour at 260°C. The two results also indicated that mass loss in air treatment is higher than in nitrogen. Similar results were reported by Mazela et

al. (2003), who obtained more mass loss in air than in water at 160°C to 220°C for treatment on pine (*Pinus sylvestris*). In timber molecule, hydroxyl groups can be oxidised, and hydrogen atom will be taken to form water, which decrease timber molecule weight. Hence, oxygen plays an important role in mass loss during timber heat treatment

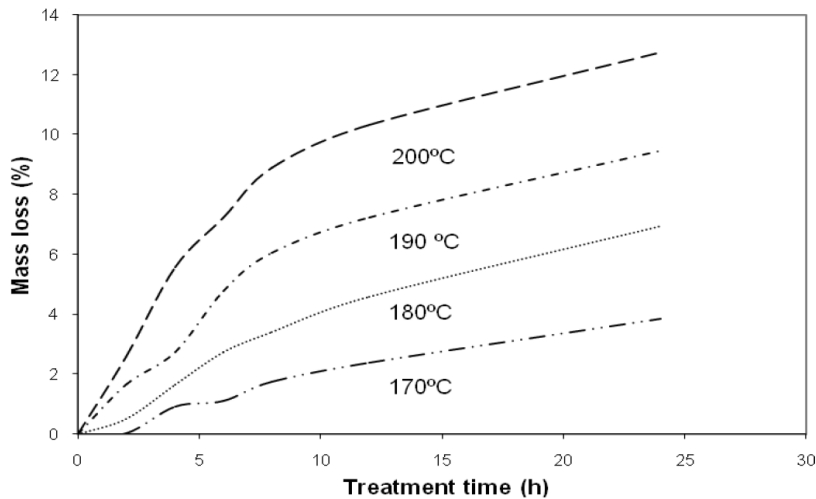


Figure 2-18 Mass Loss and Treatment Period/Atmosphere (Esteves and Pereira, 2008)

The colour of timber becomes dark during treatment and this is usually measured by the CIELAB system (Figure 2-19) which contain five basic evaluation parameters: L^* , a^* , b^* , C^* and h^* .

- L^* is the lightness coordinate, from 0 (black) to 100 (white)
- a^* is the red/green coordinate, from $+a^*$ (red) to $-a^*$ (green)
- b^* is the yellow/blue coordinate, from $+b^*$ (yellow) to $-b^*$ (blue)
- C^* is the chroma coordinate, the distance from the lightness axis
- h^* is the hue angle, expressed in degrees, with 0° for $+a^*$ axis, 90° for the $+b^*$ axis, 180° for $-a^*$ and, 270° for $-b^*$.

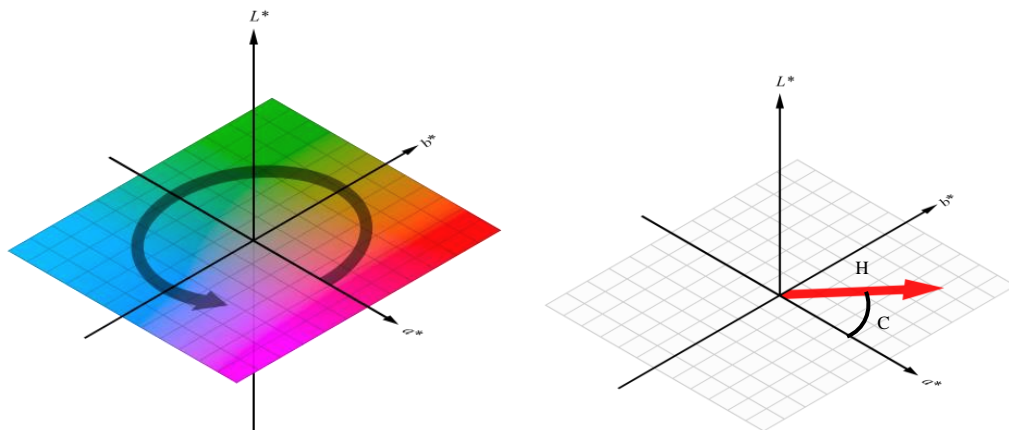


Figure 2-19 CIELAB System

Bekhta and Niemz (2003) studied the effect of heat treatment on timber colour on spruce wood (*Picea abies*). they found that lightness (L^*) starts to decrease at 100°C and decreases more with the treatment period. The red (a^*) and yellow colours (b^*) increase at 150°C reaching 12 times and 7 time higher, respectively, than with untreated wood. At 200°C , the red (a^*) continues increase to 4.4 times higher than for 150°C , but the yellow (b^*) shows a dramatic decrease. The change of C^* is same as for yellow (b^*) in that it increases at 150°C but decreases sharply at 200°C . Similar results were reported by Sundqvist et al. (2006), who detected colour changes (L^* , C^* and h^*) on birch wood (*Betula pubescens Ehrh*) after hydrothermal treatment at 180°C for 4 hours. This study demonstrated that the dark colour is attributed to hemicellulose degradation, secondary condensation products and/or quinone and quinonemethide degradation, which result from the breaking of the α -and β -ether of lignin.

In addition, many studies have reported that extractives also have a close relationship with colour changes. Burtin et al. (1998) measured the colour of sapwood and heartwood of a walnut tree (*Juglans nigra*, *J. regia* and *hybrid*) and compared this with the content of four

main extractives (hydrojuglone glucoside, quercitrin and two unknown compounds). Chemical reactions of hydrolysis, oxidation and polymerisation on hydrojuglone glucoside were the reason given for the colour change. Sundqvist and Morén (2002) also compared extracted, un-extracted Scots pine (*Pinus sylvestris L.*) and birch (*Betula pubescens Ehrh.*), reporting that extractives affect the colour of both natural aged and heat-treated timber. Gierlinger et al. (2004) also found high correlation between the red hue (+a*) related to phenols extractives and brown rot resistance on 293 trees of various species, with R²=0.84. Matsuo et al. (2009) reported that cellulose is also involved in the colour changes of timber during heat treatment.

Matsuo et al. (2010) studied colour changes of heat-treated wood (*Chamaecyparis obtuse Endl*) for 90°C to 180°C treatment by chemical kinetic analysis and defined colour changes according to the following equation:

$$\Delta L^* = L^* - L_0^*;$$

$$\Delta a^* = a^* - a_0^*;$$

$$\Delta b^* = b^* - b_0^*$$

$$\Delta E_{ab}^* = \sqrt{\Delta L^{*2} + \Delta a^{*2} + \Delta b^{*2}}$$

where, ΔE_{ab}^* is the total colour change.

The relationship between colour changes with temperature and treatment period (Figure 2-20) was discussed in this study to produce an appropriate equation for wood colour changing prediction. For ΔL^* and ΔE_{ab}^* :

$$f(x) = \frac{\alpha}{1 + \beta \exp(-\gamma x)}$$

where $f(x)$ is the colour parameter, while α , β and γ are constants. For Δa^* and Δb^* , x is the related treatment temperature and reference temperature.

$$g(x) = \sum_{k=3}^7 Pk x^k$$

where $g(x)$ is the colour properties and Pk are the coefficients.

The two equations were examined by coefficients of determination (R^2) and showed 0.996, 0.900, 0.861 and 0.995 for ΔL^* , Δa^* , Δb^* and ΔE_{ab}^* , respectively, which indicates high accuracy for prediction.

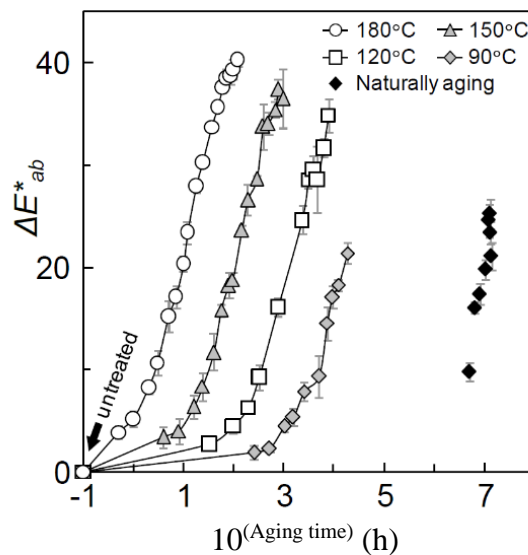


Figure 2-20 Colour Changes during Natural Aging and Heat Treatment (Matsuo et al., 2010)

Matsuo et al. (2011) studied colour changes of natural aged wood 560, 737, 921, 1,215, 1,470, 1,505, 1,395 and 1,773 years old, finding that the two equations also match natural aged wood prediction (Figure 2-21). Hence, colour change is an important evaluation on timber ageing

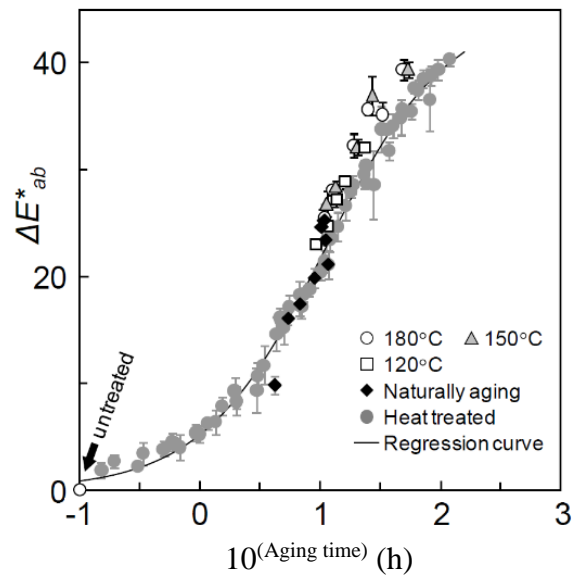


Figure 2-21 Timber Colour Regression Model (Matsuo et al., 2011)

2.2.5 Summary

The chemical composition of timber is affected by the environment, with oxygen playing an important role in changes regarding both its natural ageing and artificial treatment. Temperature increases the rate of chemical change and a few changes to timber happen at specific temperatures.

Hemicellulose is affected primarily in any atmosphere. Decomposition including deacetylation, dehydration and degradation normally happens in hemicellulose molecules even at low temperature, but this is much more dramatic at higher ones. Hydrolysis of hemicellulose is also an important cause of change in a water environment.

Cellulose is one of the most stable components, with no changes during hundred thousand years natural ageing or at 250°C high temperature treatment due to its crystalline structure. Uncrystallised cellulose is relatively less stable, but the structure also changes slowly. Decomposition and hydrolysis are the main chemical changes in uncrystallised cellulose.

However, cellulose cannot resist fungi or insect attack, because polysaccharides (cellulose and hemicellulose) are nutrition for these organisms.

Various chemical changes such as oxidation, condensation, hydrolysis and degradation can happen in lignin molecules, depending on the environment. For instance, lignin condensation and cross-linking reaction is promoted at 160°C to 200°C in an atmosphere without oxygen, but when it is present, oxidation reaction inhibits condensation and cross-linking reaction. In addition, oxygen would appear to play an important role in lignin degradation, in that its molecular structure in water is more stable than in air. Moreover, the cross-linked and condensed structure of lignin is stable as crystallised cellulose. That is, the two structures are non-hydrolysable residues which increase with time during the natural ageing process.

Mass loss due to decomposition products (liquid or gaseous) being released from samples increases directly with temperature and treatment period. Hemicellulose, uncrystallised cellulose, un-crosslinked/un-condensed lignin and moisture are mainly responsible for the mass loss. Colour changes are also owing to chemical changes including hydrolysis, oxidation and polymerisation.

Chemical changes in all three kinds of timber molecules are variant. Figure 2-22, Figure 2-23 and Figure 2-24 shows many ways of chemical changes for cellulose, hemicellulose and lignin. In fact, timber molecules consist of many chemical functional groups and chemical changes are based on the activity of these groups. A chemical functional group is a specific atom group within molecules, which can involve specific chemical changes. For instance, an oxygen bridge (-O-) can have a reaction with water (H-OH) and compose hydroxyl (-OH) under specific conditions, which is termed hydrolysis. Conversely, two hydroxyl groups in the same or different molecules could form an oxygen bridge and water,

which is called condensation. Hence, theoretically, chemical changes in timber molecule can be reflected in the changes of chemical functional groups.

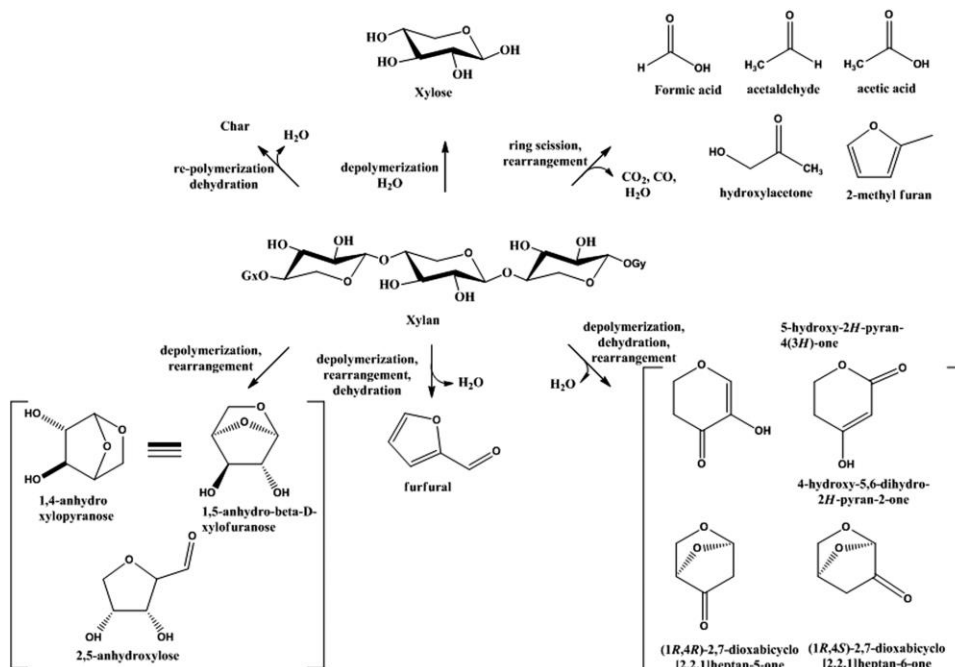


Figure 2-22 Hemicellulose Changes During Heat Treatment (Zhou et al., 2016)

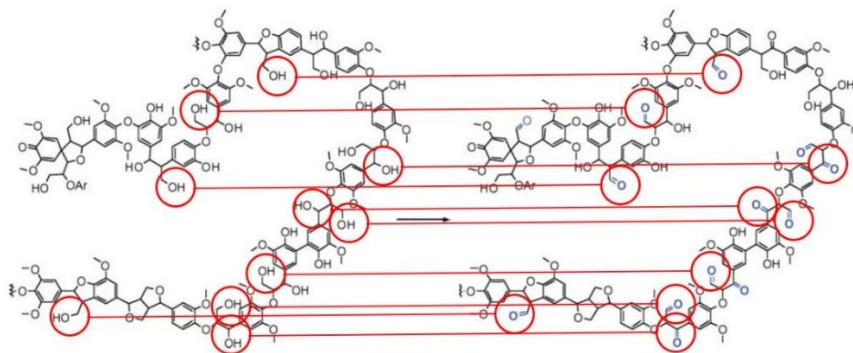


Figure 2-23 Oxidation Reaction During Heat Treatment (Liu et al., 2019)

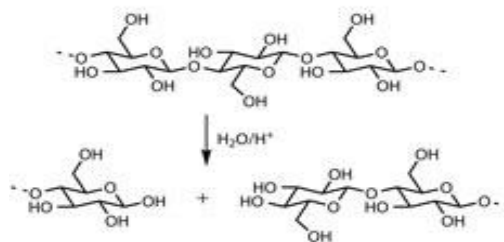


Figure 2-24 Hydrolysis Reaction During Heat Treatment (Shevchenko et al., 1999)

The chemical analysis methods regarding timber molecules were discussed in the first section of this chapter. As was explained, classic wet chemical analysis can detect the quantity change of the main molecules, especially holocellulose and lignin, but the detailed change of the molecular structure cannot be illustrated through this method. The pyrolysis method breaks up high weight molecules into many pieces with short chains and deduces the original molecular status by analysing these. However, temperature might cause unexpected changes to molecular composition, so this method is not sufficiently sensitive for detecting low degrees of chemical composition changes. The FTIR technique can reflect chemical composition changes by sensitively detecting functional groups of molecules and it is quick for investigating large numbers of samples. In addition, this technique is a form of non-destructive analysis in that the chemical composition of samples is not affected during testing. However, FTIR is not good at quantitative analysis, density change is not easy to illustrate so mass loss of samples should be recorded as an assistant analysis.

Chemical composition changes and their corresponding impact on the peak area of the FTIR spectrum will be studied in the first section of chapter 4.

2.3 Changes in Timber Mechanical Properties

In relation to timber as a type of building material, mechanical behaviours are the most critical evaluation. In general, mechanical properties are examined by static or dynamic testing. Bending and compression testing are the two main static method for the evaluation of the mechanical properties of timber in the radial and longitudinal directions, respectively. A bending test involves a three- or four-point test. Brancheriau et al. (2002) compared the two tests in the longitudinal direction, finding a high correlation between them. The modulus of elasticity (MOE) of all samples tested by four-point bending was 1.24 times greater than for the three-point test, with $R^2=0.99$. MOE and modulus of rupture (MOR) describe the static mechanical properties. MOE is the resistance ability to bending and MOR shows the maximum load on samples. In addition, MOE is also called Young modulus.

A dynamic mechanical test is sensitive to identifying polymer molecule status. However, unlike static mechanical tests, which has a long history, it is a new test method for investigating timber mechanical properties. Hence, the volume of the literatures regarding this technique is significantly smaller than that for static mechanical testing, but there are some valuable studies from this new area.

2.3.1 Static Mechanical Properties of Natural Aged Timber.

Due to the conservation philosophy, which restricts old timber structures being destructively tested and the lack of natural aged timber resource, the literature on mechanical properties of old timber is limited. In this part, approximately 30 studies are reviewed, with the sample ages ranging from 8 years to 1,800 years in various species for different environments. Some of these studies have involved identifying the mechanical

properties of samples by a non-destructive methods, namely ultrasonic testing, the results of ultrasonic testing may be different compared to 3-point bending test.

Two thirds of studies reported that the MOE in the longitudinal direction changes only slightly during the first 400 years (Kránitz et al., 2016). For instance, the MOE of the samples of fir between 29 and 90 years old (*Pseudotsuga menziesii*) did not show significant changes, when compared to new fir, according to Leichti et al. (2005), who studied replaced wood structural members from the Pacific northwest (USA). Ninety two 375 years old wood samples, including zelkova (*Keyaki*), cedar (*Sugi*), cypress (*Hinoki*) and pine (*Akamatsu*) showed no change or just a slight increase in the MOE compared with recent wood (Ooka et al., 2012). However, a few of the zelkova and pine samples were attacked by rot. Erhardt et al. (1996) studied 300 to 400 year old pine (*Pinus sylvestris L.*) from Norway and reported that even though the xylans are hydrolysed, the MOE did not show significant changes. Similar results were reported for the species *Cyclobalanopsis longinux*, *Castanopsis carlesii*, *Litsea acuminata*, *Cyclobalanopsis gilva*, *Pasania harlandii* (Lin et al., 2007), *Picea jezoensis*, *Abies sachalinensis* (Horie, 2002) and an unidentified one by Fridley et al. (1996) and Nakajima and Murakami (2010).

However, a few reports have indicated that the MOE increases or decreases significantly when compared to new wood. Chini (2001) graded 100 years old pine from a historic timber structure and found an increase of 5% to 37% in the MOE. However, Attar-Hassan (1976) tested 150 year old white pine and illustrated that the MOE decreased significantly. In this study, both mechanical and ultrasonic testing were conducted. The ultrasonic pulse velocity increased with the MOE decrease, which violate the principle of ultrasonic. Hence, the results of ultrasonic testing may not reflect accurately static mechanical properties. Saito et al. (2008b) observed a clear decrease in the MOE of 200-500 year old baulk samples from a historic building. However, the researchers also observed an insect attack by *Nicobium*

hirtum, which could have been an essential factor in the MOE decrease. A reasonable explanation of MOE changes put forward by Kohara (1955) is that it increased for the first 100 years and following this decreased.

The MOR, also called bending strength, likewise changes differently. More than of half studies observed slight changes in the MOR such as that of Kránitz (2014) on spruce and oak, Leichti et al. (2005) on fir, Lin et al. (2007) on oak and Fridley et al. (1996) on unidentified species. According to Noguchi et al. (2012), who tested both the MOR and MOE on 115, 270 and 290 year old Akamatsu pine (*Pinus densiflora*) by ultrasonic testing and found that even though the MOE increased with time, the ratio of vibrational MOE/vibrational bending strength did not change. Similar results were reported by Yokoyama et al. (2009), who investigated 360 year old Hinoki wood (*Chamaecyparis obtusa*). However, one study reported a 17% decrease in the MOR for 115 to 290 years old *Zelkova serrata* and *Pinus densiflora* (Hirashima, 2005), whilst another found a 15% decrease for 85 years old pine (Chini, 2001).

Compressive strength, tensile strength and shear strength have also been investigated by a few studies and the majority of the reports show few mechanical changes (Ooka et al., 2012; Falk and Green, 1999; Rug and Seemann, 1991; Deppe and Rühl, 1993). In fact, the three strength changes are the same as for the MOR.

The changes in mechanical property of natural aged wood over time vary due to different environment and position on structure (Cavalli et al., 2016). Few samples are from old structure with the function of loading, MOR of the samples decreased significantly. Crews and MacKenzie (2008) tested many structural members and found that the MOR decreased by 35% on light loaded structures such as a roof and 50% on long term and high loaded structures such as storage room floor. Smith (2012) reported a 20% decrease in MOR on

loaded structural samples. Falk et al. (1999) and Nakajima and Murakami (2010) also found a 15% MOR decrease for a 100 year old column sample (*Pseudotsuga menziesii*) and 13% for a deconstructed structure. In addition, it was found that sample size affects the results of mechanical properties, according to Nicholas et al. (2009), who did not find changes to the MOR of 300 year old spruce (*Picea abies*) by the size of 27×55×200mm. However, MOR increases of 17.3% and 42.1% on 270- and 290-years old samples were observed respectively of the size 20×20×320mm (Hirashima, 2005). Finally, decay, including insect and fungal attacks reduce the mechanical properties of aged samples (Rammer, 1999; Saito et al., 2008b; Saito et al., 2008a).

To sum up regarding the mechanical changes to natural aged timbers, previous loaded structure, storage environment and sample size affect the results significantly. However, mechanical properties during the first 400 years changes only slightly.

2.3.2 Static Mechanical Properties of Heat-Treated Timber

Bending tests are common and important in mechanical property research, because timber is invariably used as bending structural members and the bending is the weakest type of loading. MOE (Modulus of elasticity) and MOR (Modulus of rupture) reflect the bending strength, with the moduli being affected by temperature and treatment period, according to Kim (1998), who studied timber heat treatment on pine (*Pinus radiata*) at 120°C, 150°C and 180°C in air. The influence on the maximum load of samples or the MOR is more significant than for the MOE during heat treatment (Kim, 1998). A similar result was reported by Bekhta and Niemz (2003), who found 44% to 50% reduction in the bending strength (MOR), but only 4% to 9% decrease in the MOE during 200°C treatment of spruce wood (*Picea abies*) between 2 and 24 hours.

The treatment atmosphere affects mechanical properties significantly. Mitchell (1988) heated loblolly pine with different moisture contents (0%, 12% and green) at 150°C in air, oxygen and nitrogen for 1 to 16 hours. It was elicited that both the MOE and MOR of dry samples (0% moisture content) increased significantly compared to green wood, even reaching 14 times greater for the MOE after 16 hours of treatment. Both the MOE and MOR of the dry samples treated in oxygen were reduced by approximately 20%, but there were no significant changes in air and only slight increases in nitrogen. Kubojima et al. (1998) treated Sitka spruce (*Picea sitchensis Carr.*) in nitrogen and air at 120°C to 200°C for 2 hours to 16 hours and found that Young's modulus (MOE) increased both in the longitudinal and radial direction at the beginning in the temperature 120°C and 160°C. 200°C treatment increased the MOE at the beginning, which was followed by a reduction. The MOR was not studied in the experiment. A short period of treatment in any atmosphere did not cause changes, according to Kubojima et al. (2000), who compared heat treatment in nitrogen on green (60% moisture content) and dry spruce (*Picea sitchensis Carr.*) at 160°C for half an hour. Young's modulus (MOE) did not show significant changes between the green and dry samples.

In a steam atmosphere, heat treatment on pine (*Pinus pinaster*) between 190°C and 210°C for 2 to 12 hours caused a 7% increase in the MOE before 4% mass loss, then following a decrease, but MOE decreased constantly on eucalyptus wood (*Eucalyptus globulus*) (Esteves et al., 2007). The bending strength (MOR) of both eucalyptus and pine decreased constantly with the treatment period. Varga and van der Zee (2008) also observed a decrease in the bending strength and hardness for four hardwoods, *Robinia pseudoacacia L.*, *Quercus robur L.*, *Intsia bijuga* and *Hymenolobium petraeum* after steam treatment in a cylindrical pressure chamber. Inoue et al. (1993) compared dry and steaming treatment at 180°C, 200°C and 220°C on sugi (*Cryptmeria japonica D. Don*), reporting a reduction

in the MOE of 3.3%, 8.6% and 20%, respectively in steam. In the dry atmosphere, the MOE increased slightly during the first 8 hours of treatment at 180°C, whilst following this it decreased at 200°C and did so significantly when heated at 220°C. No significant change in the MOR occurred at 180°C and 200°C in steam treatment but decreased at 220°C. Steam treatment also improved dimensional stability, according to Santos (2000).

In an inert gas atmosphere, Poncsak et al. (2006) heated samples by a thermogravimetric system in nitrogen and carbon dioxide for birch (*Betula papyrifera*). The MOE showed a slight decrease between 150°C and 200°C treatment, while the MOR reduced with rising temperature by approximately 40% at 200°C. In addition, in this study also a slight increase in the MOE was observed with the humidity increasing, whereas there was a huge increase in the MOR, which suggests that moisture decreases the MOR significantly at high temperatures. Mburu et al. (2008) reported that the MOR reduced by approximately 60% and that the reduction of the MOE was approximately 30% for oak (*Grevillea robusta*) after 240°C treatment in an inert atmosphere. Hence, it is concluded that high temperatures (above 200°C) timber strength decreases dramatically in any atmosphere.

Wood species show different behaviour under the same treatment condition, according to Shi et al. (2007), who studied mechanical property changes in Quebec spruce (*Pices spp.*), pine (*Pinus spp.*), fir (*Abies spp.*), aspen (*Populus spp.*) and birch (*Betula spp.*) by applying the ThermoWood method treatment (at 200°C or higher in a low oxygen atmosphere for 3 hours). The results show that apart from a 6% rise for birch wood, the MOR decreased by 49%, 28%, 37% and 35% in the spruce, pine, fir and aspen respectively. Only spruce and pine showed a slight reduction in the MOE after treatment. The MOE of fir, aspen and birch increases 17%-25%, 15% and 30%, respectively, than untreated wood. Boonstra et al. (2007a) treated two pines (*Pinus radiata D.* and *Pinus sylvestris L.*) and one Norway spruce (*Picea abies Karst*) with a two-step technique involving 30 minutes treatment in water at

165°C, and 6 hours treatment in steam or nitrogen at 180°C. The MOR of scots pine and Norway spruce reduced 3% and 31%, respectively, the same treatment. Wood density and different molecule (cellulose, hemicellulose and lignin) content are responsible for the changes after heat treatment.

The results of compression tests have been reported in many studies. Unsal and Ayrimis (2005) studied compression parallel to the grain of river red gum tree wood (*Eucalyptus camaldulensis Dehn.*) for 120°C to 180°C treatment for 2 to 10 hours, eliciting that the compression strength (MOR) decreases with treatment period and as temperature rise. Similar results were reported for Scots pine (*Pinus sylvestris L.*) by Korkut et al. (2008), who undertook treatment with same method. This study also reported a decrease in bending strength, tension strength, hardness, impact bending strength and tension strength.

Timber is an anisotropic material, which means that the mechanical properties of the three directions are different. Boonstra et al. (2007b) found that the compressive strength in the longitudinal and tangential directions increases by 28% and 8%, respectively, but decreased by 43% in the radial direction with Scots pine (*Pinus sylvestris L.*) after an industrially-used-two-stage heat treatment.

2.3.2 Dynamic Mechanical Properties of Timber

Dynamic mechanical thermal analysis (DMTA) is a technique based on stress-versus-strain or load-versus-deformation curves (Figure 2-25), which connects the mechanical property of timber with the molecular structure (Birkinshaw et al., 1986; Wetton et al., 1991). The technique involves applying a sinusoidal stress to the sample and then, measuring the strain response from it; a phase lag appears between the stress and strain. The stress and strain can be evaluated by the following equation.

Stress: $\sigma = \sigma_0 \sin(t\omega + \delta)$

Strain: $\varepsilon = \varepsilon_0 \sin(t\omega)$

where, ω is the frequency of strain oscillation and t is time.

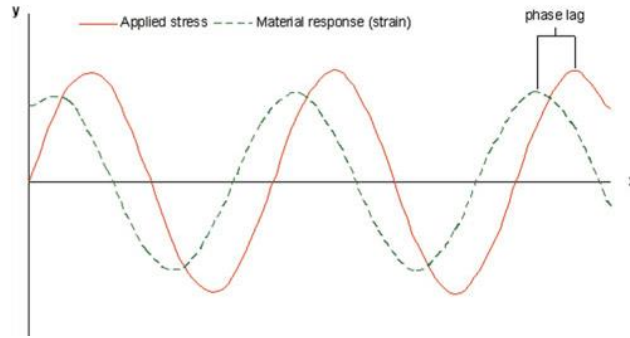


Figure 2-25 Theory of DMTA Technique

Phase lag also represents the viscoelastic behaviour of materials, especially for high weight polymer materials. DMTA is based on three modulus for describing the viscoelasticity, namely the storage modulus (E'), loss modulus (E'') and phase angle ($\tan \delta$), the relationship for which is shown in Figure 2-26. The storage modulus is the energy stored in the sample, the loss modulus is the energy dissipated to heat or other kinds of energy. E^* is complex modulus to describe materials viscoelasticity.

Storage modulus: $E' = \frac{\sigma_0}{\varepsilon_0} \cos \delta$

Loss modulus: $E'' = \frac{\sigma_0}{\varepsilon_0} \sin \delta$

Phase angle: $\delta = \arctan \frac{E''}{E'}$

Complex modulus: $E^* = E' + iE''$

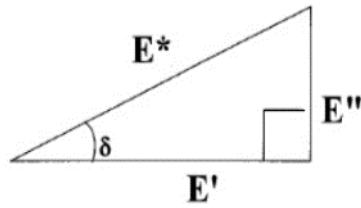


Figure 2-26 Relationships between Complex Modulus, Storage Modulus and Loss Modulus

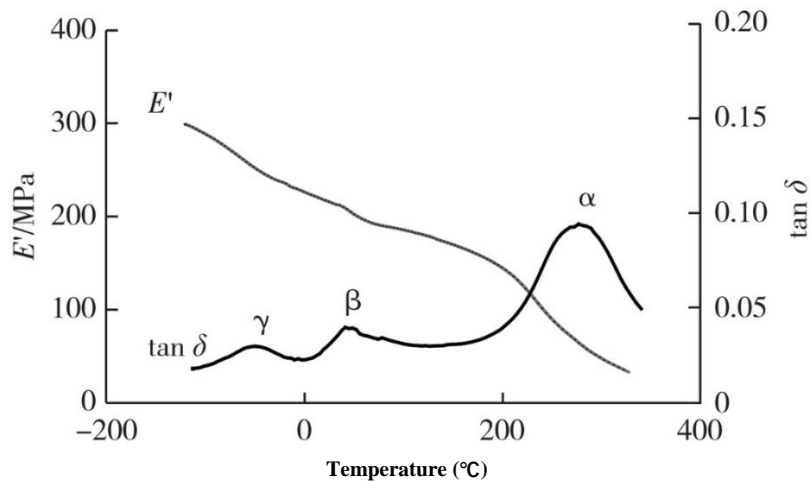


Figure 2-27 Tan δ Curve During Temperature Scanning (Havimo, 2009)

Temperature is an important factor that affects DMTA results (Wetton et al., 1991) and $\tan \delta$ can show the characteristics of the materials. In general, in a temperature scan from -150°C to 300°C, the storage modulus decreases constantly due to molecule softening (Figure 2-27) (Havimo, 2009). $\tan \delta$ shows three peaks in the temperature range and from low to high temperature are peak γ , peak β and peak α . Peak α is located between 150°C and 300°C, which is considered as the glass transition temperature and timber molecules, become very soft and elastic above this temperature. However, this peak is appeared during pulping process of making paper, which is rare in sample of solid timber. Timber samples at these temperatures experience dramatic decomposition and are carbonised (Esteves and Pereira, 2008). Peak β appears between -10°C and 100°C, with most studies having shown

that the peak is related to water molecule rearrangement in the timber molecules (Obataya et al., 2001; Kelley et al., 1987; Backman and Lindberg, 2001). However, Peak β still appear in timber samples with low moisture content after impregnation treatment in formaldehyde or polyethylene glycol as followed by Scandola and Ceccorulli (1985) as well as in a few organic diluents utilised by Handa et al. (1982). Obataya et al. (2001) concluded that Peak β relaxation is not related to the timber molecule main chain but rather, can be affected by short molecules, such as water. Peak γ appears at the temperature range between -150°C and -10°C . According to Obataya et al. (2001), Peak γ relaxation is affected by methylol groups ($\text{CH}_2\text{-OH}$) in the amorphous region of cellulose, hemicellulose and lignin molecules, because the peak is absent when other functional groups replace these groups. In addition, Peak γ may contain two small peaks with dry samples, according to Montes and Cavallé (1999), who elicited that these two small peaks are affected by the methylol groups and hydroxyl groups, respectively. In fact, the three peaks are impacted upon by the DMTA testing frequency, testing method (bending or compression) and the sample size.

A DMTA temperature scanning from -150°C to 300°C test is about 1 and a half hours for each sample. However, higher temperature scan may cause changes of chemical composition in the timber molecules, especially above 200°C . Hence, timber samples are normally tested from -150°C to 150°C owing to much less chemical composition changes in the molecules.

Different species of wood have different behaviours under DMTA. Birkinshaw et al. (1986) measured the shear storage modulus and $\text{Tan } \delta$ on ash (*Fraxinus excelsior*), Brazilian mahogany (*Swietenia macrophylla*), Iroko (*Chlorophora excelsa*), Keruing (*Dipterocarpus spp.*), Kingwood (*Dalbergia cearensis*), Obeche (*Triplochiton scleroxylan*), Parana pine (*Araucaria augustifolia*), pine (*Pinus sylvestris*), sapele (*Entandophragma cylindricum*)

and spruce (*Picea abies*) with temperature scanning from -100°C to 150°C. Even though the storage modulus of all the species decreased with temperature rising, Tan δ showed significant variations due to different compositions and densities (Figure 2-28). In general, Tan δ has two increasing periods from -100°C to -50°C and 50°C to 150°C. The first transition is because of molecular branch chain movement, whilst the second, is due to increasing thermo-plasticity of lignin. Sugiyama et al. (1998) studied spruce (*Picea sitchensis* Carr.) with four chemical modifications and reported that tan δ decreased due to the formation of oxygen bridges between the hydroxyl groups (condensation reaction, normally on lignin). Moreover, lignin becomes soft at around 85°C, according to Attack (1981), who studied spruce (*Picea mariana*) with temperature 20°C to 140°C and scanned by DMTA.

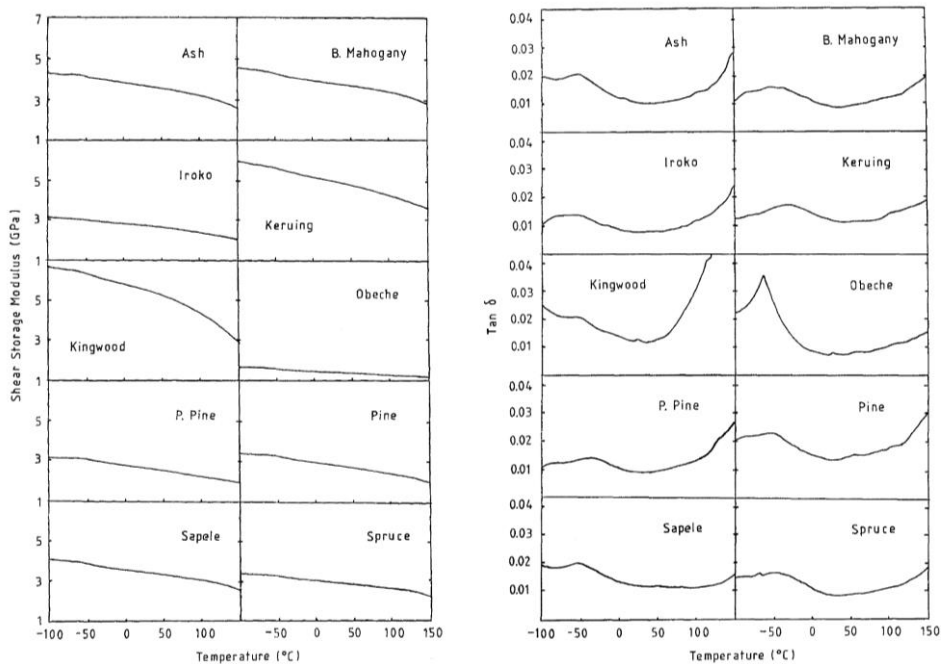


Figure 2-28 Storage Modulus and Tan δ Curve under Temperature Scanning of Different Species (Birkinshaw et al., 1986)

Dynamic mechanical behaviour is different in the longitudinal, radial and tangential directions possibly due to the direction of the cellulose microfibrils (Backman and

Lindberg, 2001). $\tan \delta$ is the highest in the longitudinal direction, while in the radial direction it is slightly higher than in the tangential direction at the same temperature. For this study, three peaks (molecule relaxation) appear on $\tan \delta$ and but the author obtained different conclusions to other results. First peak is from -120°C to -40°C and is affected by water adsorption of the methylol group. Both the second peak and third peak at 0°C and 40°C to 60°C , respectively, reflect the glass transition of hemicellulose.

Moisture content affects DMTA results. Sun et al. (2007) studied dry yellow-poplar (*Liriodendron tulipifera*) and pine (*Pinus spp.*) through DMTA and reported that moisture content increases from 0% to 1%, which results in a significant storage modulus rise.

Oxidation is also an important factor affecting $\tan \delta$, according to Subramanian and Hofmann (1983), who studied oxidised and unoxidised fir by DMTA at 72°C . That is, $\tan \delta$ of the oxidised samples was found to be significantly higher than for the unoxidised one. Hence, oxidation may cause molecular decomposition or diminish the length of the molecules of timber.

In terms of research on fungi degradation, Ormondroyd et al. (2017) reported a close relationship between storage modulus (E') and gDNA (a technique for detecting fungi activity better than mass loss) on scots pine (*Pinus sylvestris L.*) attacked by brown rot (*P. placenta*), with $R^2=0.9776$. The storage and complex moduli decreased constantly over 17 days of fungi exposure. However, the change of $\tan \delta$ is not significant, according to McCarthy et al. (1991), who utilised DMTA with a temperature scan on a pine (*Pinus sylvestris*) for 42 days fungi exposure, the result of which indicated that the chemical composition structure degrades uniformly.

DMTA technique is also popular in the study of wood adhesives which provide valuable information for the relationship between high weight molecule composition and DMTA.

High hydroxyl groups content of adhesives leads to an increase in the storage modulus, because of hydrogen bonds and cross-linking (Kim and Kim, 2003). In addition, DMTA has also been used for the glass transition temperature and creep response of adhesives to define their operating temperature and maximum load (Roseley et al., 2011).

2.3.3 Summary

Most naturally aged samples do not show significant changes in static mechanical properties (MOE and MOR) for the first 400 years and the changes in older samples are not defined due to their scarcity. However, the static mechanical properties of natural aged timber are affected by previous loading and decay. In addition, specimens size affects the mechanical testing results significantly in that a large one shows fewer changes to the MOE and MOR than a small one. Timber static mechanical property changes during heat treatment are also affected by the environment. That is, the MOR and MOE increase with gentle treatment temperature (approximately 120°C-160°C) in an inert atmosphere and decrease dramatically at higher temperatures (above 200°C) in air or oxygen. For the literature of all heat treatment, oxidation and decomposition reaction of the molecules lead to a decrease in mechanical strength, whereas crystallisation, cross-linking and condensation improve mechanical behaviour, in particular, regarding the MOR.

Tan δ of DMTA is an important measure reflecting the dynamic behaviour of timber, which illustrates three relaxation (γ , β and α) transitions of timber in the temperature range from -150 to 300. Peak γ , peak β and peak α are affected by motions of methylol groups, motions of moisture and lignin glass transition, respectively. Theoretically, from low temperature to high, Tan δ is affected by the following order: water molecule (glassy state) \rightarrow side groups and chain ends (glassy state) \rightarrow side chain (glassy state) \rightarrow main chain (Glass transition temperature) \rightarrow chain slippage (rubbery state). However, in the range from -

150°C to 150°C, timber does not show state changes. Many studies prove that carbonisation of timber starts from 212°C. Timber may not show rubbery state but stay in glassy state at the temperature between -150°C to 150°C.

However, even though DMTA can identify the molecular status of timber, the study on timbers is less reported.

2.4 Conclusions

Cellulose, hemicellulose and lignin molecules comprise timber cell walls, playing an important role in the mechanical behaviour of timber with moisture. Cellulose with 45%-50% content is a single long chain molecule supporting cell walls, a large part of which is arranged into a crystalline structure. The orientation of cellulose is parallel to the cell axis, which leads to different mechanical behaviour in three directions. The increase of cellulose crystallinity results in an increase in the MOE, which means high resistance to bending. Hemicellulose is shorter chains and bind celluloses, so degradation of hemicellulose can decrease mechanical strength lignin is full of branch chains that unite all the single molecules of the cell wall. Condensation and cross-linking reaction on lignin can expand its molecules' spatial influence and consequently, improve the mechanical properties in terms of both the MOE and MOR. However, hydrolysis or degradation can decrease this spatial influence, thus impairing the timber mechanical behaviour. Water invades the gap between timber molecules and connect hydroxyls on them by hydrogen bonding, such that the moisture provides an additional force of attraction force between molecules. However, excessive moisture swells timber molecules and leads to lose strength in the cell wall. Hence, cellulose, hemicellulose, lignin and water are main molecules affecting timber mechanical properties.

Dynamic mechanical thermal analysis results are also affected by molecule status. Due to different molecule contents and composition (cellulose, hemicellulose and lignin), each species of timber shows distinctive changes on an DMTA scan. Chemical reactions related to methylol groups, such as oxidisation, condensation, cross-linking reaction on the molecule also affect the DMTA results as with moisture content.

Some important information for experimental design has been obtained after comprehensively reviewing the literature. Firstly, the experiment atmosphere should be diverse. For, when all chemical changes in timber molecules, including decomposition, hydrolysis, oxidisation, condensation, cross-linking and crystallisation are observed, the level of reaction depends on the environment, such as temperature, oxygen content and humidity. Secondly, experiments can quickly be conducted in a lab environment. However, chemical composition changes of naturally aged wood are extremely slow and, UV as well as fungi exposure affect samples more seriously on the surface than inside. Hence, such wood is not suitable for chemical change analysis in the lab and instead, heat treatment is a suitable method for causing chemical composition changes to whole samples. Aerobic and anaerobic environment of heat treatment is easy to create by a few specific facilities in a lab. In addition, equilibrium moisture content change and mass loss of timber during heat treatment should be recorded to facilitate the analysis of chemical composition changes.

Since timber molecular weight are high, including more than 5,000 units and changes can happen in any part, traditional wet chemical analysis cannot identify these changes, whilst pyrolysis analysis destroys the original status of the molecule. Hence, a non-destructive detecting method, FTIR, based on changes of molecule chemical functional groups is deemed a suitable method for overcoming these issues. However, FTIR technique cannot detect sample mass loss, which is caused by decomposition or pyrolysis, so density data should be recorded at the same time.

Various static moduli, including the MOR and MOE in the different directions of timber and dynamic moduli, such as the storage modulus, loss modulus and $\tan \delta$ can be calculated by utilising specific testing facilities. However, all moduli are affected by sample size significantly. Hence, timber samples of both static and dynamic mechanical testing should be the same size. In addition, sample moisture content and testing temperature also affect mechanical testing results, which thus should be recorded before and after any kind of mechanical experiment.

Chapter 3 Materials and Experiment Plan

3.1 Materials

A few pieces of timber construction members have been replaced during a restoration project on a historic building, the Hall of Fusheng in Qufu, China (Figure 3-1 upper right). One piece of old timber can be used for testing. Its original position was as a girder of a veranda (Figure 3-1 upper left). One part, which does not show any cracks, is cut out for the study (Figure 3-1 lower right). Despite the piece of timber being exposed to the air, there was not much of a damp problem. The meteorological data of Qufu shows that the average temperature is 17°C with a high of 35°C in July and low of -6°C in January, whilst average humidity is 38%, a which is relatively dry environment. Hence, the piece of old timber had naturally aged in this environment.

A carbon 14 radiation report indicates that the age of the old timber is 580 ± 30 years (Figure 3-2) and a species detection report showed that it belongs to *Pinus Densiflora*. Figure 3-3 shows that the cell wall of the old pine timber is in good condition. Another piece of new pine of the same species was found in a forest farm in the northeast of China, because historical records revealed that all the timbers of the Hall of Fusheng are from the area. Hence, the new and old pine were grown in relatively the same climate condition. Moreover, the cell walls of the new specimen are also in good condition (Figure 3-4).

Even though two pieces of timber are the same species, the density and equilibrium moisture content of the new and old timber are significantly different. In the conditioning chamber at 20°C with 65% relative humidity, based on the samples with dimensions of 2mm×4mm×35mm, density was 0.46 g/cm³ and 0.38 g/cm³ for the old and new samples, respectively. The growing environment, timber age and different parts of tree trunk are responsible for this difference (Fengel, 1991; Yokoyama et al., 2009).

The equilibrium moisture content (EMC) at 20°C with 65% relative humidity was 10% and 10.5% on old and new pine, respectively. Hence this had decreased only slightly after 580 years of natural ageing. However, resin may have affected the EMC results for both the new and old samples. The moisture content detecting method was to dry the samples at 105°C for approximately 24 hours and measure the weight before and after drying. With the size 2mm×4mm×35mm, EMC is 10% and 10.5%, respectively, for the old and new pine, whilst for 20mm×20mm×40mm, these figures are 9.36% and 9.9%. Resin is easy to evaporate off in a small sample, but this is not so with large one (Figure 3-5), which leads to slightly higher values in the former.



Figure 3-1 Pine Structure Member after Restoration of the Hall of Fusheng

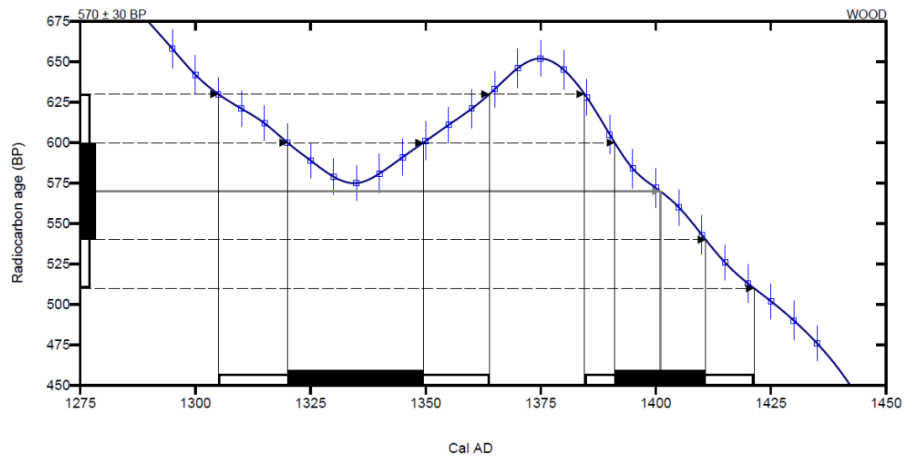


Figure 3-2 C14 Radiation of Old Pine

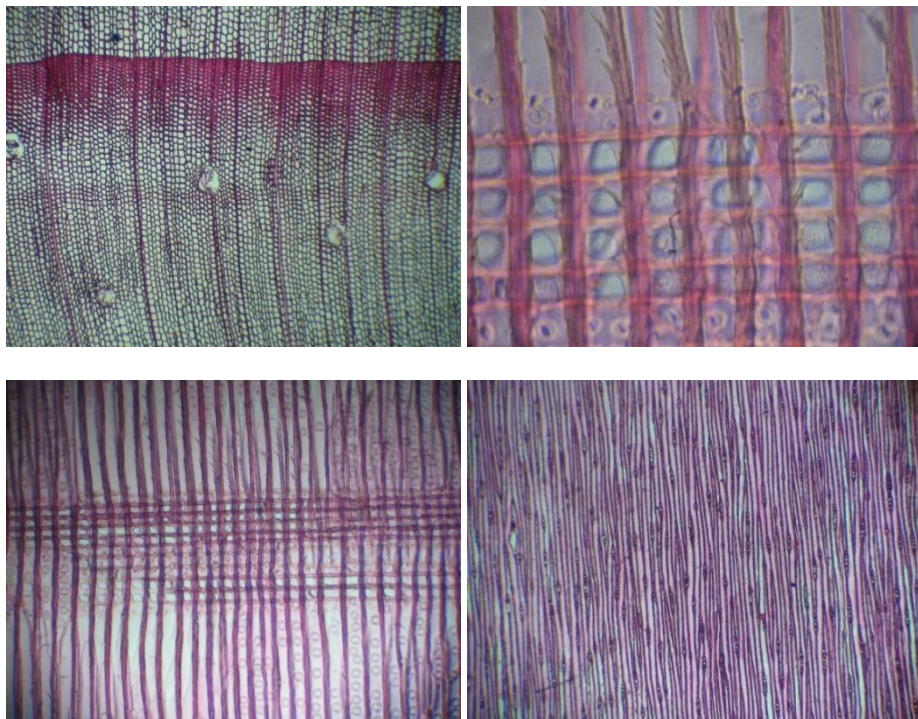


Figure 3-3 Cells of Old Pine

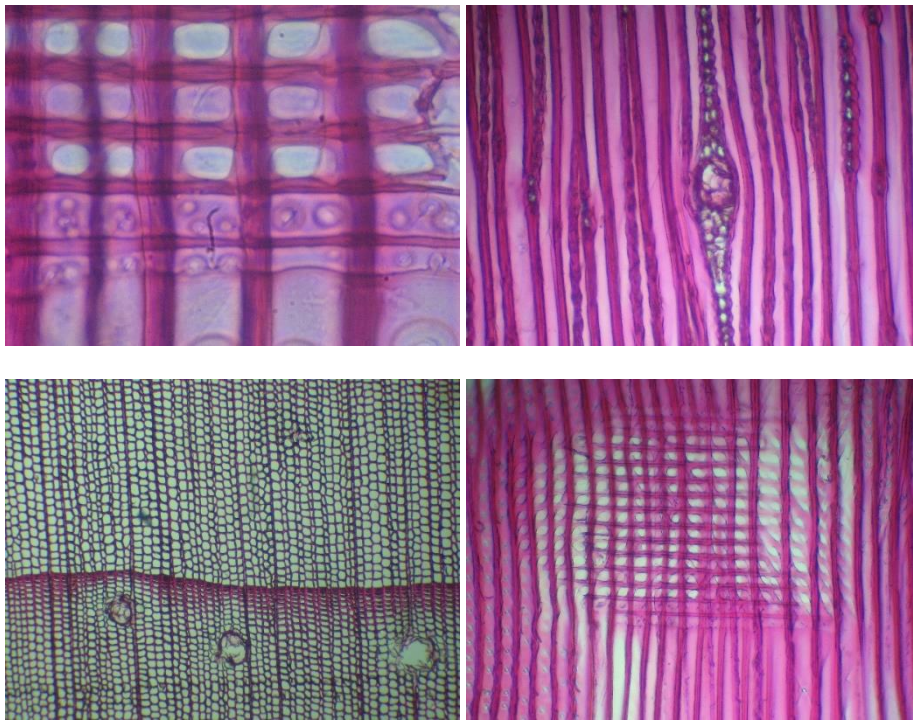


Figure 3-4 Cells of New Pine

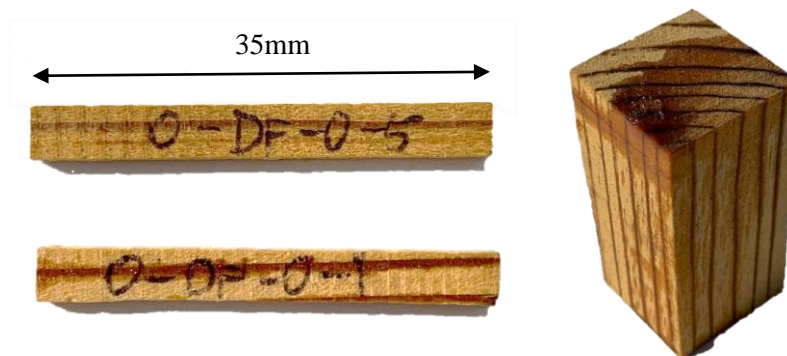


Figure 3-5 Resin in Small and Big Samples

The FTIR technique does not require a specific sample size but static and dynamic mechanical tests need. Mechanical testing results are affected by sample size (Cavalli et al., 2016; Esteves and Pereira, 2008) and annual ring direction (Backman and Lindberg, 2001). Hence, the samples under DMTA and 3-point bending test were set as

2mm×4mm×35mm (radial × tangential × longitudinal) with an annual ring vertical to the longitudinal direction of the cross section (Figure 3-6). In addition, each sample contained earlywood and latewood.

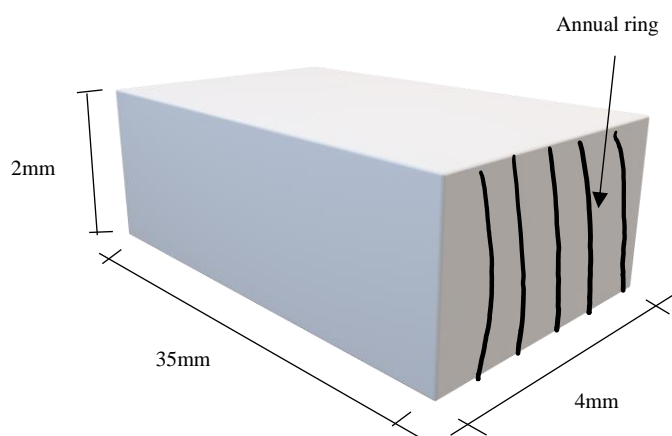


Figure 3-6 Sample Size and Annual Ring Direction in the Experiment

A compression mechanical test on new pine was considered in the experiment. However, 2mm×4mm×35mm was too small to fit the test facility, so the sample size for the compression test was set at 20mm×20mm×40mm.

3.2 Experiment Design

Evidence for the existence of a relationship between timber's chemical composition and mechanical behaviour has been provided in the chapter 2. Mechanical testing results are also affected by density and moisture content and hence, these two influencing factors were recorded in this experiment:

- Equilibrium moisture content of samples at 20°C with 65% relative humidity before and after heat-treatment;
- Mass loss during heat-treatment of dry samples;
- Chemical composition by FTIR before and after heat-treatment;

- Mechanical properties by a 3-point bending test and DMTA after heat-treatment.

In the experiment, all the samples started in a conditioning chamber at 20°C and 65% relative humidity for at least two weeks to allow to reach equilibrium moisture content. After conditioning, FTIR tests were conducted for chemical composition analysis of all the samples, then the weight was measured. The samples were subsequently placed in a dry oven at 105°C for approximately 24 hours until the weight did not change. Equilibrium moisture content before heat-treatment was obtained. Heat-treatment was started immediately after weight scaling. The sample weights were scaled after heat-treatment to calculate the mass loss and then, placed back into the conditioning chamber for approximately two weeks for equilibrium moisture content after heat-treatment. FTIR ascertained the chemical composition changes after heat treatment. Finally, a 3 point-bending test and DMTA were carried out. The experimental process applied to the samples is shown in Figure 3-7.

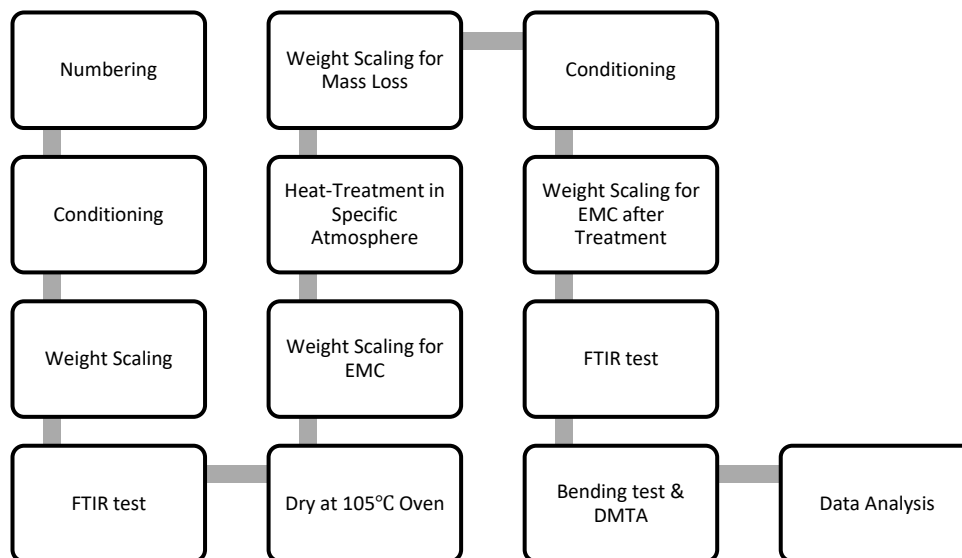


Figure 3-7 Experimental Process

Temperature treatment is a core process for implementing changes to timber. The temperature as set at 120°C, 160°C and 200°C for 8, 12, 16, 20 and 24 hours. Two treatment atmospheres, air (aerobic atmosphere) and vacuum (anaerobic atmosphere) were created using a specialised oven. Hence, there are three temperature levels × five treatment periods × two treatment atmospheres, which gives a total of 30 groups, with an additional non-treated reference group. Each group contained 20 new pine samples for 3-point bending testing and six samples for DMTA, so the total sample quantity for the new pine as 806. However, due to the limited volume of old pine, 3-point bending test samples were only carried out at 120°C and 200°C for 8, 16 and 24 hours, but the sample quantity for DMTA was not affected, so the total quantity of old pine samples was 458. Table 3-1 shows the heat treatment design and sample distribution in the experiment.

In addition, three supplementary experiments were conducted to investigate:

- The relationship between moisture content and mechanical properties;
- The relationship between moisture content and DMTA;
- The compression mechanical property changes during heat-treatment.

To examine the first objective, 132 samples were placed in the conditioning chamber with 20°C and 65% relative humidity for two weeks and then, dried in an oven at 105°C for approximately 24 hours. Subsequently, the samples were returned to the conditioning chamber for a different period to provide different moisture content. The static mechanical property was tested immediately by the 3-point bending test, whilst DMTA was undertaken for approximately 1-hour from -150°C to 150°C. Since moisture content would change significantly, but the facility could not control humidity, only six dry samples and six samples with 10.5% moisture content were tested. The 3-point bending test assesses timber strength in the tangential direction, while the compression measures that in the longitudinal

direction, with a total of 210 samples, 20mm×20mm×40mm, being processed during the heat-treatment. However, due to limited volume, the samples were processed only in the treatment at 160°C and 200°C both in air and vacuum atmospheres. All these three supplementary experiments involved only new timber, due to the aforementioned limited volume of the old pine.

Table 3-1 Sample Quantity and Distribution During Heat Treatment

Period (hours)	Air			Vacuum			
	120°C	160°C	200°C	120°C	160°C	200°C	
New Pine	0						
	20 (Bending)						
	6 (DMTA)						
	10 (Com.)						
	8	20 (Bending)	20 (Bending)	20 (Bending)	20 (Bending)	20 (Bending)	20 (Bending)
		6 (DMTA)	6 (DMTA)	6 (DMTA)	6 (DMTA)	6 (DMTA)	6 (DMTA)
			10 (Com.)	10 (Com.)	10 (Com.)	10 (Com.)	10 (Com.)
	12	20 (Bending)	20 (Bending)	20 (Bending)	20 (Bending)	20 (Bending)	20 (Bending)
		6 (DMTA)	6 (DMTA)	6 (DMTA)	6 (DMTA)	6 (DMTA)	6 (DMTA)
			10 (Com.)	10 (Com.)	10 (Com.)	10 (Com.)	10 (Com.)
16	20 (Bending)	20 (Bending)	20 (Bending)	20 (Bending)	20 (Bending)	20 (Bending)	
	6 (DMTA)	6 (DMTA)	6 (DMTA)	6 (DMTA)	6 (DMTA)	6 (DMTA)	
		10 (Com.)	10 (Com.)	10 (Com.)	10 (Com.)	10 (Com.)	
20	20 (Bending)	20 (Bending)	20 (Bending)	20 (Bending)	20 (Bending)	20 (Bending)	
	6 (DMTA)	6 (DMTA)	6 (DMTA)	6 (DMTA)	6 (DMTA)	6 (DMTA)	
		10 (Com.)	10 (Com.)	10 (Com.)	10 (Com.)	10 (Com.)	
24	20 (Bending)	20 (Bending)	20 (Bending)	20 (Bending)	20 (Bending)	20 (Bending)	
	6 (DMTA)	6 (DMTA)	6 (DMTA)	6 (DMTA)	6 (DMTA)	6 (DMTA)	
		10 (Com.)	10 (Com.)	10 (Com.)	10 (Com.)	10 (Com.)	
Old Pine	0						
	20 (Bending)						
	6 (DMTA)						
	8	20 (Bending)		20 (Bending)	20 (Bending)		20 (Bending)
		6 (DMTA)	6 (DMTA)	6 (DMTA)	6 (DMTA)	6 (DMTA)	6 (DMTA)
12	6 (DMTA)	6 (DMTA)	6 (DMTA)	6 (DMTA)	6 (DMTA)		

16	20 (Bending)	6 (DMTA)	20 (Bending)	20 (Bending)	6 (DMTA)	20 (Bending)
	6 (DMTA)		6 (DMTA)	6 (DMTA)		6 (DMTA)
20	6 (DMTA)	6 (DMTA)	6 (DMTA)	6 (DMTA)	6 (DMTA)	6 (DMTA)
24	20 (Bending)	6 (DMTA)	20 (Bending)	20 (Bending)	6 (DMTA)	20 (Bending)
	6 (DMTA)		6 (DMTA)	6 (DMTA)		6 (DMTA)
Total	New: 806 samples with 2mm×4mm×35mm, 210 samples with 20mm×20mm×40mm					
	Old: 458 samples with 2mm×4mm×35mm					

3.3 Experiment Process and Facility

3.3.1 Heat treatment



Figure 3-8 Oven with Vacuum Pump

Temperature is one way to cause chemical and mechanical changes. Whilst mechanical properties can be improved or harmed in a specific environment, both during the natural ageing process and heat treatment, the former is not efficient due to its slow occurrence. Other methods, such as UV, biological attack or chemical modification, cannot control the rate of chemical change in timber. Moreover, the stability of timber molecules, cellulose, hemicellulose and lignin varies at different temperature levels and in atmospheres. Hence, temperature is the most suitable method to cause changes in this experiment.

An oven with a vacuum pump was utilised for the heat-treatment. The temperature was set at $120^{\circ}\text{C} \pm 5^{\circ}\text{C}$, $160^{\circ}\text{C} \pm 5^{\circ}\text{C}$ and $200^{\circ}\text{C} \pm 5^{\circ}\text{C}$. The vacuum atmosphere is created by switching off the valve and pumping all the air to out, whilst for an air atmosphere, the air valve is switched on and the pump is run to increase air flow.

None of the samples are allowed to touch the oven shelf directly, as this could cause uneven temperature distribution. Instead, many U shape supporters are made for sample heat treatment. After heat treatment, the samples are moved to a glass desiccator to cool down, which prevents moisture having an influence during the cooling down process.

Another oven at 105°C was used to dry samples before heat treatment to measure moisture content. The FTIR spectra show that the chemical composition during the drying process underwent no changes (Figure 3-9) and the mass loss was less than 0.2% (Table 3-2).

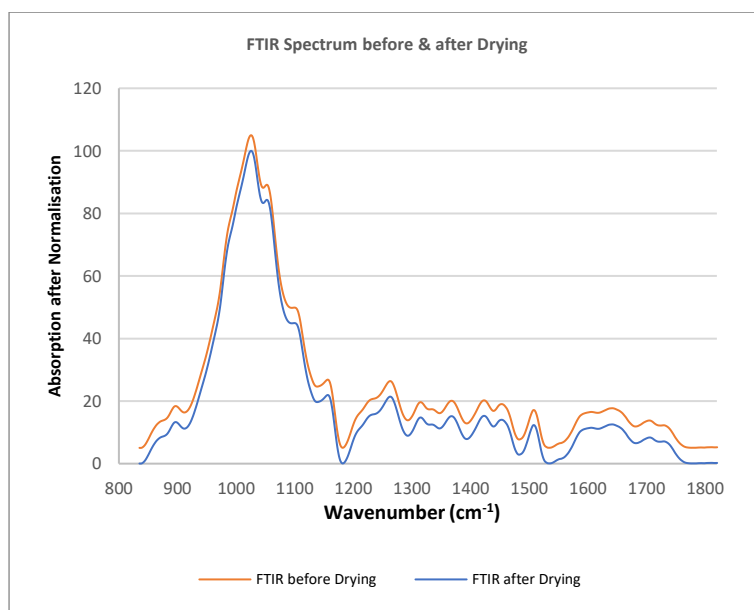


Figure 3-9 FTIR Spectrum before and after the Drying Process of New Pine

Table 3-2 Mass Loss During the Drying Process

	Weight after first conditioning (g)	Weight after drying (g)	Weight after second conditioning (g)	Moisture content	Mass loss after drying (g)
	0.1051	0.0951	0.105	10.41%	0.0001
	0.1086	0.0985	0.1086	10.25%	0
	0.1128	0.1019	0.112	9.91%	0.0008
	0.1123	0.1012	0.112	10.67%	0.0003
	0.1151	0.1045	0.1146	9.67%	0.0005
	0.1088	0.099	0.1085	9.60%	0.0003
	0.109	0.0984	0.1089	10.67%	0.0001
New pine	0.1122	0.1011	0.112	10.78%	0.0002
	0.1097	0.0997	0.1096	9.93%	0.0001
	0.1084	0.0979	0.1084	10.73%	0
	0.1124	0.1021	0.1122	9.89%	0.0002
	0.105	0.0951	0.1049	10.30%	0.0001
	0.1098	0.0992	0.1095	10.38%	0.0003
	0.1099	0.0994	0.1097	10.36%	0.0002
	0.1059	0.0961	0.1056	9.89%	0.0003
		Mean		10.5%	0.000233
	0.1575	0.1433	0.1575	9.91%	0
	0.1475	0.1348	0.1474	9.35%	0.0001
	0.1496	0.1361	0.1496	9.92%	0
	0.1437	0.13	0.1437	10.54%	0
	0.1726	0.1574	0.1725	9.59%	0.0001
	0.1501	0.1358	0.1486	9.43%	0.0015
	0.1616	0.1463	0.1611	10.12%	0.0005
Old pine	0.1542	0.1406	0.154	9.53%	0.0002
	0.1404	0.1282	0.1404	9.52%	0
	0.2126	0.1904	0.2086	9.56%	0.004
	0.1372	0.1256	0.1372	9.24%	0
	0.1476	0.1341	0.1471	9.69%	0.0005
	0.1479	0.1346	0.1478	9.81%	0.0001
	0.1343	0.1216	0.1343	10.44%	0
	0.1483	0.135	0.1483	9.85%	0
	0.1651	0.1499	0.1641	9.47%	0.001
		Mean		10.04%	0.0005

3.3.1 Chemical Analysis

Wet chemical analysis can obtain the quantities of timber molecules. However, the method is not sensitive to tiny changes in the molecules and moreover, the operation process is slow, which makes it cumbersome to investigate large numbers of samples. Hence, ATR-FTIR is a suitable method with the advantages of quick analysis and easy operation. It detects chemical composition changes by detecting the functional groups of timber molecules and can show very small changes in a molecule's functional groups. However, ATR-FTIR cannot ascertain the density of timber accurately, so mass loss data should be recorded as a reference.

The chemical composition of samples was obtained by Thermo Scientific FTIR equipment (Figure 3-10 left) with a PIKE GladiATR accessory (Figure 3-10 right). The facility was placed in a laboratory at 20°C with 65% humidity.

FTIR resolution was set as 1 cm^{-1} and scanned 30 times. For each sample, two smooth surfaces were chosen for the test. This is because smooth surface samples lead to clearer results to achieve this, all the timber specimens were made with an electric fine saw used by an expert.



Figure 3-10 FTIR Facility used in the Experiment

3.3.2 Static Mechanical Properties

The static mechanical properties, namely containing the bending modulus of rupture (MOR) and modulus of elasticity (MOE), are the fundamental properties of a building material. MOR illustrates the maximum stress that a sample can sustain, whilst MOE shows the ability of the a sample to resist to bending.

The static mechanical properties were measured by a INSTRON 3-point bending equipment (Figure 3-11) and the stress-strain curve was recorded using Bluehill software. The facility was placed in a laboratory at 20°C with 65% humidity. The span of the fixture was 28.5mm and the speed of pressing was set at 0.025mm/s.



Figure 3-11 3-Point Bending Test Facility

3.3.3 Dynamic Mechanical Properties

Dynamic mechanical testing can illustrate molecular status between timber molecules during a temperature scanning. More friction between molecules, which leads to a higher loss modulus of a sample, is responsible for an increase in $\tan \delta$, whilst expanding or extending timber molecules contributes to a low loss modulus and a low value of $\tan \delta$.

There are two peaks on the $\text{Tan } \delta$ curve of temperature scanning, which are affected by distinctive molecular components and also reflect the form changes of molecules.

The DMTA testing involved the facility made by Triton Technologies (Figure 3-12). The test was based on a 3-point bending clamp accessory with a temperature scan from -150°C to 150°C at a frequency of 1 Hz. The -150°C environment was created by liquid nitrogen and then, a heating system controlled the temperature automatically at an increasing rate of $6^{\circ}\text{C}/\text{min}$.

Temperature scanning by DMTA can cause chemical composition changes but if so, there are extremely small. The weights of the samples were recorded before and after DMTA testing, being then compared with the weight after heat-treatment. The results show that the weight after the DMTA test was heavier than that after heat treatment, which indicates that only moisture is responsible for the mass change (Table 5-1).

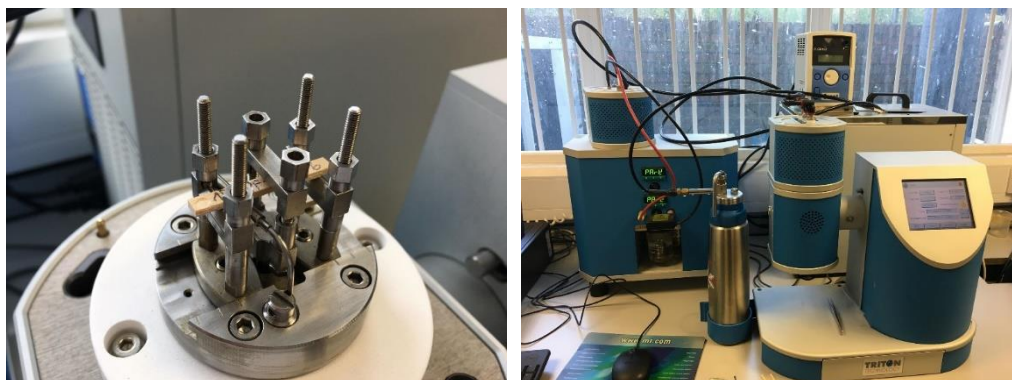


Figure 3-12 DMTA Facility

3.4 Peak Fitting of FTIR

Chemical composition analysis by the ATR accessory of FTIR is easy and quick. However, whilst high pressure of clamp improves the absorption of near infrared light (≤ 1200

wavenumber), it decreases the absorption of far infrared light (≥ 3000 wavenumber), which leads to the baseline of the spectrum tilting to a high frequency wavenumber (Spragg, 2011). A similar result was observed by Lu et al. (2017). Hence, the raw FTIR spectrum should be processed with baseline corrections. The FTIR spectrum testing range is from 600 cm^{-1} to $4,000\text{ cm}^{-1}$, but the essential peaks for analysing timber are from 800 cm^{-1} to 1800 cm^{-1} . Hence, to ensure the accuracy of baseline corrections, this range is the area focused on to be corrected. Baseline correction was calculated in Origin Pro software.

According to FTIR spectrum literature reviews, the FTIR technique is adept in qualitative analysis rather than showing the quantity change of chemical functional groups. The relative content of functional groups is more important and thus, all the spectrums were normalised as min-max from 0 to 100. Figure 3-13 shows FTIR spectrum before and after baseline correction as well as normalisation.

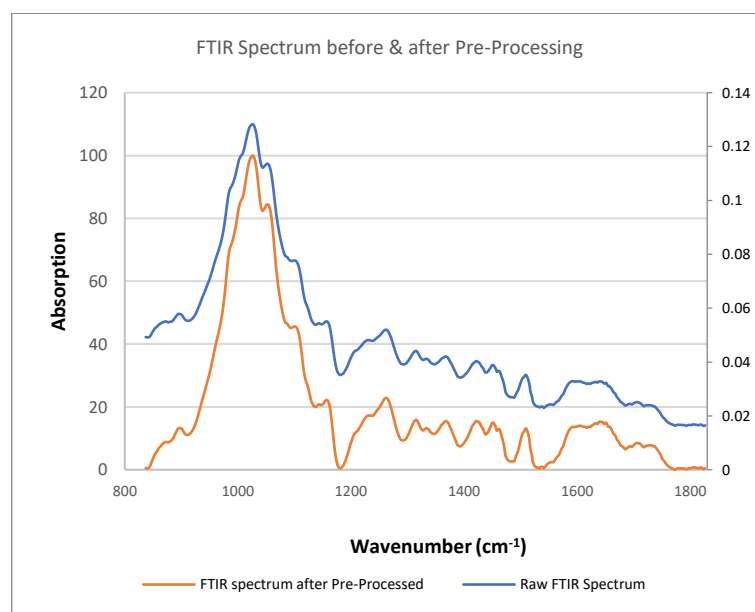


Figure 3-13 FTIR Spectrum before and after Pre-Processing

In fact, the FTIR spectrum is the result of peak superposition. According to Bradley (2007), the peak shape of solid samples is a gaussian curve, and timber is one of these. The peak

fitting process can distinguish the size of each peak and was conducted by Origin Pro software. Apart from peaks at 3,336 and 2,938-2,882, 17 peaks were found and fitted by the software. Figure 3-14 shows the peak fitting of non-treated new pine. The coefficient of determination (COD) of fitting was between 0.998 and 0.999, which indicated high correlations between the real FTIR spectrum and the predicted fitting. All 19 peak wavenumbers and the corresponding compound are shown in Table 3-3.

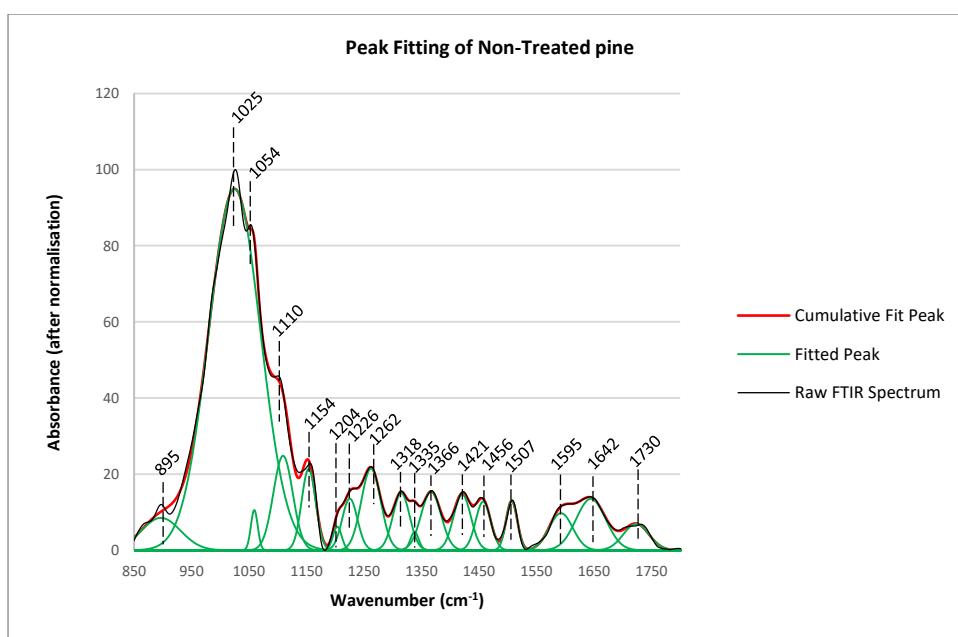


Figure 3-14 Peak Fitting of the FTIR Spectrum of Non-treated New Pine

Table 3-3 FTIR Peak Wavenumber and the Corresponding Chemical Functional Groups

No.	wavenumber	Compound
1	3336	O-H Stretch (Kondo, 1997)
2	2938	CH- stretch in methyl- and methylene groups
	2882	
-	2103	Absorption caused by the ATR crystal
	1990	
3		C=O stretching in unconjugated ketone, carbonyl, aliphatic and ester groups
	1730	(frequently of carbohydrate origin) (Harrington et al., 1964; Barker and Owen, 1999; Chow, 1971)

4	1642	-OH bending, affected by water absorption (Marchessault, 1962; Fengel and Wegener, 1984)
5	1595	C=C stretching; COO ⁻ stretching (Faix, 1991; Harrington et al., 1964)
6	1507	Aromatic skeletal vibration (Faix, 1991; Harrington et al., 1964; Marchessault, 1962)
7	1456	C-H deformation stretching in CH ₂ and CH ₃ , aromatic skeletal vibrations (Kotilainen et al., 2000; Harrington et al., 1964)
8	1421	O-H in aromatic skeletal; C-H deformation stretching in CH ₂ and CH ₃ (Harrington et al., 1964)
9	1366	C-H bending (Liang and Marchessault, 1959)
10	1335	phenol group, -OH bond to aromatic hydrocarbon group (Sarkanen and Ludwig, 1971; Marchessault and Liang, 1962)
11	1318	Condensation of guaiacyl unit and syringyl unit, syringyl unit and CH ₂ bending stretching (Evans et al., 1992; Kotilainen et al., 2000)
12	1262	C-O stretching (lignin) (Harrington et al., 1964; Marchessault, 1962)
13	1226	C-C, C-O-C (lignin) (Faix, 1991)
14	1204	C-O-C or O-H in -plane bending (Parker, 1983)
15	1154	bridge C-O-C stretching (Müller et al., 2009; Marchessault, 1962)
16	1110	C-OH stretching (Müller et al., 2009; Higgins et al., 1961)
17	1054	C-C, C-O stretching (Müller et al., 2009; Higgins et al., 1961)
18	1025	C-H in-plane deformation, C-O stretching (Kotilainen et al., 2000; Higgins et al., 1961)
19	895	Aromatic vibration at β -glycosidic linkage (Müller et al., 2009; Evans et al., 1992)

Chapter 4 Chemical Composition Changes during Heat Treatment

The chemical composition changes during heat treatment are various. In fact, pure cellulose, hemicellulose and lignin behaviour at different temperatures from low to 500°C have been discussed in detail by many studies (Yang et al., 2007; Zhou et al., 2016; Kawamoto et al., 2007). Timber mechanical properties are affected by molecule chain length, matrix and quantity (Landel and Nielsen, 1993; Tobolsky and Eyring, 1943). This chapter only discusses the chemical composition change affecting molecular shape.

The chemical composition of timber is reflected in the FTIR peak area in this research. The first section of this chapter considers chemical reaction according to chemical functional groups change and its corresponding peaks on the FTIR spectrum. The chemical composition difference between new and old pine can be obtained by FTIR and the chemical changes during natural ageing are discussed in the second section. Moisture content and mass loss, which could be treated as the change of the hydroxyl group and molecular total quantity, respectively, are studied in sections 3 and 4. Chemical composition changes during heat treatment at different temperatures and in different treatment atmospheres for the new and old timber are discussed in section 5 and section 6, respectively. Peak correlation of the FTIR spectrum study is conducted to illustrate relationships of peak variance in section 7, whilst a comprehensive discussion is provided in the final section (section 8).

4.1 Mechanism of Chemical Composition Changes of the Timber Molecule

Many studies have shown that cellulose is very stable in heat treatment under 200°C for at least 24 hours. Hence, the chemical composition changes of hemicellulose and lignin are

mainly responsible for peak area changes of the FTIR spectrum. All chemical reactions relating to chain length or the matrix are covered in this section.

Hemicellulose pyrolysis

Hemicellulose is unstable even at room temperature and temperature can accelerate the rate of the change. In many studies, acetic acid release at the beginning of hemicellulose pyrolysis have been observed (Sivonen et al., 2002; Weiland and Guyonnet, 2003; Tjeerdsmas et al., 1998). In fact, acetic acid is due to deacetylase reaction on hemicellulose, which is a process that acetyl groups detach hemicellulose main chain, so deacetylase reaction could be treated as the first stage of hemicellulose pyrolysis. Acetyl groups detach from the hemicellulose chain due to the breaking of C-O bond of the ether linkage (C-O-C). A hydrogen atom in the phenyl group near the acetyl group is attracted and forms acetic acid, which evaporates to the outside. The two chemical bond vacancies, which are the previous places of acetyl groups and hydrogen bond, respectively, link together to form alkene linkage (C=C) (Figure 4-1) (Zhou et al., 2016).

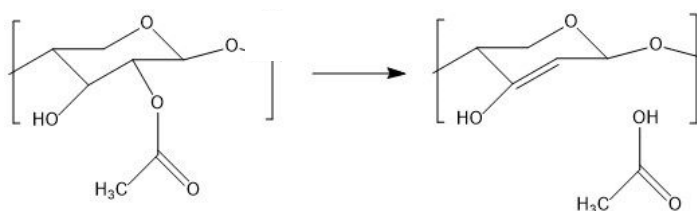


Figure 4-1 Mechanism of Hemicellulose Deacetylase

The deacetylase of hemicellulose does not change the chain length, but with rising temperature and an increasing treatment period, hemicellulose decomposes into many shorter chains. The reaction is violent and variant. A few shorter chain molecules are liquids or gas released out of the sample, which leads to a chemical functional groups decrease. However, hemicellulose pyrolysis products are rich in carbonyl (C=O) and the alkene

group (C=C), which contribute to an increase on the FTIR spectrum (Figure 4-2) (Patwardhan et al., 2011).

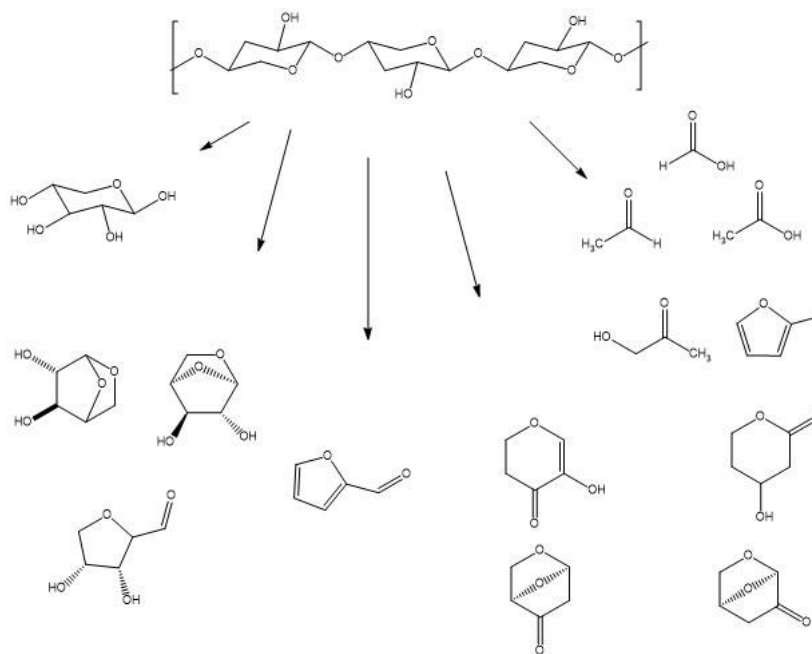


Figure 4-2 Mechanism of Hemicellulose Pyrolysis

Lignin condensation and cross-linking

Condensation and cross-linking are common chemical reactions leading to extending and expanding of lignin molecule chains. There are two kinds of condensation, both happening based on the change of ether linkage (C-O-C). In the first kind of condensation, ether linkages (C-O-C) near the phenolic ring break and one hydrogen atom of this ring is attracted by the gap. A chemical bond vacancy appears on the phenolic ring. Two phenolic ring can relink directly by C-C bond or by a methylene bridge (-CH-) (Figure 4-3) (Hemmilä et al., 2017). This reaction is termed condensation I in this research. The other kind of lignin condensation happens between two hydroxyl groups. Two hydroxyl groups can condense to ether bridge (C-O-C) and water (Figure 4-4) (Liu et al., 2019). This reaction is named condensation II. The two hydroxyl groups can be in the same or different lignin molecular chains and this reaction can also be considered as dehydration.

A lignin cross-linking reaction happens on a single chain of lignin containing an O=C-C=C- fragment (Figure 4-5). The bond of the alkene group (-C=C-) and carbonyl group (-C=O-) break to -C-C- and -C-O-, respectively, under a specific treatment. Then two or more single chains re-link to a matrix structure at the breaking position.

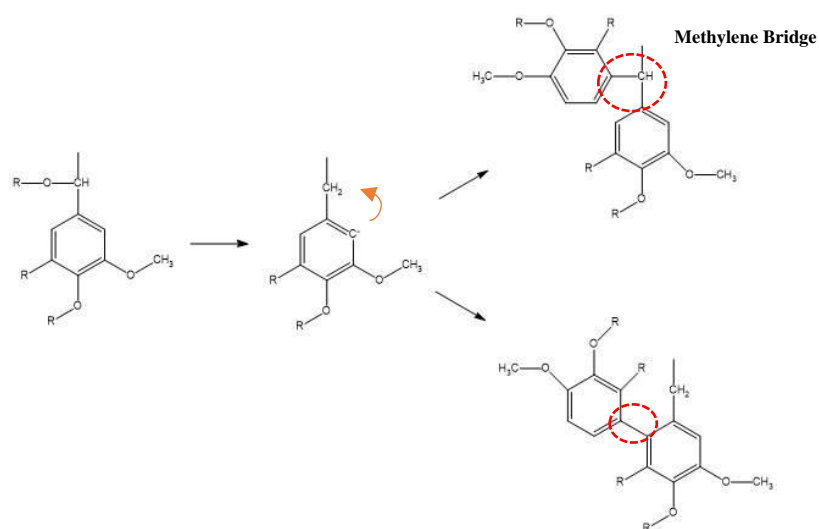


Figure 4-3 Mechanism of Lignin Condensation I

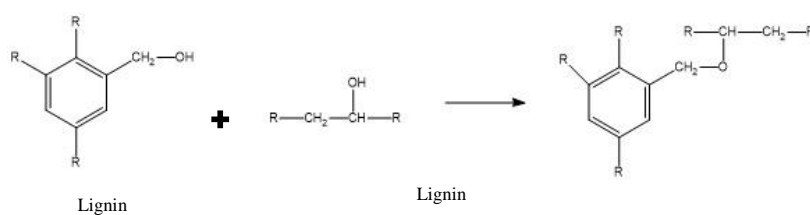


Figure 4-4 Mechanism of Lignin Condensation II

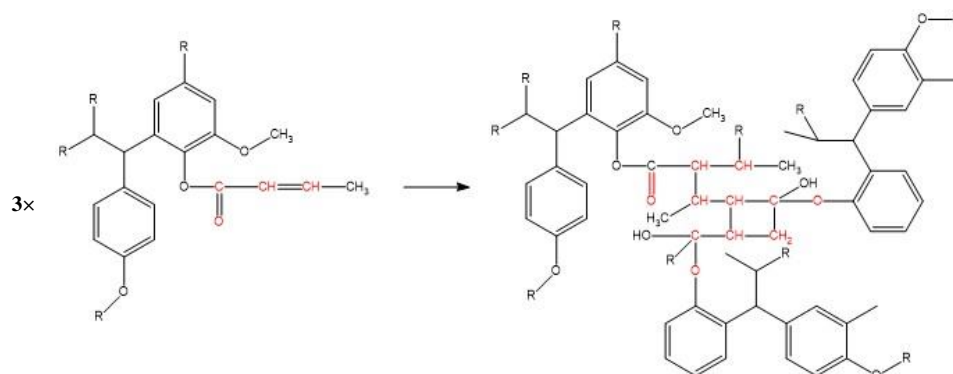


Figure 4-5 Mechanism of Lignin Cross-Linking

Lignin-carbohydrate complexes

Condensation can also happen between lignin and hemicellulose, forming lignin-carbohydrate complexes (Figure 4-6) (Imamura et al., 1994). The mechanism of the reaction is same as with lignin condensation II, where two hydroxyl groups condense to ether linkage, which links lignin and hemicellulose molecules. In addition, lignin can also condense with a pyrolysis product of hemicellulose, namely furfural, but a reaction that normally happens with lignin condensation I. An aromatic ring of furfural attaches to condensed lignin by a methylene bridge. A hydrogen atom and the -CHO group detach from the furfural and lignin, respectively, forming formaldehyde gas, which is released out of the sample (Figure 4-7) (Hemmilä et al., 2017).

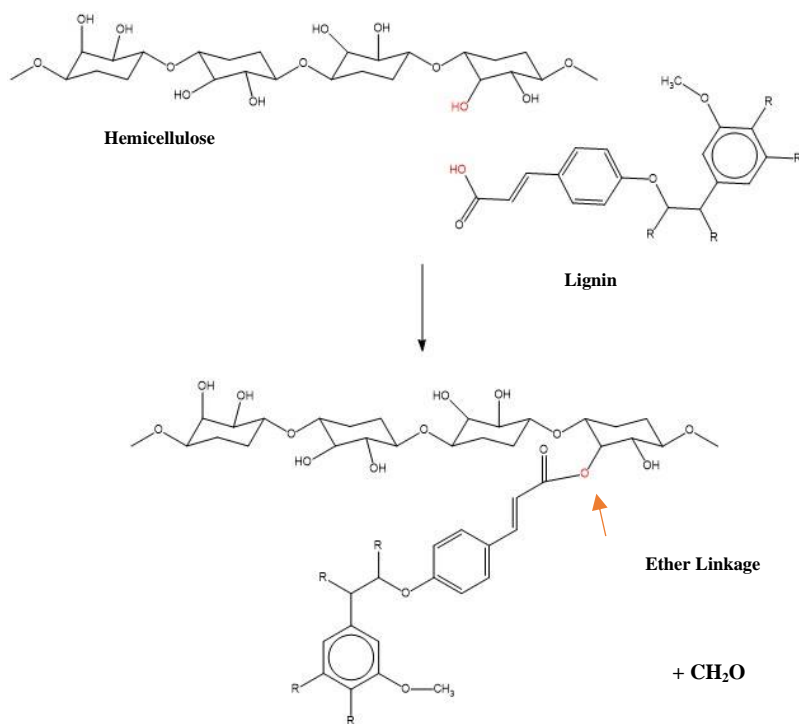


Figure 4-6 Mechanism of Lignin-Carbohydrate Complexes formation

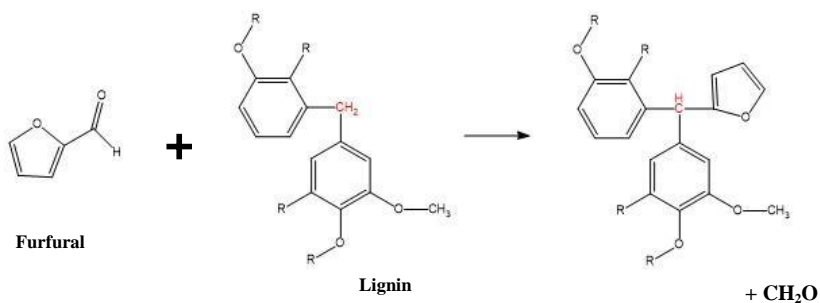


Figure 4-7 Mechanism of Lignin-Furfural Complexes formation

Lignin pyrolysis and dehydration

The lignin molecule is much more stable than hemicellulose, but a few chemical bonds can be modified at high temperatures (Kawamoto et al., 2007). Generally, chemical changes happen based on the fragment of HO-C-C-C-OH and the middle carbon atom bond to phenyl by β -O-4 linkage (a kind of ether linkage) or directly.

β -O-4 linkage detaches the fragment from the middle carbon atom at high temperature, which leads to the lignin chain breaking into two pieces. The breaking end of the two pieces form a hydroxyl group (-OH) and alkene group (C=C), respectively, (Figure 4-8 upside). In addition, phenyl can break up the fragment, forming a hydroxyl group (-OH) and alkene group (C=C) on the two breaking ends (Figure 4-9 upside).

Two hydroxyl groups of the fragment may condense to the alkene group (Figure 4-8 downside and Figure 4-9 downside), which is known as a dehydration reaction. After dehydration, the alkene group on the single lignin chain provides a suitable part for lignin cross-linking. The dehydration reaction of lignin contributes to an increase in the alkene group and a decrease in the hydroxyl one.

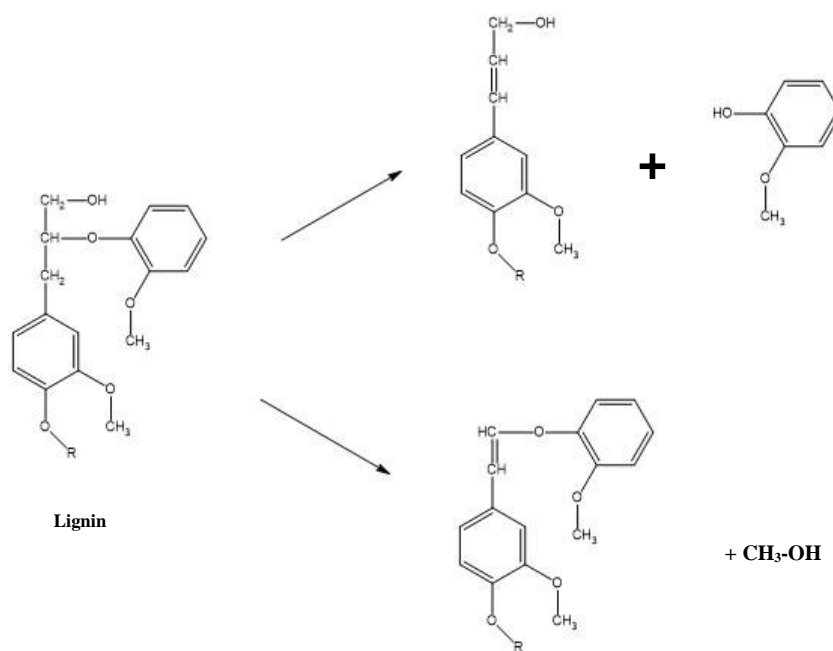


Figure 4-8 Mechanism of Lignin Pyrolysis I

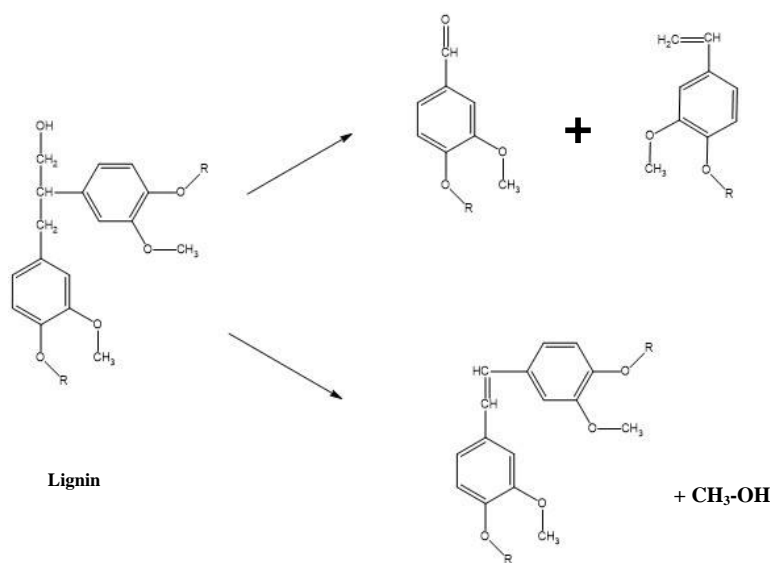


Figure 4-9 Mechanism of Lignin Pyrolysis II

Oxidation

Hydroxyl groups of hemicellulose or lignin can be oxidised from the C-OH group to the C=O group and water (Figure 4-10) (Kärkäs et al., 2016). Oxidation leads to an increase in the carbonyl group and a reduction in the hydroxyl group.

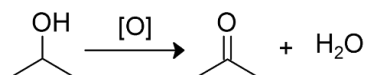


Figure 4-10 Mechanism of Hydroxyl Group Oxidation

Hydrolysis

Heat treatment process is run immediately after drying and theoretically, there is no moisture content at the beginning of it. However, water can be formed during lignin condensation II, lignin-hemicellulose condensation and dehydration on lignin or hemicellulose reaction. The new water could cause the hydrolysis of an ether group (C-O-C) (Figure 4-11). In fact, condensation and hydrolysis is considered as being reversible reactions.

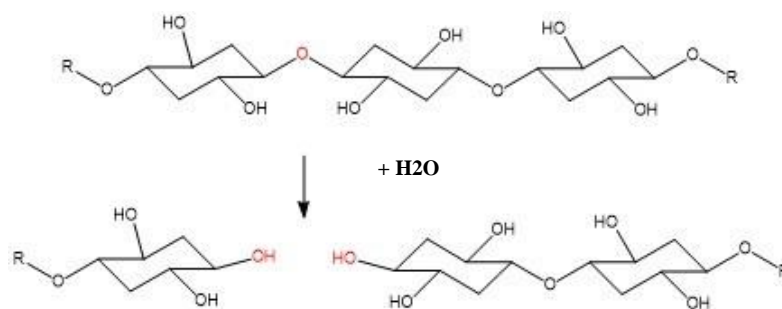


Figure 4-11 Mechanism of hydrolysis

To sum up all the chemical reactions, the changes during heat treatment could be distinguished by functional groups. However, their changes are complex in that a few groups increase with one chemical change but decrease with another (Table 4-1). Hence, FTIR composition analysis should be incorporated with mass loss change, equilibrium moisture content change and the treatment environment.

Table 4-1 Chemical Functional Group Changes and the Corresponding FTIR

Chemical Reaction	Location	Name	Functional groups	Content Change	FTIR Peak
Deacetylation	Hemicellulose	Carbonyl	C=O	↓	Peak 1730
		Alkene	C=C	↑	Peak 1595
Hemicellulose Pyrolysis	Hemicellulose	Carbonyl	C=O	↑	Peak 1730
		Alkene	C=C	↑	Peak 1595
		Others		↓	Peak 1226 to 1507
Condensation I	Lignin	Ether	C-O-C	↓	Peak 1154
		-	C-C	↑	Peak 1054
Condensation II	Lignin	Ether	C-O-C	↑	Peak 1154
		Hydroxyl	-OH	↓	Peak 3336
Cross-linking	Lignin	Alkene	C=C	↓	Peak 1595
		-	C-C	↑	Peak 1054
		Carbonyl	C=O	↓	Peak 1730
Lignin-carbohydrate complexes	Lignin	Hydroxyl	-OH	↓	Peak 3336
	Hemicellulose	Ether	C-O-C	↑	Peak 1154
	Lignin	Carbonyl	C=O	↓	Peak 1730

Lignin-Furfural Complexes	Furfural	Methylene	C-H	↑	Peak 2938
		-	C-C	↑	Peak 1054
Lignin Pyrolysis	Lignin	Hydroxyl	-OH	↓	Peak 3336 and 1110
		Alkene	C=C	↑	Peak 1595
		-	C-C	↓	Peak 1054
		Ether	C-O-C	↓	Peak 1154
Lignin dehydration	Lignin	Hydroxyl	-OH	↓	Peak 3336 and 1110
		Alkene	C=C	↑	Peak 1595
		-	C-H	↓	Peak 1025
Oxidation	Lignin	Hydroxyl	-OH	↓	Peak 3336
	Hemicellulose	Ketone	C=O	↑	Peak 1730
Hydrolysis	Hemicellulose	Hydroxyl	-OH	↑	Peak 3336
		Ether	C-O-C	↓	Peak 1154

4.2 Chemical Composition Change of the Natural Ageing Process

The FTIR spectra illustrate a few differences in functional groups between new and old pine, which indicates that chemical changes happen during the natural ageing process. As discussed in chapter 3.1, chemical composition changes of ageing are affected by the environment, the environment is introduced.

On the FTIR spectrum (Figure 4-12 and Table 4-2), the increase in ether linkage (C-O-C, Peak 1154) and the decrease in hydroxyl groups (-OH, peak 1110) of 580 year old pine illustrate condensation between the hydroxyl groups. Lignin condensation II (Figure 4-4) or lignin-carbohydrate complexes (Figure 4-6) cause the change. A decrease in the hydroxyl groups also leads to a fall in the moisture content. Lignin cross-linking might happen during the natural ageing process due to a slight decrease in the C-H bond (Peak 1421 and Peak 1456) and slight increase in the carbonyl (C=O, Peak 1730) and alkene groups (C=C, Peak 1595). Hence, condensation and lignin cross-linking happen, which extends and/or expands molecule chains of old pine timber.

Hemicellulose is decomposed after a long period of natural ageing due to the decrease in all the peak relating to its functional groups, namely Peak 1054 and Peaks from 1226 to 1507 (Table 4-2). The carbonyl group (C=O, Peak 1730) and alkene group (C=C, Peak 1595) increase significantly in the FTIR spectrum of old pine. These peak changes indicate a few complex chemical reactions during natural ageing. Firstly, decomposition of hemicellulose leads to more decomposition products, which contain abundant carbonyl and alkene groups (Figure 4-2). Hemicellulose experiences a joint condensation and decomposition reaction during natural ageing. Secondly, the deacetylase of hemicellulose (Figure 4-1) and dehydration of lignin (below of Figure 4-8 and Figure 4-9) are responsible for the increase in the alkene group (C=C). Finally, the decrease in the hydroxyl groups could be also due to as oxidation reaction which is attributed to an increase of the carbonyl group (C=O) (Figure 4-10).

Ether linkage, the carbonyl group and the alkene group increase in the process of natural ageing, which indicates that these three functional groups are the most stable groups in timber.

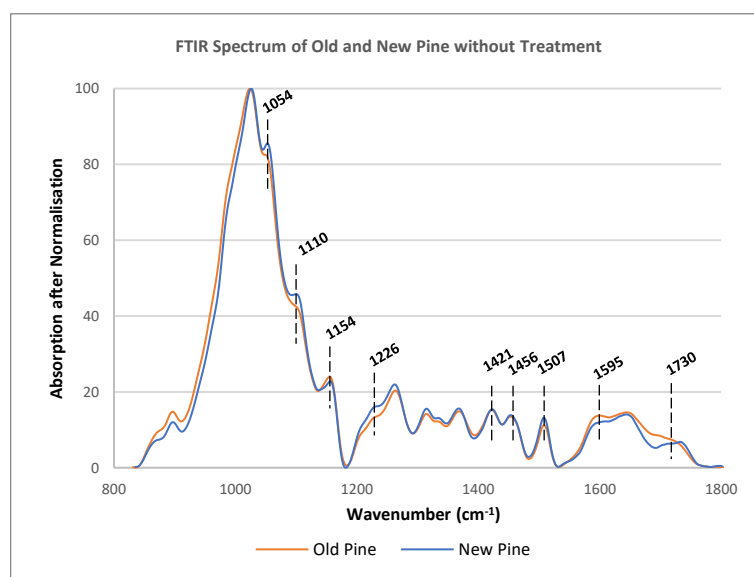


Figure 4-12 FTIR Spectrum of Non-Treated New and Old Pine

Table 4-2 FTIR Peak area of New and Old Pine without Treatment

	Peak 1054	Peak 1110	Peak 1154	Peak 1204	Peak 1226	Peak 1262	Peak 1318
new	146	1052	610	116	432	895	494
old	85	905	634	82	385	813	450
	Peak 1335	Peak 1366	Peak 1421	Peak 1456	Peak 1507	Peak 1595	Peak 1730
new	92	650	568	425	288	355	480
old	75	723	559	389	275	408	534

4.3 Equilibrium Moisture Content Change During Heat Treatment

The ability of timber to absorb moisture is based on the hydrogen bonds between its timber molecules and moisture. The equilibrium moisture content (EMC) can illustrate the moisture composition of the timber molecule indirectly.

4.3.1 EMC Changes of New and Old pine

The EMC of new pine and old pine at 20°C with 65% humidity is 10.5% and 10%, respectively. Boonstra and Tjeerdsma (2006) and Esteves et al. (2008) reported that lignin cross-linking and condensation contribute to the decrease in the EMC. On the FTIR spectrum, decomposition, condensation, cross-linking and oxidation reactions on old pine can be observed (Figure 4-12), with all the reactions being based on the activity of hydroxyl group. Hence, hydroxyl groups or hydrogen atoms are responsible for the EMC. Similar results were reported by Jämsä and Viitaniemi (2001).

Figure 4-13, Table 4-3 and Figure 4-14 shows the EMC changes after heat treatment in different atmospheres. The EMC of new pine at 120°C changes slightly at 10.5% after 24 hours heat treatment. However, it is reduced significantly with temperature rising and oxygen content. In the treatment at 200°C, EMC reduce to 5.3% and 6% in air and vacuum respectively. At 160°C treatment, after 24 hours, the EMC drops to 8.2% and 8.5% in air

and vacuum, respectively. The EMC of old samples during heat treatment have same trends as with the new (Figure 4-15, Table 4-4 and Figure 4-16).

Chemically, Jämsä and Viitaniemi (2001) reported that EMC is affected by hydroxyl groups on the molecule due to hydrogen bonding with water. However, whilst the FTIR spectrum of the treatment at 120°C of the new (Figure 4-23 and Figure 4-29) and old pine (Figure 4-36 and Figure 4-40) clearly show a hydroxyl group decrease due to condensation, the moisture content is less affected. Hence, the hydroxyl group is not the only functional group affecting EMC. Any functional groups containing hydrogen atoms may also bond with water by hydrogen bonding, where the reduction of the EMC will be due to a hydrogen atom decrease.

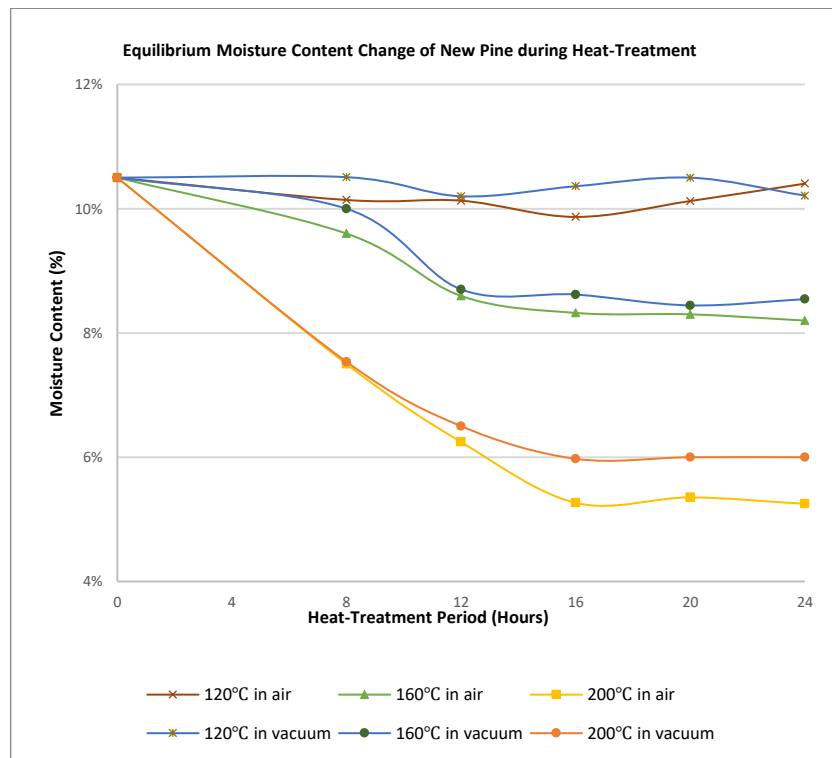


Figure 4-13 Equilibrium Moisture Content Change of New Pine during Heat-Treatment

Table 4-3 EMC Change and Standard Deviation of New Pine during Heat-Treatment

Treatment Period	Treatment in Vacuum			Treatment in Air			
	Temperature	120°C	160°C	200°C	120°C	160°C	200°C
0	EMC	10.50%					
	Standard Deviation	0.33%					
8	EMC	10.44%	10.27%	7.51%	10.11%	9.84%	8.17%
	Standard Deviation	0.37%	0.40%	0.45%	0.35%	0.34%	0.36%
12	EMC	10.10%	8.72%	6.10%	10.10%	8.57%	6.22%
	Standard Deviation	0.36%	0.37%	0.53%	0.33%	0.37%	0.14%
16	EMC	10.28%	8.56%	5.97%	10.01%	8.29%	5.30%
	Standard Deviation	0.67%	0.40%	0.27%	0.37%	0.33%	0.21%
20	EMC	10.60%	8.48%	6.12%	10.12%	8.30%	5.38%
	Standard Deviation	0.33%	0.36%	0.42%	0.34%	0.32%	0.26%
24	EMC	10.16%	8.48%	6.20%	10.38%	8.38%	5.61%
	Standard Deviation	0.41%	0.43%	0.51%	0.49%	0.34%	0.27%

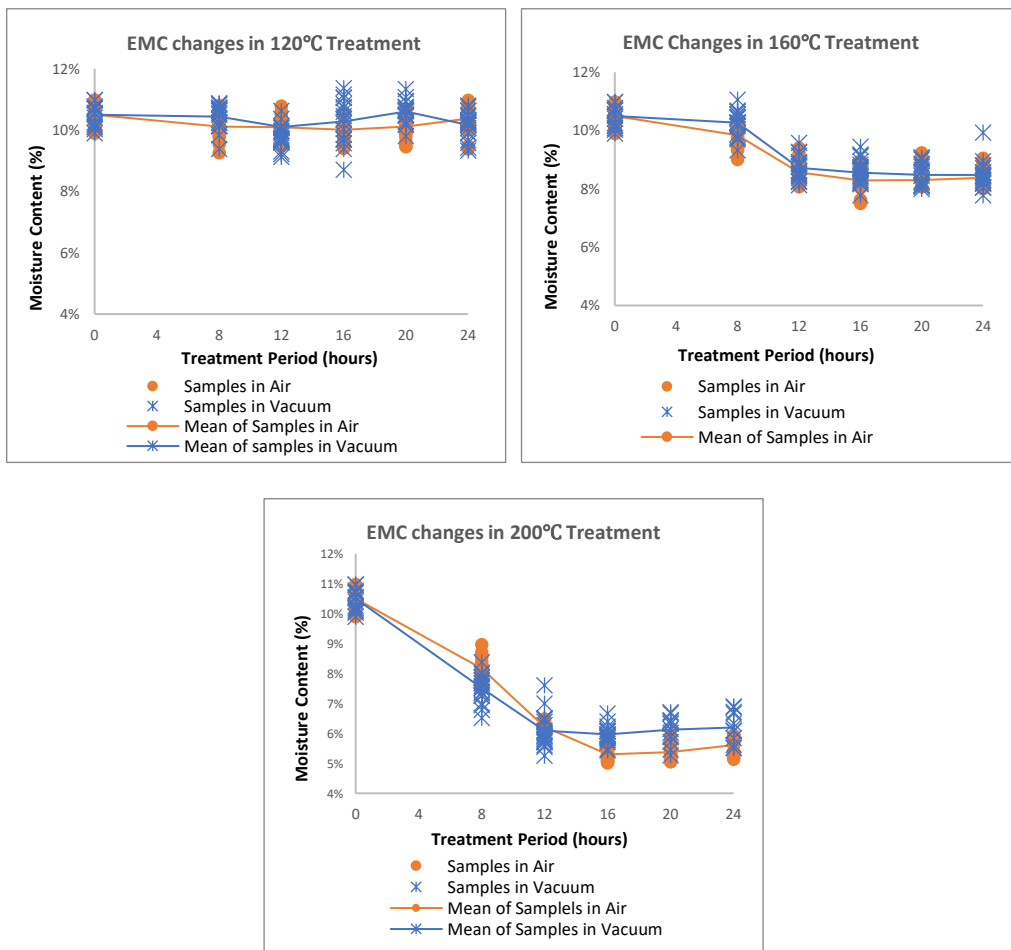


Figure 4-14 Equilibrium Moisture Content Variation of New Pine during Heat-Treatment

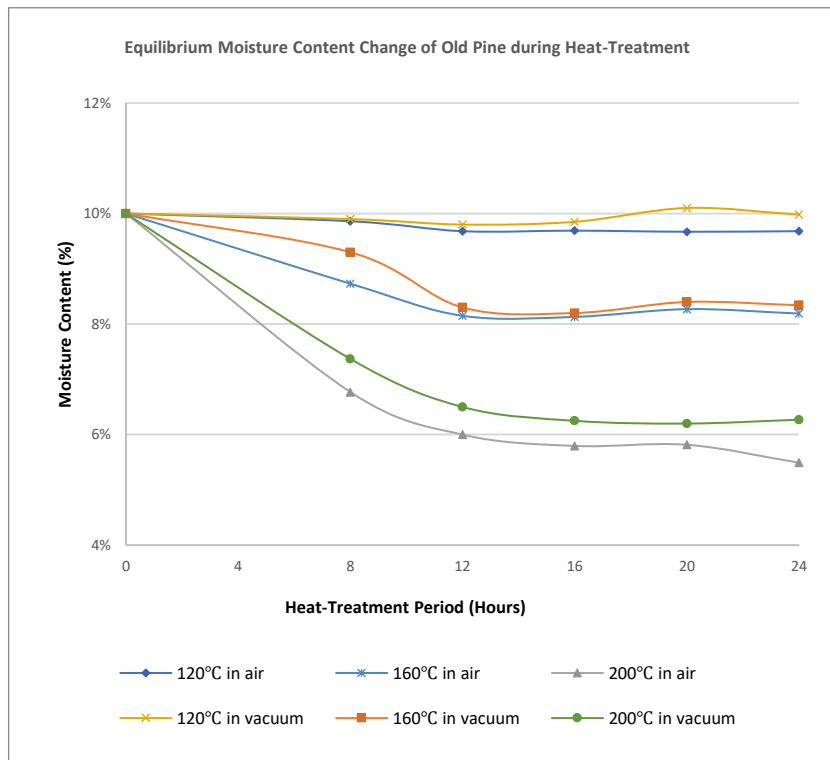


Figure 4-15 Equilibrium Moisture Content Change of Old Pine during Heat-Treatment

Table 4-4 EMC Change and Standard Deviation of Old Pine during Heat-Treatment

Treatment Period	Treatment in Vacuum			Treatment in Air			
	Temperature	120°C	160°C	200°C	120°C	160°C	200°C
0	EMC	10.00%					
	Standard Deviation	0.33%					
8	EMC	9.90%	8.73%	7.37%	9.86%	9.30%	6.77%
	Standard Deviation	0.26%	0.12%	0.65%	0.33%	0.24%	0.36%
12	EMC	9.80%	8.15%	6.50%	9.68%	8.30%	6.00%
	Standard Deviation	0.26%	0.42%	0.27%	0.20%	0.24%	0.21%
16	EMC	9.85%	8.13%	6.25%	9.69%	8.20%	5.80%
	Standard Deviation	0.49%	0.26%	0.26%	0.37%	0.39%	0.14%
20	EMC	10.10%	8.27%	6.20%	9.67%	8.40%	5.82%
	Standard Deviation	0.51%	0.25%	1.42%	0.72%	0.60%	0.06%
24	EMC	9.98%	8.19%	6.27%	9.68%	8.34%	5.49%
	Standard Deviation	0.26%	0.46%	0.33%	0.13%	0.34%	0.22%

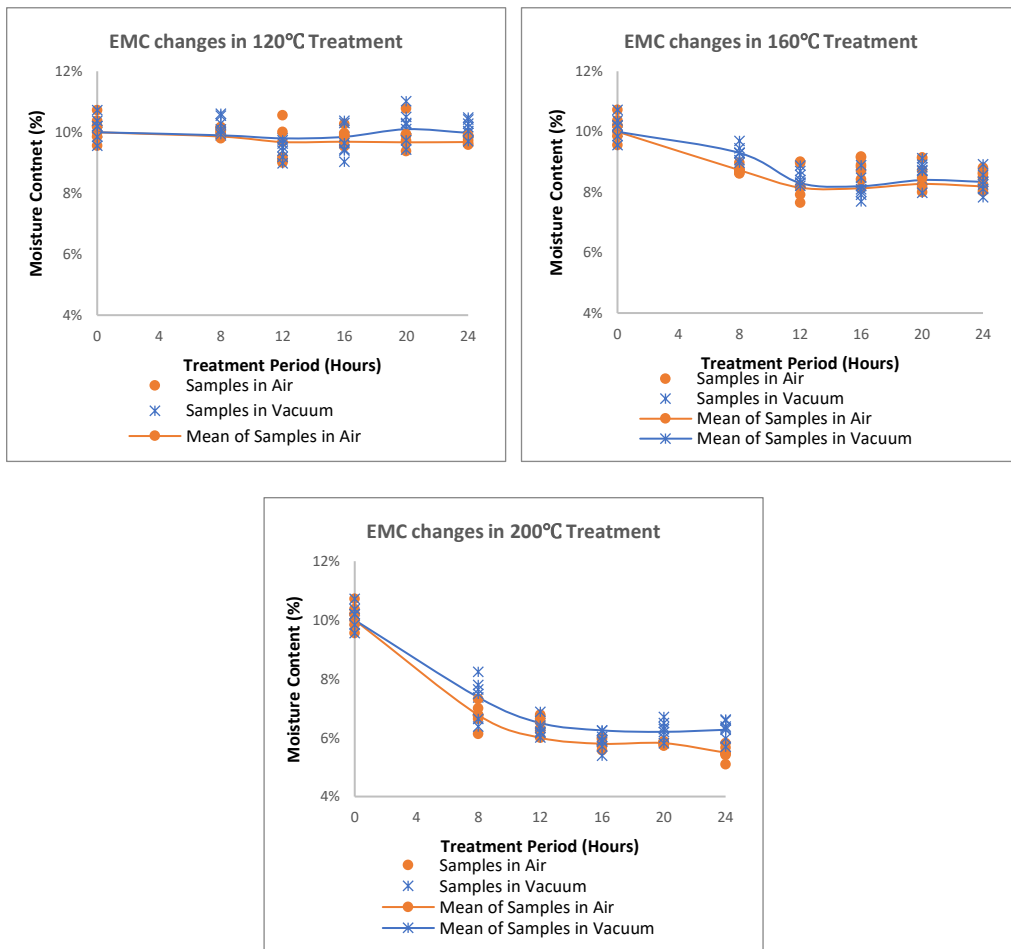


Figure 4-16 Equilibrium Moisture Content Error of Old Pine during Heat-Treatment

4.3.2 Moisture Content Related to FTIR

Marchessault (1962) and Fengel and Wegener (1984) indicated that Peak 1642 is affected by water absorption, thus having a high relationship with moisture content. Figure 4-17 shows the relationship between the size of Peak 1642 and moisture content of both new and old pine during heat treatment. The moisture content (MC) can be calculated by the size of peak 1642 on the FTIR spectrum, and the curve is fitted by Origin with COD (R^2) = 0.8:

$$MC = (6.69494E - 10) \times Wv_{1642}^{2.774}$$

Where, $W_{v_{1642}}$ is peak area of 1642.

The MC is measured at 20°C with 65% humidity and different values in these different results for the EMC. Hence, the mathematic model has more potential for predicting moisture content than oven drying method by FTIR spectrum.

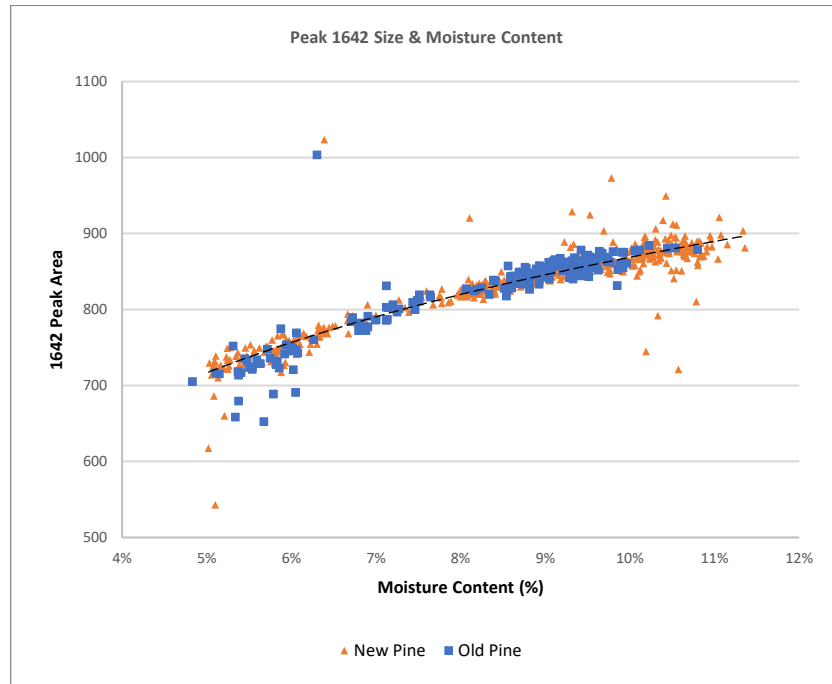


Figure 4-17 Relationship between Peak 1642 Area and Moisture Content

4.4 Mass Loss of New and Old Timber During Heat Treatment

Bourgois and Guyonnet (1988) and Tjeerdsma et al. (1998) demonstrated that hemicellulose pyrolysis is responsible for mass loss, because few pyrolysis products are gas or liquid, which release out of the sample. On the FTIR spectrum, the peaks from 1226 to 1507 are related to hemicellulose and a decrease in the indicates hemicellulose pyrolysis.

The mass loss of new pine during heat treatment in air is higher than it is in a vacuum atmosphere and increases with temperature and treatment period (Figure 4-18, Table 4-5 and Figure 4-19). It reaches the highest loss at approximately 14.5% after 24 hours

treatment at 200°C in air, whereas this only approximately 8% in a vacuum. For 160°C and 120°C treatment, mass loss both in air and a vacuum are between 2% to 4%, with the loss in the former being slightly higher. In the treatment in air, the hydroxyl group (C-OH) is oxidised to the carbonyl one (C=O) (Figure 4-10). One hydrogen atom is attracted by oxygen to form a water molecule and hence, the oxidation reaction leads to more mass loss. In addition, oxygen promotes hemicellulose pyrolysis by a series of chemical changes.

For old pine, the mass decreases with temperature and oxygen content (Figure 4-20, Table 4-6 and Figure 4-21), which is the same as with new pine. Moreover, the mass loss is less than for new timber at 120°C, but more at 200°C treatment. The highest and lowest mass loss of 19% and 1.42% happen at 200°C treatment in air and 120°C treatment in a vacuum after 24 hours, respectively. The chemical composition of old timber molecules resists pyrolysis at 120°C due to hemicellulose linked to lignin by forming lignin-carbohydrate complexes during the natural ageing process (Figure 4-6) (Watanabe et al., 1989). However, hemicellulose cannot resist the energy at 200°C treatment and so, is largely pyrolysed (Figure 4-2). Part of lignin may also be pyrolysed with the decomposition of lignin-carbohydrate complexes (Figure 4-8 and Figure 4-9). In addition, mass loss in air and vacuum atmosphere is nearly the same for 120°C and 160°C treatments, which indicates that oxygen plays less of a role in the mass loss of old pine under the latter. Timber molecules of old pine have been oxidised during the 580 years ageing process.

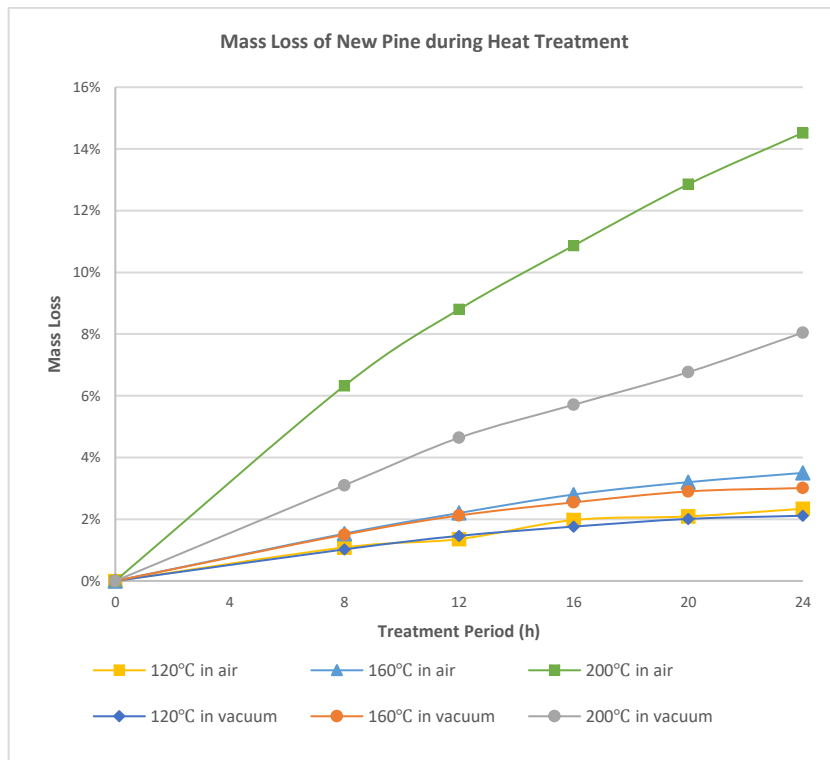


Figure 4-18 Mass Loss of New Pine During Heat Treatment

Table 4-5 Mass Loss and Standard Deviation of New Pine During Heat Treatment

Treatment Period	Treatment in Vacuum			Treatment in Air			
	Temperature	120°C	160°C	200°C	120°C	160°C	200°C
0	Mass Loss	0					
	Standard Deviation	0					
8	Mass Loss	1.02%	1.02%	4.56%	1.09%	1.53%	6.33%
	Standard Deviation	0.08%	0.40%	1.04%	0.16%	0.14%	0.96%
12	Mass Loss	1.46%	2.37%	4.64%	1.36%	2.00%	10.63%
	Standard Deviation	0.14%	0.12%	1.13%	0.12%	0.09%	1.29%
16	Mass Loss	1.76%	2.45%	5.71%	1.97%	2.50%	11.86%
	Standard Deviation	0.18%	0.14%	0.49%	0.08%	0.20%	0.73%
20	Mass Loss	2.01%	2.64%	6.76%	2.09%	2.69%	12.85%
	Standard Deviation	0.17%	0.12%	0.79%	0.36%	0.17%	1.35%
24	Mass Loss	2.11%	2.98%	8.05%	2.34%	3.21%	14.52%
	Standard Deviation	0.15%	0.09%	0.72%	0.24%	0.20%	1.62%

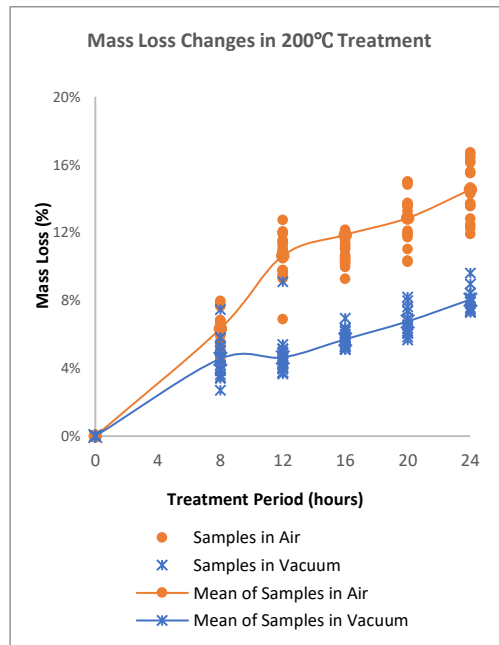
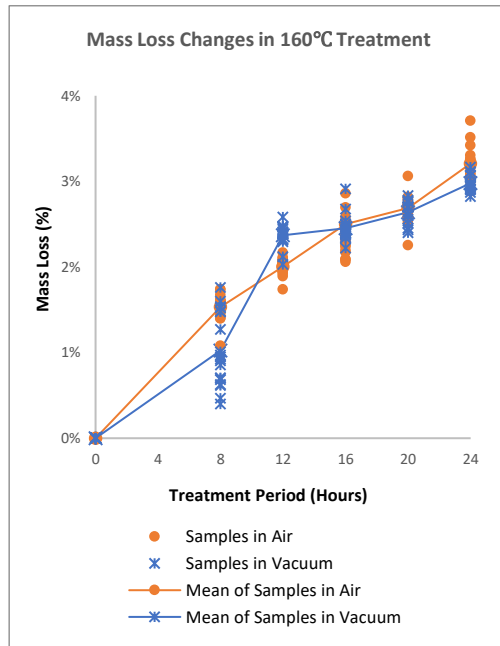
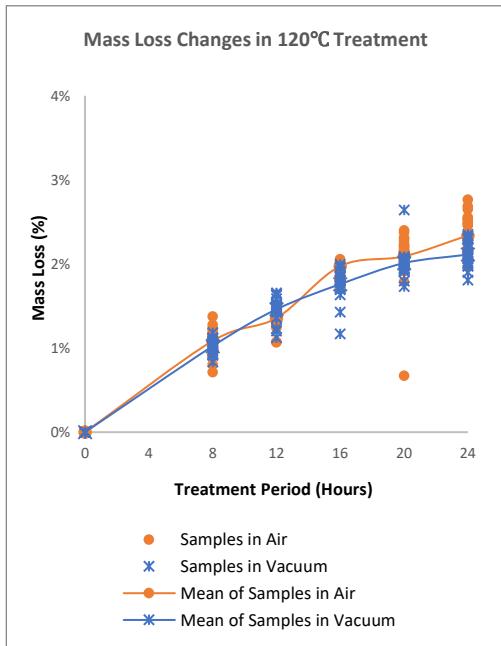


Figure 4-19 Mass Loss Variation of New Pine During Heat Treatment

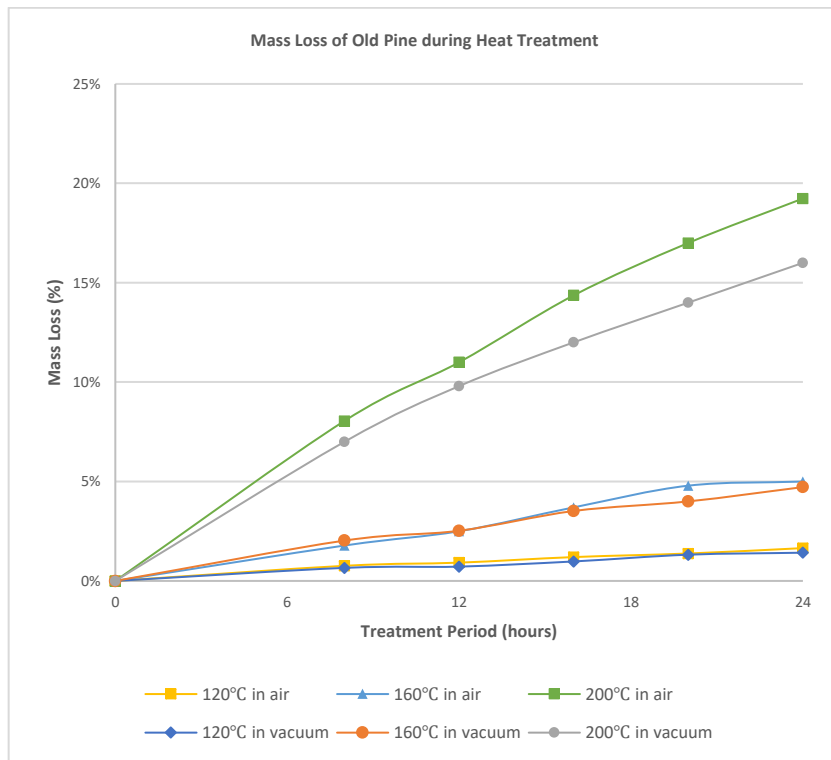


Figure 4-20 Mass Loss of Old Pine During Heat Treatment

Table 4-6 Mass Loss and Standard Deviation of Old Pine During Heat Treatment

Treatment Period	Treatment in Vacuum			Treatment in Air			
	Temperature	120°C	160°C	200°C	120°C	160°C	200°C
0	Mass Loss	0			0		
	Standard Deviation	0			0		
8	Mass Loss	0.66%	2.03%	7.00%	0.76%	1.78%	8.05%
	Standard Deviation	0.17%	0.95%	4.99%	0.18%	0.16%	3.88%
12	Mass Loss	0.72%	2.52%	9.80%	0.92%	2.50%	11.00%
	Standard Deviation	0.24%	0.69%	3.62%	0.42%	0.58%	1.75%
16	Mass Loss	0.98%	3.52%	12.00%	1.20%	3.70%	14.36%
	Standard Deviation	0.31%	2.15%	2.87%	0.23%	0.22%	1.12%
20	Mass Loss	1.32%	4.00%	14.00%	1.38%	4.79%	17.00%
	Standard Deviation	0.30%	0.33%	1.55%	0.77%	3.19%	1.73%
24	Mass Loss	1.42%	4.72%	16.00%	1.65%	5.00%	19.23%
	Standard Deviation	0.18%	2.16%	0.73%	0.79%	1.04%	2.03%

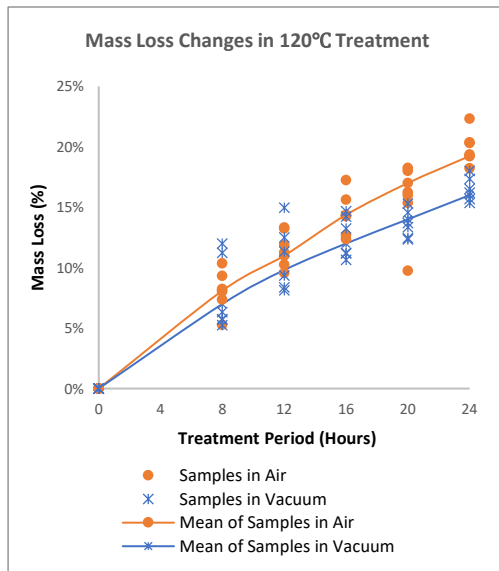
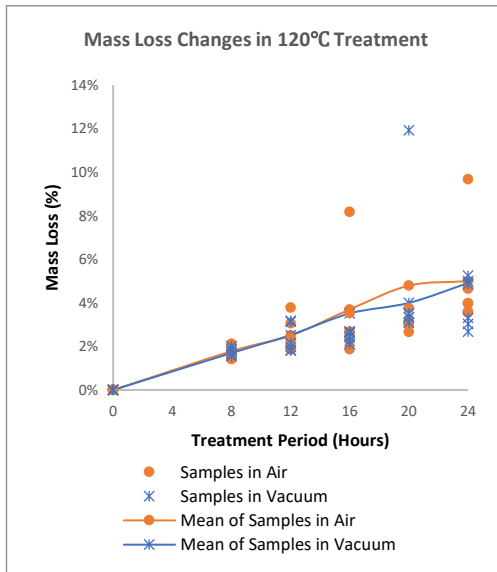
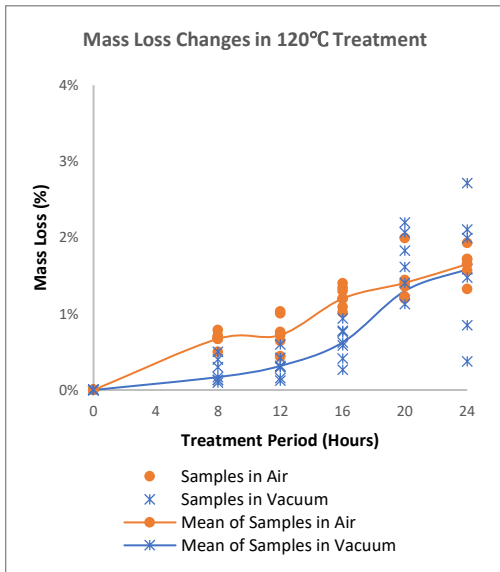


Figure 4-21 Mass Loss Variation of Old Pine During Heat Treatment

4.5 New Timber Chemical Composition Changes During Heat Treatment

New timber can be treated as a no chemical changes sample. Different temperature levels and oxygen content atmospheres can cause distinctive changes in the timber molecule, which provide a meaningful database for the timber natural ageing or accelerated ageing process.

4.5.1 New Samples in Vacuum Treatment

Figure 4-22 and Figure 4-23 shows FTIR spectrum changes of new timber at 120°C in vacuum treatment and each peak area change.

In the first 12 hours of treatment, there is an increase in the alkene group (C=C, Peak 1595) and a decrease in the carbonyl group (C=O, Peak 1730), which indicates deacetylase reactions on hemicellulose (Figure 4-1). Deacetylase is the first stage of hemicellulose pyrolysis to form acetic acid (CH₃COOH), which is released out of the sample. Decreases in Peak 1226, Peak 1262, Peak 1456, and Peak 1595 related to C-C, C-O, C-H, and COO⁻ functional groups, respectively, also demonstrate that deacetylase reaction happens. The alkene group increase may also be due to dehydration of lignin (Figure 4-8 and Figure 4-9). After 12 hours, the alkene group decreases along with the carbonyl group, which indicates that lignin is cross-linked during the treatment. The carbonyl (C=O) group rises again after 16 hours of treatment, which is due to slight pyrolysis in hemicellulose. Hence, the deacetylase reaction rate is slow in the 120°C treatment in a vacuum, but lignin cross-linking reaction is higher at least in the first 16 hours of treatment. Deacetylase and pyrolysis of hemicellulose contribute to 2% mass loss after 24 hours treatment.

Peak 1154 relates to an ether linkage (C-O-C) increase and Peak 110 to a significant decrease in the hydroxyl group, which indicates that this group condenses to ether linkage. Two kinds of chemical reaction are responsible for the change. Firstly, hydroxyl groups on

the lignin chain condensed as condensation II (Figure 4-4). Another explanation is that lignin and hemicellulose condensed to lignin–carbohydrate complexes (Figure 4-6). The condensation reaction extends and/or expands molecule chains and thus, enhances the stability of timber molecules.

Peak 1318 corresponding to lignin aromatic ring condensation increases, which indicates that lignin condensation I happens (Figure 4-3).

To sum up, 120°C treatment in a vacuum improves condensation and cross-linking reactions and causes low mass loss.

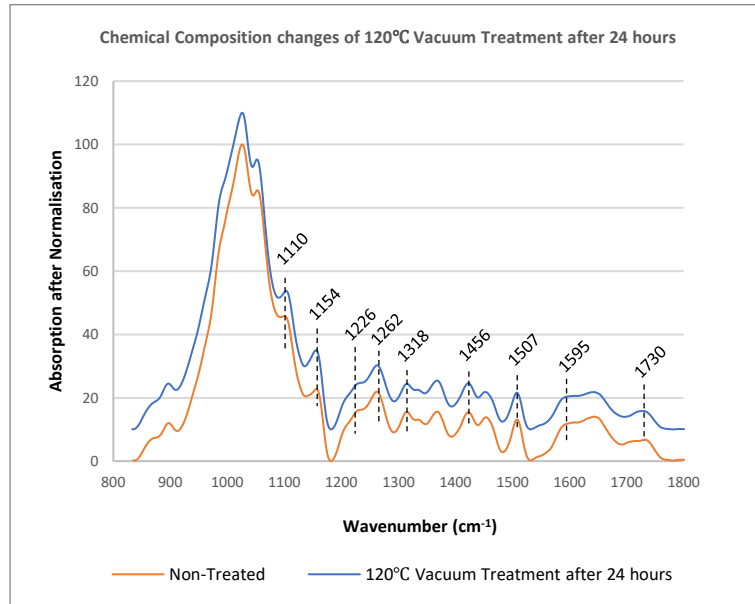


Figure 4-22 FTIR Spectrum Change of New Pine in 120°C Vacuum Treatment After 24 hours

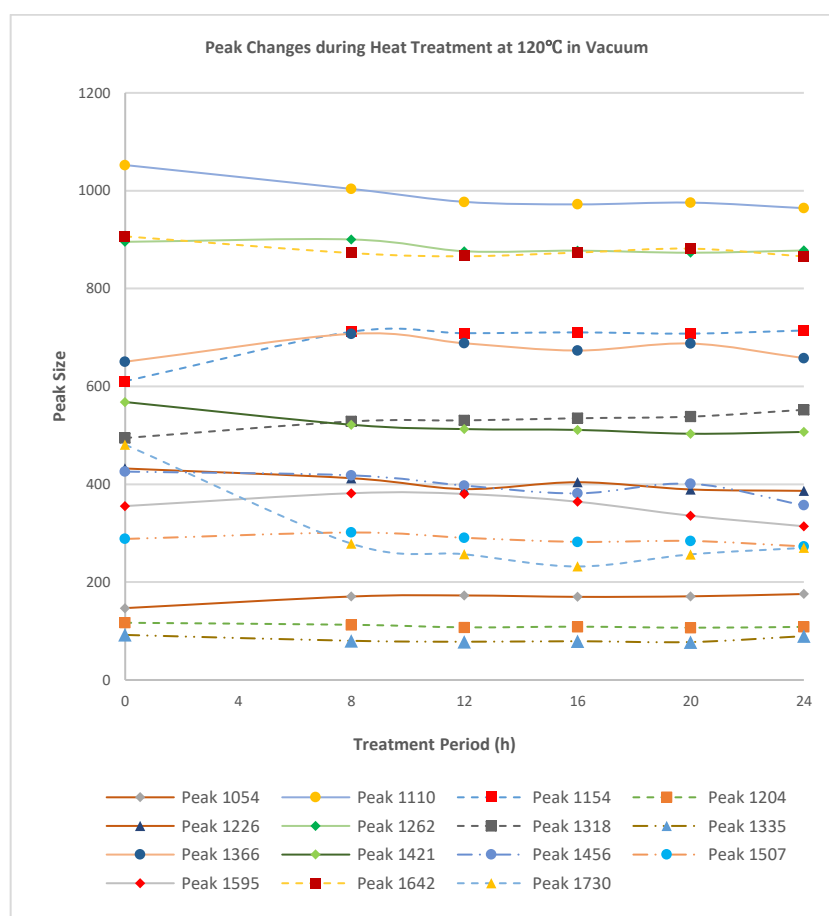


Figure 4-23 FTIR Peak Area Change of New Pine during 120°C Vacuum Treatment

At 200°C treatment, pyrolysis is the main feature due to a marked decrease in Peak 1226 to 1507 relating to the hemicellulose functional group (Figure 4-24 and Figure 4-25) after 24 hours. A few hemicellulose liquid or gas pyrolysis products evaporate out of samples, which leads to C-C, C-O, C-H and aromatic ring group reduction.

Pyrolysis products of hemicellulose (Figure 4-2) and lignin (Figure 4-8 and Figure 4-9) contain rich alkene (C=C) and carbonyl (C=O) groups, which contribute to dramatically increasing on Peak 1595 and Peak 1730, respectively. Condensed S- or G-ring lignin (Peak 1318) decreases gradually, which provides evidence that lignin is pyrolysed during heat treatment (Figure 4-8 and Figure 4-9). In the first 8 hours, the carbonyl group rate of increase is slower than between 8 and 24 hours, which indicates that lignin crosslinking

and condensation might happen in the first few hours, but the rate is much slower than that for pyrolysis. Peak 1154 relating to ether linkage (C-O-C) shows an increase after 24 hours of treatment. The increase is because ether linkage is not easy to pyrolyse. Lignin condensation II (Figure 4-4), hemicellulose linking to lignin (Figure 4-6) may happen during the treatment. Therefore, timber molecule cannot resist high temperature. The pyrolysis reaction is easily observed on the FTIR spectrum and mass loss. The alkene (C=C) and carbonyl groups (C=O) as well as ether linkage (C-O-C) are relatively stable chemical functional groups in molecules.

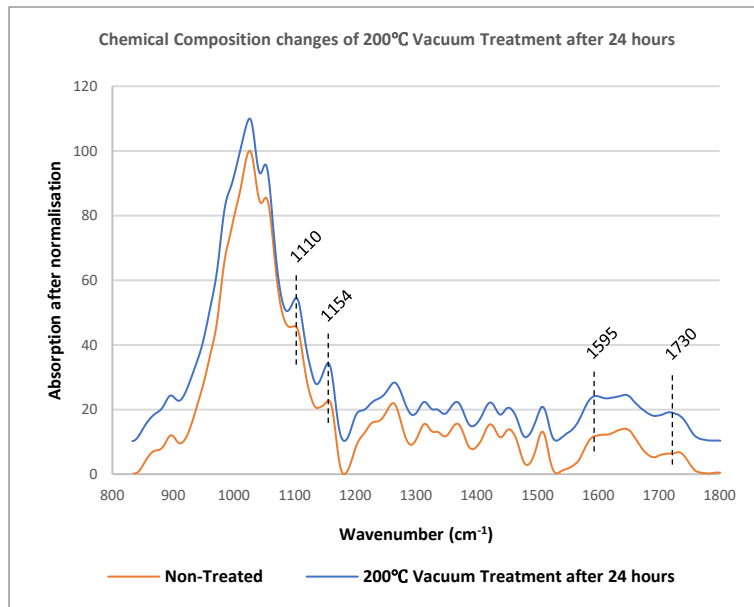


Figure 4-24 FTIR Spectrum Change of New Pine in 200°C Vacuum Treatment After 24 hours

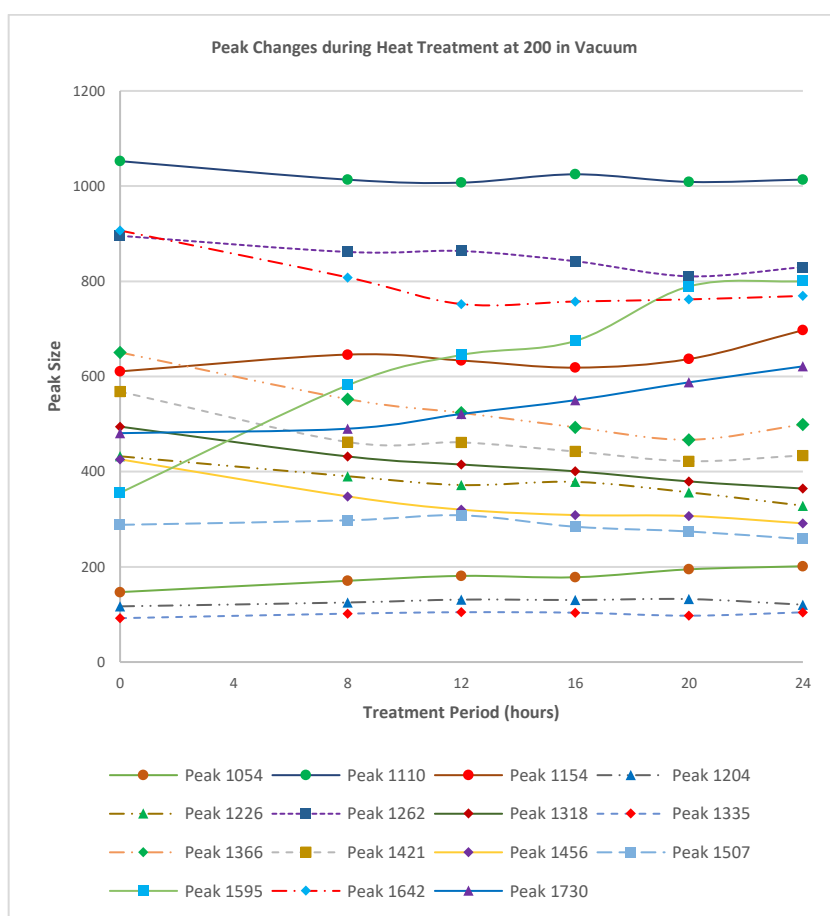


Figure 4-25 FTIR Peak Area Change of New Pine During 200°C Vacuum Treatment

Timber molecule composition changes at 160°C treatment in a vacuum are complex. Chemical changes of condensation, cross-linking and pyrolysis are observed on the FTIR spectrum, but the changing rate varies according to different treatment periods (Figure 4-26 and Figure 4-27).

The decrease in the carbonyl group (C=O, peak 1730) and increase in the alkene group (C=C, Peak 1595) in the first 16 hours are attributed to a series of chemical changes. Hemicellulose deacetylase, lignin dehydration and lignin cross-linking reaction might be responsible for the changes in the carbonyl and alkene groups. In the first 8 hours, deacetylase, dehydration and cross-linking reaction happen together. In the 8 to 16 hours treatment, Peak 1730 and Peak 1595 change quicker than in the first 8 hours, which

indicates that cross-linking is the main chemical reaction, while the deacetylase and dehydration reaction rates decrease. The pyrolysis reaction rate is stable, and the carbonyl and alkene groups increase dramatically due to pyrolysis products after 16 hours treatment. while deacetylase, dehydration and the cross-linking reaction rate are slow after 16 hours treatment.

Ether linkage (C-O-C, Peak 1154) increases but not as much as when treated at 120°C. Lignin-hemicellulose condensation (Figure 4-6) and lignin condensation II (Figure 4-4) and hemicellulose pyrolysis happen together in the treatment. In the first 8 hours of treatment, Peak 1154 (ether linkage) and Peak 1110 (hydroxyl group) changes greatly while the mass loss is less than 2%, which demonstrates that the condensation reaction relates to the hydroxyl group being in a dominant position in the first 8 of hours treatment at 160°C treatment.

Peak 1318 relates to condensation of G- or S- lignin units increasing in the first 16 hours due to lignin condensation I (Figure 4-3), then following this there is decrease due to pyrolysis of lignin.

Consequently, 160°C is a temperature for improving all chemical changes in timber. In the first few hours, condensation and cross-linking reaction are the main reactions, but these rates are slower than pyrolysis after 16 hours treatment.

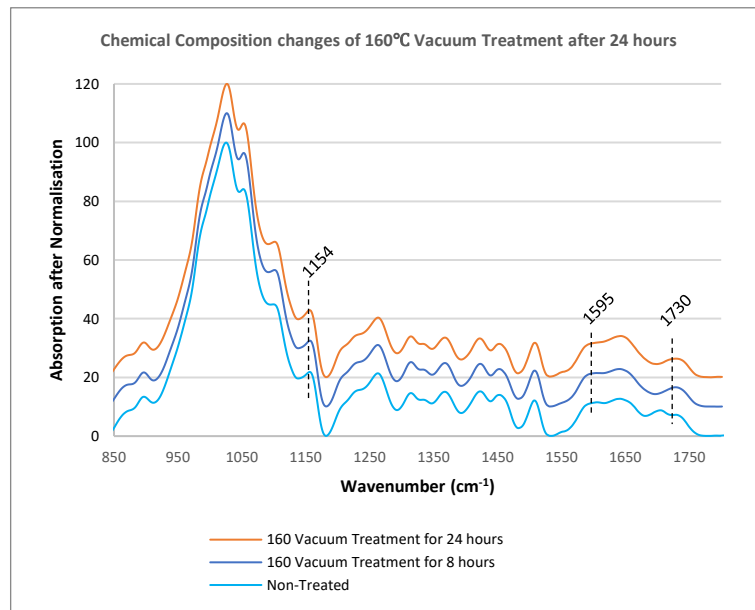


Figure 4-26 FTIR Spectrum Change of New Pine in 160°C Vacuum Treatment after 24 hours

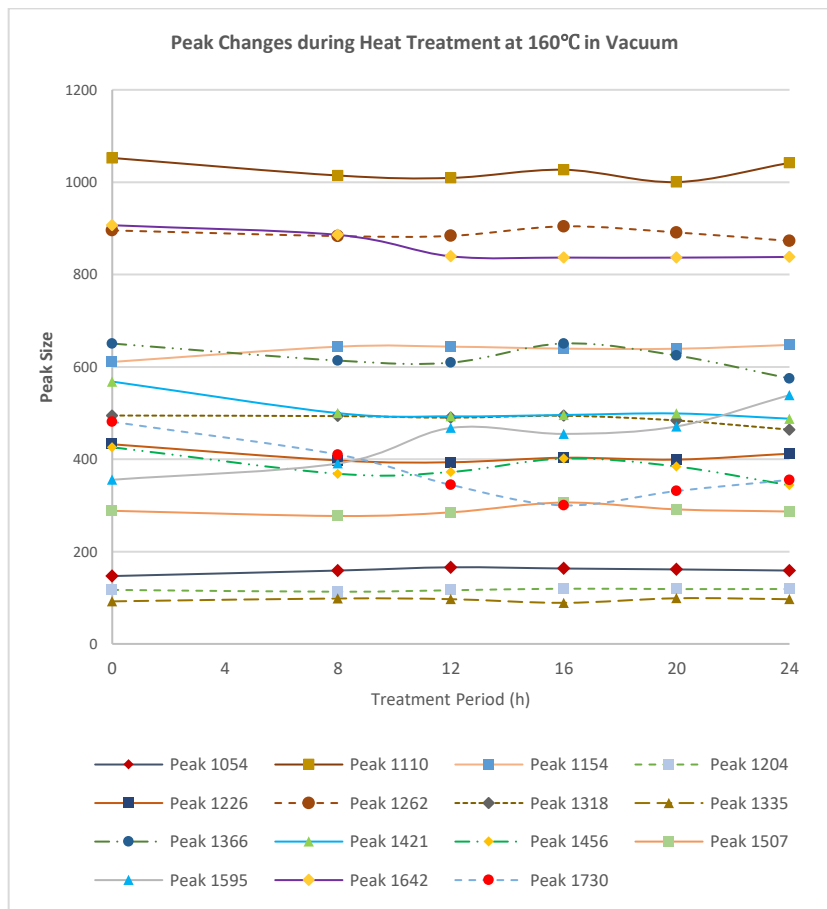


Figure 4-27 FTIR Peak Area Change of New Pine during 160°C Vacuum Treatment

4.5.2 New Samples in Air Treatment

With the treatment at 120°C in air (Figure 4-28 and Figure 4-29), generally, the peak changes are the same as for vacuum treatment at 120°C, despite oxygen being involved. Both the change of the carbonyl group (C=O, Peak 1730) in air and in a vacuum are the same, which clearly indicates deacetylase and cross-linking reactions, so oxidation reaction might not affect the two reactions. However, all the peaks from 1226 to 1507 relating to hemicellulose decrease a bit more than in a vacuum, especially in the first 8 hours of treatment. Hence, oxygen improves hemicellulose deacetylase and pyrolysis. In terms of chemical change rate in the first 8 hours of treatment, both the carbonyl and alkene groups decrease slightly, which demonstrates that the cross-linking reaction rate is higher than that for deacetylase. The alkene group starts to increase after 8 hours treatment, which means that the lignin cross-linking reaction tends to slow.

Peak 1154 relates to an ether linkage (C-O-C group) increase, while Peak 1110 pertains to the hydroxyl group decreasing dramatically in the first 8 hours of treatment. Lignin condensation II (Figure 4-4) and lignin-hemicellulose condensation (Figure 4-6) are responsible for the change. Lignin condensation I (Figure 4-3) also happens in the first 8 hours due to Peak 1318 (condensed S- or G-ring on lignin) increasing. After 8 hours treatment, condensation reaction is slow due to a slight change in Peak 1154 and Peak 1318. In summary, 120°C treatment in air leads to similar changes in timber as in a vacuum, but slightly greater pyrolysis results in 0.2% more mass loss.

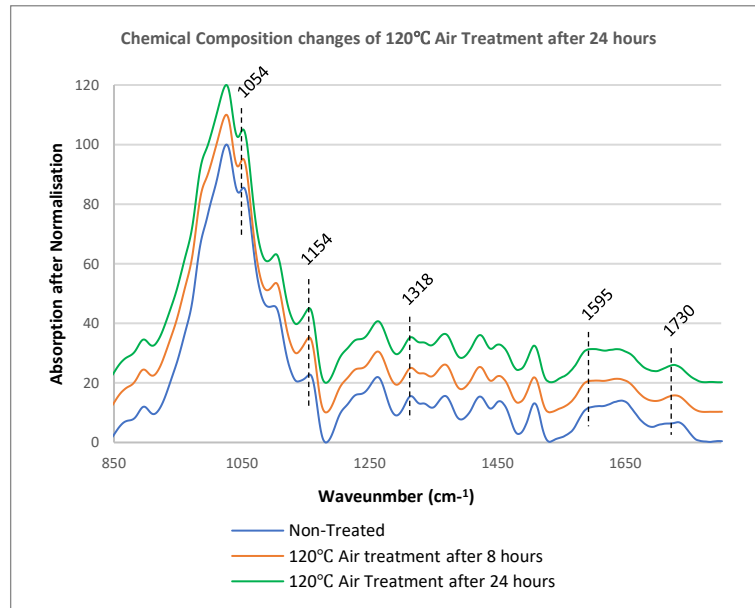


Figure 4-28 FTIR Spectrum Change of New Pine in 120°C Air Treatment After 24 hours

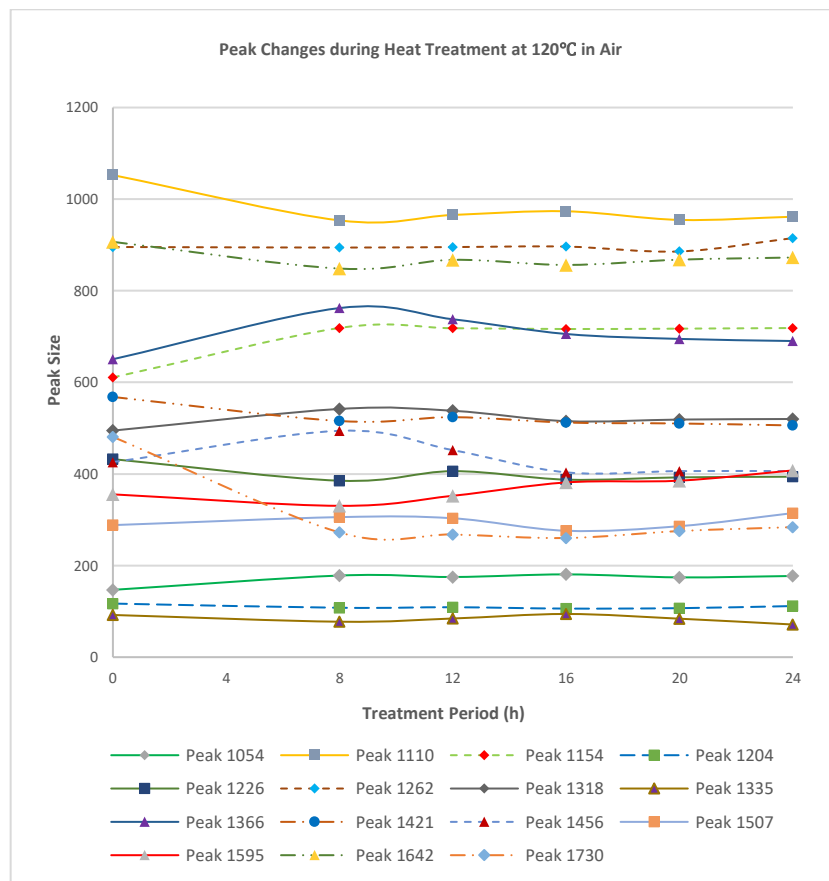


Figure 4-29 Peak Area Change of New Pine During 120°C Air Treatment

All chemical changes of 160°C treatment in air are more significant and quicker than with 120°C treatment (Figure 4-30 and Figure 4-31), leading to 3.5% mass loss after 24 hours.

A decrease in the carbonyl group (C=O, Peak 1730) and an increase in the alkene group (C=C, Peak 1595) in the first 8 hours treatment illustrates that hemicellulose deacetylation and lignin cross-link reactions happen together, with the former being the greater. Hence, compared with 120°C treatment in the first 8 hours, 160°C treatment improves deacetylation, but does not affect or suppress the cross-linking of lignin. The carbonyl group and alkene group increase significantly after 8 hours, which is attributed to pyrolysis.

Lignin condensation I (Figure 4-3), condensation II (Figure 4-4) and lignin-hemicellulose condensation (Figure 4-6) are observed due to an increase in ether linkage (C-O-C, Peak 1154) and the C-C bond (Peak 1054), especially in the first 8 hours of treatment. Lignin-furfural condensation (Figure 4-7) also happens, but in a low rate. The decrease in Peak 1110 relates to the hydroxyl group, which also indicates hydroxyl group condensation.

Lignin S- and G-ring condensation happens in the first 8 hours of treatment due to the increase in Peak 1318. However, pyrolysis of hemicellulose and lignin lead to a decrease in the peak after 8 hours treatment.

After 8 hours treatment, the carbonyl group increases significantly than under vacuum treatment. Oxidation and pyrolysis reactions are responsible for this increase.

The treatment at 160°C is more complex than for a vacuum due to the oxygen involved into the chemical reactions. Oxygen can oxidise hydroxyl groups and inhibit the reactions relating to the hydroxyl group, such as condensation II. Condensation I and a cross-linking reactions happen significantly in the first few hours of treatment. Pyrolysis reaction is the main one in the following period and leads to a 4% mass loss.

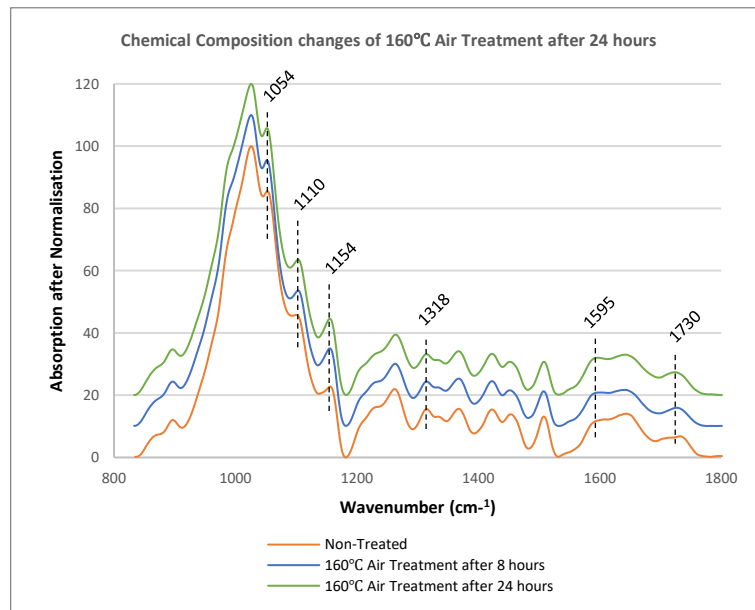


Figure 4-30 FTIR Spectrum Change of New Pine in 160°C Air Treatment After 24 hours

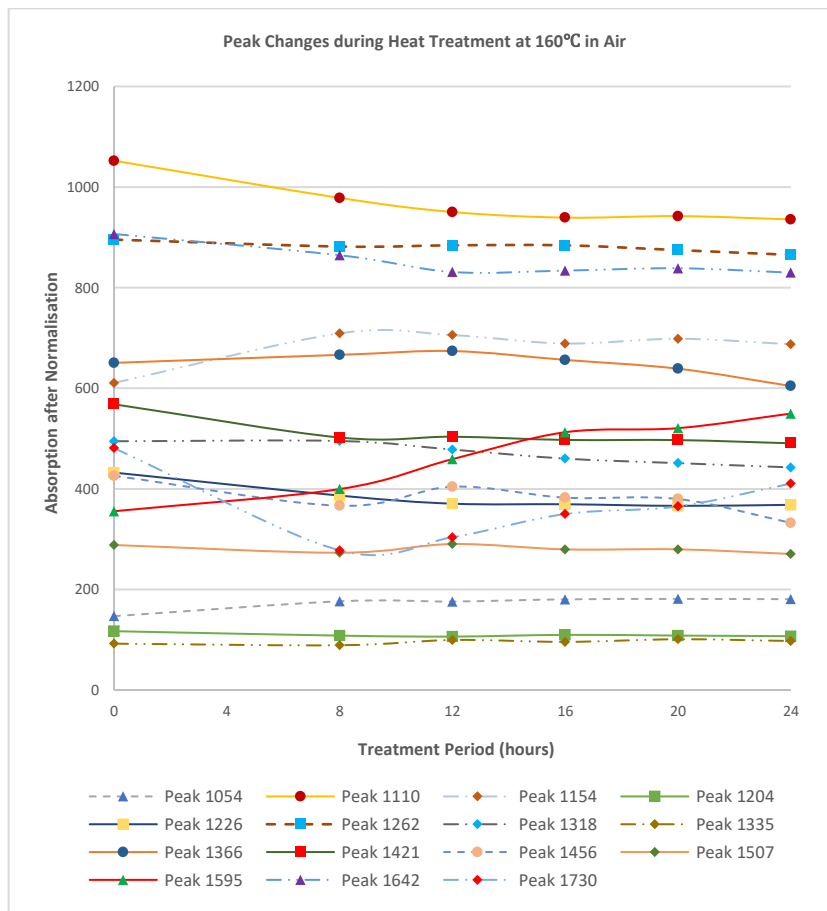


Figure 4-31 Peak Area Change of New Pine during 160°C Air Treatment

In heat treatment at 200°C in air (Figure 4-32 and Figure 4-33), pyrolysis of hemicellulose and part of the lignin is the dominant reaction due to the decrease in Peak 1226 to 1507, which results in 14.5% mass loss after 24 hours.

Peak 1595 (C=C alkene group) increases in the first 8 hours treatment, but the rate is much slower than from 8 to 16 hours. Hence, apart from a pyrolysis reaction, lignin cross-linking may happen in the first few hours of treatment. Peak 1730 (C=O, carbonyl group) increases dramatically due to massive creation of pyrolysis products. In addition, the hydroxyl group substantially decreases, which is more than with the treatment at 200°C in a vacuum. An oxidation reaction (Figure 4-10) of the hydroxyl group is also responsible for the carbonyl group increasing. As a result, lignin condensation II (Figure 4-4) and lignin-hemicellulose condensation (Figure 4-6) occur less due to a decrease in the hydroxyl group.

The peak area of ether linkage (C-O-C, Peak 1154) is not changed during 200°C treatment. Ether linkage content reaches a balance due to interactions of lignin condensation II (Figure 4-4) Lignin-hemicellulose condensation (Figure 4-6), pyrolysis of hemicellulose (Figure 4-2) and lignin (Figure 4-8).

The highest temperature treatment in air leads to the largest mass loss due to pyrolysis. Condensation and a cross-linking reaction may happen in the treatment, but at a slow rate.

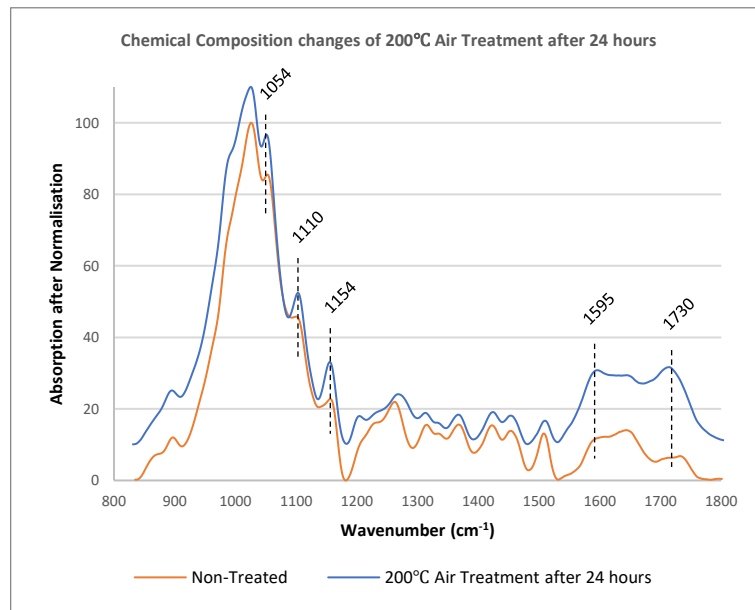


Figure 4-32 FTIR Spectrum Change of New Pine in 200°C Air Treatment After 24 hours

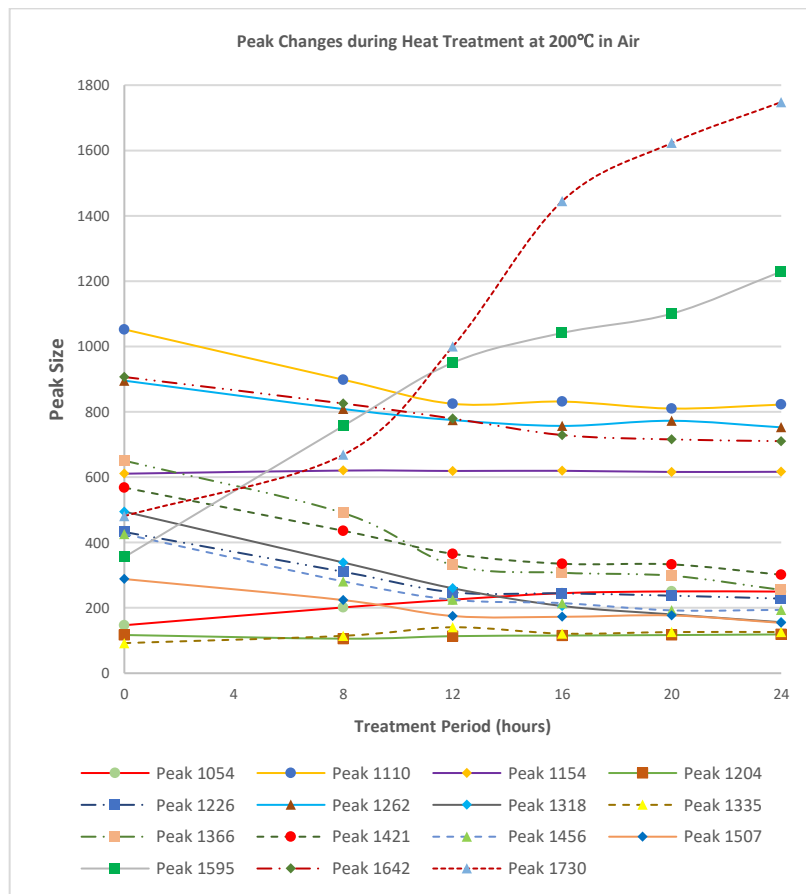


Figure 4-33 Peak Area Change of New Pine during 200°C Air Treatment

4.5.3 Summary

Chemical composition changes of new pine are mainly in hemicellulose and lignin and the changes are affected by the treatment atmosphere, including temperature and oxygen.

Hemicellulose is easy to affect even at low treatment temperatures. The acetyl group in the hemicellulose molecule is its most unstable chemical group, detaching from the hemicellulose chain at 120°C temperature treatment to form acetic acid (Figure 4-1). Deacetylase does not affect the length of hemicellulose chain until higher temperatures of more than 160°C are reached, when it starts to break into many shorter chains (Figure 4-2). Oxygen and temperature promote the rate of pyrolysis, which leads to large mass loss.

Lignin condensation and cross-linking reactions are observed in all treatments with different temperature and oxygen content; however, the rate of the two changes differ. Lignin condensation I (Figure 4-3) happens at 120°C without oxygen treatment for at least 24 hours, but only during the first 16 hours at 160°C in a vacuum and for the first 8 hours treatment at 120°C and 160°C in air. In 200°C treatment, lignin condensation I may happen in the first few hours. Lignin condensation II (Figure 4-4) and lignin-hemicellulose condensation (Figure 4-6) are based on the hydroxyl group and the two reactions happen only in the first 8 hours in all treatment environments. A cross-linking reaction (Figure 4-5) in lignin is also observed throughout 24 hours treatment at 120°C in a vacuum atmosphere, whilst this is only for 16 hours at 160°C treatment without oxygen, 8 hours at 120°C in air, 160°C in air and 200°C in a vacuum treatment. Hence, an aerobic atmosphere inhibits condensation and a cross-linking reactions.

Additionally, an oxidation reaction (Figure 4-10) is not observed easily at 120°C treatment even in air treatment because the carbonyl group (C=O) changes similarly.

Figure 4-34 shows the chemical reaction for the different treatment periods, temperatures and atmospheres (air and vacuum).

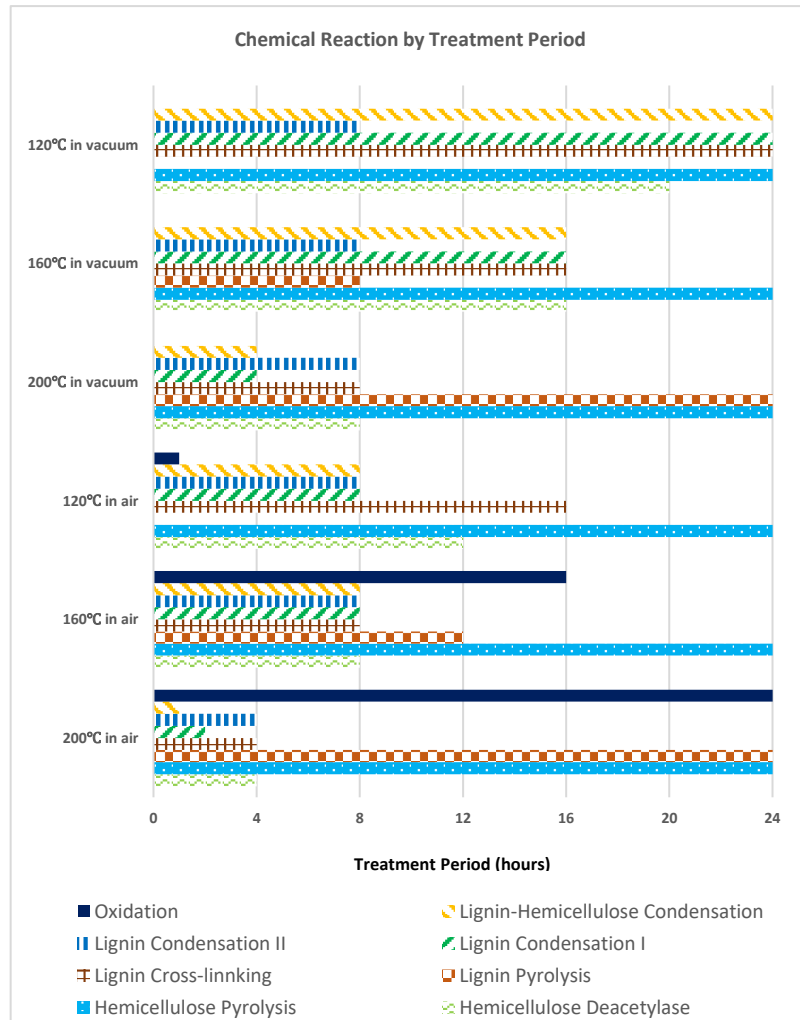


Figure 4-34 New Pine Chemical Reaction for Different Temperatures, Treatment Period and Atmospheres (air and Vacuum)

4.6 Old Timber Chemical Composition Changes during Heat Treatment

Compared to new pine, chemical composition of old pine is different. Lignin-hemicellulose condensation (Figure 4-6), oxidation (Figure 4-10) and decomposition (same as pyrolysis, Figure 4-2) are observed after 580 years natural ageing. However, the volume of old pine was limited, with only six samples being treated at 160°C, whilst 26 samples were treated at both 120°C and 200°C. Given the small sample size at 160°C treatment and hence, issues concerning validity, the behaviour of old pine at this temperature is not discussed.

4.6.1 Old Samples in a Vacuum

Regarding the treatment at 120°C in a vacuum, hemicellulose is less affected, with only approximately 1.6% mass loss after 24 hours and the peak relating to it also shows a very slight change (Figure 4-35 and Figure 4-36). The decrease on Peak 1730 and Peak 1595 pertaining to the carbonyl group (C=O) and alkene group (C=C), respectively, indicates cross-linking reaction in lignin. The increase of the C-C (Peak 1054) bond also gives evidence of the changes to lignin. Lignin condensation I (Figure 4-3) is also observed due to a slight increase in Peak 1318. However, ether linkage (C-O-C, Peak 1154) content is less affected during the treatment, which indicates very little of the hydroxyl group is condensed in the reaction of lignin condensation II (Figure 4-4) and lignin-hemicellulose condensation (Figure 4-6).

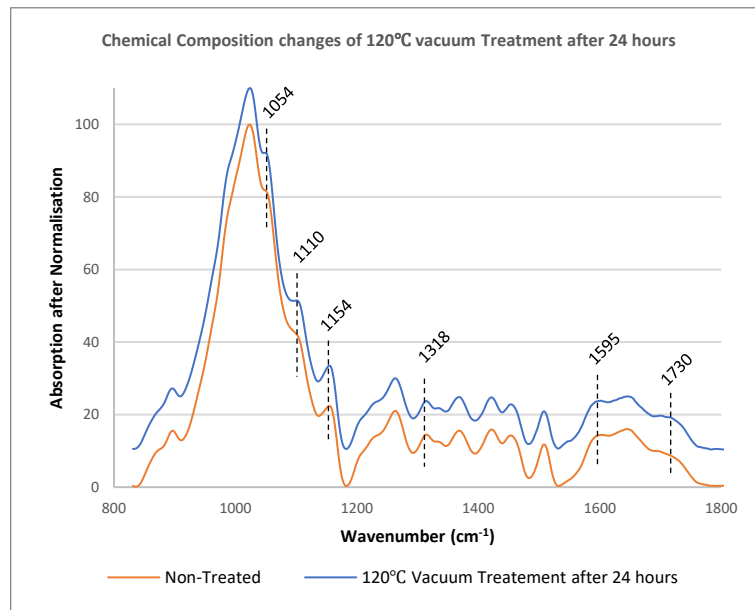


Figure 4-35 FTIR Spectrum Change of Old Pine in 120°C Vacuum Treatment After 24 hours

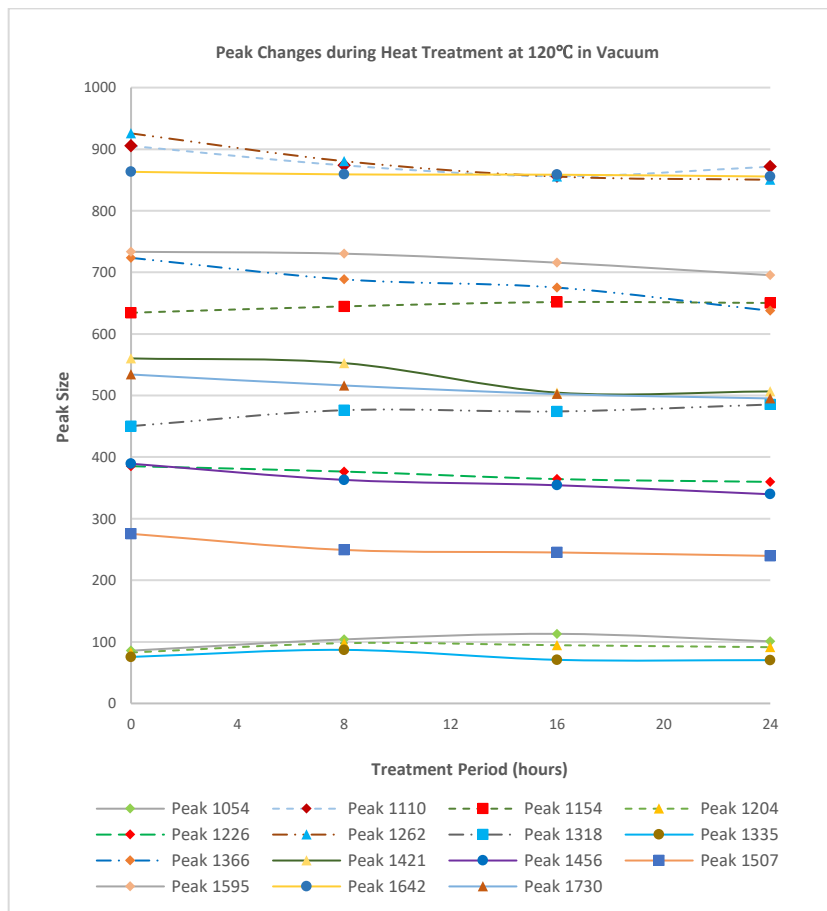


Figure 4-36 Peak Area Change of Old Pine During 120°C Vacuum Treatment

Whilst the mass loss of old pine at 120°C is lower than for new pine in the same treatment, a 200°C temperature destroys the chemical composition of old pine, resulting in more intense mass loss than for new pine. The decrease of Peak 1226 to 1456 relating to hemicellulose and increase of Peak 1730 and Peak 1595 pertaining to hemicellulose pyrolysis products during treatment, indicate that hemicellulose is greatly decomposed (Figure 4-37 and Figure 4-38). A lignin cross-linking reaction may happen in the first few hours of treatment due to C-C bond increases (Peak 1054 and Peak 1204).

The ether linkage (Peak 1154, C-O-C) decreases in the first 8 hours treatment, with pyrolysis in the lignin-carbohydrate complex (Figure 4-6) being responsible for the decrease. After 8 hours treatment, pyrolysis of carbohydrate complex tends to slow and lignin condensation I continues to happen (Figure 4-3) which leads to the ether linkage content increasing. Pyrolysis products of hemicellulose (Figure 4-2) and lignin (Figure 4-8) also contain many ether linkage and contribute to an increase on Peak 1154.

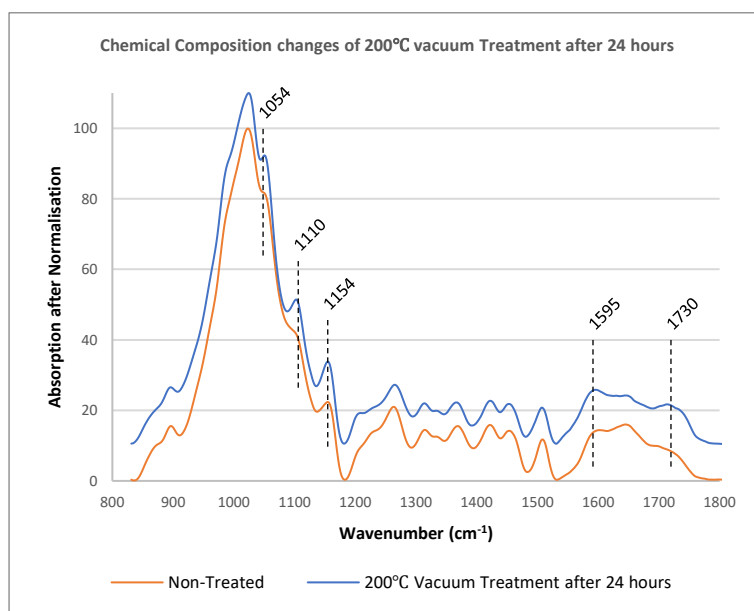


Figure 4-37 FTIR Spectrum Change of Old Pine at 200°C vacuum Treatment After 24 hours

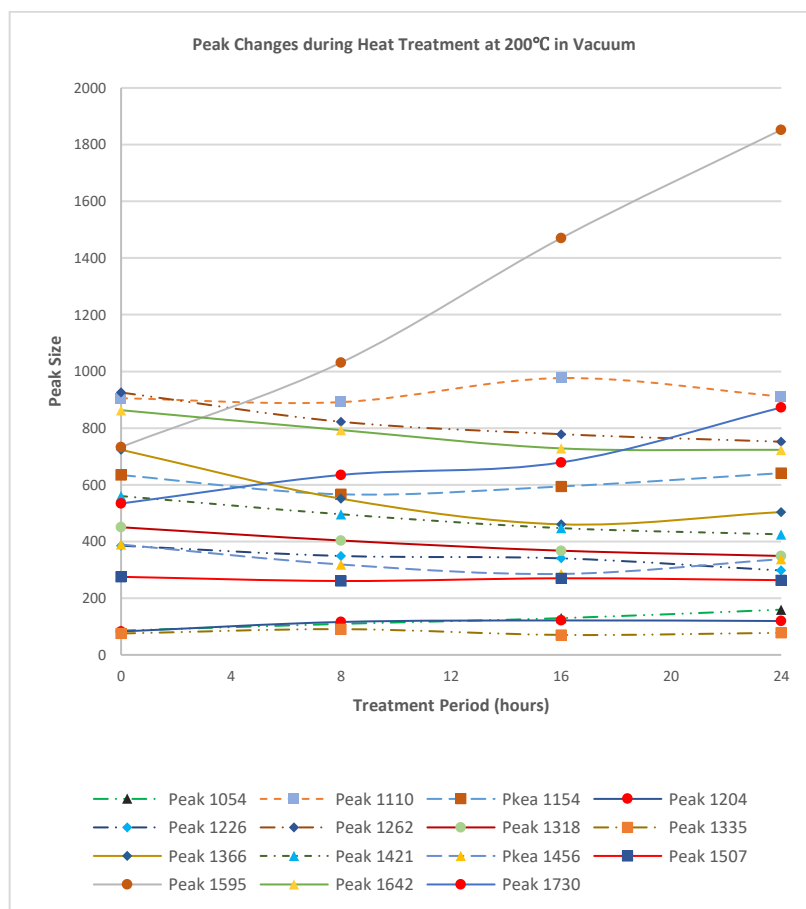


Figure 4-38 Peak Area Change of Old Pine During 200°C Vacuum Treatment

4.6.2 Old Samples in Air Treatment

In treatment at 120°C in air, apart from Peak 1730, Peak 1595, Peak 1318 and Peak 1154 relating to the carbonyl group, the alkene group, the condensed lignin ring and ether linkage, respectively, the decreases of the other peaks are same as with the vacuum treatment, but decrease a bit more after 24 hours treatment (Figure 4-39 and Figure 4-40). Hemicellulose pyrolysis is mainly responsible for the decrease and this leads to a similar mass loss as for the vacuum treatment at 120°C.

The alkene group (C=C, Peak 1595) increases gradually due to pyrolysis products of hemicellulose. Cross-linking reaction of lignin also happens during the treatment due to a C-C bond increase (Peak 1054) but the rate is much lower than regarding pyrolysis.

Ether linkage (C-O-C, peak 1154) changes slightly and there is only approximately 1.65% mass loss after treatment, which means that lignin condensation II and lignin-hemicellulose condensation do not happen. The hydroxyl groups (Peak 1110) decreases significantly in the first 16 hours treatment and no condensation happens, thus lignin dehydration (Figure 4-8 and Figure 4-9) is responsible for the change. The alkene group (Peak 1595) also increases, thereby providing evidence of a dehydration reaction. A lignin condensation I reaction happens in the first 16 hours due to an increase of Peak 1318, whereas, lignin pyrolysis contributes to decreasing this peak after 16 hours of treatment.

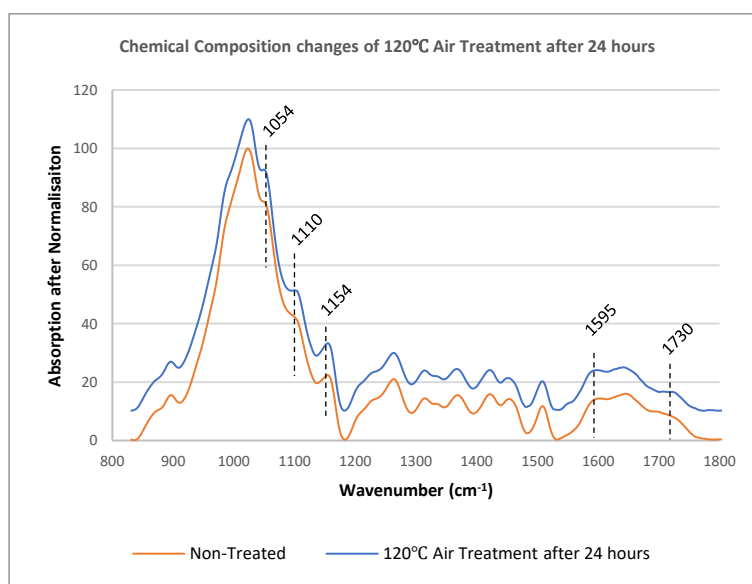


Figure 4-39 FTIR Spectrum Change of Old Pine in 120°C Air Treatment after 24 hours

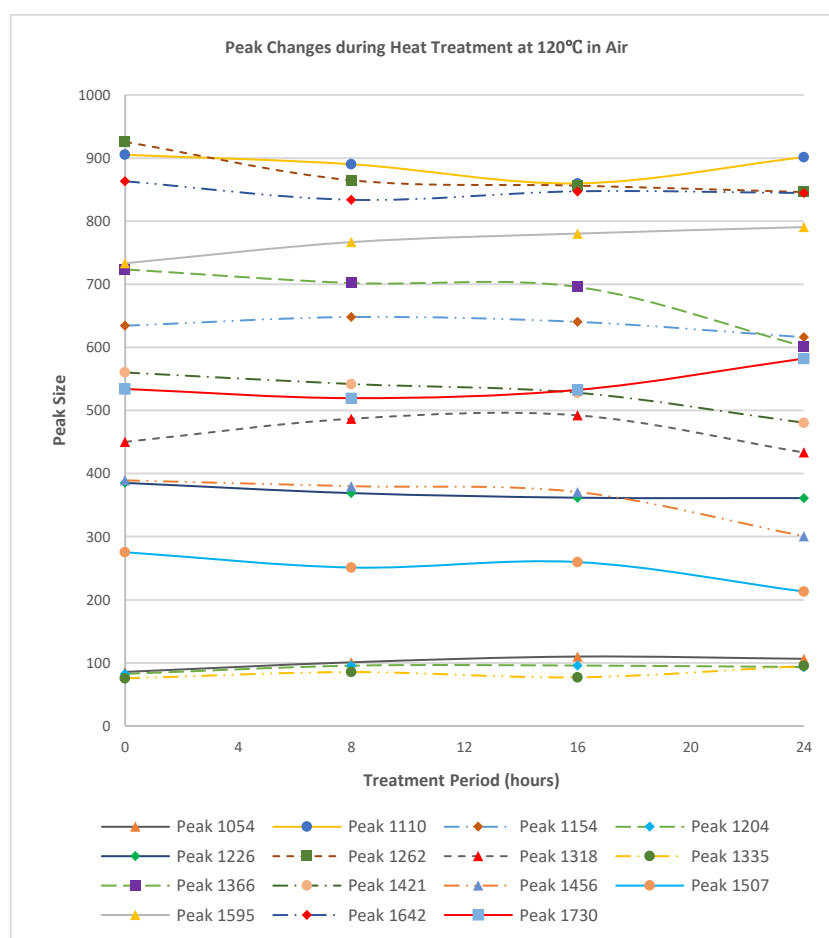


Figure 4-40 Peak Area Change of Old Pine during 120°C Air Treatment

With the treatment at 200°C in air, pyrolysis of hemicellulose and lignin are dominant, leading to 19.2% mass loss after 24 hours (Figure 4-41 and Figure 4-42). The carbonyl group (C=O, Peak 1730) and alkene group (C=C, Peak 1595) increase much more than with the vacuum treatment, which indicates pyrolysis. Other chemical reactions, such as condensation in and a cross-linking reaction of lignin, might happen in the first few hours, because the peak changes of ether linkage (Peak 1154), carbon-carbon bond (Peak 1054), carbonyl group and alkene group in the first 8 hours are slower than 8-24 hours treatment. The carbonyl group (C=O) increases more than in the vacuum treatment, which means that oxidation occurs.

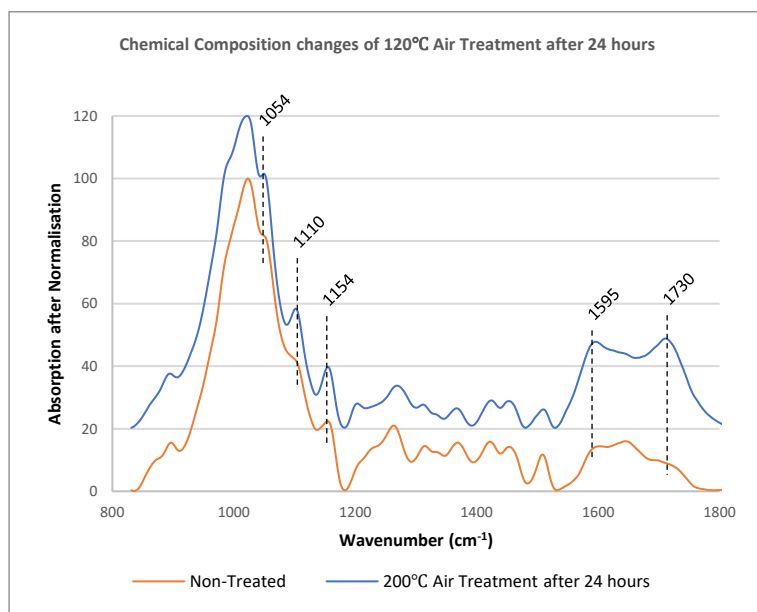


Figure 4-41 FTIR Spectrum Change of Old Pine in 200°C Air Treatment After 24 hours

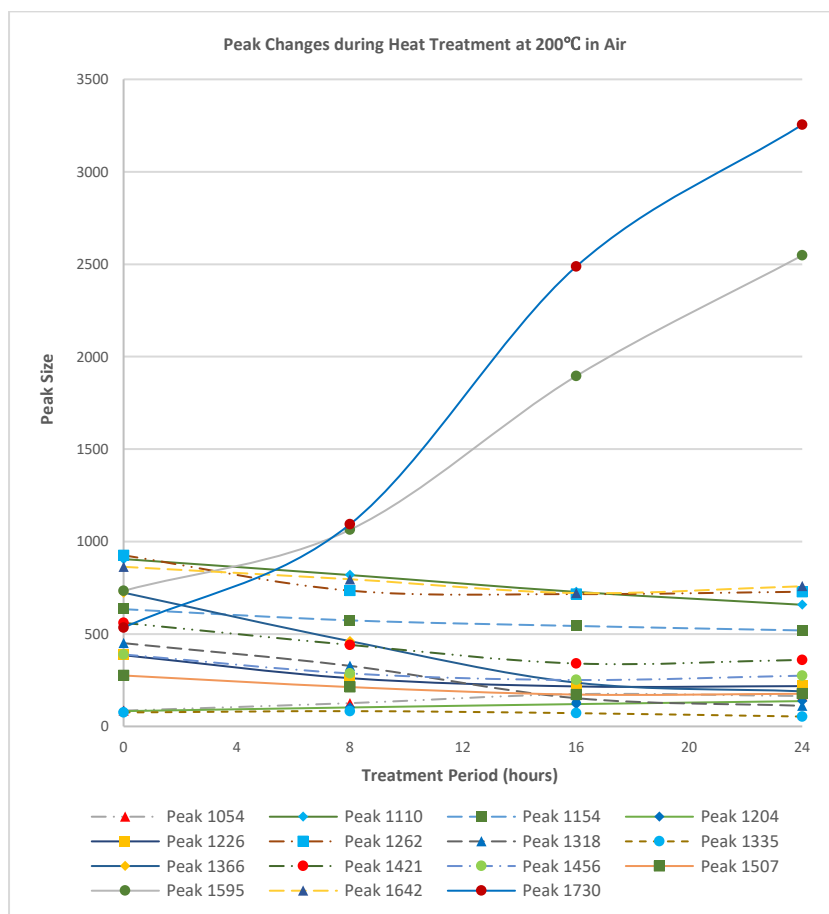


Figure 4-42 Peak Area Change of Old Pine during 200°C Air Treatment

4.6.3 Summary

Old pine molecules are stable at 120°C treatment but cannot resist high temperature. The reason is that parts of the hemicellulose and lignin are condensed or cross-linked during the natural ageing process. Both the FTIR spectrum and mass loss provide evidence for this phenomenon.

Lignin cross-linking happens throughout the vacuum treatment period, but only happens for the first 16 hours of treatment in air. Compared to the lignin cross-linking of new pine, the reaction rate on old pine is much slower. Higher temperatures improve cross-linking, but a pyrolysis reaction occurs as well.

Due to no changes in the Peak 1154 and Peak 1110 at 120°C treatment, relating to ether linkage and hydroxyl groups, respectively, lignin condensation II and lignin-hemicellulose condensation occurs less. Peak 1318 relating to S- and G-ring condensation in lignin increases in the first 8 hours both under air and vacuum treatment, which indicates that lignin condensation I happens. However, 200°C treatment obstructs the reaction due to serious pyrolysis of the hemicellulose and lignin. Moreover, and oxidation reaction is an important feature with 200°C air treatment.

The chemical change duration period is shown in Figure 4-43.

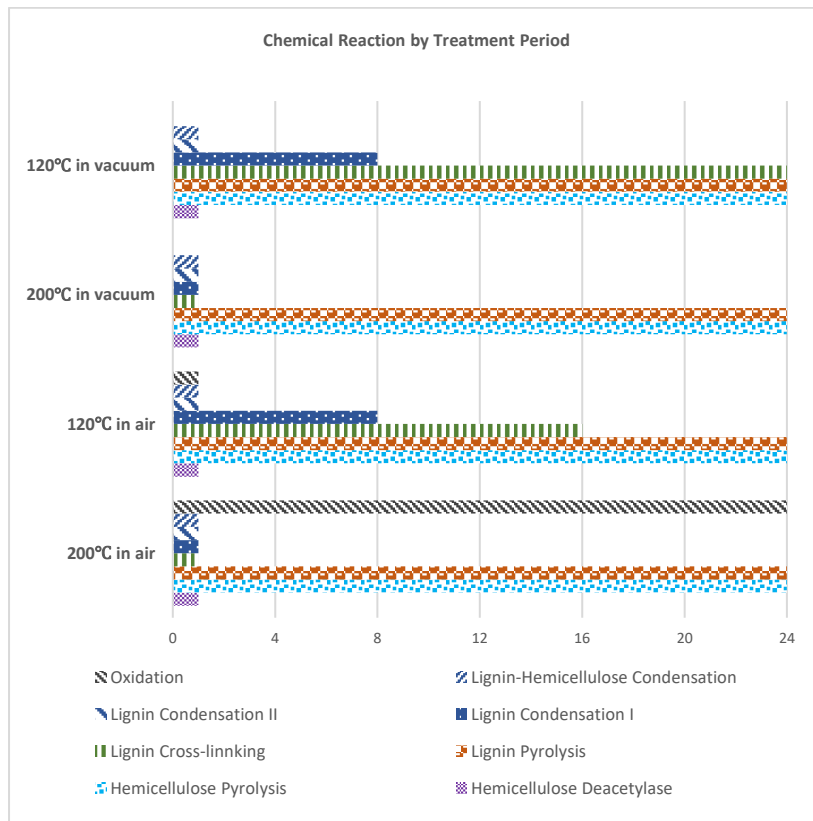


Figure 4-43 Old Pine Chemical Reaction for Different Temperatures, Treatment Periods and atmosphere

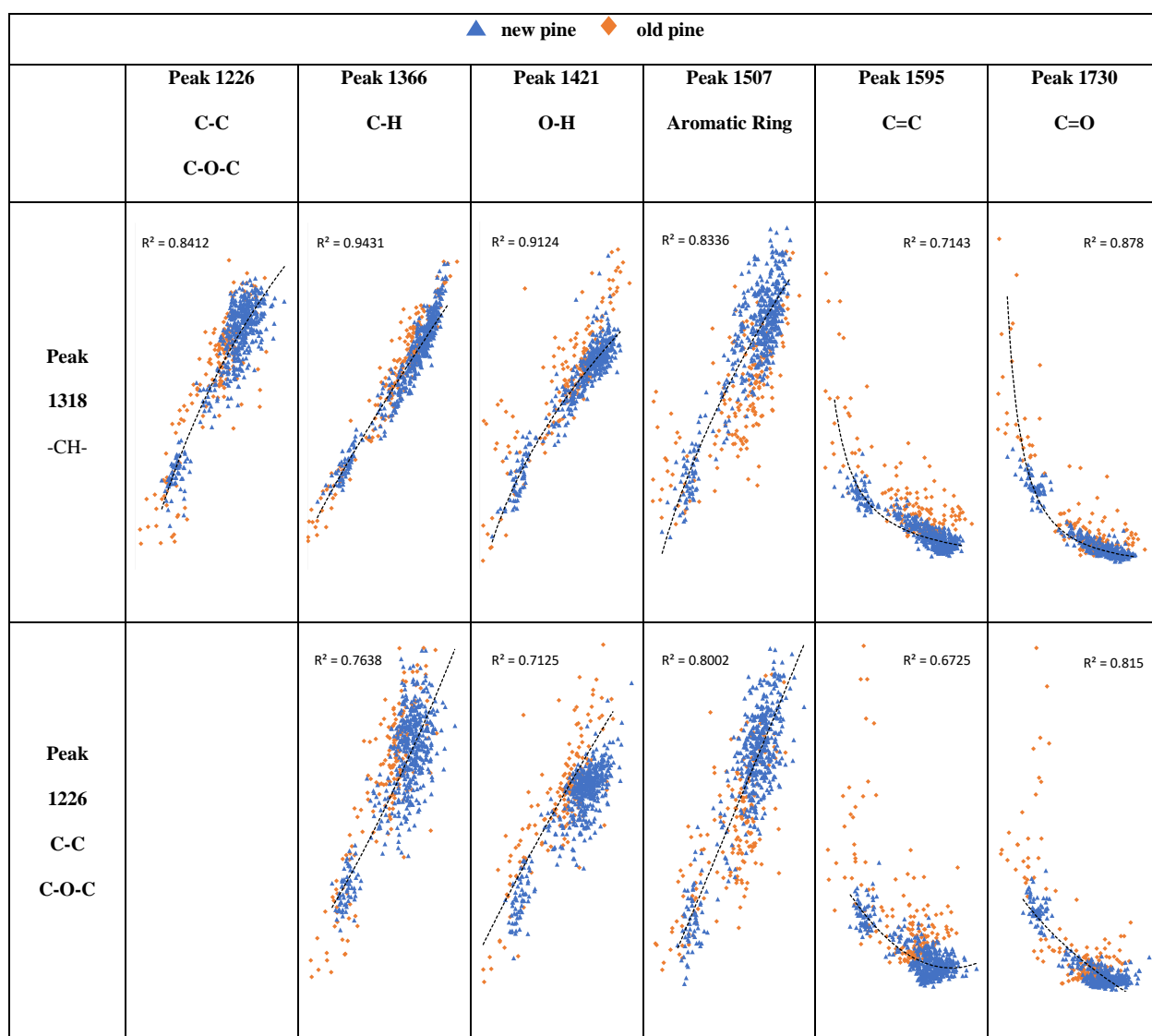
4.7 Peak Interaction Correlation

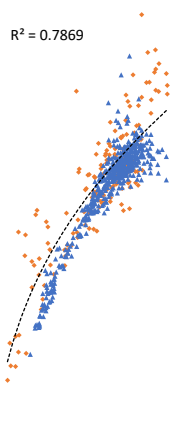
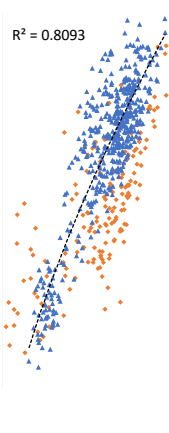
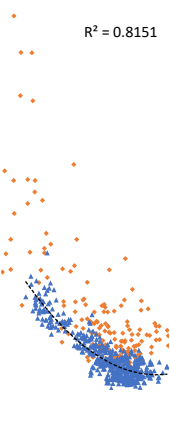
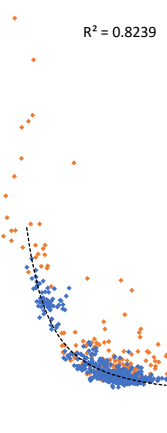
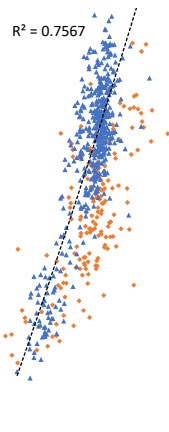
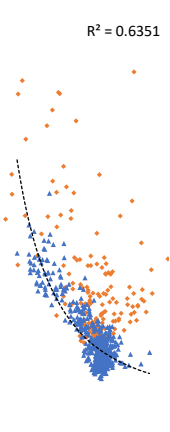
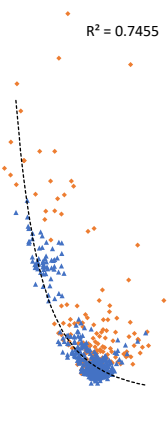
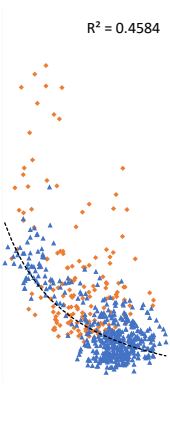
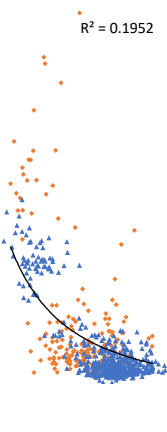
Even though the new and old timbers are heat-treated in different atmospheres, a few peaks of the FTIR spectra have a positive or negative relationship to each other. In section 4.1, Table 4-1 shows that the chemical composition changes involve at least two functional groups, so it is reasonable that a few peaks change with others (Table 4-7).

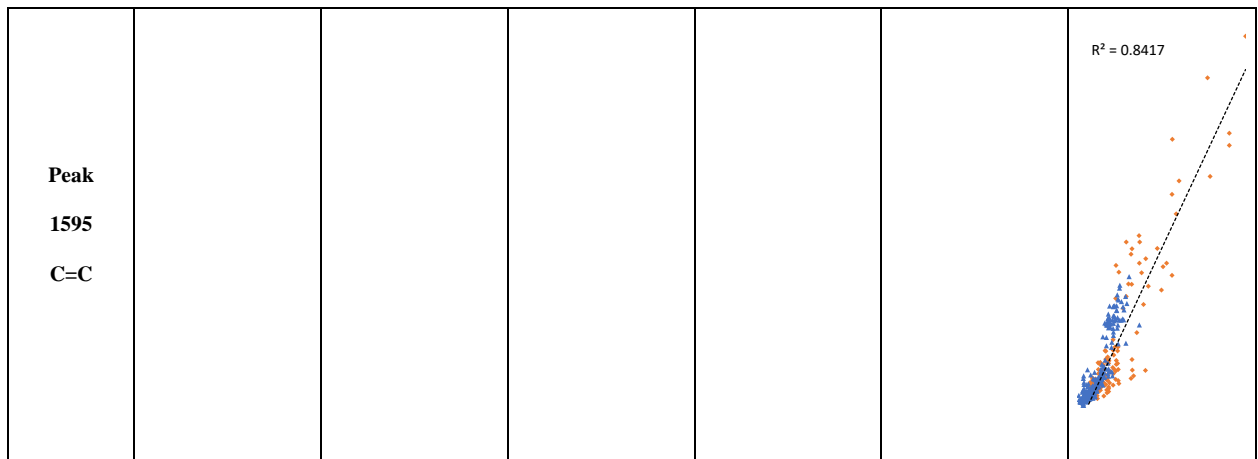
Peak 1421 and Peak 1366 relating to the C-H bond change identically during any heat-treatment. C-H bond is a common bond existing in cellulose, hemicellulose and lignin but the two peaks are related to the C-H bond on hemicellulose and lignin. Hence, hemicellulose and lignin are the two active molecules during heat treatment.

The Peak 1318 relating to S- or G-ring condensation in lignin, Peak 1507 pertaining to the aromatic skeleton and Peak 1226 relating to C-C bond have high positive correlation with the C-H bond. All the five peaks change together, which demonstrates the pyrolysis reaction of hemicellulose and lignin. Pyrolysis products also contain high quantities of the carbonyl and alkene groups, which leads to the increase of both peak 1595 and peak 1730 and these have high a negative correlation relationship to others.

Table 4-7 Correlation of FTIR Peak Area Changes



<p>Peak 1366 C-H</p>			<p>$R^2 = 0.7869$</p> 	<p>$R^2 = 0.8093$</p> 	<p>$R^2 = 0.8151$</p> 	<p>$R^2 = 0.8239$</p> 
<p>Peak 1421 O-H</p>				<p>$R^2 = 0.7567$</p> 	<p>$R^2 = 0.6351$</p> 	<p>$R^2 = 0.7455$</p> 
<p>Peak 1507 Aromatic Ring</p>					<p>$R^2 = 0.4584$</p> 	<p>$R^2 = 0.1952$</p> 



4.8 Discussion and Conclusion

Equilibrium moisture content and mass have been discussed in sections 4.3 and 4.4. The results of the experiments and other literature are covered in that section and will not be repeated in this part.

Various chemical reactions during the natural ageing process, heat treatment on old pine and heat treatment on new pine are discussed in this chapter. Generally, the changes can be divided into two categories: extending or expanding the length of the molecule or diminishing its length.

Timber molecule length reduction is due to pyrolysis of hemicellulose and lignin. Hemicellulose pyrolysis starts from a deacetylase reaction. The acetyl group attaches the hemicellulose chain by ether linkage (C-O-C), but the C-O bond near the chain can break under heat energy and form acetic acid. The reaction is deacetylase. With rising temperature, hemicellulose is pyrolyzed to many shorter molecular chains. A few gas and liquid pyrolysis products are released from the sample and these are responsible for mass loss. Deacetylase and hydrolysis reactions during the heat treatment process were observed by Kocafe et al. (2008) and Alen et al. (2002) in an anaerobic environment treatment,

whilst Sivonen et al. (2002), Weiland and Guyonnet (2003) did so with aerobic treatment. Other studies have also reported similar results (Tjeerdsma et al., 1998; Nuopponen et al., 2005; Dirol and Guyonnet, 1993; Bourgois et al., 1989). Zhou et al. (2016) reported comprehensive pyrolysis behaviour of hemicellulose and all the chemical changes in the current experiments according to the reaction atmosphere confirm this report. In addition, lignin pyrolysis also leads to a decrease in the lignin molecule chain length, but this needs a high temperature. Kawamoto et al. (2007) also found that lignin is pyrolysed at high temperatures.

Typical reactions to extend or expand molecule chain are lignin-hemicellulose condensation, lignin condensation and lignin cross-linking. The hydroxyl group of lignin and hemicellulose molecules could condense to water (H_2O) and ether linkage (C-O-C) as a bridge. Condensed lignin by ether linkage and the lignin-carbohydrate complex is observed on the new pine and naturally aged old pine with treatment at $120^{\circ}C$. The chemical composition structure of the condensation is stable at low temperatures, which leads to lower mass loss for old pine than new pine. However, at high temperatures, the molecules are pyrolysed dramatically, which results in older pine having the greater mass loss. A condensation reaction between lignin S- or G-rings is evidenced on new pine during heat treatment, but this is not significant for old pine. Funaoka et al. (1990), Li and Gellerstedt (2008) studied lignin behaviours during heat treatment and reported the same results as with the current experiment. A lignin cross-linking reaction happens in all treatments with various atmosphere. Apart from carbonyl (C=O) and alkene group (C=C), lignin cross-linking reaction is also observed by the changes of methylene bridge in other studies (Tjeerdsma et al., 1998; Nuopponen et al., 2005; Wikberg and Maunu, 2004). The lignin cross-linking reaction is also observed in old pine. Lignin-hemicellulose condensation, lignin condensation and cross-linking may affect analysis results regarding

the wet chemical method. A few studies have reported lignin increasing dramatically under inert atmosphere treatment by the wet chemical method, even reaching 84% (Bourgois and Guyonnet, 1988; Zaman et al., 2000; Dirol and Guyonnet, 1993). However, the lignin may not be pure. The reactions extending or expanding the molecule are responsible for the increase.

A few chemical changes do not affect the molecule length, but rather the functional groups, which are involved in the reactions of condensation and cross-linking. Oxidation and dehydration are the reactions based on activity of hydroxyl groups (-OH). In an aerobic atmosphere, hydroxyl groups can be oxidised to the carbonyl group (C=O), which leads to a low condensation rate. Two neighbouring hydroxyl groups on a single chain (HO-C-C-C-OH) on lignin could have a dehydration reaction with the reaction products of alkene group (-C=C-), formaldehyde (CH₂O) and water (H₂O). Alkene group could be further involved in the cross-linking reaction of lignin. Hence, oxidation inhibits a condensation reaction, whereas dehydration increases the opportunity for cross-linking.

Different atmospheres contribute to different rates of chemical composition change. Figure 4-44 shows functional group changes in different atmospheres. According, next there is discussion on the reaction promoting and inhibiting in distinctive atmospheres. The old pine compositions have undergone 580 years of the natural ageing process, show different FTIR behaviours during heat treatment. The functional group changes of old pine during heat treatment are exhibited in Figure 4-45.

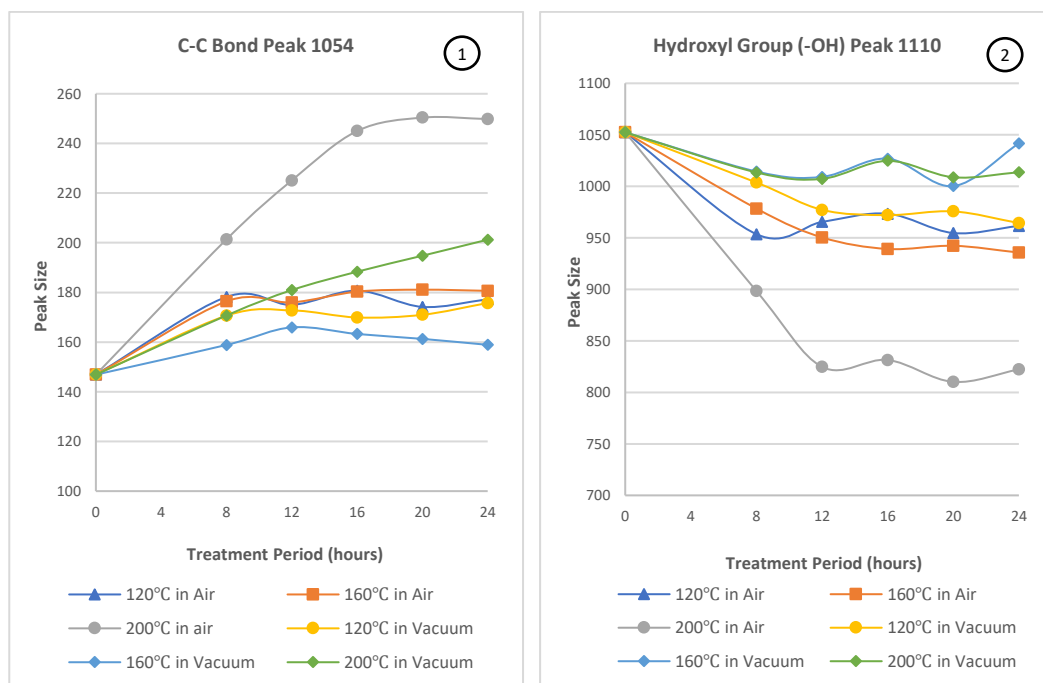
The carbon-carbon bond is a stable chemical bond in the timber molecule. The bond content increase with mass loss both on new (① of Figure 4-44) and old pine (① of Figure 4-45). Haw and Schultz (1985), Nakamura et al. (2008) and Kawamoto et al. (2007) also reported similar results. The C-C bond of new pine at 120°C both in air and vacuum treatment

increases significantly than other treatments. The increasing in C-C content, decrease on alkene group (C=C, ⑤ of Figure 4-44) and carbonyl (C=O, ⑥ of Figure 4-44) at 120°C treatment indicates a clear cross-linking reaction in lignin. The old pine sample also shows cross-linking reaction for lignin due to the decrease in the alkene (⑤ of Figure 4-45) and carbonyl (⑥ of Figure 4-45) groups. However, the related peak changes for old pine are slower than for new pine, which provides evidence that lignin has cross-linked in the natural ageing process. In addition, a deacetylase reaction on hemicellulose also leads to an increase on alkene group and reduction in the carbonyl group. The alkene group of new pine decreases under 120°C treatment, which indicates that the cross-linking reaction rate is higher than the deacetylase one, but at 160°C treatment, the opposite is the case. Hence, lignin cross-linking reaction of new pine is encouraged by the following treatment order: 120°C in a vacuum → 120°C in air → 160°C in a vacuum → 160°C in air → 200°C in a vacuum → 200°C in air.

The hydroxyl group in the timber molecule condenses to ether linkage due to the decrease on Peak 1110 and increase on 1154. Ether linkage (③ of Figure 4-44) and hydroxyl group (② of Figure 4-44) change for new pine during the first 8 hours is quicker than for 8-24 hours treatment, which shows that hydroxyl group condensation reaction is promoted first as opposed to other reactions. At 120°C treatment, the condensation reaction in air and in a vacuum is extremely close, which suggest that oxygen may not affect the hydroxyl groups at low temperatures. In treatment above 160°C in air after 8 hours, a pyrolysis reaction leads to a decrease in ether linkage. Treatment above 160°C in a vacuum is complex due to various chemical changes, especially lignin condensation I and pyrolysis. Lignin condensation I is based on the breaking of the ether linkage and so, it is promoted under vacuum treatment, but obstructed by oxygen. The changes of Peak 1318 (④ of Figure 4-44) relating to lignin condensation I also support this complex change. Ether linkage of old

pine increases at a lower rate, so the quantity of the hydroxyl group in it is less than for new pine due to the oxidation reaction during natural ageing process.

Compared to the FTIR spectrum of 120°C treatment in air and 580 years old pine, oxidation reaction is very slow during natural ageing process. In fact, there are decorative paintings on the old pine, which could be have acted as a protective layer. Finally, the carbonyl group (C=O), alkene group (C=C) and ether group's (C-O-C) content increases even when there is high mass loss; there three functional groups being relatively more stable than others.



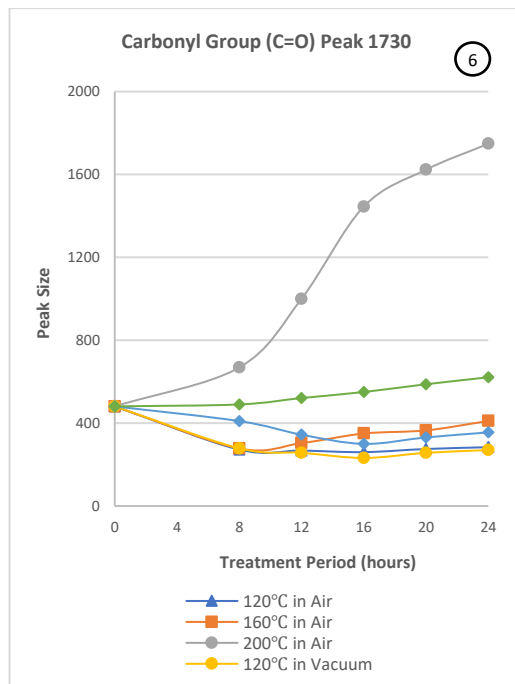
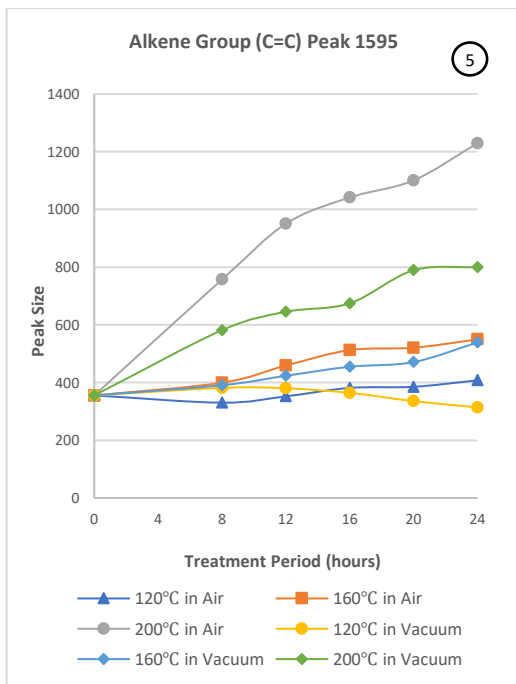
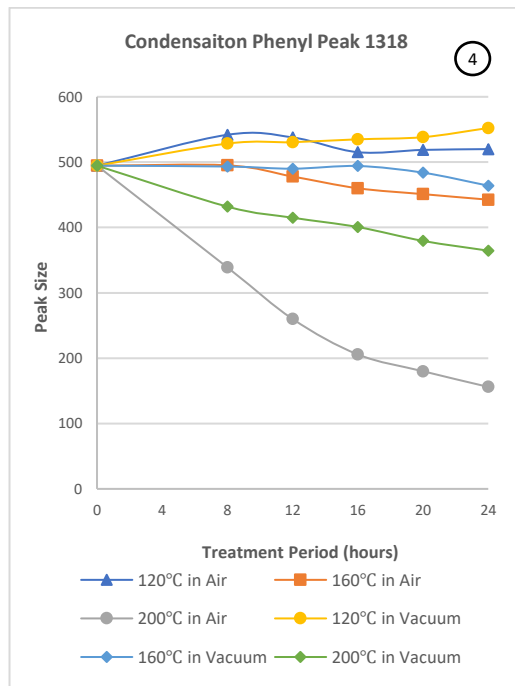
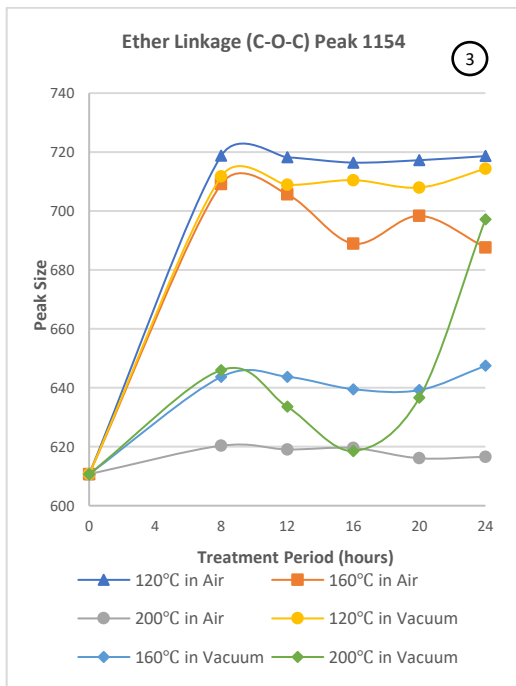
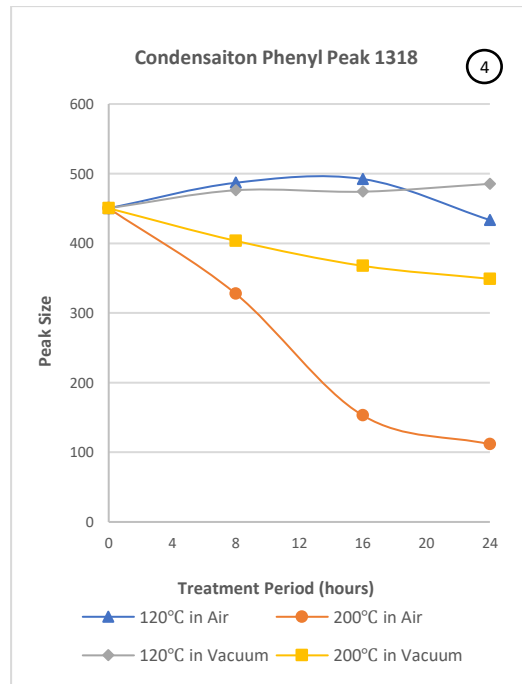
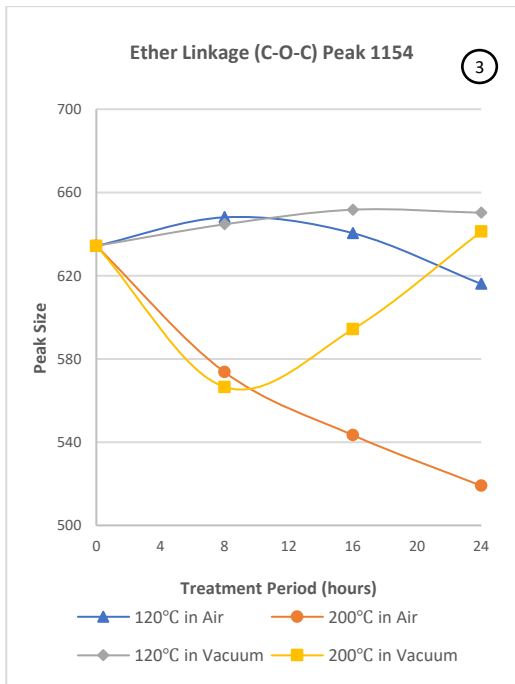
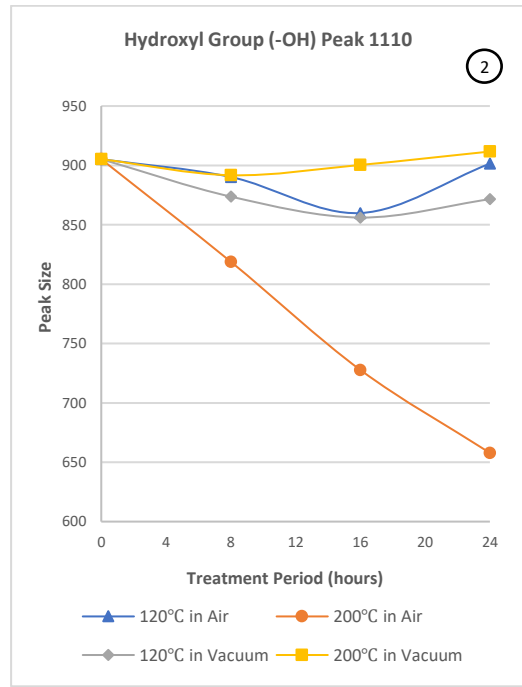
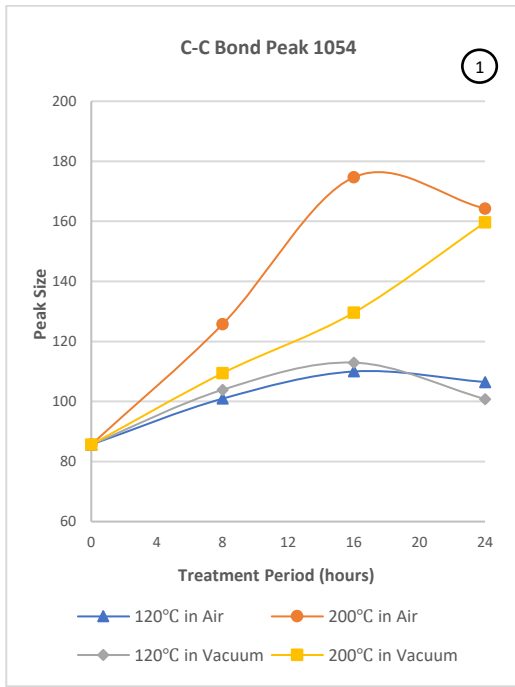


Figure 4-44 Peak Area Change of New Pine in Different Treatment



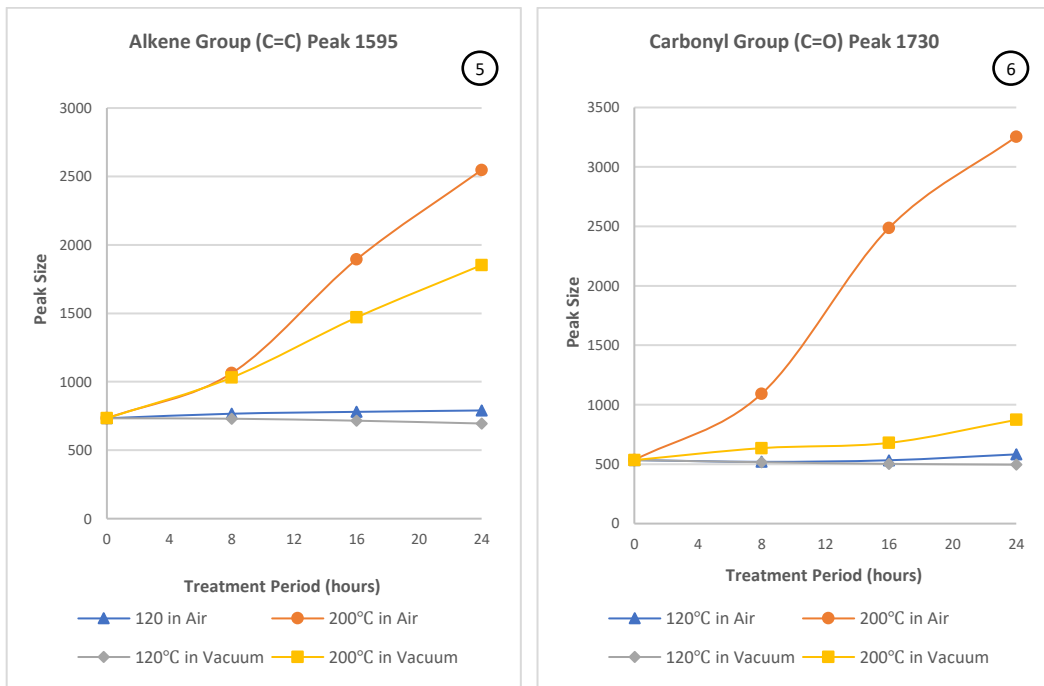


Figure 4-45 Peak Area Change of Old Pine in Different Treatment

Chapter 5 Mechanical Property Changes during Heat Treatment

Static and dynamic mechanical properties are discussed in this chapter. Moisture plays a significant role in timber strength and its influence is studied in the first section. Section 2 shows the mechanical difference between new and old timber. Section 3 and 4 discuss the static and dynamic mechanical behaviours of new and old pine during heat treatment, respectively. In this research, the modulus of elasticity (MOE) and modulus of rupture (MOR) are two essential evaluations for determining static timber mechanical properties. Storage modulus, loss modulus, complex modulus and $\text{Tan } \delta$ are the factors reflecting dynamic mechanical properties.

MOE and MOR are calculated with a 3-point bending test (Figure 5-1) by a stress-strain curve (Figure 5-2). MOE is calculated by the elastic deformation stage which is a linear area. The slope of the elastic deformation stage is calculated as:

$$s = \frac{\Delta a}{\Delta b}$$

where, Δa is the applied force change of elastic deformation and Δb is the change in deformation. The MOE is given as:

$$E_f = \frac{L^3 s}{4wd^3}$$

Whilst MOR is the highest stress in the moment of mechanical failure:

$$\sigma = \frac{3F_{max}L}{2wd^2}$$

Where, for both MOE and MOR, L is length of the supporter span, s is the slope of elastic deformation, w is the sample width and d is the sample thickness.

The MOE is the modulus for describing the sample's resistance ability to mechanical deformation and a higher MOE contributes to low strain when applying the same force. MOR is one property that defines sample maximum strength.

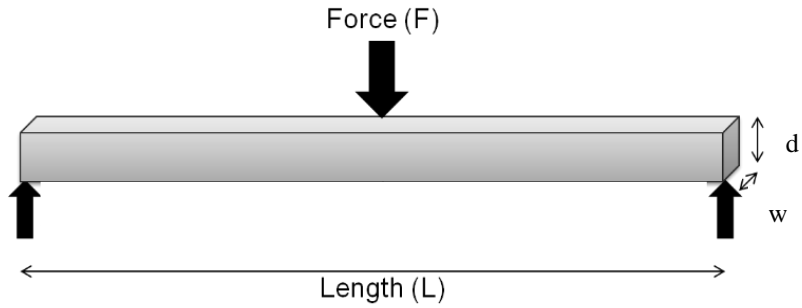


Figure 5-1 Schematic Diagram of a 3-Point Bending Test

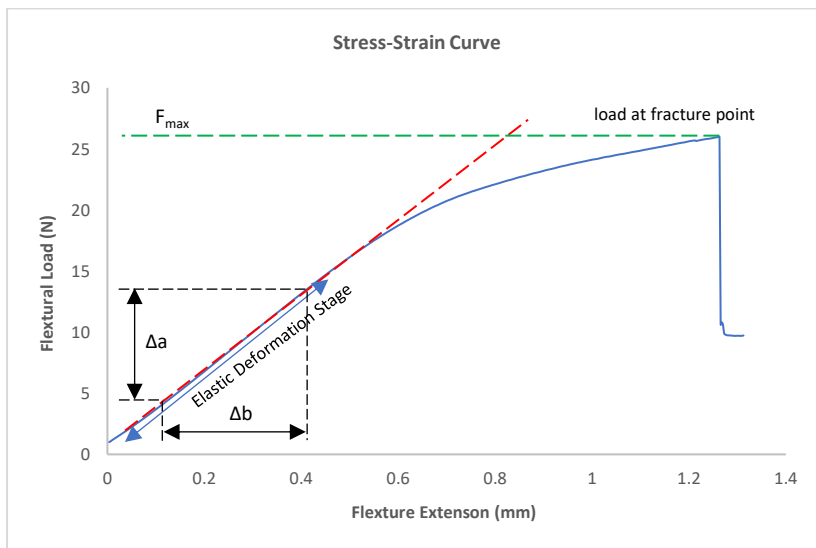


Figure 5-2 Stress-Strain Curve of a 3-Point Bending Test

The dynamic mechanical properties during temperature scanning are tested by DMTA (dynamic mechanical thermal analysis) facility and the results are calculated by a computer. Tan δ is the ratio of loss modulus (E'') / storage modulus (E') for describing materials' viscoelasticity. When applying an external force, part of the energy is stored by molecule deformation and another part is dissipated by molecule friction. An increase in Tan δ

indicates intermolecular sliding, while a decrease means that energy is stored by molecule bending or stretching. A complex modulus used to describe the property and the relationships between the dynamic mechanical properties is shown in Figure 5-3. An absolute value of the complex modulus is calculated as follows:

$$|E^*| = \sqrt{E'^2 + E''^2}$$

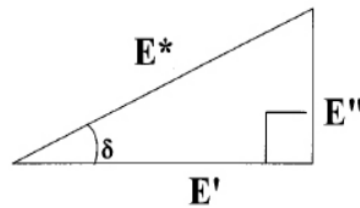


Figure 5-3 Relationships Between Dynamic Mechanical Properties

However, the values of both the static and dynamic mechanical properties might not be the same as in other studies. The main reason for this being the samples size. That is, in this research, sample is designed to fit both a 3-point bending test and DMTA test together for comparing static and dynamic mechanical properties, rather than using international standards.

5.1 Moisture Content and Bending Mechanical Properties

5.1.1 Static Mechanical Properties and Moisture Content

Moisture content (MC) affects timber's static mechanical properties significantly such that MOR and MOE decrease with moisture content rising (Figure 5-4 and Figure 5-5). Specifically, the MOR and MOE decrease by approximately 30% and 10%, respectively, in samples from dry to 10% MC. Hence, MOR is affected by moisture content more significantly than MOE. Similar results were reported by Dinwoodie (1975); Kretschmann and Green (2007). However, regarding the stress-strain curve (Figure 5-6), dry samples and

10% MC samples show a different behaviour. Dry samples show elastic deformation and yield stages before mechanical failure, whilst 10% MC samples illustrate a second elastic deformation between the yield stage and mechanical failure. Hence, moisture contributes to a molecule rearrangement process under external force to form a new balance between stress and strain, which gives more deformation extension than with dry samples. Steiner (2002) also reported that moisture can improve molecule re-arrangement in a larger deformation.

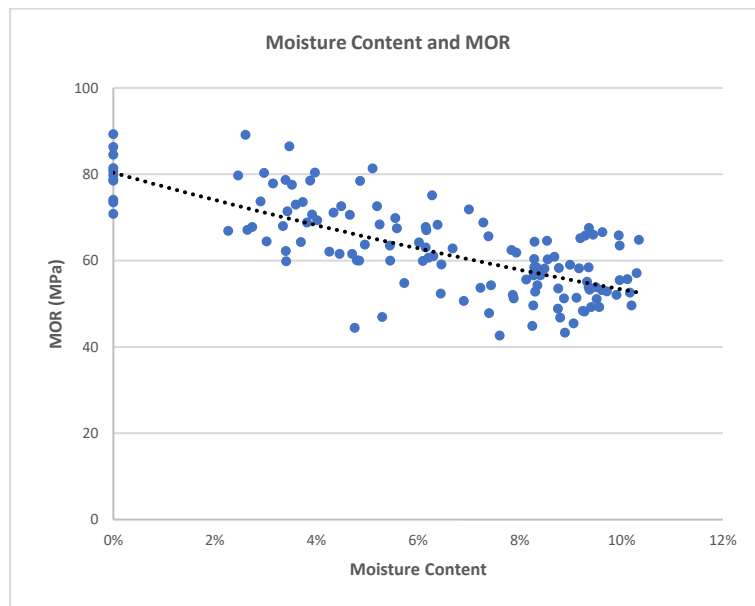


Figure 5-4 MOR and Moisture Content of New Pine

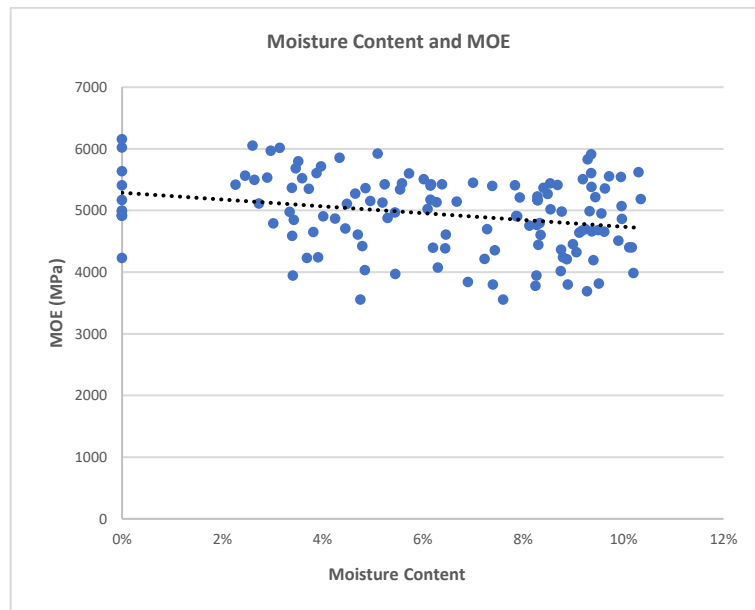


Figure 5-5 MOE and Moisture Content of New Pine

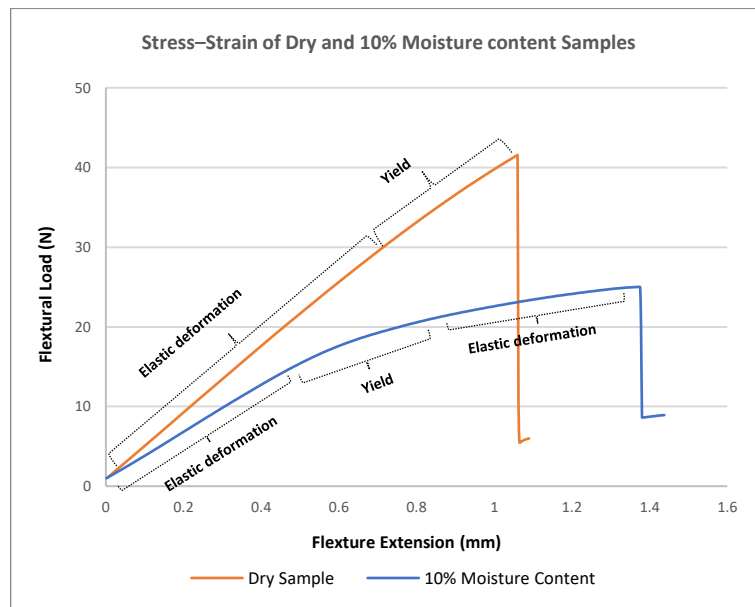


Figure 5-6 Stress-Strain Curve of Dry and 10% Moisture Content Samples

5.1.2 Dynamic Mechanical Properties and Moisture Content

During a DMTA test, which can reach 150°C, the mass loss of dry samples both new and old, is very low (Table 5-1), which can be taken as that chemical composition is little changed. The mass loss of moisture samples during DMTA test is due to moisture. The

testing period of each sample is approximately 1 hour, which can be treated as no chemical changes happen.

Both the storage moduli of dry and moisture sample decreases with temperature in new pine (Figure 5-7) and old pine (Figure 5-10), but with the latter the decrease is greater at the temperature from -150°C to -120°C in new pine and -150°C to -90°C in old pine, dry samples have a large storage modulus. The storage modulus and Young's Modulus (MOE) have the same concept and calculation method but the values shown are slightly different. Hence, water molecules decrease friction movement between timber molecules at low temperatures, which enhance the elasticity of timber samples. Moisture starts to improve timber's molecule with temperature rising and this leads to a lower MOE.

The loss moduli of dry and moisture samples have complex changes both in new (Figure 5-8) and old samples (Figure 5-11) and mainly responsible for the behaviours of $\text{Tan } \delta$ curve of new (Figure 5-9) and old samples (Figure 5-12). In general, $\text{Tan } \delta$ of dry samples is lower than for moisture samples, especially above -120°C for new pine and -90°C for old pine, which means that the timber molecules of dry samples are not subject easily to friction and this leads to higher elasticity. All the moisture samples show Peak β for temperature scanning between 0°C and 100°C , with the peaks appearing at nearly the same temperature (68°C for new pine and 71°C for old pine). However, the peak has disappeared and changed to a flat curve in the dry samples. Hence, moisture is responsible for the Peak β . Water molecules contribute to molecule friction for temperatures between approximately 10°C and 70°C . Hydrogen bonds between timber and water molecules start to lose bond attractions in the temperature range, which leads to an increase in $\text{Tan } \delta$. Above 70°C , moisture motion is intense and does not affect timber molecules significantly. Timber molecules are not easily subject to friction in this higher temperature range, which causes a decrease in $\text{Tan } \delta$. The relationship was also discussed by Obataya et al. (2001); Kelley

et al. (1987) and Backman and Lindberg (2001). Peak γ is affected by methylol groups, according to Obataya et al. (2001) and both moisture and dry samples for new and old pine have a peak during DMTA temperature scanning. However, the peak γ decreases and divides into two peaks in dry samples. Hence, moisture also plays a significant role in peak γ . Montes and Cavail  (1999) reported that the two peaks are caused by methylol and the hydroxyl groups, respectively.

Table 5-1 DMTA of Dry and 10% Moisture Content Samples

	Sample Number	Dry Density (Kg/m ³)	Moisture Content	Dry Weight (g)	Weight after DMTA test (g)	Mass Loss during DMTA (g)
New	Dry	ND1	0	0.0959	0.0954	0.0005
		ND2	0	0.1035	0.1032	0.0003
		ND3	0	0.0992	0.099	0.0002
		ND4	0	0.0938	0.0935	0.0003
		ND5	0	0.0901	0.09	0.0001
		ND6	0	0.096	0.0958	0.0002
	Moisture	NM1	10.23%	0.1036	0.1055	-0.0019
		NM2	10.25%	0.0946	0.0971	-0.0025
		NM3	9.82%	0.1028	0.1052	-0.0024
		NM4	10.02%	0.1258	0.1271	-0.0013
		NM5	10.74%	0.1015	0.1061	-0.0046
		NM6	9.81%	0.0999	0.1004	-0.0005
Old	Dry	OD1	0	0.1201	0.1200	0.0001
		OD2	0	0.1349	0.1347	0.0002
		OD3	0	0.1195	0.1193	0.0002
		OD4	0	0.1304	0.1303	0.0001
		OD5	0	0.1348	0.1348	0
		OD6	0	0.1306	0.1304	0.0002
	Moisture	OM1	9.8%	0.1565	0.1567	-0.0002
		OM2	9.78%	0.1315	0.1318	-0.0003
		OM3	10.02%	0.1326	0.1331	-0.0005
		OM4	9.2%	0.1228	0.1232	-0.0004
		OM5	9.89%	0.1333	0.1333	0
		OM6	9.75%	0.1425	0.1448	-0.0023

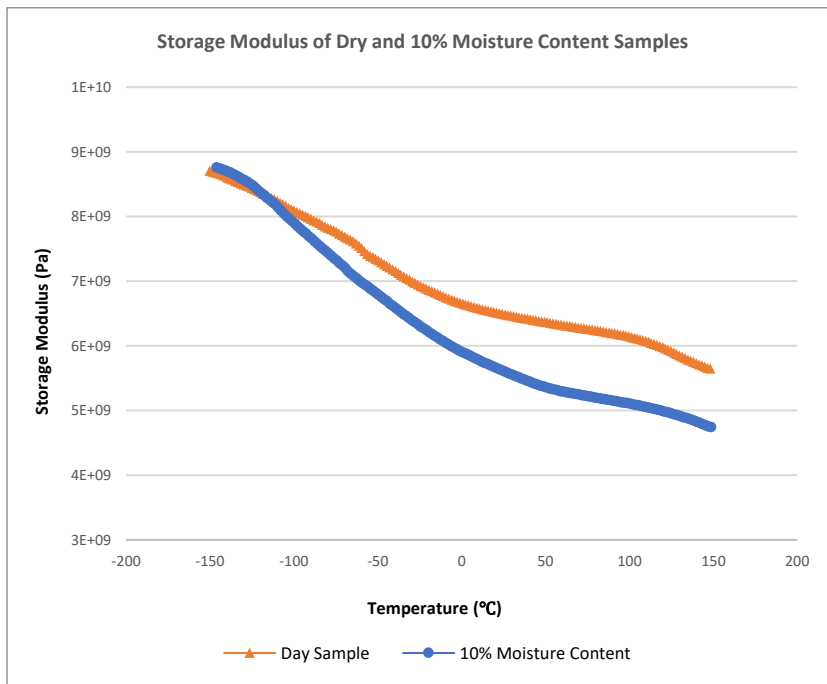


Figure 5-7 DMTA Storage Modulus of a New Sample in Dry and Moisture Samples

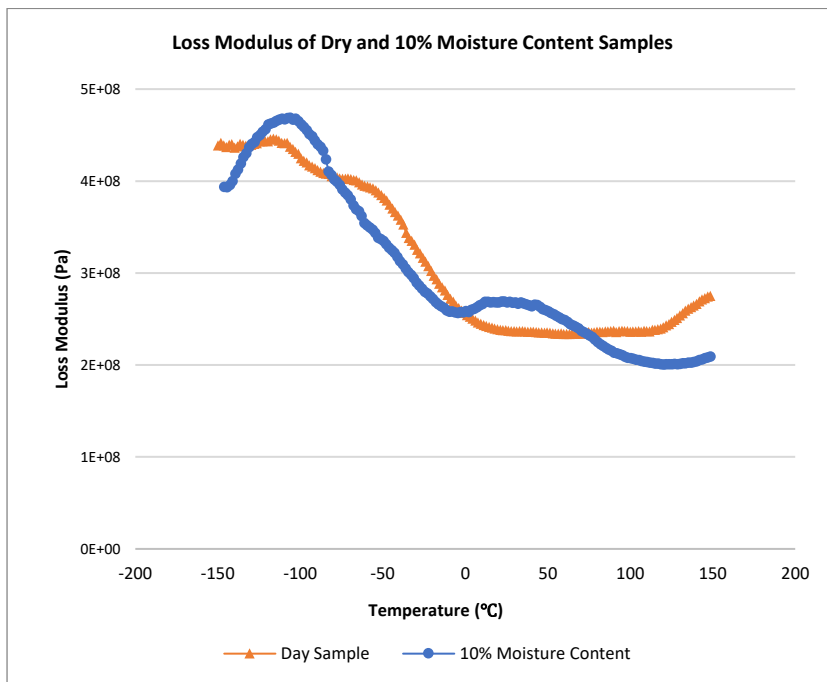


Figure 5-8 DMTA Loss Modulus of a New Sample for both Dry and Moisture Samples

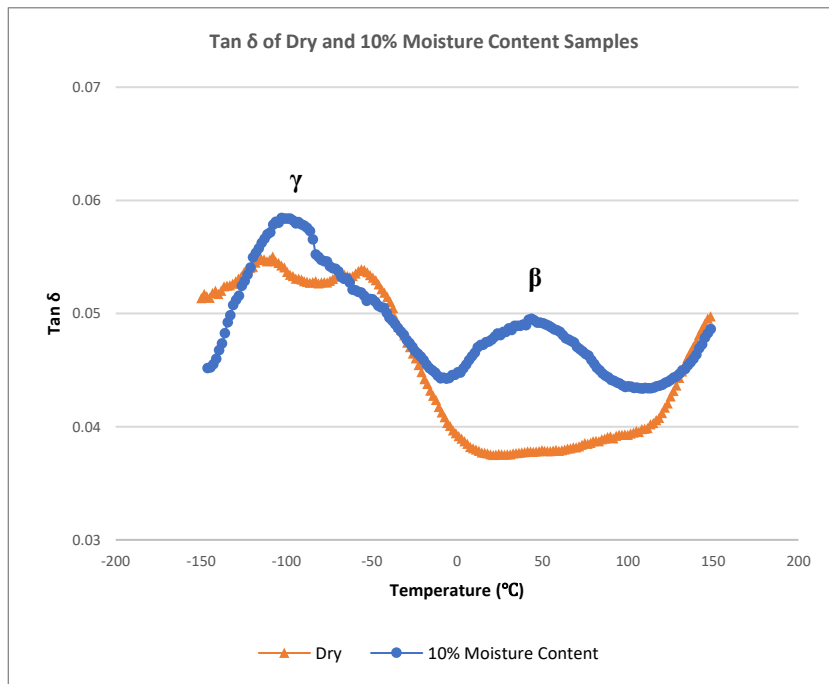


Figure 5-9 DMTA Tan δ of a New Sample for both Dry and Moisture Samples

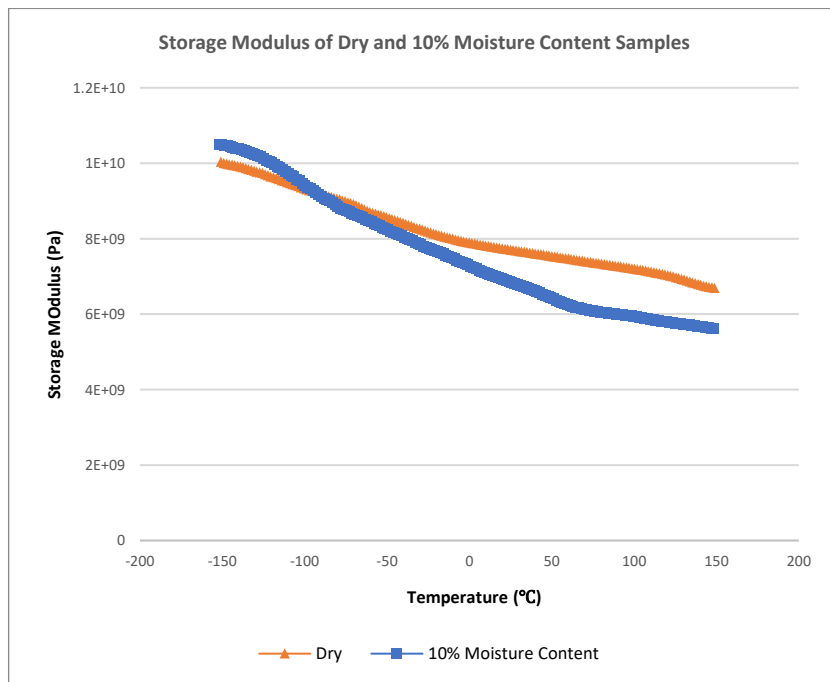


Figure 5-10 DMTA Storage Modulus of an Old Sample for both Dry and Moisture Samples

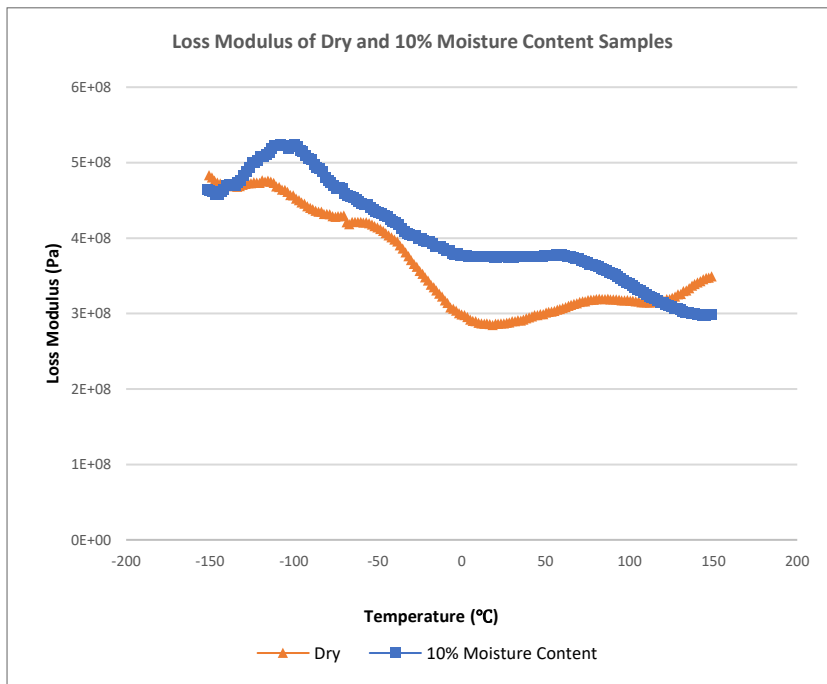


Figure 5-11 DMTA Loss Modulus of an Old Sample for both Dry and Moisture Samples

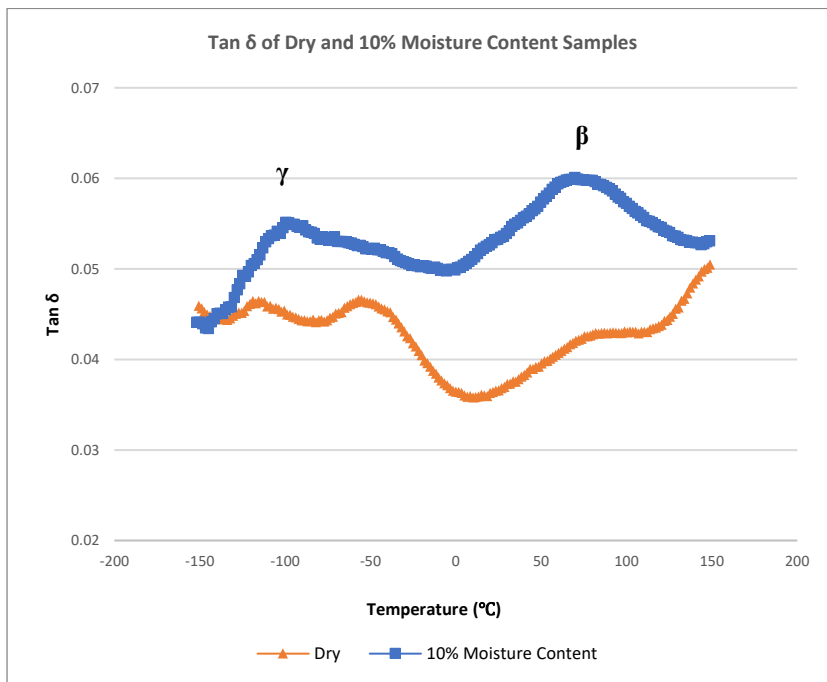


Figure 5-12 DMTA Tan δ of an Old Sample for both Dry and Moisture Samples

To sum up, moisture decreases the static mechanical properties (MOE and MOR) significantly but can enhance strain extension by re-arranging timber molecules in the yield stage. In dynamic mechanical test with temperature scanning, both peak β and peak γ are affected by the moisture while peak β disappeared if no moisture was present in samples.

5.2 Dynamic Mechanical Difference Between New and Old Pine

Dynamic mechanical thermal analysis (DMTA) highlights a different viscoelasticity behaviours for new and old pine samples (Figure 5-13). Generally, two clear peaks, γ and β , are clearly shown in the Tan δ curve. Peak γ of both the new and old samples is illustrated at approximately -100°C . Moreover, the small peak (γ_1), which is affected by the methylol group, in the Tan δ curve of dry new and old samples is illustrated for two slightly different temperatures (Figure 5-14). γ_1 of the old pine samples is found at a slightly lower temperature than for the new pine samples, which indicates that the methylol group in the former's molecules is slightly less. Peak β shows a large difference between the new and old pine samples. The peak β temperature of old pine is higher than new pine. Peak β is affected mainly by moisture content though affecting energy dissipation of molecule main chains. Hence, in the old pine samples, the molecule main chain is relatively stable, which is affected by moisture at a higher temperature.

Moisture plays a more significant role in the old pine samples than the new. Below -65°C , Tan δ of the old samples is slightly lower, but it is higher than for the new samples above -65°C and the gap increases with temperature. However, in the dry samples, Tan δ of both new and old pine decreases, with the latter decreasing more. Tan δ of old pine samples is significantly lower than for new pine under 0°C , but similar above this temperature. Hence,

dry old pine samples perform better as elastic materials, which also indicates their stable structure.

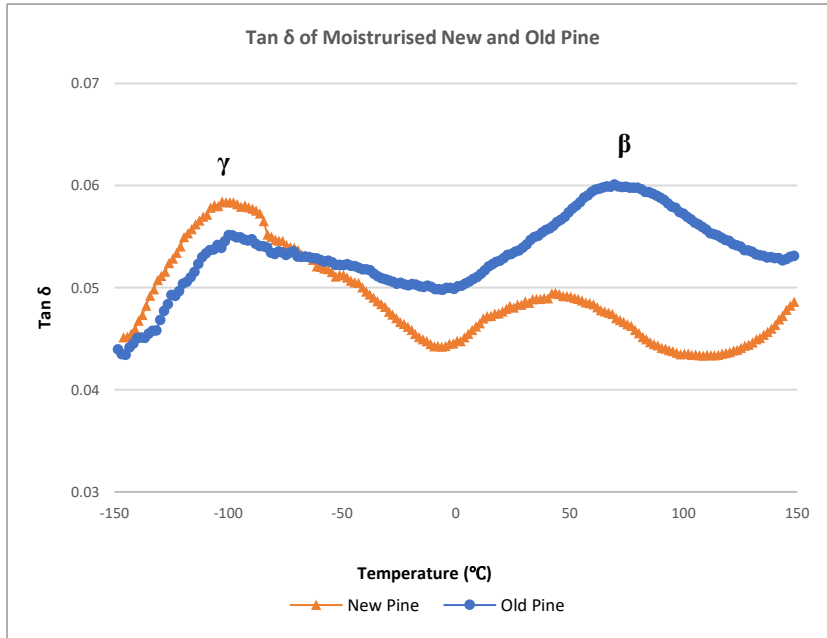


Figure 5-13 DMTA Tan δ of Moisturised New and Old Pine

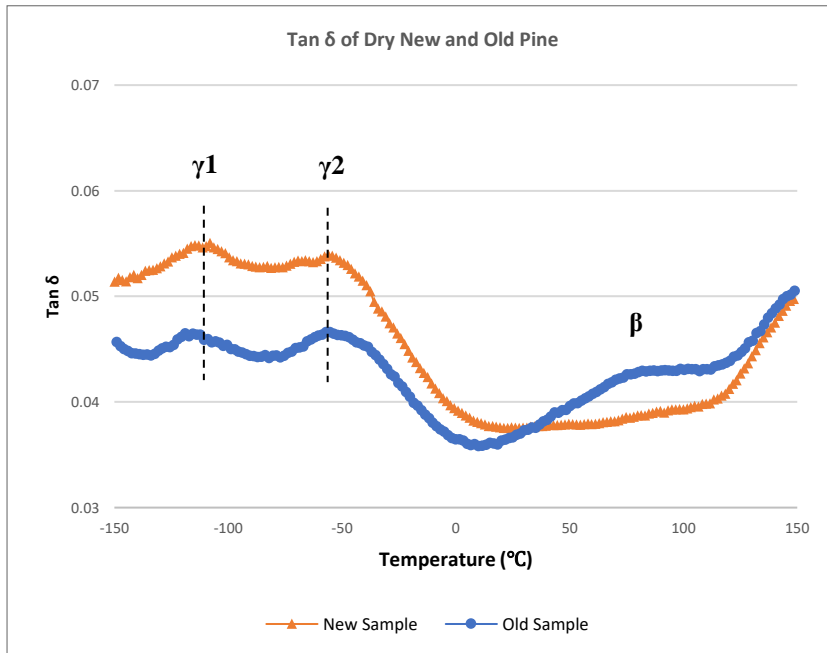


Figure 5-14 DMTA Tan δ of Dry New and Old Pine

5.3 Mechanical Property Changes in New Timber

New pine samples were treated at 120°C, 160°C and 200°C for 8, 12, 16, 20, 24 hours in air and vacuum atmospheres. The mean MOR and MOE are calculated by 15-20 samples in each treatment group.

5.3.1 Static Bending Mechanical Properties of New Pine

The MOR during heat treatment varies significantly (Figure 5-15 and Table 5-2). In general, the changes are affected by a treatment environment such that MOR increases at 120°C treatment in a vacuum but decreases at 200°C treatment in an air atmosphere after 24 hours.

MOR of new pine treated at 120°C in a vacuum has a 15% increase from 55.3 MPa to 63.9 MPa after 24 hours, with only 2.11% mass loss. In air treatment at 120°C, MOR increases significantly after the first 8 hours by approximately 11%, remains stable up to 16 hours and then drops significantly at 24 hours treatment. Compared to non-treated samples, the treatment at 120°C both in air and vacuum for 24 hours, MOR is improved. 200°C treatment contributes to a constant decrease in MOR for both air and vacuum environments. In air treatment, MOR decreases dramatically by 42% while in vacuum treatment, this decrease is only for approximately 15%. Hence, oxygen and a high temperature contribute to the decrease in MOR of new pine samples. Under 160°C treatment both in air and a vacuum MOR increases in the first 8 hours by approximately 8% in both, followed by a decrease. After 24 hours, MOR decreases by approximately 4% and 2% in air and vacuum treatment, respectively.

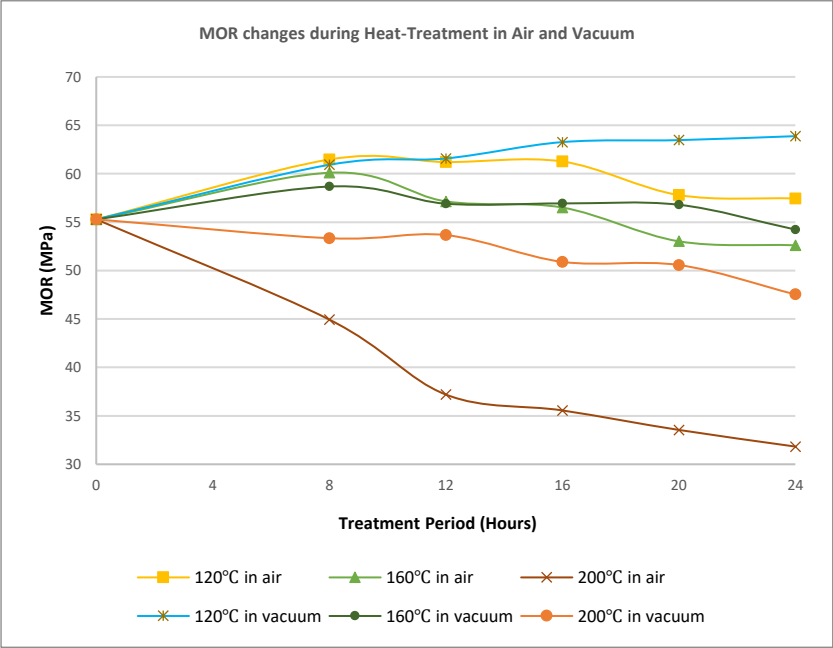


Figure 5-15 Changes in the Mean MOR of New Pine During Heat Treatment

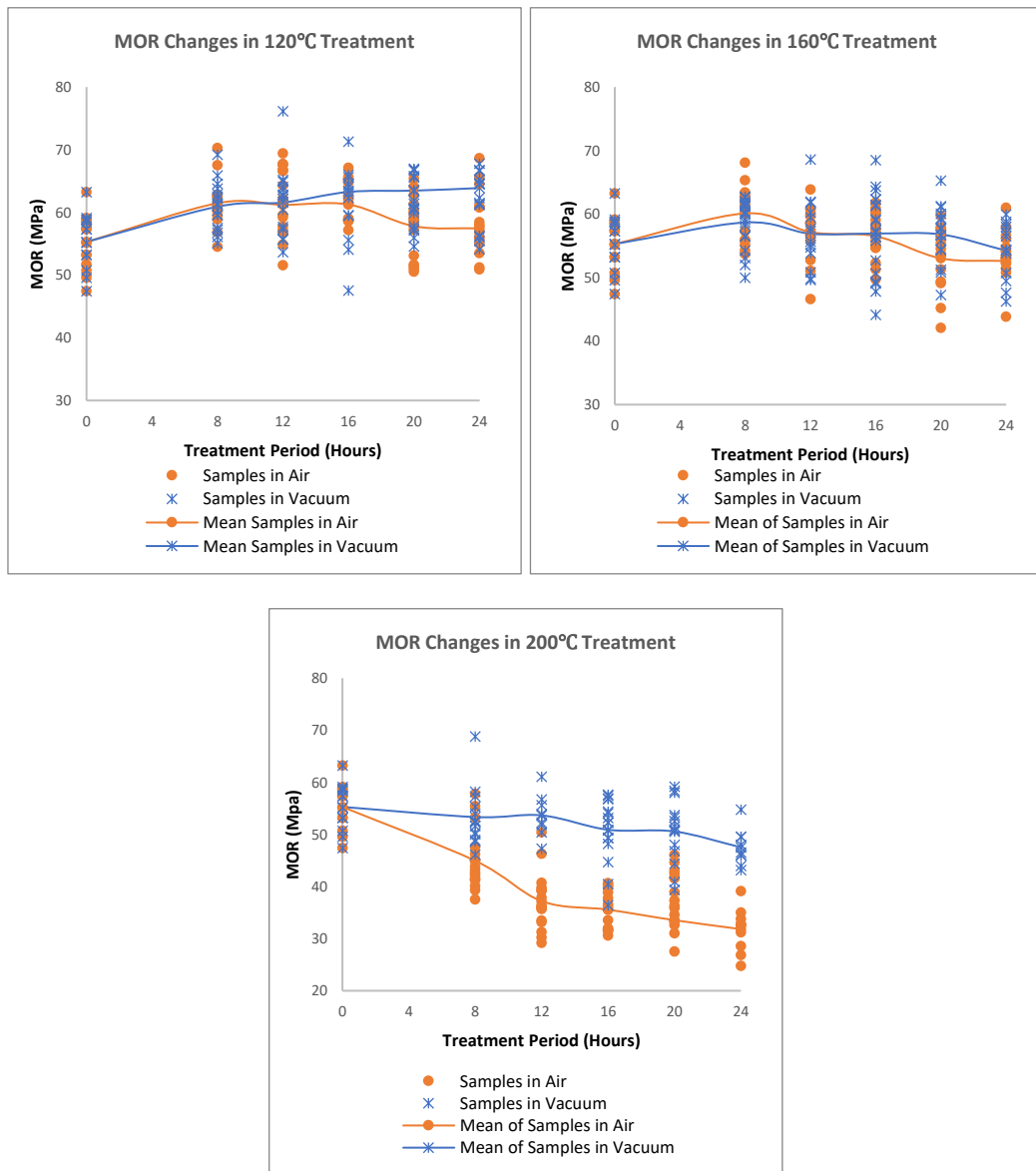


Figure 5-16 Change in the MOR Variation of New Pine During Heat Treatment

Table 5-2 Mean MOR (MPa) Changes of New Pine During Heat Treatment

Temperature		Treatment Period (hours)					
		0	8	12	16	20	24
Air	120°C	55.29	61.47	61.20	61.26	57.80	57.44
	160°C		60.10	57.15	56.51	53.02	52.61
	200°C		44.94	37.20	35.56	33.54	31.83
Vacuum	120°C		60.92	61.57	63.26	63.47	63.88
	160°C		58.67	56.91	56.93	56.79	54.23
	200°C		53.34	53.66	50.90	50.57	47.54

The MOE of new pine during heat treatment changes complexly (Figure 5-17 and Table 5-3), but with fewer changes for MOR. Comparing non-treated samples to treatment after 24 hours, MOE increase approximately 12%, 3%, 2%, 2%, 1% at 120°C in a vacuum, 120°C in air, 160°C in a vacuum, 200°C in a vacuum and 160°C in air, respectively, whilst it decreases by approximately 5% at 200°C in air.

The mass loss, which is up to 8%, does not affect MOE significantly. In treatment at 200°C in air after 8 hours, and the treatment at 200°C in a vacuum after 24 hours, MOE increases 6% and 1%, respectively, whilst the mass losses are 6% and 8%. MOE increases in all treatments for the first 8 hours. Unlike MOR changes, which decreased by oxygen, the highest MOE increase in the first 8 hours happens at 200°C in air, being 6%. Treatment at 160°C in air also contributes to a 4% increase in MOE in the first 8 hours. Moreover, the MOE increase in treatment at 200°C and at 160°C in a vacuum is 5% and 2.1%, respectively. After 8 hours treatment, MOE decreases constantly in treatment at 200°C in air and results in a 6% decrease after 24 hours treatment, with 14.5% mass loss. Hence, oxygen improves timber's MOE before 8% mass loss.

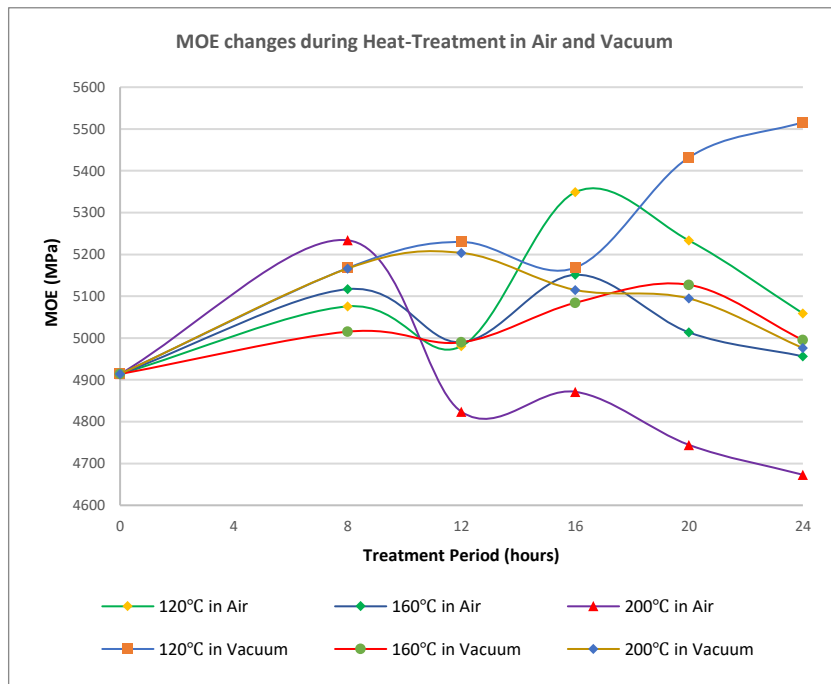


Figure 5-17 Mean MOE Changes of New Pine During Heat Treatment

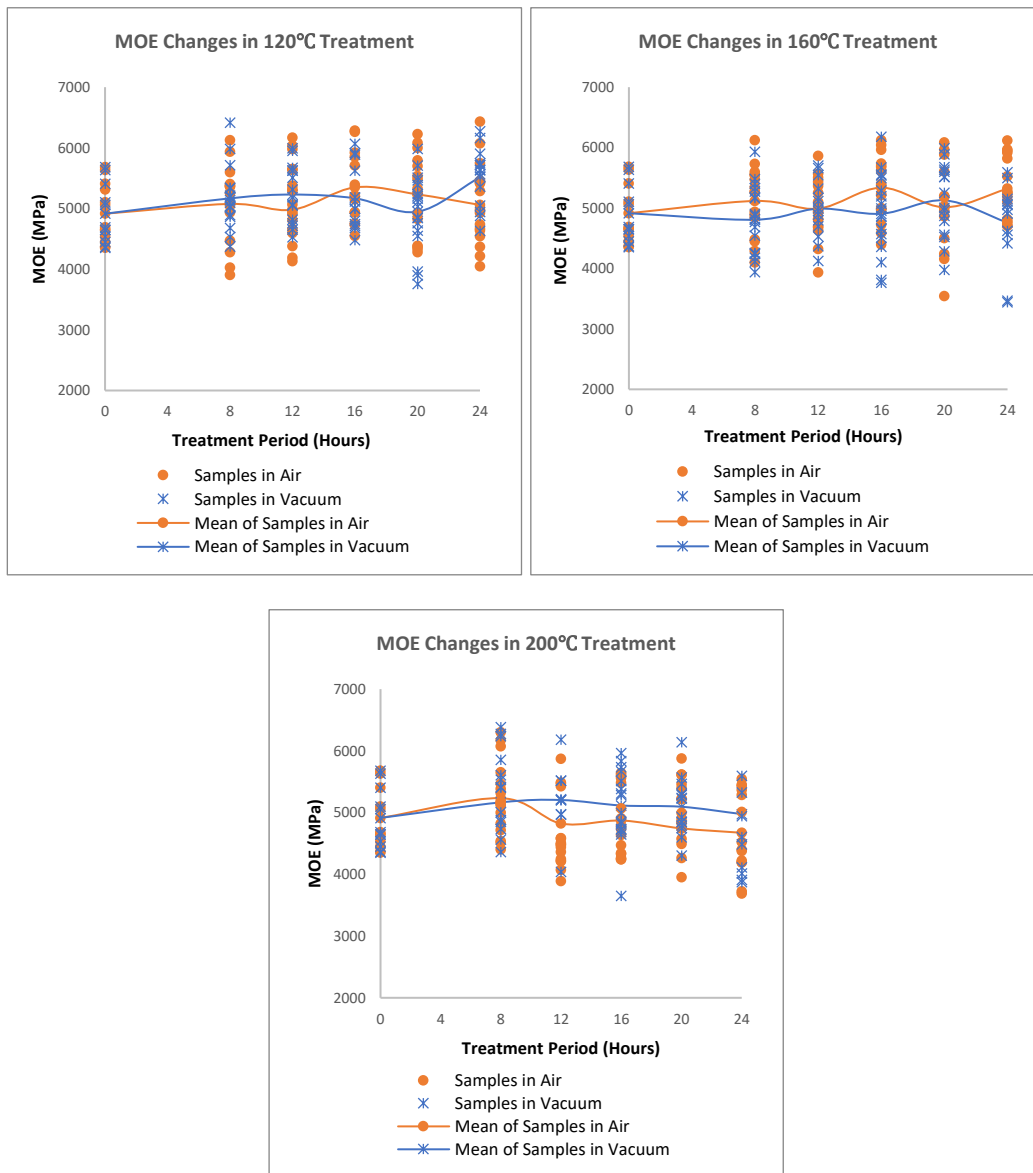


Figure 5-18 MOE Variation Changes of New Pine During Heat Treatment

Table 5-3 Mean MOE (MPa) Changes of New Pine During Heat Treatment

Temperature		Treatment Period (hours)					
		0	8	12	16	20	24
Air	120°C	4913	5075	4980	5348	5233	5058
	160°C		5116	4989	5013	5013	4956
	200°C		5233	4823	4871	4744	4672
Vacuum	120°C		5167	5229	5168	5432	5516
	160°C		5015	4987	5084	5127	4995
	200°C		5166	5203	5115	5094	4976

5.3.2 Bending Dynamic Mechanical Properties of New Pine

Tan δ of the dynamic mechanical properties decreases after 24 hours treatment at 120°C in a vacuum but it increases after treatment at 200°C in air (Figure 5-19). Compared to the static mechanical test, the former also enhances MOR and MOE, whilst the latter decreases them. The increase in the elasticity of timber also leads to an improvement in the static mechanical properties but an increase in viscosity contributes to a decrease on Tan δ .

Peaks γ and β on the Tan δ curve have appeared, but move to a higher temperature (Table 5-4 and Table 5-5), which indicates that timber molecules tend to acquire a stable status after any kind of heat treatment. In treatment at 120°C in a vacuum Peaks γ and β move to -80.9°C and 65.2°C, respectively, under a DMTA temperature scan, whilst with treatment at 200°C in air, they increase to -85.8°C and 60.3°C, respectively. The peaks on the Tan δ curve are affected by specific functional groups or moisture. When the peaks appear at a higher temperature, it means that the related functional groups need higher energy to cause friction between the timber molecules. Hence, the timber molecule is stable after treatments even though the static mechanical strength is decreased.

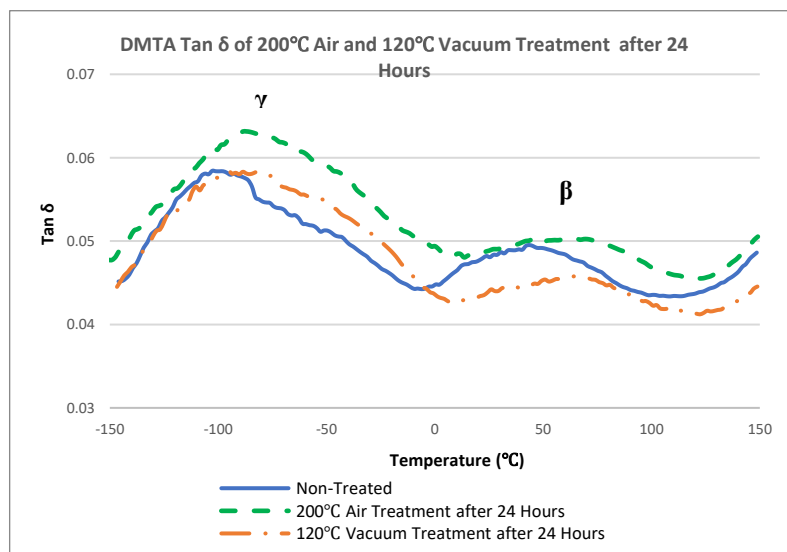


Figure 5-19 DMTA Mean Tan δ of New Pine Samples after Heat Treatment

Table 5-4 Dynamic Mechanical Properties of Peak γ of New Pine after 24 Hours Treatment

Treatment Atmosphere	Treatment Temperature	Peak Temperature	Storage Modulus	Loss Modulus	Tan δ	Absolute value of Complex Modulus
	(°C)	(°C)	(GPa)	(GPa)		(GPa)
Non-Treated		-101	7928	465	0.059	7942
Air	120	-92.2	7519	450	0.059	7532
	160	-92.2	7223	452	0.063	7237
	200	-85.8	6624	419	0.063	6637
Vacuum	120	-80.9	7330	434	0.059	7342
	160	-92	7090	426	0.060	7103
	200	-93.9	8004	460	0.057	8017

Table 5-5 Dynamic Mechanical Properties of Peak β of New Pine after 24 Hours Treatment

Treatment Atmosphere	Treatment Temperature	Peak Temperature	Storage Modulus	Loss Modulus	Tan δ	Absolute value of Complex Modulus
	(°C)	(°C)	(GPa)	(GPa)		(GPa)
Non-Treated		43.6	5393	279	0.051	5400
Air	120	52.6	5269	249	0.048	5275
	160	49.1	5267	274	0.052	5274
	200	60.3	5016	255	0.051	5023
Vacuum	120	65.2	5234	259	0.050	5241
	160	52.8	5163	252	0.049	5163
	200	58.5	6001	278	0.046	6008

5.3.3 Compression Tests Parallel to the Grain of New Pine

Compression tests parallel to the grain during heat treatment carried out to show the mechanical behaviours in different directions. Compression samples were cut into 20mm×20mm×40mm cuboids to fit the compression test facility. However, because of the limited sample quantities, the samples were only treated at 160°C and 200°C both in air and vacuum atmospheres. All the data are illustrated in Table 5-6.

The changes of mass loss (Figure 5-20 and Figure 5-21) and equilibrium moisture content at 20°C with 65% relative humidity (EMC) (Figure 5-22 and Figure 5-23) during heat treatment are much less than for small samples in the same treatment atmosphere, but the trend is the same. Mass loss increases with temperature and oxygen. The highest mass loss, 8.76%, happens at 200°C in air after 24 hours, which is much less than with small samples in the same treatment atmosphere, at 14.5%. In other treatments, the mass loss at 200°C in a vacuum, at 160°C in air and a vacuum after 24 hours are 4.8%, 1.34% and 1.31%, respectively. The EMC drops to 7.55% and 8.62% in the treatment at 200°C both in air and a vacuum after 24 hours, respectively, which is higher than with small samples, standing at 5.25% and 6%, respectively, after the same treatments. However, the EMC is less affected in 160°C treatment both in air and a vacuum.

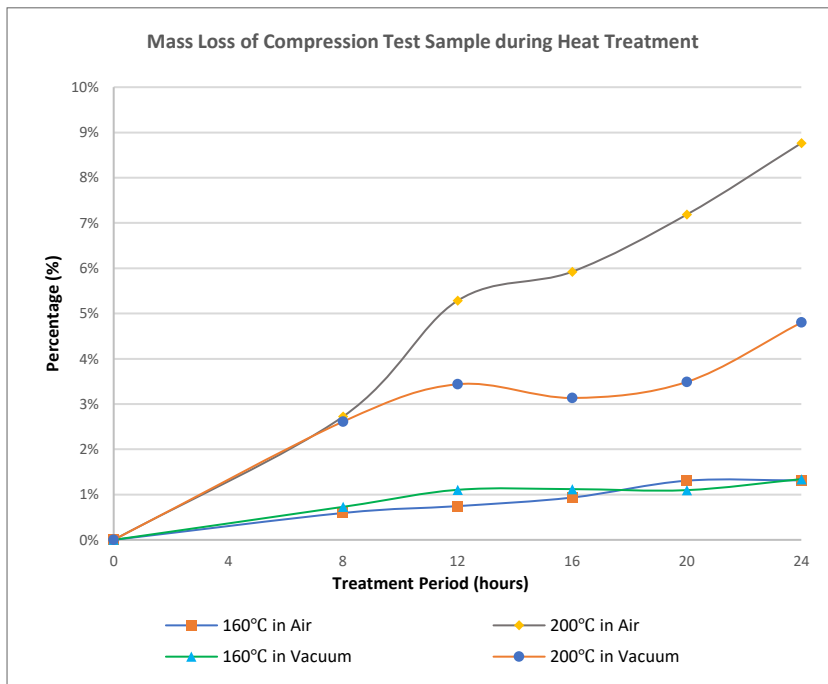


Figure 5-20 Mass loss of Compression Test Samples During Heat Treatment

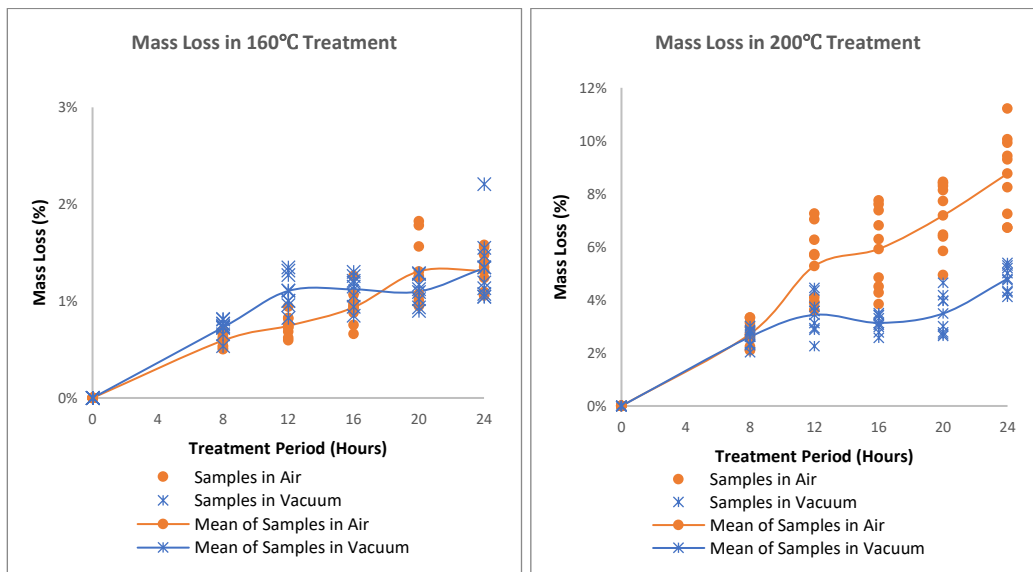


Figure 5-21 Mass loss Variation of Compression Test Samples During Heat Treatment

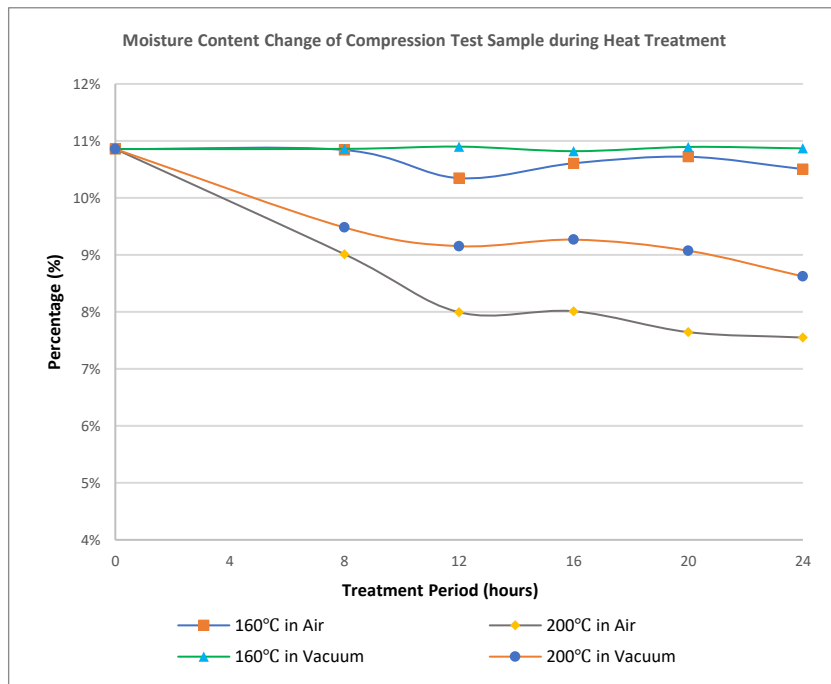


Figure 5-22 EMC Change of Compression Test Samples During Heat Treatment

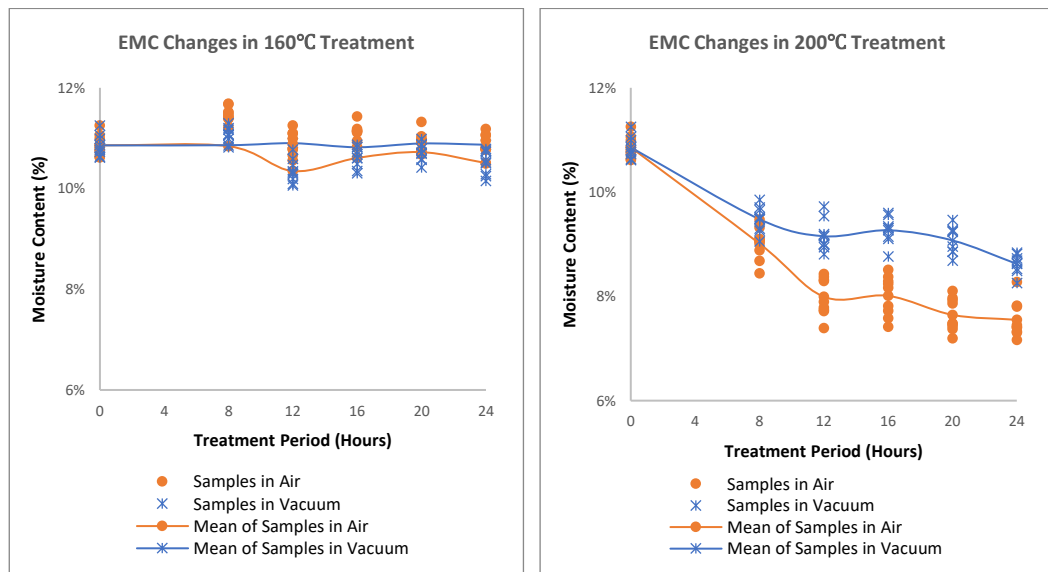


Figure 5-23 EMC Error Change of Compression Test Samples During Heat Treatment

The compression MOE (Figure 5-24 and Figure 5-25) and MOR (Figure 5-26 and Figure 5-27) shows a different behaviour compared to the bending test. In general, the

compression MOR (modulus of rupture) is more complex than that for MOE (modulus of elasticity).

The compression MOE increases constantly in the treatment at 160°C in a vacuum by approximately 11% after 24 hours, whilst it increases in the first 12 hours treatment in air treatment followed by a decrease. In treatment at 200°C, the compressive MOE both in air and vacuum treatment increases during the first 8 hours followed by a decrease. However, a vacuum atmosphere improves compression MOE significantly more than with air. Comparing compression MOE with bending MOE, the static mechanical properties of large samples at 160°C treatment are the same as those for small samples at 120°C treatment. Hence, large samples need higher temperatures to cause a similar mechanical change to small ones.

The compressive MOR of all the samples decrease slightly after 24 hours treatment, with the changes being complex and less than 10%. Apart from treatment at 200°C in air, which leads to a constant decrease in the compression MOR, other treatment atmospheres contribute to unpredictable wave changes in MOR.

Hence, the compression MOE are affected by heat treatment atmosphere but compression MOR does not show significant changes before 6% mass loss.

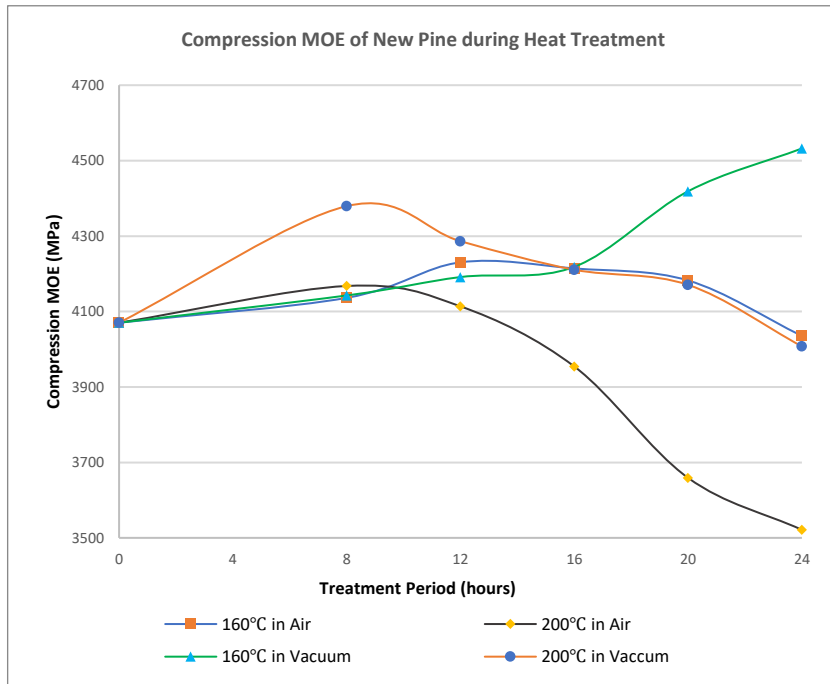


Figure 5-24 Compression MOE Parallel to the Grain of New Pine

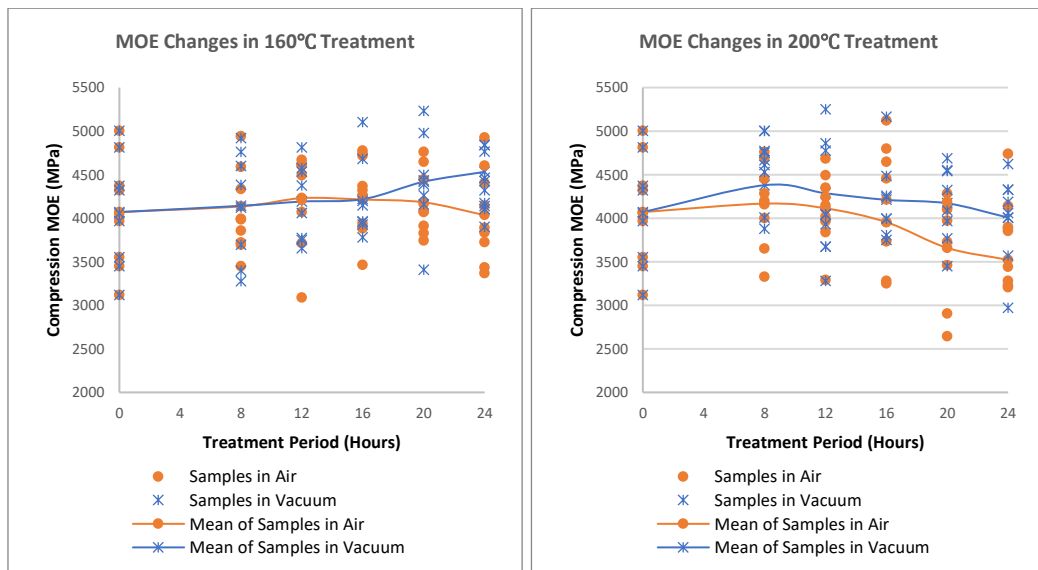


Figure 5-25 Compression MOE Variation Parallel to the Grain of New Pine

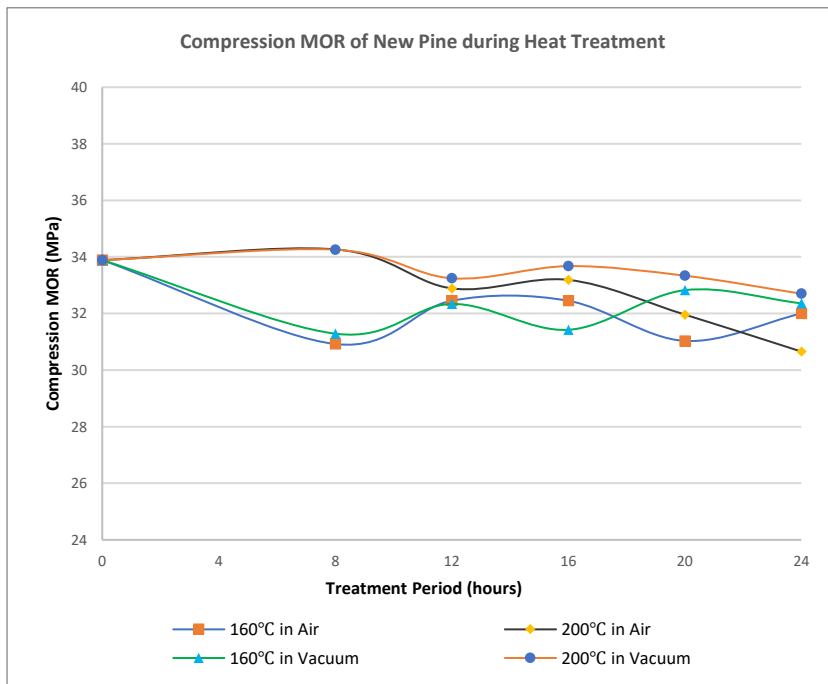


Figure 5-26 Compression MOR Parallel to the Grain of New Pine

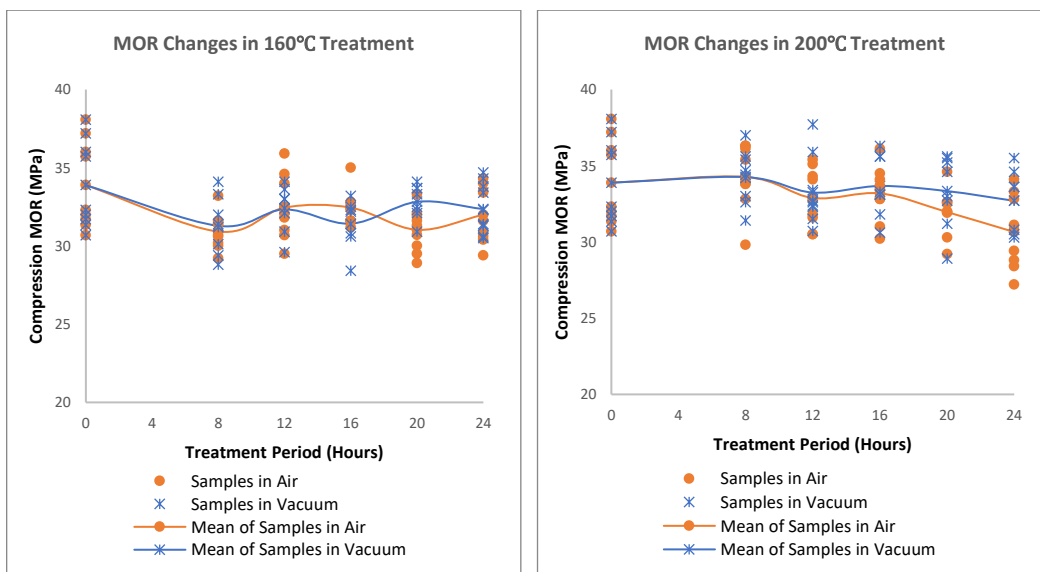


Figure 5-27 Compression MOR Variation Parallel to the Grain of New Pine

Table 5-6 Mass Loss, EMC Change and Static Compression Mechanical Property

		Mass loss	EMC	MOE	MOR		
		(%)	(%)	(MPa)	(MPa)		
Non-Treated		0	10.86	4070	33.88		
Air	160	8	0.59	4136	30.92		
		12	0.75	4230	32.45		
		16	0.93	4214	32.4		
		20	1.31	4182	31.03		
		24	1.34	4035	32		
	200	8	2.72	4167	34.26		
		12	5.28	4113	32.89		
		16	5.92	3954	33.19		
		20	7.18	3658	31.96		
		24	8.76	3521	30.66		
		Vacuum	160	8	0.73	4142	31.28
				12	1.1	4191	32.33
16	1.12			4218	31.43		
20	1.1			4418	32.82		
24	1.31			4532	32.36		
200	8		2.61	4379	34.26		
	12		3.44	4286	33.24		
	16		3.13	4210	33.68		
	20		3.49	4170	33.33		
	24		4.8	4007	32.7		

5.3.4 Summary

Heat treatment affects mechanical properties of new pine samples by improving or weakening the strength of timber cell walls. The cell wall is a long tube (Figure 5-28), which gives the feature of anisotropy for timber materials. The modulus of elasticity (MOE) of a bending test and the modulus of rupture (MOR) of a compression test are complex

such that the changing trends are difficult to predict. Hence, molecular structures are also an important factor affecting the mechanical property changes of timber. The bending MOR and compression MOE are affected by the molecule cell wall strength, whilst the bending MOE and compressive MOR are affected by the cell structure.

In general, the changes in the bending MOR and compression MOE are similar. In treatment at 120°C in a vacuum, (for compression samples with a large size, it is 160°C), the bending MOR and compression MOE increase constantly, whilst at 200°C in air the two decrease significantly. In other treatments, the two properties increase at first, followed by a decrease and mass loss is an important reason for these mechanical properties decreasing.

The dynamic mechanical properties by bending shows that the timber molecule stability is enhanced after any kind of heat treatment, due to Peak β and γ appearing at higher temperatures. Moreover, the $\tan \delta$ curve also indicates that the elasticity of new pine is enhanced in treatment at 120°C in a vacuum whilst the viscosity is increased at 200°C in air. Hence, the bending MOR and compression MOE is improved by the increasing in viscosity of sample but decreased by the elasticity increasing.

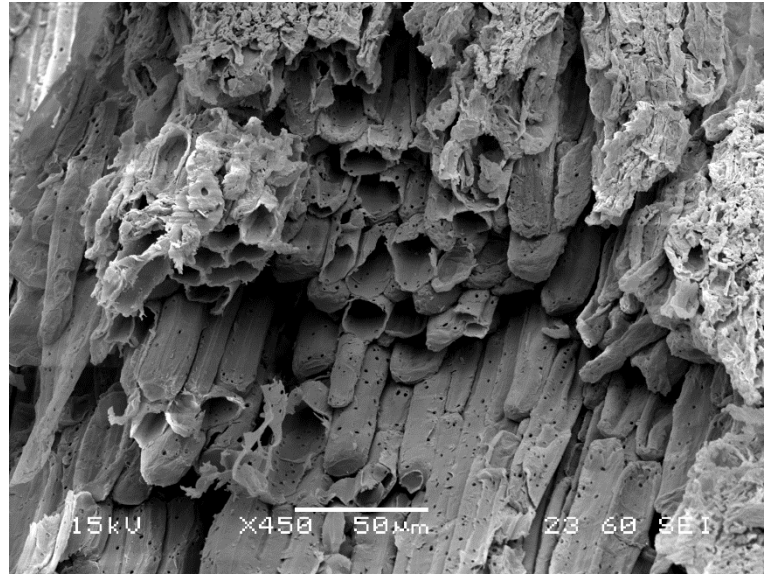


Figure 5-28 Scanning Electron Microscope (SEM) of Timber Cells

5.4 Mechanical Property Changes in Old timber

Due to limited volume, the old pine samples were only cut into 2mm × 4mm × 35mm size and treated only in 120°C and 200°C both in air and a vacuum. Hence, the bending mechanical property changes of old samples during 160°C treatment and the compression mechanical properties are not covered in this section.

5.4.1 Static Bending Mechanical Properties of Old Pine

In general, the MOR of the old pine samples has similar changes during heat treatment at 120°C and 200°C as with new ones (Figure 5-29, Figure 5-30 and Table 5-7). It increases by approximately 8% after 24 hours treatment at 120°C in a vacuum, whilst in air, it increases during the first 16 hours of treatment by approximately 7%, followed by a decrease. The mass losses of the two treatment after 24 hours are 1.42% and 1.65%, respectively. A lower mass loss does not lead to a MOR decrease. In treatment at 200°C, timber strength reduces dramatically by approximately 60% and 32% in air and a vacuum, with a mass loss of 19% and 16%, respectively.

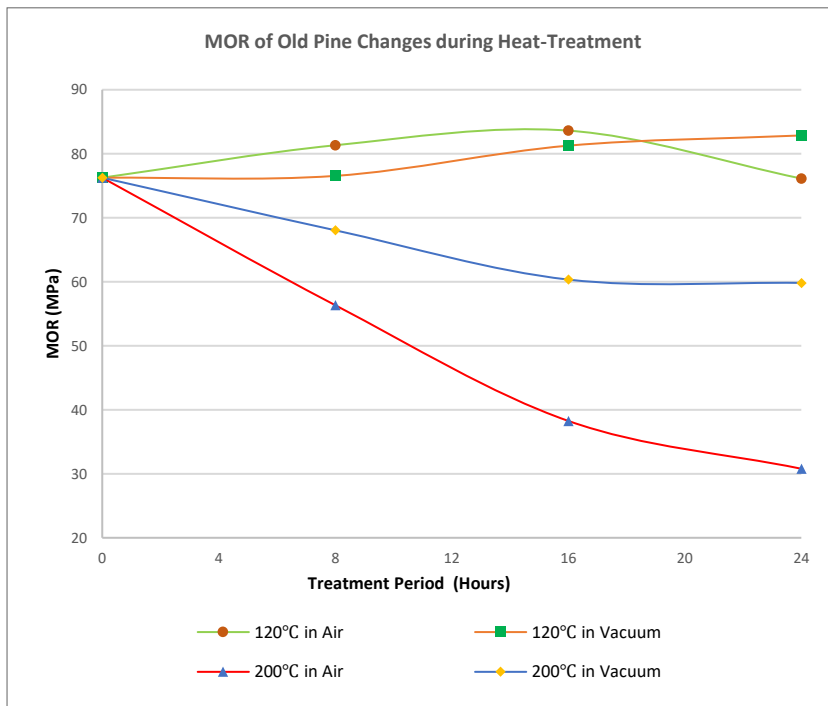


Figure 5-29 MOR of Old Pine Changes During Heat Treatment

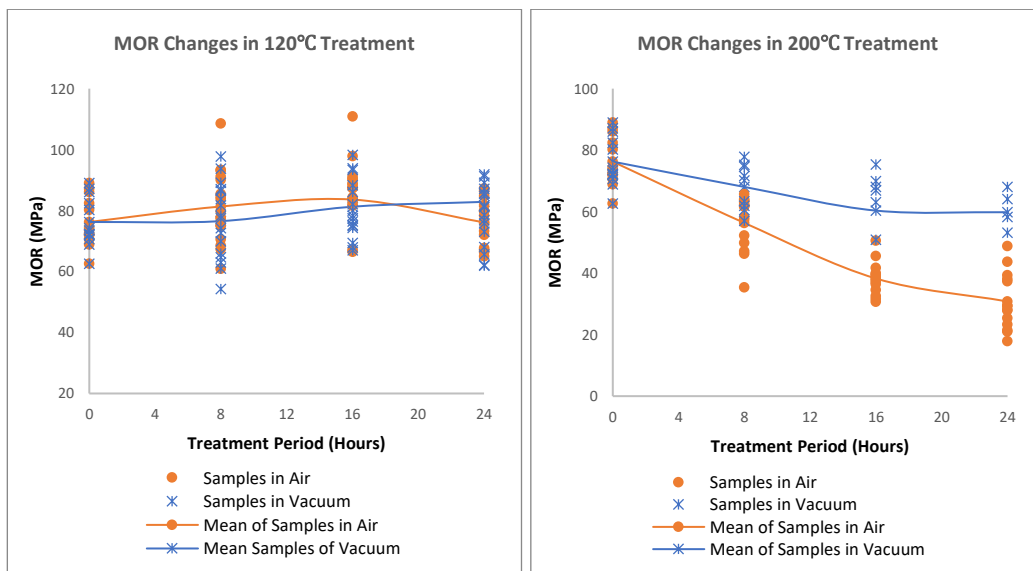


Figure 5-30 MOR Variation Changes of Old Pine During Heat Treatment

Table 5-7 MOR (MPa) Changes of Old Pine During Heat Treatment

	Temperature	Treatment Period (hours)			
		0	8	16	24
Air	120°C	76.25	81.33	83.61	76.12
	200°C		56.34	38.26	30.78
Vacuum	120°C		76.54	81.26	82.85
	200°C		68.04	60.34	59.82

The MOE of the old samples also shows complex changes during heat treatment, as with the new ones. It improves for all treatments in the first 8 hours (Figure 5-31, Figure 5-32 and Table 5-8), increasing by approximately 9%, 5%, 3% and 1% at 120°C in air, 200°C in air, 120°C in a vacuum and 200°C in a vacuum respectively. Vacuum treatment at 120°C and 200°C improves MOE significantly by approximately 15% and 6% after 24 hours treatment, with at mass loss of 1.42% and 16%, respectively. Moreover, a large decrease in MOE happens at 200°C in air of 11% after 24 hours. Hence, same as the mechanical behaviour of the new pine samples during heat treatment, oxygen can improve MOE over a short treatment period with low mass loss, but for a long period, vacuum atmosphere and 120°C treatment lead to a higher MOE.

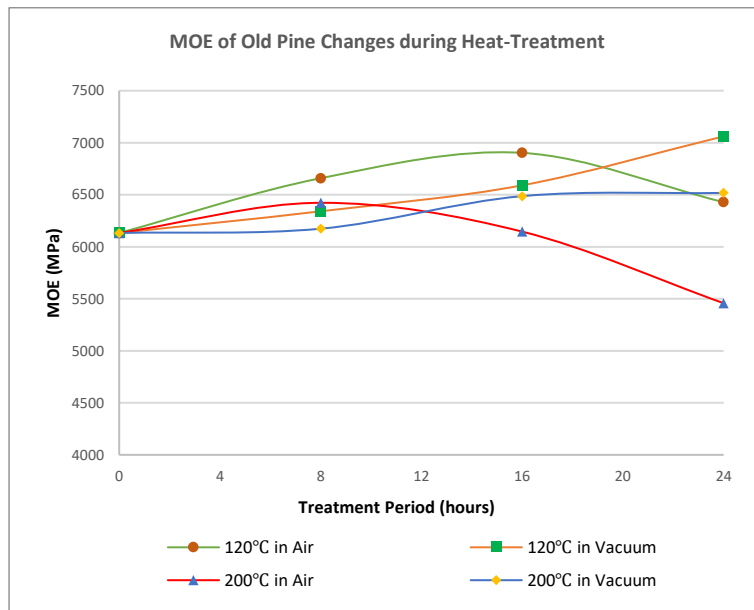


Figure 5-31 MOE Changes of Old Pine During Heat Treatment

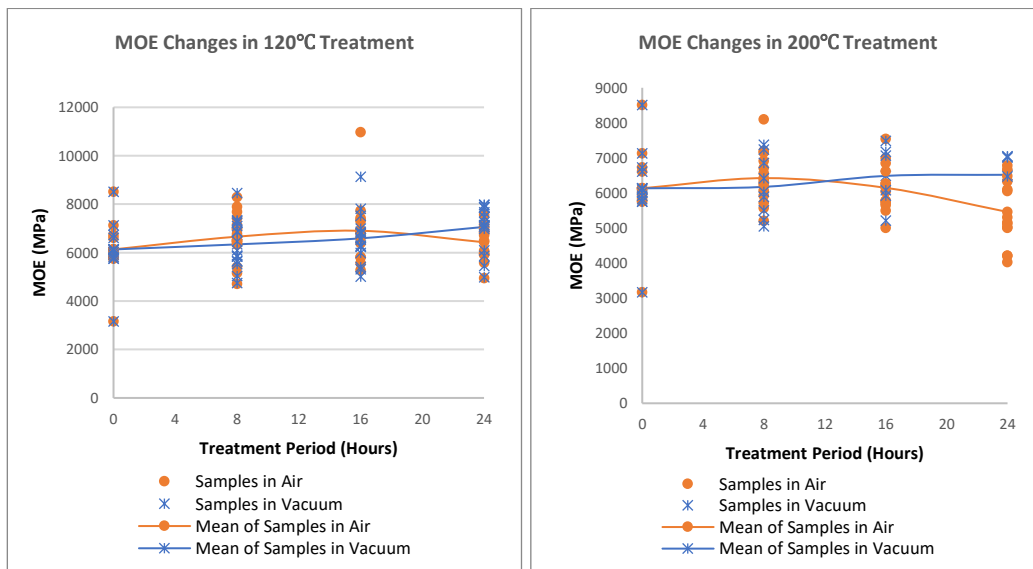


Figure 5-32 MOE Variation Changes of Old Pine During Heat Treatment

Table 5-8 MOE (MPa) Changes of Old Pine During Heat Treatment

	Temperature	Treatment Period (hours)			
		0	8	16	24
Air	120°C	6132	6658	6902	6428
	200°C		6422	6145	5457
Vacuum	120°C		6340	6590	7061
	200°C		6173	6486	6517

5.4.2 Dynamic Mechanical Properties of Old Pine

In the DMTA test, $\text{Tan } \delta$ of the old pine samples non-treated and treated at 200°C in air for 24 hours, is similar under temperature scanning from -150°C to 150°C (Figure 5-33). The 19% mass loss does not affect the viscoelasticity of the old samples. However, $\text{Tan } \delta$ decreases significantly in treatment at 120°C in a vacuum due to a loss modulus decrease, which indicates low friction between the timber molecules. Hence, the connection between the timber molecules are improved in the treatment.

On the $\text{Tan } \delta$ curve, both Peak γ (Table 5-9) and Peak β (Table 5-10) are less affected, appearing at temperatures from -98°C to -91°C and 69°C to 75°C, respectively. As the two peaks are influenced by the methylol groups and moisture in the main chain, respectively, the methylol groups and the structure of old pine molecule single chain is less affected by heat treatment. Hence, the molecules of old pines show more stability than new pine.

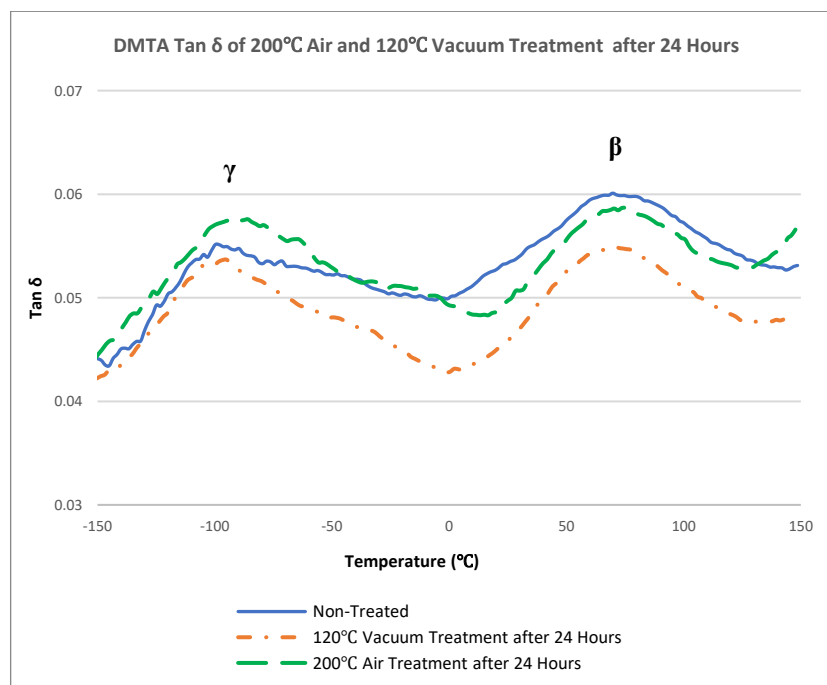


Figure 5-33 DMTA Mean $\text{Tan } \delta$ of Old Pine Samples after Heat Treatment

Table 5-9 Dynamic Mechanical Properties of Peak γ of Old Pine after 24 Hours Treatment

Treatment Atmosphere	Treatment Temperature (°C)	Peak Temperature (°C)	Storage Modulus (GPa)	Loss Modulus (GPa)	Tan δ	Absolute value of the Complex Modulus (GPa)
Non-Treated		-97.2	9353	523	0.056	9368
Air	120	-95.8	9664	534	0.055	9679
	160	-96.6	9882	544	0.056	9897
	200	-91.24	8601	507	0.059	8616
Vacuum	120	-95.7	10487	560	0.054	10502
	160	-94.8	10222	520	0.051	10236
	200	-91.4	9087	502	0.056	9103

Table 5-10 Dynamic Mechanical Properties of Peak β of Old Pine after 24 Hours Treatment

Treatment Atmosphere	Treatment Temperature (°C)	Peak Temperature (°C)	Storage Modulus (GPa)	Loss Modulus (GPa)	Tan δ	Absolute value of the Complex Modulus (GPa)
Non-Treated		69.2	6103	381	0.063	6115
Air	120	70.2	6680	378	0.057	6691
	160	74.9	6789	413	0.061	6802
	200	70.7	6210	371	0.06	6221
Vacuum	120	70.3	7068	389	0.055	7079
	160	70.7	7288	383	0.053	7298
	200	74.76	6671	337	0.05	6680

5.4.3 Summary

The static mechanical properties of old pine samples experience similar changes to new pine ones. Both the modulus of rupture (MOR) and modulus of elasticity (MOE) are improved in treatment at 120°C in a vacuum by 8% and 15% but decrease in treatment at 200°C in air by 60% and 11%, respectively.

The elasticity increases in vacuum treatment at 120°C, but there is less change in air treatment even though the mass loss is high. The temperature at which the Peak γ and β on the Tan δ curve appeared are similar after all heat treatments, which indicates that the molecule structure of old pine is much more stable than new pine.

5.5 Discussion and Conclusion

The mechanical properties of timber changes distinctively in different directions. The bending MOR and compression MOE change sensitively during heat treatment, but the bending MOE and compression MOR are not affected as much as the two former properties even with high mass loss. Korkut et al. (2008) obtained similar changes for treatment at 120°C, 150°C and 180°C for 5, 6, 10 hours on maple. Heat treatment can enhance or diminish the strength of cell walls and lead to distinctive changes in mechanical properties. Moreover, timber cells, which are long tubes, play an essential role in the differences of three direction mechanical properties. Hence, the distinct cell structures also affect the bending MOE and compression MOR as well as the cell wall strength. However, according to Backman and Lindberg (2001), the Tan δ temperature scanning curve from -150°C to 150°C, which contains two peaks, is not changed.

Density and moisture content play significant roles in static mechanical properties even in non-treated samples. The density of old pine samples is more than in new pine by approximately 20%. The reason is the two pieces of samples are from different parts of

trunks, which lead to different MOE and MOR. Yang and Evans (2003) found that density has high positive correlations with MOE and MOR in different species of *E. globulus*, *E. nitens* and *E. regnans* wood with age ranging from 15 to 33 years old. Similar results were found by Dinwoodie (1975), who also reported that moisture content affect timber mechanical properties with negative correlations. A mathematical model to predict mechanical properties by moisture content works well, according to Kretschmann and Green (2007), who studied non-treated pine samples (*Pinus echinata* and *Pinus taeda*) by means of testing. Moisture content also affects the dynamic mechanical properties, especially the β peak of $\text{Tan } \delta$. Dry samples show higher static mechanical properties and elasticity than moist samples, with both new and old samples exhibiting this influence.

In terms of the bending static mechanical properties, the MOR changes in both new and old samples during heat treatment is more significant than those for MOE, due to the coefficient of variation (CV) of MOE being largely more than for MOR both in new (Table 5-11) and old pine (Table 5-12) samples. CV illustrates the degree of variation by the following equation:

$$C_v = \frac{\sigma}{\mu} \times 100\%$$

where C_v is coefficient of variation, σ is the standard deviation and μ is the mean of the data. Kim (1998); Bekhta and Niemz (2003) also reported that MOE is more unpredictable than MOR during heat treatment in any atmosphere.

Table 5-11 Coefficient of Variation of MOE and MOR of New Pine During Heat Treatments (20 samples)

Temperature		Treatment Period (hours)						
		0	8	12	16	20	24	
Air	120°C	MOE		13%	17.4%	10%	12.5%	13.3%
		MOR		6.4%	8.6%	5.3%	8.3%	8.5%
	160°C	MOE		11.2%	10%	9.6%	14.6%	9.4%
		MOR		7%	7.2%	6%	8.6%	6.8%
	200°C	MOE		10.8%	12.6%	11.2%	13.5%	14%
		MOR	9.7%	12.6%	10%	10.4%	9.2%	12.4%
Vacuum	120°C	MOE	8%	10.7%	10.1%	10.3%	12.4%	10.4%
		MOR		6.1%	7.8%	7.5%	6.3%	7.2%
	160°C	MOE		11.4%	9.5%	12.7%	11.7%	14%
		MOR		6.6%	7.2%	10.1%	7.5%	8.2%
	200°C	MOE		12.2%	11.8%	11.6%	12.2%	13.9%
		MOR		6.6%	7.8%	10.9%	9%	7.3%

Table 5-12 Coefficient of Variation of MOE and MOR of Old Pine During Heat Treatments (20 samples)

Temperature		Treatment Period (hours)				
		0	8	16	24	
Air	120°C	MOE		14.1%	18.7%	11.2%
		MOR		12.1%	9.2%	10%
	200°C	MOE		11.8%	11.3%	17.3%
		MOR	19.1%	10.7%	14.6%	30%
Vacuum	120°C	MOE	10.4%	15.2%	15.3%	13.1%
		MOR		10.2%	11.7%	11.4%
	200°C	MOE		13.8%	13.6%	12.6%
		MOR		11%	11.6%	9.2%

*upper (MOE), below (MOR)

In addition to treatment at 200°C in air, other treatments (200°C in a vacuum, 160°C in air and vacuum, 120°C in air and vacuum) improve MOR values in specific period. Similar results with the same treatment method and sample preparation were reported by Mitchell (1988), who treated pine samples at 150°C in air and nitrogen. Bekhta and Niemz (2003) also observed the MOR of spruce samples increases in a specific period treatment at 100°C and 150°C in air but decrease at 200°C. Shi et al. (2007) reported that MOR decreases constantly from 24 hours to 60 hours treatment at approximately 200°C in air. However, Goroyias and Hale (2002) reported a slight increase in the MOR of pine (*Pinus Sylvestris*) samples after 20 minutes treatment. Hence, in any heat treatment atmosphere, MOR is improved in a specific treatment period even though in a higher temperature. A few authors have obtained a constant decrease in MOR, which is different to the outcome of the

experiments. One important reason for this is that these authors did not consider the sample moisture content influence during heat treatment. Boonstra et al. (2007b) reported a different level of decrease in few pine and spruce samples with 165°C to 185°C treatment after 6 hours. The author recorded that samples are treated with 16%-20% moisture content, but in this experiment, samples were dried before heat treatment. Moisture was involved in the decomposition changes by a hydrolysis reaction, which also contributed to 13% decrease in density. Mitchell (1988) observed that the MOR of green samples decrease more than dry samples in the same treatment. Similar MOR decreases in moisture samples during heat treatment were reported by Poncsak et al. (2006), Kamdem et al. (2000) and Mburu et al. (2008). In the treatment of old pine, MOR changes are similar as with new.

The reported bending MOE changes during heat treatment vary, with some studies registering increases (Inoue et al., 1993; Santos, 2000), other decreases (Shi et al., 2007; Mburu et al., 2008; Rusche, 1973) and some found little affect (Kim, 1998; Rapp and Sailer, 2000; Goroyias and Hale, 2002). Mass loss is an important factor, according to Rusche (1973), who found that MOE changes slightly before 8-10% mass loss. In addition, MOE is also significantly affected by the microfibril angle, especially the S2 layer of the cell wall (Evans and Elic, 2001; Evans et al., 2000). In current experiments, the microfibril angles of each sample are slightly different, which is a factor contributing to a large variation in MOE. The close relationship between the microfibril angle and MOE was also reported by Yang and Evans (2003).

Dynamic and static mechanical properties show a close relation between each other. The increase in elasticity due to the decrease in $\tan \delta$ also leads to an improvement in the bending MOE and MOR. The increase in viscosity owing to the increase in $\tan \delta$, has the effects of the decrease of the bending MOE and MOR. Moreover, the two peaks on the \tan

δ curve increase after any kind of heat treatment, which indicates that the molecules are stable after being subjected to it.

Chapter 6 Chemical Composition and Mechanical Properties

In this chapter, the mechanical properties and chemical compositions of all the samples, including new and old pine, are discussed together to address the relationships between the two. Both the static and dynamic mechanical properties are predicted by the peak areas of the FTIR spectrum through a suitable regression analysis method. Curve fitting, multiple regression analysis and ridge regression analysis are the three essential analysis methods for the mathematic models.

6.1 Static Mechanical Properties and Chemical Composition

The modulus of rupture (MOR) and modulus of elasticity (MOE) are two essential measurements in static mechanical property tests used to describe timber strength. In this section, the mathematic models are produced to predict the bending MOR and MOE from the peaks on the FTIR spectrum. In general, the bending MOR is predicted by a curve fitting method with logarithm relation and multiple regression analysis. The bending MOE is predicted by multiple regression analysis and ridge regression analysis. The four mathematical models have their own advantages, and all are suitable for prediction.

The relationships between the compression mechanical properties and timber chemical compositions are also discussed. However, since the compression testing samples are too large to fit the FTIR facility, the regression mathematic models for the compression MOR and compression MOE are not provided.

6.1.1 Bending Modulus of Rupture and Chemical Composition

Comparing chemical composition and MOR changes during heat treatment, the latter increase due to chemical reactions, which can expand or extend the molecule length or the

matrix. The reactions happen in hemicellulose and lignin molecules, including lignin condensation, lignin-hemicellulose condensation and lignin cross-linking changes. MOR is reduced as a result of timber molecules changing into shorter chains including lignin and hemicellulose pyrolysis. Moreover, condensation which is based on the hydroxyl groups, is inhibited by oxygen since this group can be oxidised to carbonyl group (C=O). High temperature and oxygen also improve pyrolysis in hemicellulose and lignin.

In heat treatment at 120°C in a vacuum, MOR of both new and old pine increases constantly by approximately 15% and 8%, respectively. In terms of new pine, the FTIR spectrum shows clear lignin-hemicellulose condensation (Figure 4-6) and lignin condensation II (Figure 4-4) due to the increase in the ether linkage (C-O-C, peak 1154) and the decrease in the hydroxyl group (-OH), lignin condensation I (Figure 4-3) due to the increase of peak 1318 and lignin cross-linking (Figure 4-5) due to the increase in the C-C bonds and decrease in the carbonyl group (C=O). Hemicellulose deacetylase and a low rate of pyrolysis of hemicellulose are also observed due to an increase in the C=C bonds and at decrease in the peaks relating to hemicellulose, which leads to 2.11% and 1.42% mass loss in new and old pine during the treatment, respectively. In terms of old pine samples treatment, MOR increases, which is mainly due to cross-linking, but there are lesser condensation reactions, which contribute to a lower increase in MOR than with new pine. The FTIR spectrum shows that hemicellulose and lignin molecules have been condensed during the natural ageing process, which enhances timber molecules to resist 120°C temperature and leads to lower mass loss than with the new pine samples. In addition, with the treatment at 120°C for the old samples, MOR changes in air and vacuum atmospheres are the same. Oxygen does not play a significant role in the MOR of old pine which is different to the same treatment in new pine. Hence, old pine also has been oxidised during natural ageing.

MOR shows a 42% and 60% decrease at 200°C treatment in air after 24 hours for new and old pine samples, respectively. A condensation reaction and cross-linking reaction may happen in the first few hours of treatment, whilst pyrolysis of hemicellulose (Figure 4-2) and lignin (Figure 4-8 and Figure 4-9) contribute to large decrease on MOR. In fact, pyrolysis is not only responsible for gas or liquid being released from the samples, for it also leads to molecule lengths decreasing in hemicellulose and lignin. Old pine samples show more mass loss than new ones, which indicates that hemicellulose and lignin-carbohydrate complexes are greatly pyrolysed and this contributes to a 12% MOR decrease.

In other treatments in new timber at 120°C in air, both 160°C in air and vacuum and 200°C in vacuum, MOR increases in a specific period following a decrease. The MOR increase is attributed to condensation and cross-linking reactions, which consume the hydroxyl group, ether linkages and C=C bonds. The three functional groups, which can experience condensation and cross-linking reactions, decrease after a certain period of treatment. Hence, these reactions stop earlier than pyrolysis and oxidation. Pyrolysis is the dominant reaction after condensation and cross-linking reactions stop, which leads to mass loss and MOR decrease. Oxidation enhances pyrolysis but inhibits condensation and cross-linking.

MOR has high correlations with the chemical composition of samples as detected by the FTIR technique. Table 6-1 and Table 6-2 show the Pearson Correlation coefficients between MOR and the peak areas of the FTIR spectrum for new and old pine samples, respectively. The highest positive and negative correlation coefficients are Peak 1318 and Peak 1730, respectively. Peak 1318 is between the S- or G- units of lignin. An increase of Peak 1318 indicates lignin condensation and a decrease means lignin pyrolysis. Peak 1730 is the carbonyl bond (C=O), where a decrease represents lignin cross-linking and an increase signifies hemicellulose pyrolysis. In the table, the next two positive correlations with high values for both new and old pine are Peak 1366 and Peak 1226, which correspond

to C-H bonds and ether linkages (C-O-C), respectively. The C-H bond is highly related to pyrolysis in a negative way. Ether linkage increases due to condensation between lignin and hemicellulose or between lignin itself but decrease owing to pyrolysis. The second highest negative correlation is Peak 1642, which is affected by lignin cross-linking and hemicellulose pyrolysis. Hence, MOR can be predicted by three peaks on the FTIR spectrum with a positive correlation and two peaks with negative correlation. In addition, density is also an essential factor affecting MOR, because the FTIR spectrum does not illustrate significant mass loss.

Table 6-1 Pearson Correlation of New Pine Sample between MOR and FTIR Peaks

	Peak	Peak	Peak	Peak	Peak	Peak	Peak	Peak	Peak
	1318	1335	1366	1421	1456	1507	1595	1642	1730
Pearson Correlation	.852**	-.645**	.804**	.789**	.647**	.707**	-.796**	.677**	-.821**
Sig. (2-tailed)	0.000	0.000	0.000	0.000	0.000	0.000	0.000	0.000	0.000
N	467	467	467	467	467	467	467	467	467
MOR	Peak	Peak	Peak	Peak	Peak	Peak	Peak	Peak	Peak
	895	1025	1054	1110	1154	1204	1226	1262	
	Pearson Correlation	.280**	-.197**	-.645**	.538**	.561**	-.205**	.793**	.739**
	Sig. (2-tailed)	0.000	0.000	0.000	0.000	0.000	0.000	0.000	0.000
	N	467	467	467	467	467	467	467	467

Table 6-2 Pearson Correlation of Old Pine Sample between MOR and FTIR Peaks

	Peak 1318	Peak 1335	Peak 1366	Peak 1421	Peak 1456	Peak 1507	Peak 1595	Peak 1642	Peak 1730
Pearson Correlation	.846**	-.248**	.798**	.665**	.362**	.498**	-.698**	.677**	-.769**
Sig. (2-tailed)	0.000	0.001	0.000	0.000	0.000	0.000	0.000	0.000	0.000
N	170	170	170	170	170	170	170	170	170
MOR	Peak 895	Peak 1025	Peak 1054	Peak 1110	Peak 1154	Peak 1204	Peak 1226	Peak 1262	
Pearson Correlation	-0.98	.117	-.622**	.556**	.586**	-.629**	.760**	.478**	
Sig. (2-tailed)	0.204	0.128	0.000	0.000	0.000	0.000	0.000	0.000	
N	170	170	170	170	170	170	170	170	

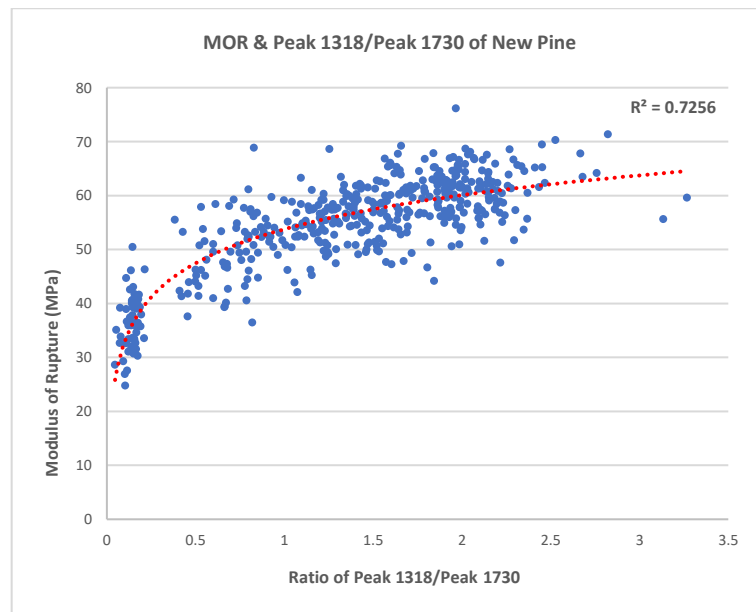


Figure 6-1 MOR & Peak 1318 / Peak 1730 of New Pine

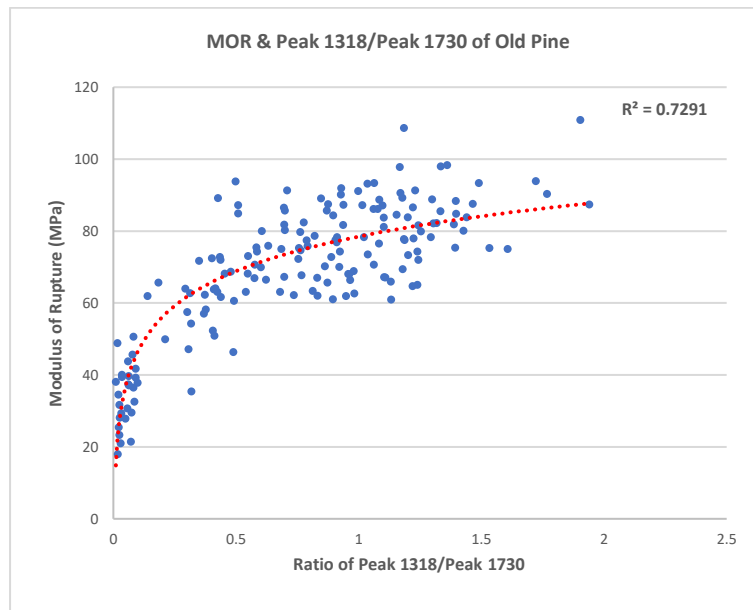


Figure 6-2 MOR & Peak 1318 / Peak 1730 of Old Pine

Regarding the total 637 samples containing both new and old pine samples, each is tested by FTIR and static mechanical analysis. The MOR of both new and old pine samples shows high correlation to the size ratio of Peak 1318/Peak 730 (Figure 6-1 and Figure 6-2). Hence, three independent variables, namely density (ρ), size of Peak 1318 (W_{v1318}) and size of Peak 1730 (W_{v1730}) can predict MOR reasonably accurately. In fact, Figure 6-1 and Figure 6-2 illustrate that the relationship between MOR and the ratio_{1318/1730} is a natural logarithmic one. However, according to Missanjo and Matsumura (2016); Węgiel et al. (2018) and Guller (2007), the relationship between MOR and density is linear. Hence, mathematic model should have in the following form:

$$\sigma = a \times \rho \times \left(\ln \frac{\text{Peaks with positive correlation}}{\text{Peaks with negative correlation}} + b \right)$$

where a and b are parameters, σ is MOR and ρ is density.

The independent variables (peak area and density) and the dependent variable (MOR) are fitted with R^2 (Coefficient of determination) = 0.818.

$$\sigma_1 = 22.85425 \times \rho \times \left(\ln \frac{Wv_{1318}}{Wv_{1730}} + 6.71716 \right)$$

where σ_1 is MOR, ρ is the density of the sample, Wv_{1318} is the size of Peak 1318 and Wv_{1730} is the size of Peak 1730.

R-squared and adjusted R-Squared are 0.818 and 0.817, respectively, which indicates that the mathematic model is appropriate. However, the model only contains Peak 1318 and Peak 1730 of the FTIR spectrum. There are more positive and negative correlation peaks detected by Pearson Correlation, which could be used in the model. In the result of MOR curve fitting, R-squared and adjusted R-Squared are less affected (Table 6-3).

$$\sigma_2 = 24.75646 \times \rho \times \left(\ln \frac{Wv_{1318}}{\sqrt{Wv_{1730}^2 + Wv_{1595}^2}} + 6.70748 \right)$$

$$\sigma_3 = 23.84291 \times \rho \times \left(\ln \frac{\sqrt{Wv_{1318}^2 + Wv_{1366}^2}}{Wv_{1730}} + 5.90796 \right)$$

$$\sigma_4 = 25.43515 \times \rho \times \left(\ln \frac{\sqrt[3]{Wv_{1318}^3 + Wv_{1366}^3 + Wv_{1226}^3}}{Wv_{1730}} + 5.55012 \right)$$

$$\sigma_5 = 25.8844 \times \rho \times \left(\ln \frac{\sqrt{Wv_{1318}^2 + Wv_{1366}^2}}{\sqrt{Wv_{1730}^2 + Wv_{1595}^2}} + 5.90611 \right)$$

$$\sigma_6 = 27.8036 \times \rho \times \left(\ln \frac{\sqrt[3]{Wv_{1318}^3 + Wv_{1366}^3 + Wv_{1226}^3}}{\sqrt{Wv_{1730}^2 + Wv_{1595}^2}} + 5.54231 \right)$$

where Wv_{1595} , Wv_{1366} and Wv_{1226} are the size of Peak 1595, Peak 1366 and Peak 1226, respectively.

In fact, more permutations of positive/negative correlations, such as addition $(Wv_{1318} + Wv_{1366} + Wv_{1226}) / (Wv_{1730} + Wv_{1595})$ and multiplication $(Wv_{1318} \times Wv_{1366} \times Wv_{1226}) / (Wv_{1730} \times Wv_{1595})$ are tested, but R-squared and adjusted R-Squared are much lower.

Table 6-3 MOR Curve Fitting with Different Peaks of the FTIR Spectrum

Equation	Related Peak	R-Squared (COD)	Adj. R-Squared
σ_1	Peak 1318	0.81769	0.8174
	Peak 1730		
σ_2	Peak 1318	0.80188	0.80156
	Peak 1730, Peak 1595		
σ_3	Peak 1318, Peak 1366	0.81927	0.81898
	Peak 1730		
σ_4	Peak 1318, Peak 1366, Peak 1226	0.81659	0.8163
	Peak 1730		
σ_5	Peak 1318, Peak 1366	0.80214	0.80183
	Peak 1730, Peak 1595		
σ_6	Peak 1318, Peak 1366, Peak 1226	0.79854	0.79822
	Peak 1730, Peak 1595		

Figure 6-3 shows the relationship between predicted MOR and measured MOR, including both new and old samples. As MOR increases, the predicted MOR is increasingly higher than the measured MOR. There are two reasonable hypotheses to explain this deviation. First, Peak 1730 is not only affected by lignin cross-linking and hemicellulose pyrolysis reactions, but also, by a deacetylase reaction in hemicellulose. Deacetylase is a reaction that does not affect the hemicellulose length or matrix, but it leads to a decrease in the carbonyl group (C=O). Hence, as a denominator in the mathematic model, the predicted MOR becomes slightly higher than the measured MOR. Regarding the second hypothesis, a relationship between the quantity of the chemical functional groups and the size of their

corresponding peaks on the FTIR spectrum is not proven. The chemical functional groups are fitted by a gaussian curve, where a slight increase in peak height can lead to a significant increase in the size. A higher predicted MOR might indicate that above a certain value, a change in the FTIR peak area is much quicker than changes in the functional group quantity.

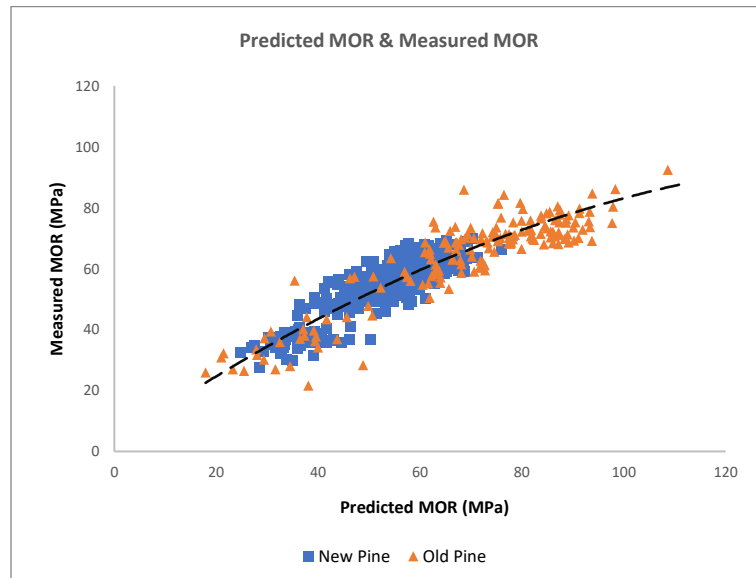


Figure 6-3 Relationship between Predicted MOR and Measured MOR by Curve Fitting

Another method to predict MOR is Multiple Regression Analysis (MRA). MRA can predict the dependent variable (MOR) by several independent variable (density and peak area), with it being presumed that the relationship between the dependent variable and independent variables is linear. MRA predicts the dependent variable by the following equation:

$$Y = \beta_0 + \beta_1 X_1 + \beta_2 X_2 + \beta_3 X_3 + \beta_4 X_4 \dots + \beta_n X_n$$

where, Y is the dependent variable, and $X_1, X_2, X_3 \dots X_n$ are independent variables. $\beta_0, \beta_1, \beta_3 \dots \beta_n$ are regression parameters, which will be defined in the analysis. MRA predicts

MOR by the following mathematic model with R square being 0.819 and Adjusted R square being 0.817:

$$\sigma = -4.916 - 0.039 \times Wv_{1054} + 0.045 \times Wv_{1366} + 137.258 \times \rho - 0.054 \times Wv_{1456} + 0.059 \times Wv_{1318} - 0.032 \times Wv_{1421}$$

where, σ is MOR, Wv_{1054} , Wv_{1366} , Wv_{1456} , Wv_{1318} and Wv_{1421} are the sizes of Peak 1054, 1366, 1456, 1318 and 1421 respectively, whilst ρ is the sample density.

Table 6-4 shows the MRA summaries of the different mathematic models. The R-square and Adjusted R square are the highest in the last model, which indicates that the model is suitable. In fact, model 4, 5 and 6 are similar due to similar R, R square and Adjusted R square. Hence, Peaks 1054, 1366, 1456 and density are fundamental variables for the MRA model. Density and Peak 1366 relating to the C-H bonds in hemicellulose have positive correlations, while Peak 1054 and 1456, which are related to the C-O in and C-H bonds in cellulose, respectively, have negative correlations to MOR in the model. Cellulose is the most stable molecule in timber, whilst the content increase indicates pyrolysis reactions in hemicellulose and lignin. Hence, this model predicts MOR by density and the peaks related to cellulose (Peak 1054 and 1456), hemicellulose (Peak 1366) and lignin (Peak 1318).

The relationship between predicted MOR and measure the MOR by MRA method is shown in Figure 6-4. The predicted MOR is slightly higher than that measured MOR, which is the same as with the curve fitting method. Since peak 1730 is not used in the MRA model, the possible hypothesis of the phenomenon is that there is an unclear relationship between the quantity of functional groups and the size of the FTIR peaks.

Table 6-4 Summary of Multiple Regression Analysis for MOR

	Related Peak	R	R-Squared (COD)	Adj. R-Squared	Std. Variation of estimate
1	Peak 1054	0.706	0.497	0.497	10.197
2	Peak 1054, 1366	0.806	0.649	0.648	8.530
3	Peak 1054, 1366, density	0.867	0.752	0.750	7.183
4	Peak 1054, 1366, density Peak 1456	0.897	0.805	0.803	6.377
5	Peak 1054, 1366, density Peak 1456, 1318	0.903	0.815	0.814	6.207
6	Peak 1054, 1366, density Peak 1456, 1318, 1421	0.905	0.819	0.817	6.146

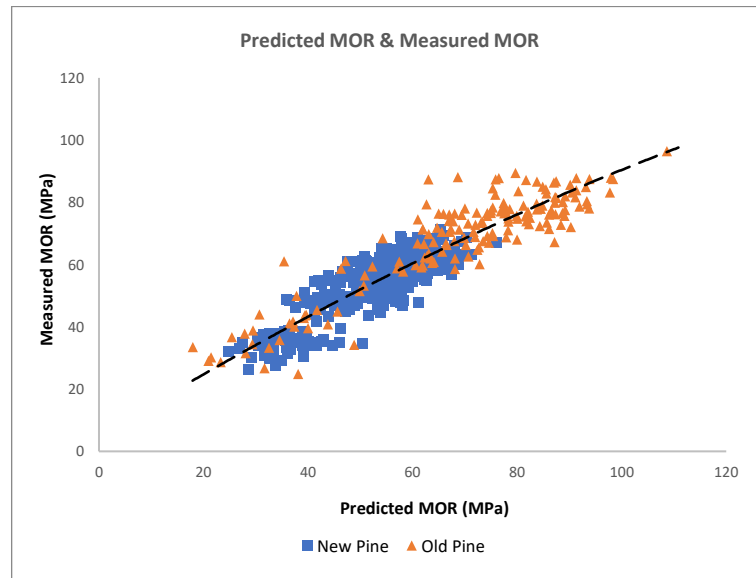


Figure 6-4 Relationship between Predicted MOR and Measured MOR by MRA

Both the curve fitting and multiple regression analysis method predict MOR with high R square and Adjusted R square. The curve fitting method can achieve a high coefficient of determination for MOR by three variables, whilst MRA needs six. In the two methods, the predicted MOR is slightly higher than that measured MOR due to the undefined relationships between the chemical functional groups quantity and FTIR peak area. To sum up, the two methods can predict MOR for both new and old pine samples.

6.1.2 Bending Modulus of Elasticity and Chemical Composition

Generally, the average modulus of elasticity (MOE) of both new and old pine in different heat treatment atmosphere shows relatively similar change as with MOR. MOE increases in treatment at 120°C in a vacuum by approximately 12% and 15% in new and old samples, respectively, due to condensation and cross-linking reactions. MOE decrease in treatment at 200°C in air by approximately 5% and 11% in new and old samples, respectively, with mass loss of 14.5% and 19.2% for new and old samples being the reason. Hence, density is an important factor affecting timber's MOE. As MOR, the MOE of both new and old pines increase in other treatments in a specific period then following a decrease, which also indicates that condensation and cross-linking reaction improve MOE at low mass loss. Moreover, an oxidation reaction is also a factor improving MOE. For treatment on new pine in air, the maximum increase in MOE is 6.5%, 4% and 8% at 120°C for 16 hours, 160°C for 16 hours and 200°C for 8 hours, respectively, whilst in a vacuum atmosphere, it is 4% and 5% in treatment at 160°C for 20 hours and 200°C for 12 hours, respectively. Hence, the treatment in air leads to a higher increase in MOE than with in a vacuum. For the old samples, that have been oxidised during natural ageing, MOE increases with condensation and a cross-linking reaction, but decreases with pyrolysis.

The MOE changes are not as significant as with MOR, in that mass losses of new and old pine at 200°C in a vacuum after 24 hours are 8% and 16% for the latter, respectively, whilst for the former, these increase 1.2% and 6.1%, respectively. Bekhta and Niemz (2003) also reported similar results. Unlike other isotropic materials, the timber cell is the fundamental unit for timber mechanical properties. Astley et al. (1998) found a close relationship between timber cell geometries and Young's Modulus (MOE) by comparing measured MOE to predicted MOE, including the variables of cell size, cell wall thickness, the shape of cell section and microfibrils angle. The relationships were also reported by Qing and Mishnaevsky Jr (2009), Mishnaevsky Jr and Qing (2008) and Harrington et al. (1998). Since condensation, cross linking reactions and pyrolysis leading to mass loss greatly affect cell wall strength but have much less impact on cell wall form, MOE changes are less than those for MOR during the heat treatment.

Table 6-5 shows that the Pearson correlations between MOE and the FTIR spectrum peaks. The highest correlation is density, which means this is an important factor for static mechanical properties, including MOR and MOE. Peaks 1025 and 895 are the next two highest correlations to MOE, which relate to C-H bond and β -glycosidic linkage (a kind of ether linkage), respectively. The C-H bond is the most prevalent in the timber molecule, which can be treated as a bond representing the quantity of timber molecule. Peak 895 is a kind of ether linkage in hemicellulose and lignin, which reflects the degree of condensation. Peak 1054, relating to C-C and C-O bonds, has the largest negative correlation to MOE.

Table 6-5 Pearson Correlation of All Samples between MOE and Density and FTIR Peaks

	Density	Peak 1335	Peak 1366	Peak 1421	Peak 1456	Peak 1507	Peak 1595	Peak 1642	Peak 1730
Pearson Correlation	.737**	-.200**	.101**	.196**	-.042	-.139**	.180**	.066	.058
Sig. (2-tailed)	0.000	0.000	0.011	0.000	0.288	0.000	0.000	.096	0.141
N	637	637	637	637	637	637	637	637	637
MOE	Peak 895	Peak 1025	Peak 1054	Peak 1110	Peak 1154	Peak 1204	Peak 1226	Peak 1262	Peak 1318
Pearson Correlation	.394**	.554**	-.467**	-.271	-.189**	.294**	.029	.027	.046
Sig. (2-tailed)	0.000	0.000	0.000	0.000	0.000	0.000	0.429	0.492	0.026
N	637	637	637	637	637	637	637	637	637

In the previous section, two mathematic models that can predict MOR with a high coefficient of determination were presented. Regarding MOE, the curve fitting method does not show reasonable prediction, where multiple regression analysis (MRA) provides a suitable model to predict it. Table 6-6 shows stepwise regression analysis and the model 7 with R square 0.642 and Adjusted R square 0.638 is the best mathematic model for MOE:

$$\begin{aligned}
 E = & -11641.87 + 13750.99 \times \rho + 0.749 \times Wv_{1025} + 7.956 \times Wv_{1054} \\
 & + 2.807 \times Wv_{1226} + 1.173 \times Wv_{895} - 2.533 \times Wv_{1456} \\
 & + 1.556 \times Wv_{1507}
 \end{aligned}$$

where ρ is density, Wv_{1025} , Wv_{1054} , Wv_{1226} , Wv_{895} , Wv_{1456} and Wv_{1507} are the size of Peaks 1025, 1054, 1226, 895, 1456 and 1507 after normalisation, respectively.

In the model, the predicted MOE is also slightly higher than that measured (Figure 6-5). The reason for this has been discussed in the subsection 6.1.2 in relation to MOR, so will not be discussed further in this subsection.

Table 6-6 Summary of Multiple Regression Analysis for MOE

	Related Peak	R	R-Squared (COD)	Adj. R-Squared	Std. Error of estimate
1	Density	0.742	0.550	0.549	634
2	Density, Peak 1025	0.758	0.575	0.574	617
3	Density Peak 1025, 1054	0.769	0.591	0.589	606
4	Density Peak 1025, 1054, 1226	0.783	0.614	0.611	589
5	Density Peak 1025, 1054, 1226, 895	0.792	0.628	0.625	578
6	Density Peak 1025, 1054, 1226, 895, 1456	0.797	0.635	0.632	573
7	Density Peak 1025, 1054, 1226, 895, 1456, 1507	0.801	0.642	0.638	568

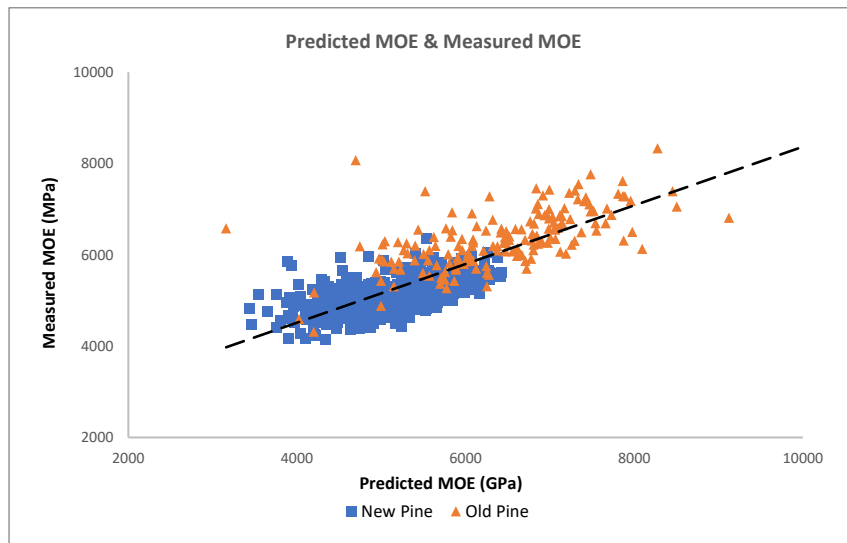


Figure 6-5 Relationship between Predicted MOE and Measured MOE by MRA

In the MRA model, peak 1054 is used as a positive variable but Pearson correlation shows that it is negative. This phenomenon is common in an MRA model due to multicollinearity, which is caused by the high correlations between two or more variables. Hence, to avoid the problem, another regression method, Ridge Regression (RR) is used to predict MOE. This is a method to processing multicollinearity data, which improves the reliability of the regression coefficient, but reduces the quantity of independent variables and thus, decreases the precision of the model. RR analysis shows the following mathematic model with R square 0.601, Adjusted R square 0.598 and standard error 599.217.

$$E = -5936.428 + 9291.654 \times \rho + 0.588 \times Wv_{1025} + 2.156 \times Wv_{1226} + 1.171 \times Wv_{895} - 1.101 \times Wv_{1456}$$

In the model, density and the size of Peak 1025, 1226, 895 and 1456 are the independent variables, which means abandoning Peaks 1054 and 1226 included in the MRA method. Figure 6-6 shows the relationship between predicted MOE and that measured by RR method. The reason for the higher predicted MOE than that measured has been discussed in subsection 6.1.1.

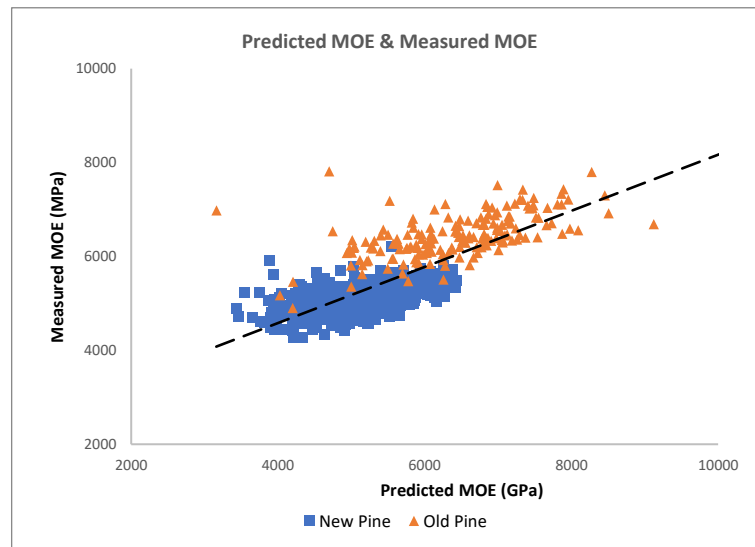


Figure 6-6 Relationship between Predicted MOE and Measured MOE by RR

Both multiple regression analysis (MRA) and ridge regression (RR) analysis create a suitable mathematic model to predict MOE by FTIR peaks, with each having its distinctive advantages. The MRA model has a high coefficient of determination (R square) but suffer from a multicollinearity problem. RR produces a model with a high reliability of regression coefficient, but the R square is slightly lower than with MRA. In sum, the two mathematic models are reasonable for the research.

6.1.3 Summary

The chemical compositions of timber molecules have close relations with the static mechanical properties. In general, condensation and cross-linking reactions can improve the static properties under low mass loss. Higher mass loss, which is caused by pyrolysis reactions, leads to a decrease in these properties. Both the bending modulus of rupture (MOR) and modulus of elasticity (MOE) can be predicted by different regression mathematic models.

MOR can be predicted by a curve fitting method or multiple regression analysis (MRA) method. In the curve fitting model, density along with Peaks 1318 and 1730, which are related to condensation, cross-linking, and pyrolysis reaction, are three independent variables. In the MRA model, density, Peak 1054, 1366, 1456, 1318 and 1421 are the variables. Both the two models have more than 0.8 R-square (coefficient of determination), which indicate that the two models are suitable for predicting MOR by the FTIR peaks.

MOE can be predicted by an MRA model with 0.64 R-square. Density as well as Peak 1025, 1054, 1226, 895, 1456 and 1507 are the important variables. However, the MRA model has a problem of multicollinearity, so another Ridge Regression method is used to solve the problems with Peaks 1025, 1226, 895 and 1456 as variables, but the R-square is reduced to 0.6.

6.2 Dynamic Mechanical Properties and Chemical Composition

In temperature scanning from -150°C to 150°C, Tan δ shows two peaks. Moreover, the Tan δ curve decreases in treatment at 120°C in a vacuum but increase at 200°C in air. Tan δ increases due to an increase in viscosity and decrease in elasticity at the same time, whilst Tan δ decreases due to the opposite occurrence. Hence, the chemical reaction, which can extend or expand timber molecules including condensation and cross-linking reactions, can improve the elasticity of timber. Pyrolysis reactions, which lead to shortening of molecules, can increase the viscosity of timber.

Two peaks, γ and β , appear on the Tan δ curve, which are affected by methylol and moisture content, respectively. Peaks γ and β move to a higher temperature after all heat treatments, which means that the related functional groups need a high temperature to cause intermolecular friction. Hence, condensation and cross-linking reaction contribute to the stability of timber molecules as well as the pyrolysis reaction, which leads to an increase

in a few stable functional groups including ether linkage, C=C bonds and the carbonyl group.

The storage modulus and loss modulus of Peak γ and β can be predicted by the peak area of the FTIR spectrum. The Tan δ value at the two peaks also can be predicted from the storage and loss moduli, which have a close relationship to each other (Figure 6-7 and Figure 6-8).

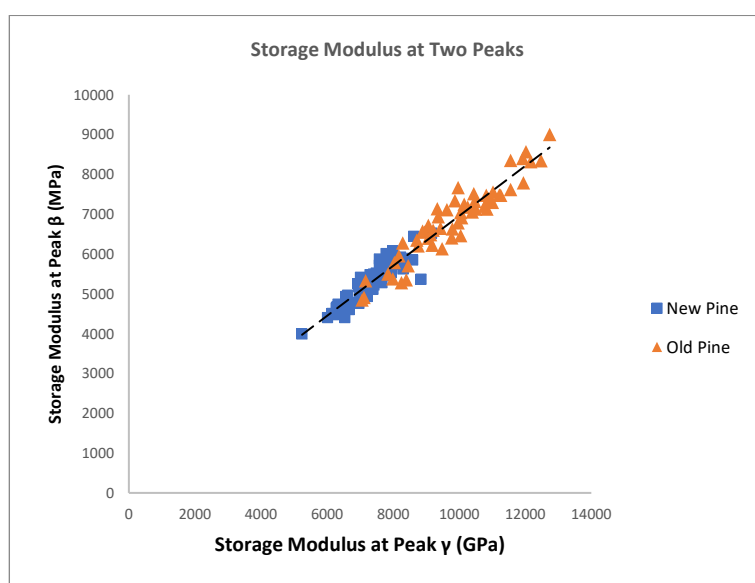


Figure 6-7 Relationships of Two Peaks Storage Modulus

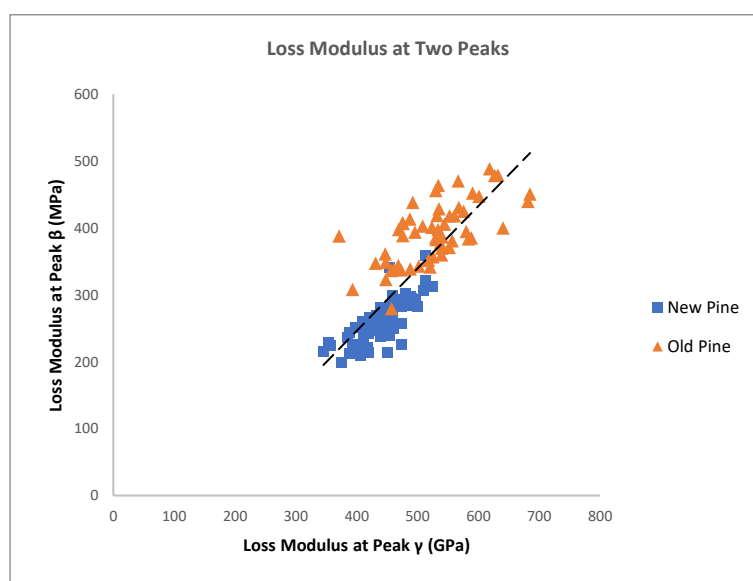


Figure 6-8 Relationships of Two Peaks Loss Modulus

6.2.1 Peak γ of $\tan \delta$

The storage modulus at Peak γ is affected significantly by density (Table 6-7). Peaks 1318 and 1025, relating to condensation reactions and C-H bonds, respectively, have high positive correlations with the storage modulus, whilst Peaks 1054 and 1110 have high negative correlations with it. Since these two peaks are related to cellulose an increase indicates mass loss caused by the pyrolysis of hemicellulose and lignin. The loss modulus at Peak γ is also affected by density with the highest positive correlation (Figure 6-8). The loss modulus reflects the viscosity of samples, whilst Pearson correlation analysis shows the same positive or negative relations to storage and loss moduli, the two regression models use different peaks as the independent variables.

Storage modulus and loss modulus can be predicted by the related functional groups by an MRA method as follows:

$$Sm_{\gamma} = -9315.670 + 13935.553 \times \rho + 0.980 \times Wv_{1025} + 2.783 \times Wv_{1318}$$

$$Lm_{\gamma} = -264.444 + 0.053 \times Wv_{1025} + 375.540 \times \rho$$

where Sm_γ and Lm_γ are the storage modulus and loss modulus at peak γ , respectively, ρ is density, whilst Wv_{1025} and Wv_{1318} , are the size of the Peaks at 1025 and 1318, respectively. The R-square and adjusted R-square of the storage modulus regression model are 0.611 and 0.600, respectively, whilst those of the loss modulus regression model are 0.383 and 0.373, respectively. The predicted and measured storage and loss moduli are shown in Figure 6-9. The predicted modulus is higher than that measured, the reason for which has been explained in the subsection 6.1.1.

Table 6-7 Pearson Correlations between the Storage Modulus of Peak γ and Density and the FTIR Peaks

	Density	Peak 1335	Peak 1366	Peak 1421	Peak 1456	Peak 1507	Peak 1595	Peak 1642	Peak 1730
Pearson Correlation	.728**	-.059	.237**	.308**	.042	.027	.104	-.069	-.008
Sig. (2-tailed)	0.000	0.521	0.009	0.001	0.652	0.773	0.259	.451	0.933
N	120	120	120	120	120	120	120	120	120
Storage Modulus	Peak 895	Peak 1025	Peak 1054	Peak 1110	Peak 1154	Peak 1204	Peak 1226	Peak 1262	Peak 1318
Pearson Correlation	.155	.633**	-.588**	-.422**	-.247**	.167	.000	.085	.228*
Sig. (2-tailed)	0.090	0.000	0.000	0.000	0.007	0.068	0.998	0.353	0.012
N	120	120	120	120	120	120	120	120	120

Table 6-8 Pearson Correlations between the Loss Modulus of Peak γ and Density and the FTIR Peaks

	Density	Peak 1335	Peak 1366	Peak 1421	Peak 1456	Peak 1507	Peak 1595	Peak 1642	Peak 1730
Pearson Correlation	.557**	-.084	.189 [†]	.258**	.061	.003	.118	-.056	.107
Sig. (2-tailed)	0.000	0.361	0.039	0.004	0.511	0.970	0.201	.544	0.245
N	120	120	120	120	120	120	120	120	120
Loss Modulus	Peak 895	Peak 1025	Peak 1054	Peak 1110	Peak 1154	Peak 1204	Peak 1226	Peak 1262	Peak 1318
Pearson Correlation	.156	.559**	-.423**	-.409**	-.229 [†]	-.031	.021	.136	.184**
Sig. (2-tailed)	0.088	0.000	0.000	0.000	0.012	0.734	0.819	0.140	0.045
N	120	120	120	120	120	120	120	120	120

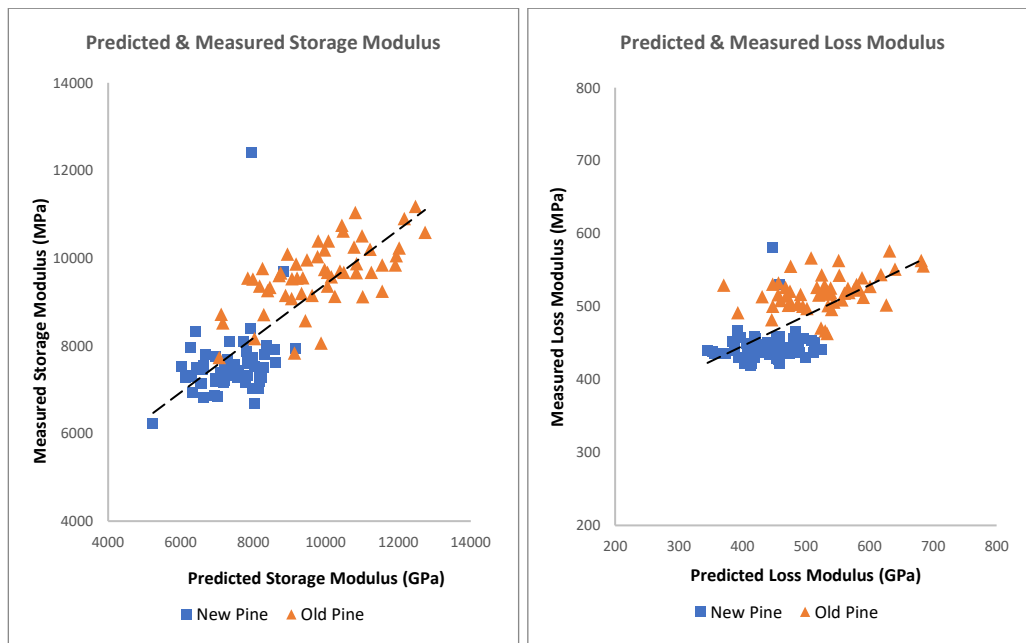


Figure 6-9 Predicted and Measured Storage and Loss Moduli of Peak γ

Tan δ at Peak γ can be calculated by the two regression models as:

$$\text{Tan } \delta_{\gamma} = \frac{Lm_{\gamma}}{Sm_{\gamma}}$$

The relationship between the predicted and measured Tan δ at Peak γ is shown in Figure 6-10, with the R-square 0.35. The temperature at which peak γ appears cannot be predicted by the FTIR peaks. One possible reason is that there are no peaks corresponding to the methylol group in the timber molecule.

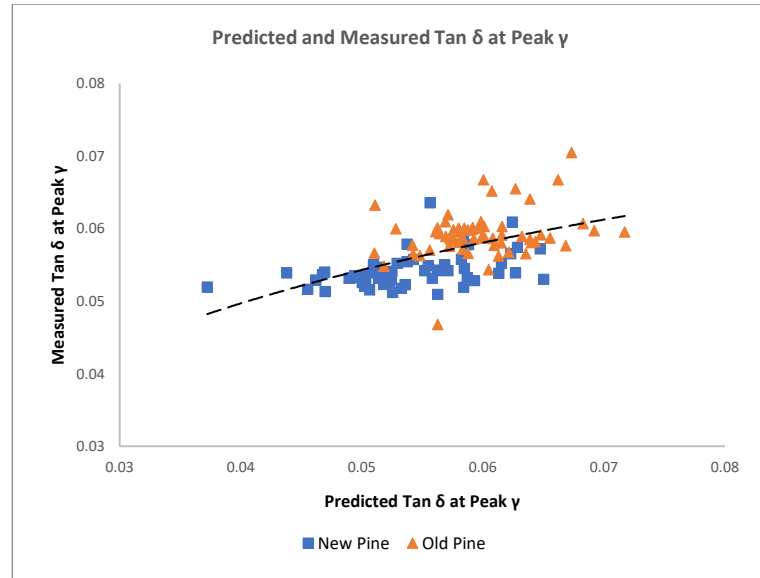


Figure 6-10 Predicted and Measured Tan δ at Peak γ

6.2.2 Peak β of Tan δ

Peak β is affected by moisture between timber molecules, whilst intermolecular friction happens on main chains and moisture acts as lubrication. Same as peak γ , the storage and loss moduli are also affected by density and Peak 1025 with positive correlations and Peaks 1054 and 1110 with negative ones (Table 6-9 and Table 6-10). MRA shows the models for storage and loss moduli by the peak areas of the FTIR spectrum as follows:

$$Sm_{\beta} = -4041.291 + 8785.265 \times \rho + 0.580 \times Wv_{1025}$$

$$Lm_{\beta} = -455.849 + 565.005 \times \rho + 0.057 \times Wv_{1025} - 30.150 \times Wv_{1335} \\ - 0.225 \times Wv_{1154} + 0.083 \times Wv_{895}$$

where Sm_{β} and Lm_{β} are the storage modulus and loss modulus at Peak β , ρ is sample density. Wv_{1025} , Wv_{1318} . The R-square and adjected R-square for the storage regression models are 0.519 and 0.510, respectively, whilst for loss modulus regression model these are 0.682 and 0.668, respectively. The predicted and measured moduli are shown in Figure 6-11, with the former being slightly higher than the later, the reason for which was discussed in subsection at 6.1.1.

The Tan δ at peak γ can be calculated by the following:

$$Tan \delta_{\gamma} = Lm_{\gamma} / Sm_{\gamma}$$

The relationship between the predicted Tan δ at peak γ and that measured one is shown in Figure 6-12.

Table 6-9 Pearson Correlations between the Storage Modulus of Peak β and Density and the FTIR Peaks

		Density	Peak 1335	Peak 1366	Peak 1421	Peak 1456	Peak 1507	Peak 1595	Peak 1642	Peak 1730
Storage Modulus	Pearson Correlation	.693**	-.116	.122	.204*	-.038	-.043	.189*	-.122	.053
	Sig. (2-tailed)	0.000	0.207	0.185	0.025	0.677	0.640	0.039	0.183	0.566
	N	120	120	120	120	120	120	120	120	120
		Peak 895	Peak 1025	Peak 1054	Peak 1110	Peak 1154	Peak 1204	Peak 1226	Peak 1262	Peak 1318
	Pearson Correlation	.144	.587**	-.530**	-.410**	-.293**	-.106	-.062	-.017	.136
	Sig. (2-tailed)	0.117	0.000	0.000	0.000	0.001	0.249	0.501	0.855	0.140
N	120	120	120	120	120	120	120	120	120	

Table 6-10 Pearson Correlations between the Loss Modulus of Peak β and Density and the FTIR Peaks

		Density	Peak 1335	Peak 1366	Peak 1421	Peak 1456	Peak 1507	Peak 1595	Peak 1642	Peak 1730
Loss Modulus	Pearson Correlation	.757**	-.144	.107	.191*	.023	-.104	.300**	-.073	.184*

Sig. (2-tailed)	0.000	0.117	0.243	0.036	0.801	0.260	0.000	0.428	0.045
N	120	120	120	120	120	120	120	120	120
	Peak	Peak	Peak	Peak	Peak	Peak	Peak	Peak	Peak
	895	1025	1054	1110	1154	1204	1226	1262	1318
Pearson Correlation	.214*	.662**	-.617**	-.568**	-.364**	-.098	-.153	-.075	.045
Sig. (2-tailed)	0.019	0.000	0.000	0.000	0.000	0.286	0.095	0.417	0.626
N	120	120	120	120	120	120	120	120	120

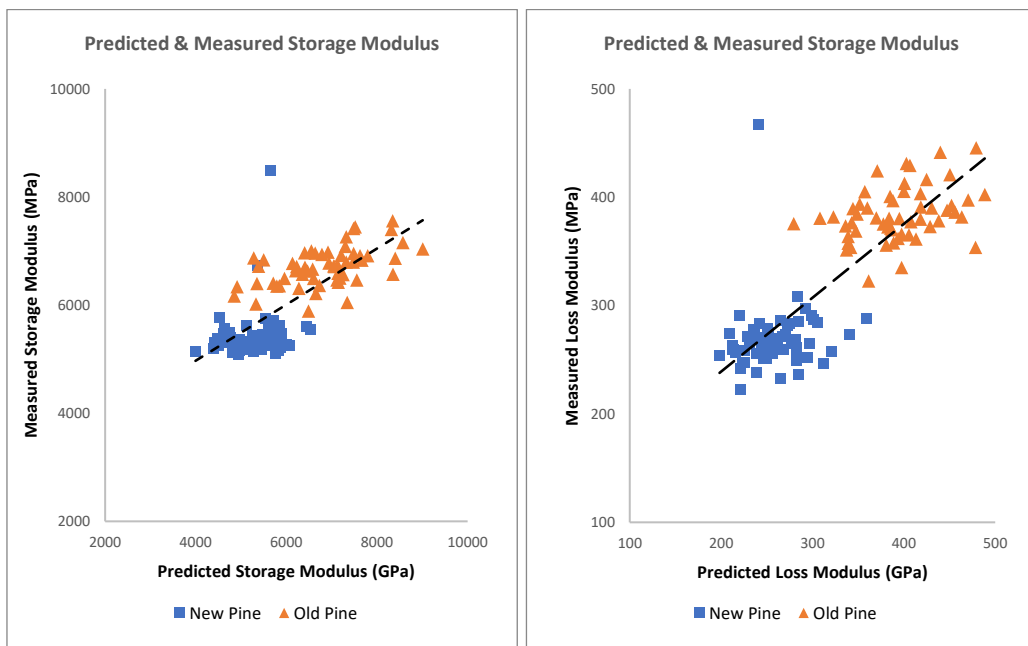


Figure 6-11 Predicted and Measured Storage and Loss Moduli of Peak β

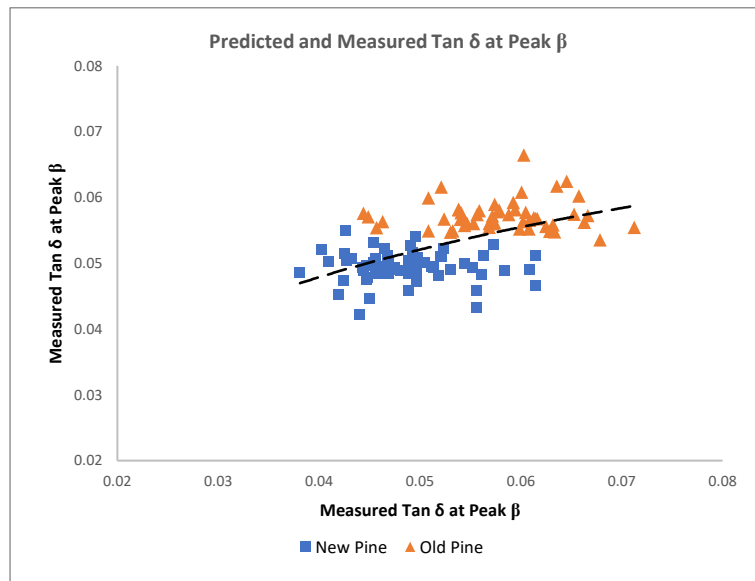


Figure 6-12 Predicted and Measured Tan δ at Peak β

The temperature at which Peak β appears can be predicted by the MRA method, with the density and moisture content being the only independent variables.

$$T_{\beta} = 31.464 + 112.455 \times \rho - 1.671 \times Mc$$

where T_{β} is the temperature when Peak β appears, ρ is the density and Mc is the sample moisture content. Moreover, the R-square and Adjusted R-square are 0.327 and 0.316, respectively. In general, this temperature is at approximately 70°C for new pine samples and between 80°C and 90°C for old pine ones, even though the mechanical properties vary dramatically. Since the largest difference between new and old pine samples is density, this is the most important factor affecting the temperature.

6.2.3 Summary

Tan δ value, temperature, storage modulus and loss modulus at Peaks γ and β have been discussed in this section. Condensation and cross-linking reaction decrease Tan δ , which

means that the elasticity is enhanced. Pyrolysis contributes to a higher $\text{Tan } \delta$, so the viscosity is increased by this reaction. Two peaks that appear on $\text{Tan } \delta$ during temperature scanning move to a higher temperature, which means that the molecule structure tends to be stable after any kind of heat treatment.

Apart from the temperature of the two peaks, other dependent variables can be predicted by the multiple regression analysis method with acceptable coefficient of determination. Both the storage and loss moduli are significantly affected by density with positive correlations. Hence, molecule quantity is an important factor affecting the moduli. However, FTIR is not a sensitive technique for identifying the quantities of functional groups. Hence, dynamic mechanical properties cannot be predicted just by FTIR techniques.

6.3 Discussion and Conclusion

Both static and dynamic timber mechanical properties have close relations to the chemical composition. Condensation and lignin cross-linking reactions play a significant role in improvement of the modulus of rupture (MOR) and modulus of elasticity (MOE). The MOE improvement also leads to a decrease in $\text{Tan } \delta$ of the dynamic mechanical properties. Mass loss, which is attributed to pyrolysis in hemicellulose and lignin, can decrease MOR and MOE, which contributes to an increase in $\text{Tan } \delta$. Hence, viscoelasticity has close relations to static mechanical properties, whereby elasticity enhances static mechanical properties, whilst viscosity reduces them.

The static mechanical properties, including the bending MOR and MOE, the dynamic mechanical properties including storage modulus, loss modulus and $\text{Tan } \delta$ value at Peak β and γ can be predicted by density and a few peaks on the FTIR spectrum. A curve fitting method by Origin software as well as multiple regression analysis and ridge regression by

SPSS software are three methods for predicting the mechanical properties. The regression models are suitable for new and old pine samples, which demonstrates their wide applicability for timbers. Moreover, for higher values of all properties, the predicted value is slightly higher than the measured one. One important reason is that the relationship between the quantities of functional groups and the size of their corresponding FTIR peaks is non linear. MOR change is more significant than MOE during heat treatment, which lead to higher coefficient of determination (R-square) of bending MOR regression model. Since the FTIR technique shows the chemical composition of cell walls, it is found that the cell wall strength, which is affected by this composition, has a more significant influence on MOR than MOE. The regression models also indicate that MOE is also affected by timber cell structure.

The temperature at which two peaks appear for $\text{Tan } \delta$ when scanning from -150°C to 150°C , β and γ , cannot be predicted by density and the FTIR peaks. Theoretically, the peaks move to a higher temperature due to the stability of the timber molecules increasing. However, the stability is not easy to define by the FTIR peaks, which might be an important reason affecting the regression model of the temperature.

Compression samples are too large to fit the FTIR facility, so in the related section, the chemical composition measured in small samples was used to discuss the relationship between compression mechanical properties and chemical composition. In fact, the compression MOE has similar changes as the bending MOR, which indicate that condensation and cross-linking reactions can improve the former whilst pyrolysis, which also contribute to mass loss, lead to a decrease on it. For compression MOR, apart from the chemical composition of timber molecules, cell structures are also an important factor affecting this.

Chapter 7 Implementation

Two implementations of the research results are produced in this chapter. Section 7.1 discusses the semi-destructive method to predict the mechanical properties of a specific structural member by density and FTIR. Section 7.2 produces a method to accelerate timber chemical composition to a specific natural ageing by heat treatment under controlled atmosphere.

7.1 Semi-Destructive Testing on Existing Building Elements

The relationships between timber chemical composition and its corresponding mechanical properties are discussed in the chapter 6, with the mechanical properties mathematic models being regressed by density and the peaks on the FTIR spectrum. Theoretically, timber's modulus of elasticity (MOE) and modulus of rupture (MOR) can be predicted by these variables.

A protective layer will be formed on timber's surface by UV exposure, even when it does not face the sunlight directly. When the chemical composition of the layer is greatly degraded and very stable (Figure 7-1), it cannot be used to predict mechanical properties. An operational method is to extract a few samples at a centimetre depth below the timber structural members. The lens of an ATR-FTIR facility is approximately 3mm in diameter, so the cross section is best set at 4mm × 4mm. Density is a variable in the regression model, which can be calculated by sample weight and volume, the thickness is chosen at approximately 2mm. In addition, for accuracy of prediction, it is appropriate to sample from multiple places on the timber structural members. In this study, all testing samples are from one large piece measuring 20cm × 20cm × 100cm and the FTIR spectrums of each

sample do not vary significantly. Hence, for a large size of structural members, in-site sampling can be extracted per meter.

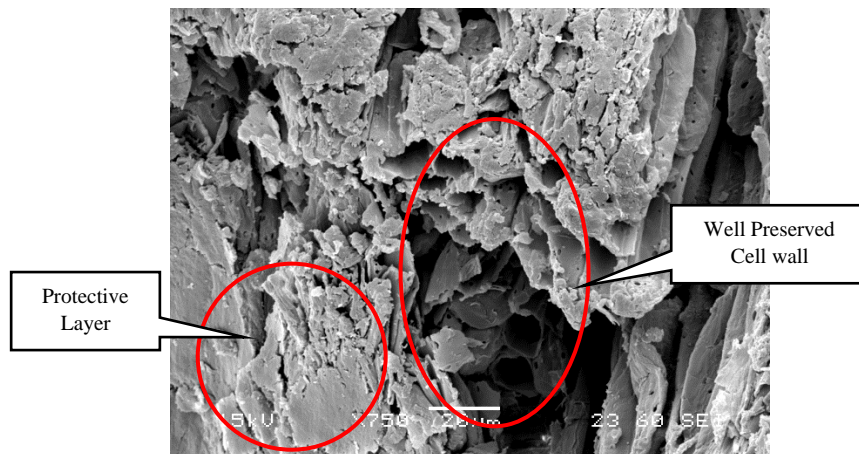


Figure 7-1 A Protective Layer after 100 hours UV Exposure

In the regression model, all independent variables are measured after conditioning at 20°C with 65% humidity. In-site sample should be also proceed in the conditioning room. Sample weights and dimensions are measured after conditioning, as well as the chemical composition, using the FTIR facility. The MOR and MOE can be calculated by the models produced in subsection 6.1. Finally, the properties are obtained by the means of the samples taken from same timber structural member.

This method can predict the static mechanical properties of timber structural members with negligible destruction at a maximum 4mm × 4mm × 10mm. If the mechanical properties of the specific timber members are reduced lower than the structural requirement, a replacement or enhancement project would be carried out immediately.

7.2 Timber Accelerated Ageing

The functional group changes of pine timber molecule during heat treatment in different temperatures, periods and atmospheres are defined in the chapter 4. The chemical

composition of 580 year old pine of the same species is also defined by FTIR techniques. Hence, an aim of the research is to obtain a piece of wood that has same chemical composition as the old pine, through temperature treatment, which will cause distinctive changes in new pine samples.

In this section, functional group change during any heat treatment is predicted according to temperature and treatment period in the first section. The accelerating method, which changes new pine to old pine chemically, is covered in the second section.

7.2.1 Regression of Functional Group Changes During Heat Treatment

The size of the peaks on the FTIR spectrum during heat treatment change complexly with trends of increase, decrease, increase-then-decrease and decrease-then-increase, all being observed during heat treatment. However, all the peak change percentages can be predicted by multiple regression analysis with oxygen content, temperature and treatment period as independent variables. The mean changes of each peak are shown in Table 7-1. Even though a few peaks change together with positive or negative correlations, which was discussed in section 4.7, these peaks are also regressed to reduce the variation for the simulation. Since one regression model cannot combine the samples treated in air and in a vacuum, the models for each peak are divided into two so as to test both atmospheres.

Table 7-1 Percentage Changes of Each Peak During Heat Treatment

Atmosphere	Period	Peak 895	Peak 1025	Peak 1054	Peak 1110	Peak 1154	Peak 1204	Peak 1226	Peak 1262	Peak 1318	
Non-treated	0	0	0	0	0	0	0	0	0	0	
air	8	7%	-1%	21%	-9%	18%	-8%	-11%	0%	10%	
	12	6%	-1%	19%	-8%	18%	-7%	-6%	0%	9%	
	120	16	10%	-1%	23%	-8%	17%	-9%	-10%	0%	4%
	20	11%	0%	19%	-9%	17%	-9%	-9%	-1%	5%	
	24	12%	-1%	21%	-9%	18%	-5%	-9%	2%	5%	
	160	8	11%	0%	20%	-7%	16%	-8%	-11%	-2%	0%
	12	14%	0%	20%	-10%	16%	-9%	-14%	-1%	-3%	

		16	10%	0%	23%	-11%	13%	-6%	-15%	-1%	-7%
		20	12%	0%	23%	-10%	14%	-7%	-15%	-2%	-9%
		24	8%	1%	23%	-11%	13%	-8%	-15%	-3%	-11%
	200	8	8%	1%	37%	-15%	2%	-10%	-28%	-10%	-31%
		12	0%	1%	53%	-22%	1%	-3%	-43%	-13%	-47%
		16	-9%	1%	67%	-21%	1%	-1%	-43%	-15%	-58%
		20	0%	2%	70%	-23%	1%	0%	-45%	-14%	-64%
		24	-7%	1%	70%	-22%	1%	1%	-47%	-16%	-68%
	120	8	13%	-2%	16%	-5%	17%	-4%	-5%	1%	7%
		12	15%	0%	18%	-7%	16%	-8%	-10%	-2%	7%
		16	17%	0%	16%	-8%	16%	-7%	-7%	-2%	8%
		20	10%	-1%	16%	-7%	16%	-9%	-10%	-2%	9%
		24	11%	0%	20%	-8%	17%	-7%	-11%	-2%	12%
	160	8	-12%	-1%	8%	-4%	5%	-3%	-8%	-1%	0%
		12	-13%	-1%	13%	-4%	5%	-1%	-9%	-1%	-1%
		16	-11%	-2%	11%	-2%	5%	2%	-7%	1%	0%
		20	-12%	0%	10%	-5%	5%	1%	-8%	0%	-2%
		24	-10%	-2%	8%	-1%	6%	2%	-5%	-3%	-6%
	200	8	-8%	-1%	16%	-4%	6%	7%	-10%	-4%	-13%
		12	-9%	-1%	23%	-4%	4%	12%	-14%	-4%	-16%
		16	-7%	-2%	21%	-3%	1%	11%	-12%	-6%	-19%
		20	0%	-3%	33%	-4%	4%	13%	-18%	-10%	-23%
		24	16%	-2%	37%	-4%	14%	3%	-24%	-7%	-26%
Atmosphere	PERIOD		Peak 1335	Peak 1366	Peak 1421	Peak 1456	Peak 1507	Peak 1595	Peak 1642	Peak 1730	
	120	8	-16%	17%	-9%	16%	6%	-7%	-6%	-43%	
		12	-8%	13%	-8%	6%	5%	-1%	-4%	-44%	
		16	2%	8%	-10%	-5%	-4%	7%	-6%	-46%	
		20	-9%	7%	-10%	-5%	-1%	8%	-4%	-43%	
		24	-23%	6%	-11%	-5%	9%	15%	-4%	-41%	
	160	8	-3%	2%	-12%	-14%	-5%	12%	-5%	-42%	
		12	8%	4%	-11%	-5%	1%	29%	-8%	-37%	
		16	4%	1%	-12%	-10%	-3%	44%	-8%	-27%	
		20	10%	-2%	-13%	-11%	-3%	46%	-8%	-24%	
		24	6%	-7%	-14%	-22%	-6%	55%	-8%	-15%	
	200	8	24%	-25%	-23%	-34%	-22%	113%	-9%	39%	
		12	53%	-49%	-36%	-47%	-39%	167%	-14%	108%	
		16	32%	-53%	-41%	-50%	-40%	193%	-20%	201%	
		20	37%	-54%	-41%	-55%	-39%	210%	-21%	237%	
		24	37%	-61%	-47%	-54%	-47%	246%	-22%	264%	
	120	8	-13%	9%	-8%	-2%	5%	7%	-4%	-42%	
		12	-15%	6%	-10%	-7%	1%	7%	-4%	-47%	
		16	-14%	4%	-10%	-10%	-2%	2%	-4%	-52%	
vacuum											

	20	-16%	6%	-11%	-6%	-1%	-6%	-3%	-47%
	24	-3%	1%	-11%	-16%	-5%	-12%	-5%	-44%
	8	7%	-6%	-12%	-13%	-4%	10%	-2%	-15%
	12	5%	-6%	-13%	-13%	-1%	19%	-7%	-28%
160	16	-3%	-4%	-13%	-11%	1%	28%	-8%	-38%
	20	7%	-4%	-12%	-10%	1%	33%	-8%	-31%
	24	5%	-12%	-14%	-19%	-1%	52%	-8%	-26%
	8	10%	-15%	-19%	-18%	3%	64%	-11%	2%
	12	14%	-19%	-19%	-25%	7%	82%	-17%	8%
200	16	12%	-24%	-22%	-27%	-1%	90%	-16%	14%
	20	6%	-28%	-26%	-28%	-5%	122%	-16%	22%
	24	13%	-23%	-24%	-32%	-10%	125%	-15%	29%

The peaks percentage changes regression models are as follow.

In air treatment

$$Pc_{895} = 0.309 - 0.001 \times T - 0.002 \times t_p$$

$$Pc_{1054} = -0.561 + 0.005 \times T + 0.008 \times t_p$$

$$Pc_{1110} = 0.139 - 0.001 \times T - 0.002 \times t_p$$

$$Pc_{1154} = 0.450 - 0.002 \times T - 0.001 \times t_p$$

$$Pc_{1204} = -0.196 + 0.001 \times T + 0.002 \times t_p$$

$$Pc_{1226} = 0.496 - 0.004 \times T - 0.004 \times t_p$$

$$Pc_{1262} = 0.245 - 0.002 \times T - 0.001 \times t_p$$

$$Pc_{1318} = 1.203 - 0.008 \times T - 0.011 \times t_p$$

$$Pc_{1335} = -0.861 + 0.006 \times T + 0.001 \times t_p$$

$$Pc_{1366} = 1.220 - 0.007 \times T - 0.011 \times t_p$$

$$Pc_{1421} = 0.448 - 0.004 \times T - 0.005 \times t_p$$

$$Pc_{1456} = 0.958 - 0.006 \times T - 0.010 \times t_p$$

$$Pc_{1507} = 0.754 - 0.005 \times T - 0.004 \times t_p$$

$$Pc_{1595} = -3.483 + 0.023 \times T + 0.039 \times t_p$$

$$Pc_{1642} = 0.191 - 0.002 \times T - 0.003 \times t_p$$

$$Pc_{1730} = -4.809 + 0.027 \times T + 0.054 \times t_p$$

In vacuum treatment

$$Pc_{895} = 0.226 - 0.002 \times T + 0.005 \times t_p$$

$$Pc_{1054} = -0.073 + 0.001 \times T + 0.004 \times t_p$$

$$Pc_{1154} = 0.277 - 0.001 \times T + 0.002 \times t_p$$

$$Pc_{1204} = -0.310 + 0.002 \times T$$

$$Pc_{1226} = 0.090 - 0.001 \times T - 0.003 \times t_p$$

$$Pc_{1262} = 0.086 - 0.001 \times T - 0.002 \times t_p$$

$$Pc_{1318} = 0.566 - 0.004 \times T - 0.003 \times t_p$$

$$Pc_{1335} = -0.477 + 0.003 \times T + 0.001 \times t_p$$

$$Pc_{1366} = 0.529 - 0.003 \times T - 0.004 \times t_p$$

$$Pc_{1421} = 0.122 - 0.001 \times T - 0.002 \times t_p$$

$$Pc_{1456} = 0.287 - 0.002 \times T - 0.006 \times t_p$$

$$Pc_{1507} = 0.073 - 0.00007620 \times T - 0.004 \times t_p$$

$$Pc_{1595} = -1.794 + 0.012 \times T + 0.017 \times t_p$$

$$Pc_{1642} = 0.164 - 0.001 \times T - 0.002 \times t_p$$

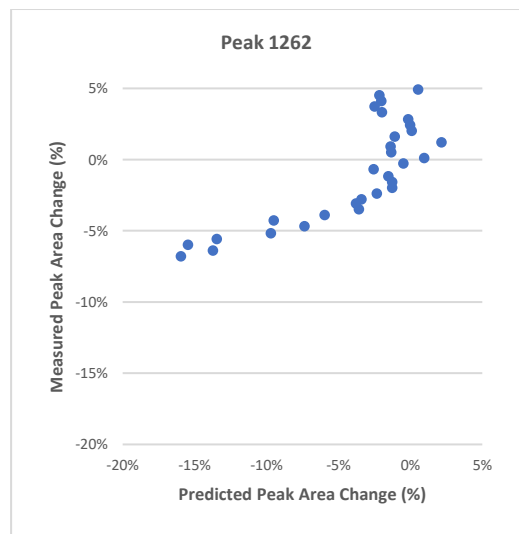
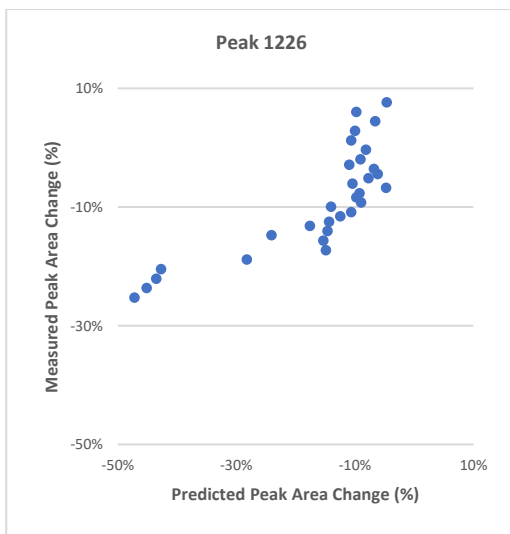
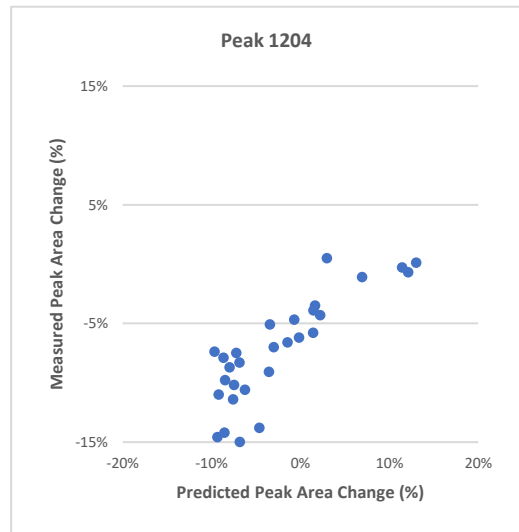
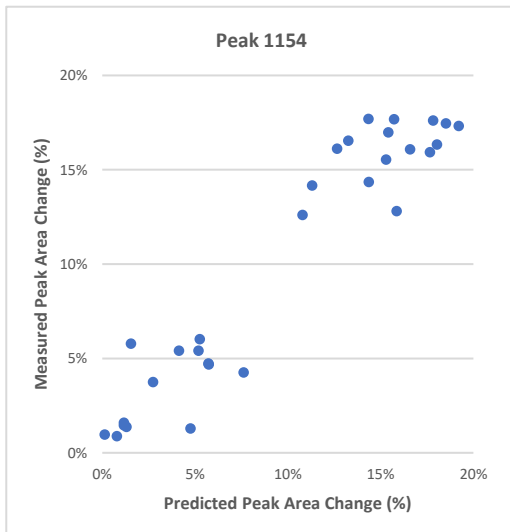
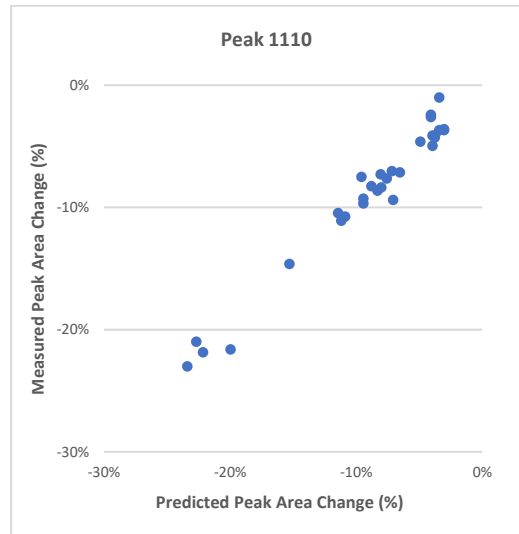
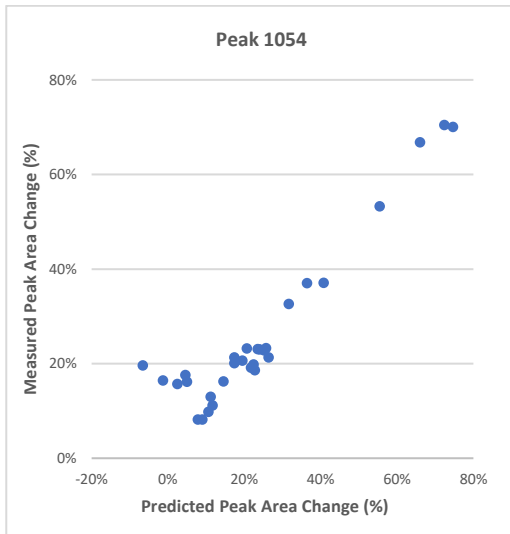
$$Pc_{1730} = -1.475 + 0.008 \times T + 0.003 \times t_p$$

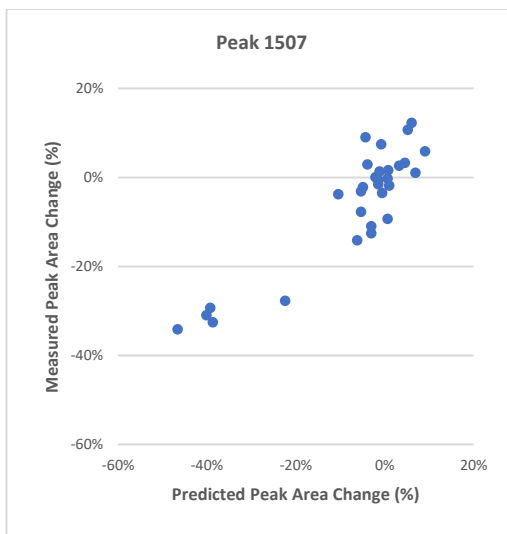
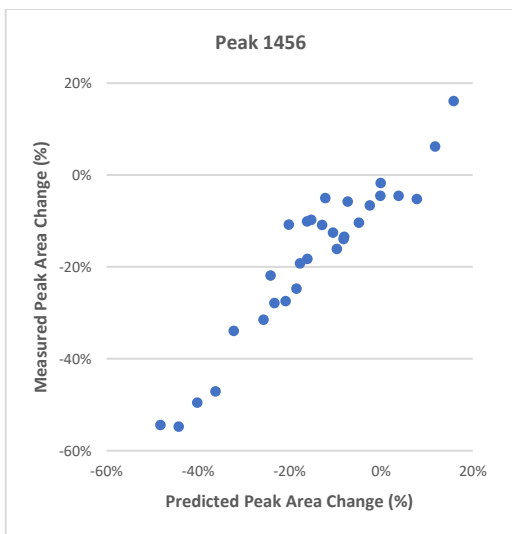
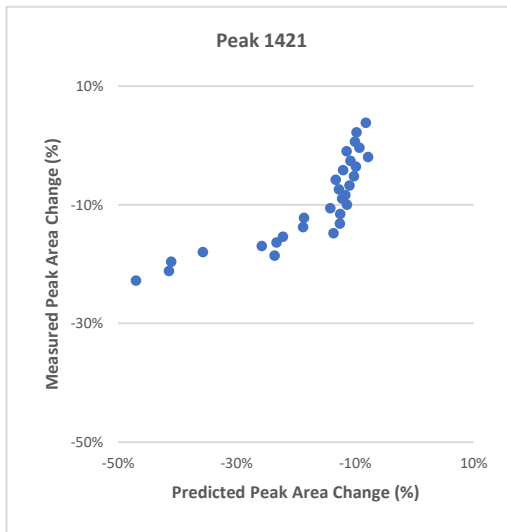
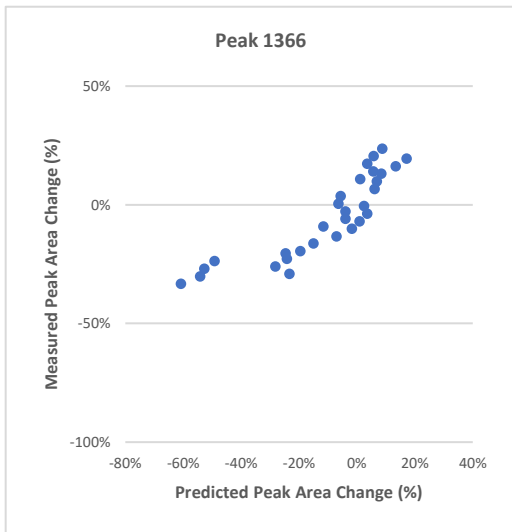
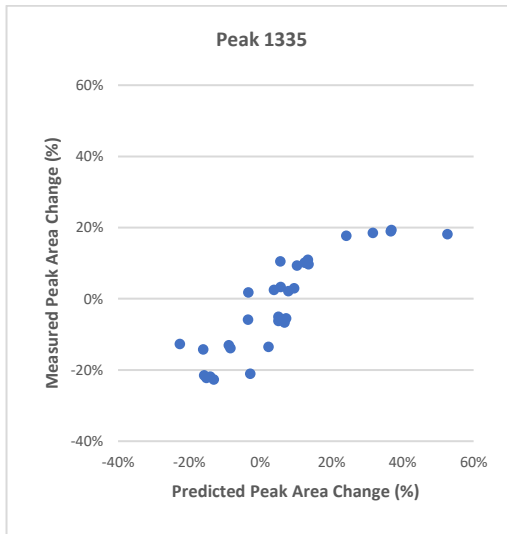
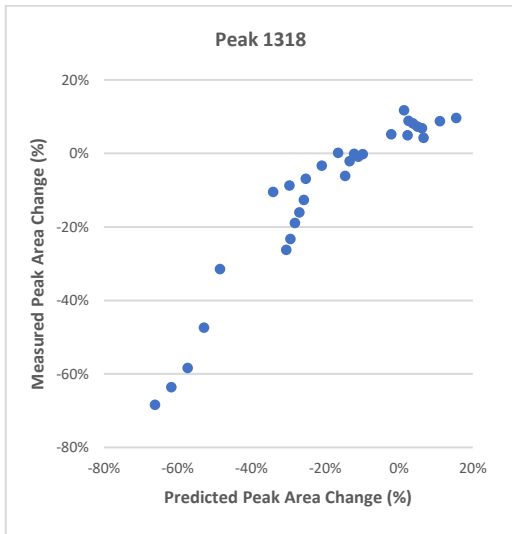
where $Pc_{wavenumber}$ are the peak percentage changes during heat treatment, T is the treatment temperature in Celsius ($^{\circ}\text{C}$) and t_p is the treatment period in hours. For high accuracy, the two independent variables are best chosen between 120°C and 200°C and between 0 and 24 hours for the treatment period. Table 7-2 shows the Pearson correlation (R), coefficient of determination (R-square), adjusted R-square and standard error of the MRA mathematical models for each peak, both in air and vacuum treatments. The R-square and Adjusted R-square are high, which means that the models are highly functional. The predicted values and measured values of the changes of each peak are shown in Figure 7-2. Since the R-square of Peaks 895 and 1025 is low, and Peak 1642 is affected by moisture content, the three peaks are not shown in the figure.

The change of Peak 1025, relating to C-Hs bond and ether linkage, cannot be predicted by the regression models. C-H bonds are the majority of bonds in the timber molecule, but the changes are not any more significant than other bonds after normalisation. Hence, peak 1025 is not discussed in the following section.

Table 7-2 MRA Models for Peak 1318, 1456 and 1595 Changes During Heat Treatment

Peak	Samples in Air				Samples in Vacuum			
	R	R-square	Adjusted R-square	Std. Error	R	R-square	Adjusted R-square	Std. Error
895	0.670	0.449	0.357	0.0561	0.572	0.327	0.214	0.1063
1054	0.841	0.707	0.658	.01185	0.555	0.308	0.193	0.0744
1110	0.876	0.767	0.729	0.0305	-	-	-	-
1154	0.941	0.885	0.866	0.0268	0.767	0.588	0.519	0.0410
1204	0.706	0.499	0.415	0.0271	0.924	0.853	0.828	0.0306
1226	0.904	0.817	0.787	0.0709	0.695	0.483	0.397	0.0395
1262	0.909	0.826	0.797	0.2921	0.783	0.545	0.469	0.0208
1318	0.932	0.869	0.847	0.1103	0.963	0.928	0.916	0.0361
1335	0.914	0.836	0.808	0.0954	0.906	0.820	0.790	0.0498
1366	0.926	0.858	0.835	0.1123	0.974	0.949	0.940	0.0293
1421	0.879	0.772	0.734	0.0719	0.935	0.874	0.853	0.0211
1456	0.952	0.906	0.890	0.0757	0.919	0.845	0.819	0.0379
1507	0.897	0.805	0.773	0.0918	0.602	0.362	0.255	0.0368
1595	0.924	0.854	0.830	0.3566	0.929	0.863	0.840	0.1811
1642	0.865	0.749	0.707	0.0338	0.912	0.832	0.804	0.0234
1730	0.848	0.720	0.673	0.6441	0.940	0.884	0.865	0.1017





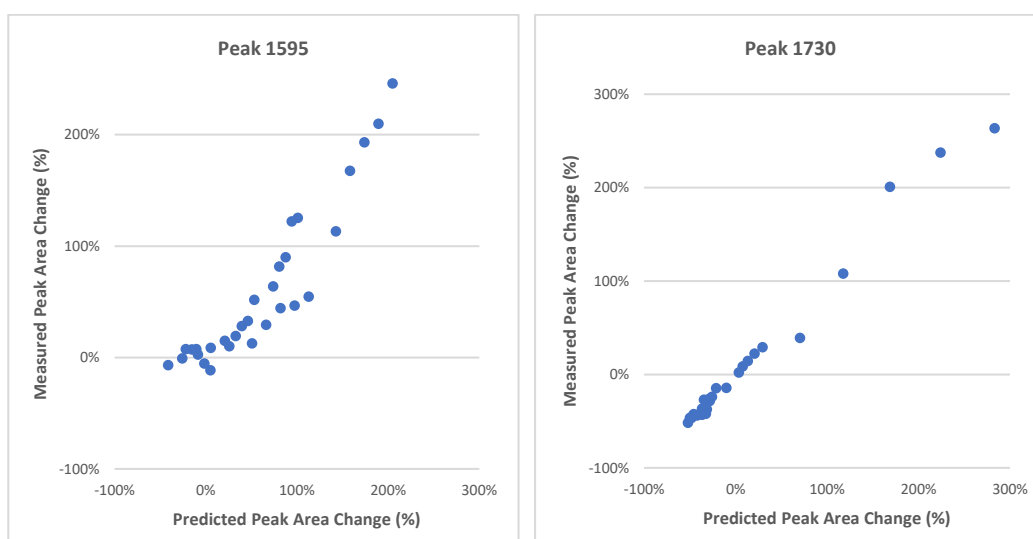


Figure 7-2 Predicted and Measured Peak Area Changes of Regression Model

7.2.2 Accelerated Ageing Method

The peak areas of untreated new and old pine are illustrated in Table 4-2 and the percentage changes are presented in Table 7-3. Hence a simultaneous equations system is set to predict two independent variables: treatment temperature and treatment period. Theoretically, three kinds of treatment might be used for the chemical change:

1. Treated in an air atmosphere;
2. Treated in a vacuum atmosphere;
3. Treated both in air and in vacuum atmospheres.

Table 7-3 New Pine Changing to Old Pine

	Peak 1054 (C-C, C-O)	Peak 1110 (C-OH)	Peak 1154 (C-O-C)	Peak 1204 (C-O-C)	Peak 1226 (C-C)	Peak 1262 (C-O)	Peak 1318 (G or S Ring)
new	0	0	0	0	0	0	0
old	-41.78%	-13.97%	+3.93%	-29.31%	-10.87%	-9.16%	-8.91%
	Peak 1335 (-OH)	Peak 1366 (C-H)	Peak 1421 (O-H)	Peak 1456 (C-H)	Peak 1507 (Aromatic Ring)	Peak 1595 (C=C)	Peak 1730 (C=O)
new	0	0	0	0	0	0	0
old	-18.47%	+11.23%	-1.58%	+8.47%	-4.51%	+14.92%	+11.25%

For the first, T_A and t_{pA} are the independent variables of temperature and treatment period.

For the second, T_V and t_{pV} are the independent variables of temperature and treatment period. For the third, the four independent variables are temperature, treatment period as well as air and vacuum atmospheres. Accordingly, three simultaneous equations systems are created as the follows:

For treatment in an air atmosphere:

$$\left\{ \begin{array}{l} -0.561 + 0.005 \times T_A + 0.008 \times t_{pA} = -0.4178 \\ 0.139 - 0.001 \times T_A - 0.002 \times t_{pA} = -0.1397 \\ 0.450 - 0.002 \times T_A - 0.001 \times t_{pA} = 0.0393 \\ -0.196 + 0.001 \times T_A + 0.002 \times t_{pA} = -0.2931 \\ 0.496 - 0.004 \times T_A - 0.004 \times t_{pA} = -0.1087 \\ 0.245 - 0.002 \times T_A - 0.001 \times t_{pA} = -0.0916 \\ 1.203 - 0.008 \times T_A - 0.011 \times t_{pA} = -0.0891 \\ -0.861 + 0.006 \times T_A + 0.001 \times t_{pA} = -0.1847 \\ 1.220 - 0.007 \times T_A - 0.011 \times t_{pA} = 0.1123 \\ 0.448 - 0.004 \times T_A - 0.005 \times t_{pA} = -0.0158 \\ 0.958 - 0.006 \times T_A - 0.010 \times t_{pA} = 0.0847 \\ 0.754 - 0.005 \times T_A - 0.004 \times t_{pA} = -0.0451 \\ -3.483 + 0.023 \times T_A + 0.039 \times t_{pA} = 0.1492 \\ -4.809 + 0.027 \times T_A + 0.054 \times t_{pA} = 0.1125 \end{array} \right.$$

Simplifying obtains:

$$\left\{ \begin{array}{l} 0.005 \times T_A + 0.008 \times t_{pA} = 0.1432 \\ -0.001 \times T_A - 0.002 \times t_{pA} = -0.2787 \\ -0.002 \times T_A - 0.001 \times t_{pA} = -0.4107 \\ 0.001 \times T_A + 0.002 \times t_{pA} = -0.0971 \\ -0.004 \times T_A - 0.004 \times t_{pA} = -0.6047 \\ -0.002 \times T_A - 0.001 \times t_{pA} = -0.3366 \\ -0.008 \times T_A - 0.011 \times t_{pA} = -1.2921 \\ 0.006 \times T_A + 0.001 \times t_{pA} = 0.6763 \\ -0.007 \times T_A - 0.011 \times t_{pA} = -1.1077 \\ -0.004 \times T_A - 0.005 \times t_{pA} = -0.4638 \\ -0.006 \times T_A - 0.010 \times t_{pA} = -0.8733 \\ -0.005 \times T_A - 0.004 \times t_{pA} = -0.7991 \\ 0.023 \times T_A + 0.039 \times t_{pA} = 3.6322 \\ 0.027 \times T_A + 0.054 \times t_{pA} = 4.9215 \end{array} \right.$$

For treatment in a vacuum atmosphere:

$$\left\{ \begin{array}{l} -0.073 + 0.001 \times T_V + 0.004 \times t_{pV} = -0.4178 \\ 0.277 - 0.001 \times T_V + 0.002 \times t_{pV} = 0.0393 \\ -0.310 + 0.002 \times T_V = -0.2931 \\ 0.090 - 0.001 \times T_V - 0.003 \times t_{pV} = -0.1087 \\ 0.086 - 0.001 \times T_V - 0.002 \times t_{pV} = -0.0916 \\ 0.566 - 0.004 \times T_V - 0.003 \times t_{pV} = -0.0891 \\ -0.477 + 0.003 \times T_V + 0.001 \times t_{pV} = -0.1847 \\ 0.529 - 0.003 \times T_V - 0.004 \times t_{pV} = 0.1123 \\ 0.122 - 0.001 \times T_V - 0.002 \times t_{pV} = -0.0158 \\ 0.287 - 0.002 \times T_V - 0.006 \times t_{pV} = 0.0847 \\ 0.073 - 0.00007620 \times T_V - 0.004 \times t_{pV} = -0.0451 \\ -1.794 + 0.012 \times T_V + 0.017 \times t_{pV} = 0.1492 \\ -1.475 + 0.008 \times T_V + 0.003 \times t_{pV} = 0.1125 \end{array} \right.$$

Simplifying obtains:

$$\left\{ \begin{array}{l} 0.001 \times T_V + 0.004 \times t_{pV} = 0.4908 \\ -0.001 \times T_V + 0.002 \times t_{pV} = -0.2377 \\ 0.002 \times T_V = 0.0169 \\ -0.001 \times T_V - 0.003 \times t_{pV} = -0.1987 \\ -0.001 \times T_V - 0.002 \times t_{pV} = -0.1776 \\ -0.004 \times T_V - 0.003 \times t_{pV} = -0.6551 \\ 0.003 \times T_V + 0.001 \times t_{pV} = 0.2923 \\ -0.003 \times T_V - 0.004 \times t_{pV} = -0.4167 \\ -0.001 \times T_V - 0.002 \times t_{pV} = -0.1378 \\ -0.002 \times T_V - 0.006 \times t_{pV} = -0.2023 \\ -0.0000762 \times T_V - 0.004 \times t_{pV} = -0.1181 \\ 0.012 \times T_V + 0.017 \times t_{pV} = 1.9432 \\ 0.008 \times T_V + 0.003 \times t_{pV} = 1.5875 \end{array} \right.$$

For treatment in both atmospheres:

$$\left\{ \begin{array}{l} -0.561 + 0.005 \times T_A + 0.008 \times t_{pA} - 0.073 + 0.001 \times T_V + 0.004 \times t_{pV} = -0.4178 \\ \quad 0.139 - 0.001 \times T_A - 0.002 \times t_{pA} = -0.1397 \\ 0.450 - 0.002 \times T_A - 0.001 \times t_{pA} + 0.277 - 0.001 \times T_V + 0.002 \times t_{pV} = 0.0393 \\ \quad -0.196 + 0.001 \times T_A + 0.002 \times t_{pA} - 0.310 + 0.002 \times T_V = -0.2931 \\ 0.496 - 0.004 \times T_A - 0.004 \times t_{pA} + 0.090 - 0.001 \times T_V - 0.003 \times t_{pV} = -0.1087 \\ 0.245 - 0.002 \times T_A - 0.001 \times t_{pA} + 0.086 - 0.001 \times T_V - 0.002 \times t_{pV} = -0.0916 \\ 1.203 - 0.008 \times T_A - 0.011 \times t_{pA} + 0.566 - 0.004 \times T_V - 0.003 \times t_{pV} = -0.0891 \\ -0.861 + 0.006 \times T_A + 0.001 \times t_{pA} - 0.477 + 0.003 \times T_V + 0.001 \times t_{pV} = -0.1847 \\ 1.220 - 0.007 \times T_A - 0.011 \times t_{pA} + 0.529 - 0.003 \times T_V - 0.004 \times t_{pV} = 0.1123 \\ 0.448 - 0.004 \times T_A - 0.005 \times t_{pA} + 0.122 - 0.001 \times T_V - 0.002 \times t_{pV} = -0.0158 \\ 0.958 - 0.006 \times T_A - 0.010 \times t_{pA} + 0.287 - 0.002 \times T_V - 0.006 \times t_{pV} = 0.0847 \\ 0.754 - 0.005 \times T_A - 0.004 \times t_{pA} + 0.073 - 0.00007620 \times T_V - 0.004 \times t_{pV} = -0.0451 \\ -3.483 + 0.023 \times T_A + 0.039 \times t_{pA} - 1.794 + 0.012 \times T_V + 0.017 \times t_{pV} = 0.1492 \\ -4.809 + 0.027 \times T_A + 0.054 \times t_{pA} - 1.475 + 0.008 \times T_V + 0.003 \times t_{pV} = 0.1125 \end{array} \right.$$

Simplifying obtains:

$$\left\{ \begin{array}{l} 0.005 \times T_A + 0.006 \times t_{pA} + 0.001 \times T_V + 0.004 \times t_{pV} = 0.2162 \\ \quad -0.001 \times T_A - 0.002 \times t_{pA} = -0.2787 \\ -0.002 \times T_A - 0.001 \times T_V - 0.001 \times T_V + 0.002 \times t_{pV} = -0.6877 \\ \quad 0.001 \times T_A + 0.002 \times t_{pA} + 0.002 \times T_V = 0.2129 \\ -0.004 \times T_A - 0.004 \times t_{pA} - 0.001 \times T_V - 0.003 \times t_{pV} = -0.6947 \\ -0.002 \times T_A - 0.001 \times t_{pA} - 0.001 \times T_V - 0.002 \times t_{pV} = -0.4226 \\ -0.008 \times T_A - 0.011 \times t_{pA} - 0.004 \times T_V - 0.003 \times t_{pV} = -1.8581 \\ 0.006 \times T_A + 0.001 \times t_{pA} + 0.003 \times T_V + 0.001 \times t_{pV} = 1.1533 \\ -0.007 \times T_A - 0.011 \times t_{pA} - 0.003 \times T_V - 0.004 \times t_{pV} = -1.6367 \\ -0.004 \times T_A - 0.005 \times t_{pA} - 0.001 \times T_V - 0.002 \times t_{pV} = -0.5858 \\ -0.006 \times T_A - 0.010 \times t_{pA} - 0.002 \times T_V - 0.006 \times t_{pV} = -1.1603 \\ -0.005 \times T_A - 0.004 \times t_{pA} - 0.0000762 \times T_V - 0.004 \times t_{pV} = -0.8721 \\ 0.023 \times T_A + 0.039 \times t_{pA} + 0.012 \times T_V + 0.017 \times t_{pV} = 5.4262 \\ 0.027 \times T_A + 0.054 \times t_{pA} + 0.008 \times T_V + 0.003 \times t_{pV} = 6.3965 \end{array} \right.$$

To obtain the most suitable results, the equation quantity is more than the number of independent variables. The results are recalculated by the least-square solution, which an application for reducing the sum of the squares of the residuals. Table 7-4 shows the results of the three simultaneous equation systems, which are simulated by air heat treatment,

vacuum heat treatment and a combined heat treatment. The highest coefficient of determination (R-square) appears in the combined heat treatment method for an air atmosphere at 137°C for 29 hours and a vacuum atmosphere at 152°C for 8 hours. For the heat treatment prediction in air and vacuum separately, 120°C for 35 hours and 165°C for 8 hours are the best methods, respectively. The prediction is very close to the measured value in all the heat treatment methods (Table 7-5, Figure 7-3, Figure 7-4 and Figure 7-5).

Table 7-4 Results of Simultaneous Equation Systems

Model	Independent Variables	Value	R-square	Adjusted R-square
Treated in air	T_A	120 (°C)	0.974	0.967
	t_{pA}	35.6621 (hours)		
Treated in a vacuum	T_V	165.078 (°C)	0.946	0.941
	t_{pV}	8 (hours)		
Treated in both atmosphere	T_A	137.2649 (°C)	0.974	0.971
	t_{pA}	29.75643 (hours)		
	T_V	152.25664 (°C)		
	t_{pV}	8 (hours)		

Table 7-5 Model-Predicted and Measured Peak Area of Regression Analysis

Peak	New Pine (Initial)	Old Pine (Aim)	Treated in Air (Model-Predicted)	Treated in vacuum (Model-Predicted)	Treated in Both (Model-Predicted)
1054	146	85	195	165	227
1110	1052	905	996	1052	991
1154	610	634	468	688	616
1204	116	82	116	119	100
1226	432	385	375	389	281
1262	895	813	865	810	791
1318	494	450	415	436	471
1335	92	75	83	94	97
1366	650	723	636	651	738

1421	568	560	445	534	530
1456	425	389	372	387	326
1507	288	275	289	296	260
1595	355	408	603	470	499
1730	480	534	668	418	520

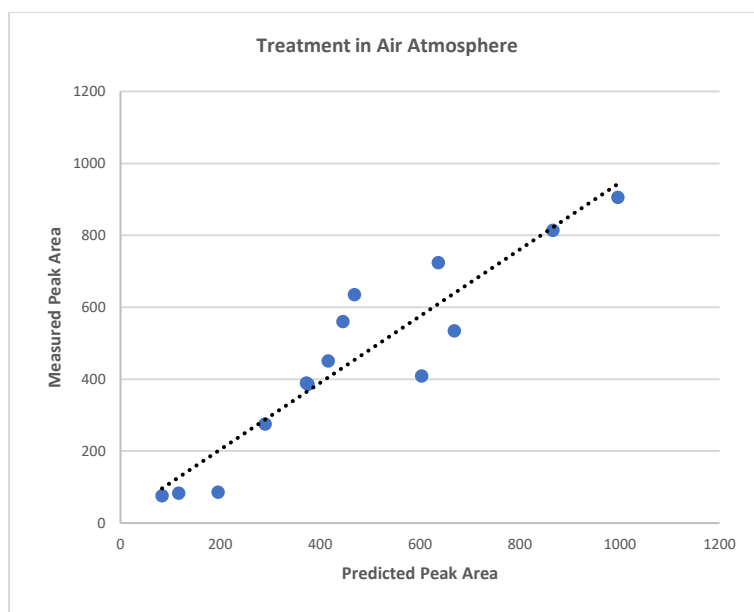


Figure 7-3 Model-Predicted and Measured Peak Area of the Air Treatment Method

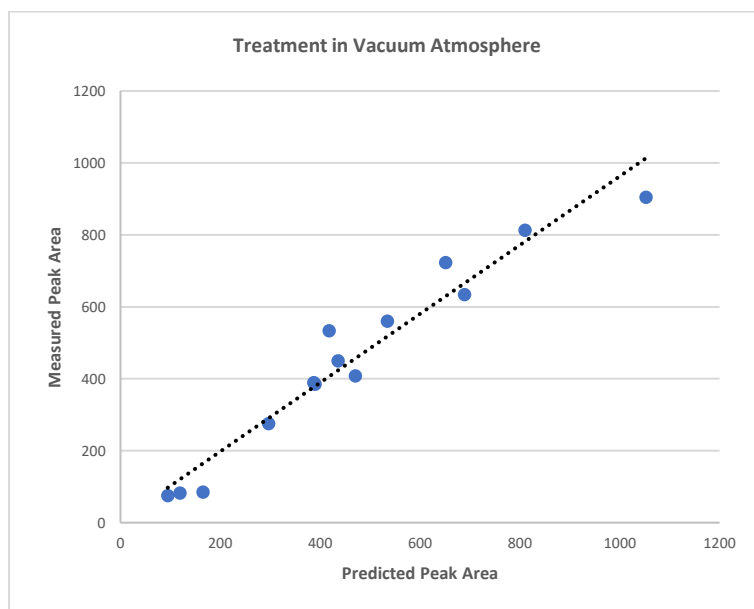


Figure 7-4 Model-Predicted and Measured Peak Area of the Vacuum Treatment Method

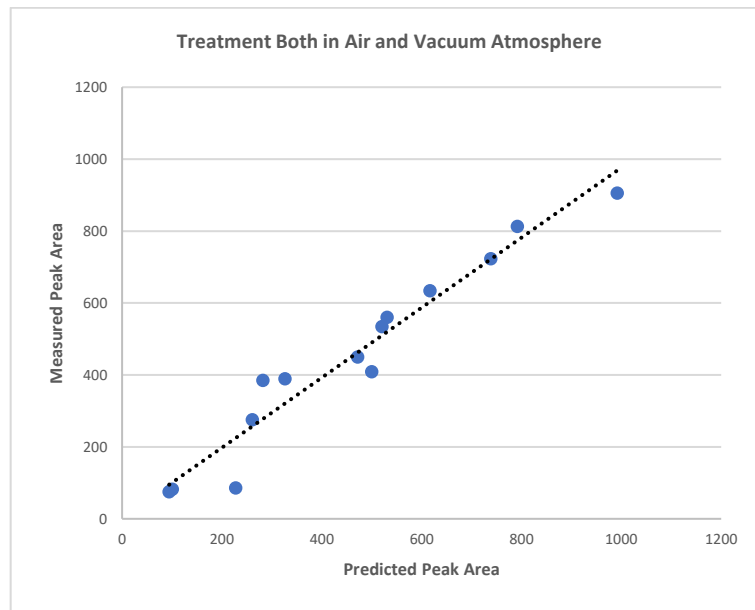


Figure 7-5 Model-Predicted and Measured Peak Area of the Combined Treatment Method

7.3 Summary

The semi-destructive testing is a quick and accurate method and cause very little destruction to predict mechanical properties of the specific timber structural members. The tests provide fundamental evaluation for the whole structure, which can help predict structural failure in advance.

The regression mathematical model shows that the chemical composition of 580 year old pine can be obtained from new pine of the same species though specific heat treatments. The most suitable method for doing so is combining treatment in air and a vacuum at a certain temperature for a specific treatment period. Since a vacuum atmosphere improves the reactions of condensation and cross-linking, while an air one promotes oxidation and pyrolysis, the timber ageing process is a combination of the four reactions at a slow rate.

Chapter 8 Conclusion

8.1 Conclusion

The objectives of this thesis were to:

- Investigate the relationship between the chemical composition of timber and the static and dynamic mechanical properties;
- Produce regression models to predict mechanical properties by timber chemical composition;
- Examine chemical composition changes during heat treatment in different atmospheres;
- Produce a mathematical model to predict the changes of timber chemical composition in different temperatures, periods and atmospheres, as a method for accelerating timber ageing.

After experimentation and data analysis, the above have been achieved.

It has been verified that timber chemical composition has close relationships with its mechanical properties, both through static and dynamic testing. Physically, the chemical reactions that can extend or expand timber molecules as well as condensation between hemicellulose and lignin, condensation between lignin and the cross-linking of lignin, improve timber mechanical static properties in terms of the bending modulus of rupture (MOR) and modulus of elasticity (MOE), whilst decreasing energy dissipation of dynamic mechanical properties ($\text{Tan } \delta$) by reducing friction between the molecules. The reactions that can diminish the length of the molecules, such as decomposition in hemicellulose and lignin, decrease the static mechanical properties and increase $\text{Tan } \delta$ significantly. Decomposition also contributes to the mass loss in timber. In addition, a deacetylase reaction leads to mass loss but does not affect the mechanical properties significantly.

Oxidation can increase the bending MOE under low mass loss, but leads to a reduction in the bending MOR. However, the bending MOR changes are more significant than those for MOE and timber cell structure also plays a close role in MOE. In terms of static compression testing, compression MOE changes are more significant for MOR, due to the same reason of specific timber cell structures. Regarding the changes in the dynamic mechanical properties, condensation and cross-linking reaction contribute to a decrease in $\text{Tan } \delta$ of these due to the lower friction between the timber molecules. Pyrolysis can increase the friction between timber molecules and lead to an increase in viscosity. The stability of the timber molecules is enhanced, which leads the peaks γ and β of the $\text{Tan } \delta$ temperature scanning curve moving to a higher temperature. The molecular structures of old pine samples tend to be stable due to condensation as well as cross-linking, oxidation reactions during the natural ageing process, which contributes to a higher temperature of the peaks γ and β of $\text{Tan } \delta$ appearing.

Timber's static and dynamic mechanical properties can be predicted by the density and the peaks of the FTIR spectrum after baseline correction and curve normalisation. The FTIR technique can illustrate the chemical compositions of timber by the peaks corresponding to specific functional groups of molecules. One natural logarithm fitting model and one multiple regression model can predict the bending MOR, which use density, Peaks 1318, 1730 and density, Peaks 1054, 1366, 1456, 1318 and 1421 as independent variables, respectively. The coefficient of determination (R-square) and adjusted R-square of the two models are more than 0.8, which indicates that the measured bending MOR is replicated by the regression models. One multiple regression model and one ridge regression model can predict the bending MOE by the independent variables of density along with Peaks 1025, 1226, 895 and 1456. The R-square and adjusted R-square of the two models are approximately 0.64 and 0.6, respectively, which can predict more than 75% of the

measured bending MOE of the samples. The two regression models also show high prediction. However, in the MOE analysis, a multiple regression model illustrates the problem of multicollinearity, which means that some independent variables have high correlations with each other. A ridge regression model can solve the problem, but this reduces R-square. In terms of dynamic mechanical properties, the Tan δ value at the peaks γ and β during temperature scanning can be predicted by the FTIR peaks, which show viscoelasticity of the timber samples. However, the temperatures at peak γ and β cannot be predicted. The main reason is that FTIR is a technique showing the relative content of molecular functional groups rather than their quantity. All the regression models, including MOR, MOE and the Tan δ of peaks γ and β , are suitable for both new and old samples. That is, the regression models are widely functional.

Temperature and specific atmospheres can cause distinctive changes to timber chemical composition. For new pine samples in heat treatment, oxygen, temperature and treatment period affect the chemical changes in timber molecules significantly. In temperature at 120°C in a vacuum atmosphere for 24 hours, condensation and cross-linking are promoted, whilst at 200°C with oxygen for more than 8 hours, the two are inhibited and pyrolysis reaction increase improved dramatically, leading to high mass loss. In other treatments, both MOR and MOE increase firstly for a certain period, followed by a decrease. Hence, condensation and cross-linking reactions happen immediately under heat treatment, but stopped after a certain period. Pyrolysis can happen in a long period. For old pine samples, the chemical changes are less than new pine at 120°C but much intense than it at 200°C. Lignin-carbohydrate complexes, which are condensed between lignin and hemicellulose during natural ageing, are responsible for this. The changes of new pine's FTIR peaks during heat treatment can be predicted by multiple regression analysis with temperature and treatment period as independent variables.

The regression models of each peak provide fundamental support for the notion of timber chemical composition changes during heat treatment and accelerated timber ageing. That is, an accelerated ageing method can be deduced by the regression models. Comparing the FTIR peaks of the new and 580 year old pine samples, the former can be treated in air, a vacuum or both to obtain similar chemical compositions as with the latter. The accelerating method is calculated by simultaneous equations and the results show that a combined treatment method, including air and vacuum atmosphere treatment is the most suitable method.

In conclusion, this study has shown that timber mechanical properties can be predicted by chemical compositions analysed by the FTIR technique through various mathematical regression models. Heat treatment in specific atmospheres contributes to distinctive changes, which can be regressed by a multiple regression analysis method. Timber accelerated ageing can be conducted by heat treatment in certain atmospheres. However, few limitations exist. Firstly, even though all regression models are suitable for the new and old pine samples (*Pinus Densiflora*), it has not been proven that the models are suitable for other tree species. Secondly, oxygen affects timber's chemical composition significantly during heat treatment, but the effects of oxygen concentration influence have not been studied in the experimentation due to this being an uncontrollable operation. A regression model that contains oxygen content as an independent variable, may provide more accuracy for the prediction of timber accelerated ageing. Thirdly, the dynamic mechanical properties seem not only to be affected by the chemical functional groups of timber molecule. Other factors, such as crystallinity, angles of the microfibrils of cell, cell shape and cell wall thickness, could affect these properties and a more comprehensive experiment design would be needed to capture these influence. Finally, the samples of old

timber with different ages were so few that the chemical composition change during natural ageing could not be evaluated.

8.2 Further Research

Given the limitations of this study addressed above, further research should contain the following.

- More tree species should be studied in heat treatment to improve the prediction regression models of timber mechanical properties. More old timber samples with different ages should be analysed to produce the regression model of natural ageing.
- The relationships between the changes of timber FTIR peaks during heat treatment and moisture content should be defined. Theoretically, timber chemical composition changes during heat treatment are affected by temperatures, treatment period and oxygen content. In addition, moisture content is also an important factor playing a significant role in the changes. The four independent variables can improve accuracy of regression models, thus providing valuable prediction for timber accelerated ageing study. However, a more advanced experimental facility is needed to improve upon this prediction capability.
- A comprehensive experiment containing more composition analysis methods needs to be conducted. Crystallinity, microfibril angles and cell wall status can be detected by XRD and SEM technique. Increasing the number of independent variables could uncover the relationships between chemical composition and dynamic mechanical properties.

Bibliography

ÅKERHOLM, M. & SALMÉN, L. 2001. Interactions between wood polymers studied by dynamic FT-IR spectroscopy. *Polymer*, 42, 963-969.

ÅKERHOLM, M. & SALMÉN, L. 2003. The oriented structure of lignin and its viscoelastic properties studied by static and dynamic FT-IR spectroscopy. *Holzforschung*, 57, 459-465.

ALEN, R., KOTILAINEN, R. & ZAMAN, A. 2002. Thermochemical behavior of Norway spruce (*Picea abies*) at 180-225 degrees C. *Wood Science and Technology*, 36, 163-171.

ANDO, K., HIRASHIMA, Y., SUGIHARA, M., HIRAO, S. & SASAKI, Y. 2006. Microscopic processes of shearing fracture of old wood, examined using the acoustic emission technique. *Journal of Wood Science*, 52, 483-489.

ASSARSSON, A. & AKERLUND, G. 1967. Studies on Wood Resin Especially Changes during Seasoning of Wood .5. Changes in Composition of Nonvolatile Extractives during Water Seasoning of Unbarked Spruce Pine Birch and Aspen Logs. *Svensk Papperstidning-Nordisk Cellulosa*, 70, 205.

ASTLEY, R. J., STOL, K. A. & HARRINGTON, J. J. 1998. Modelling the elastic properties of softwood. *Holz als Roh- und Werkstoff*, 56, 43-50.

ATAK, D. 1981. Dynamic mechanical loss properties of wood. *Philosophical Magazine A*, 43, 619-625.

ATTAR-HASSAN 1976. The effect of ageing on the mechanical properties of Eastern white pine. *Bulletin of the Association for Preservation Technology*, 8, 64-73.

BACKMAN, A. & LINDBERG, K. 2001. Differences in wood material responses for radial and tangential direction as measured by dynamic mechanical thermal analysis. *Journal of Materials Science*, 36, 3777-3783.

BAMBER, R. K. 1976. Heartwood, Its Function and Formation. *Wood Science and Technology*, 10, 1-8.

BARBOUR, R. J. The condition and dimensional stabilization of highly deteriorated waterlogged hardwoods. Les Bois Gorgés d'Eau: Étude et conservation. Actes de la 2^e conférence du groupe de travail, 1985. Centre d'Étude et de Traitement des Bois Gorgés d'Eau, 23-37.

- BARCELÓ, A. R. 1997. Lignification in plant cell walls. *International review of cytology*. Elsevier.
- BARKER, B. & OWEN, N. L. 1999. Identifying softwoods and hardwoods by infrared spectroscopy. *Journal of chemical education*, 76, 1706.
- BECKER, H. & NOACK, D. 1968. Studies on dynamic torsional viscoelasticity of wood. *Wood Science and Technology*, 2, 213-230.
- BEKHTA, P. & NIEMZ, P. 2003. Effect of high temperature on the change in color, dimensional stability and mechanical properties of spruce wood. *Holzforschung*, 57, 539-546.
- BERTAUD, F. & HOLMBOM, B. 2004. Chemical composition of earlywood and latewood in Norway spruce heartwood, sapwood and transition zone wood. *Wood Science and Technology*, 38, 245-256.
- BERTHIER, S., KOKUTSE, A. D., STOKES, A. & FOURCAUD, T. 2001. Irregular heartwood formation in maritime pine (*Pinus pinaster* Ait): consequences for biomechanical and hydraulic tree functioning. *Annals of Botany*, 87, 19-25.
- BHUIYAN, M. T. R. & HIRAI, N. 2005. Study of crystalline behavior of heat-treated wood cellulose during treatments in water. *Journal of Wood Science*, 51, 42-47.
- BHUIYAN, M. T. R., HIRAI, N. & SOBUE, N. 2000. Changes of crystallinity in wood cellulose by heat treatment under dried and moist conditions. *Journal of Wood Science*, 46, 431-436.
- BIRKINSHAW, C., BUGGY, M. & HENN, G. 1986. Dynamic mechanical analysis of wood. *Journal of Materials Science*, 5, 898-900.
- BLANCHETTE, R. A. 2000. A review of microbial deterioration found in archaeological wood from different environments. *International Biodeterioration & Biodegradation*, 46, 189-204.
- BLANCHETTE, R. A., CEASE, K. R., ABAD, A., KOESTLER, R. J., SIMPSON, E. & SAMS, G. K. 1991. An evaluation of different forms of deterioration found in archaeological wood. *International biodeterioration*, 28, 3-22.

- BLANCHETTE, R. A., HAIGHT, J. E., KOESTLER, R. J., HATCHFIELD, P. B. & ARNOLD, D. 1994. Assessment of deterioration in archaeological wood from ancient Egypt. *Journal of the American Institute for Conservation*, 33, 55-70.
- BOONSTRA, M. J. & TJEERDSMA, B. 2006. Chemical analysis of heat treated softwoods. *Holz Als Roh-Und Werkstoff*, 64, 204-211.
- BOONSTRA, M. J., VAN ACKER, J. & KEGEL, E. 2007a. Effect of a two-stage heat treatment process on the mechanical properties of full construction timber. *Wood material science and engineering*, 2, 138-146.
- BOONSTRA, M. J., VAN ACKER, J., TJEERDSMA, B. F. & KEGEL, E. V. 2007b. Strength properties of thermally modified softwoods and its relation to polymeric structural wood constituents. *Annals of Forest Science*, 64, 679-690.
- BORGIN, K., FAIX, O. & SCHWEERS, W. 1975a. The effect of aging on lignins of wood. *Wood Science and Technology*, 9, 207-211.
- BORGIN, K., PARAMESWARAN, N. & LIESE, W. 1975b. The effect of aging on the ultrastructure of wood. *Wood Science and Technology*, 9, 87-98.
- BOURGOIS, J., BARTHOLIN, M. C. & GUYONNET, R. 1989. Thermal-Treatment of Wood - Analysis of the Obtained Product. *Wood Science and Technology*, 23, 303-310.
- BOURGOIS, J. & GUYONNET, R. 1988. Characterization and Analysis of Torrefied Wood. *Wood Science and Technology*, 22, 143-155.
- BRADLEY, M. 2007. Curve fitting in Raman and IR spectroscopy: basic theory of line shapes and applications. *Thermo Fisher Scientific, Madison, USA, Application Note*, 50733.
- BRANCHERIAU, L., BAILLERES, H. & GUITARD, D. 2002. Comparison between modulus of elasticity values calculated using 3 and 4 point bending tests on wooden samples. *Wood Science and Technology*, 36, 367-383.
- BRASCH, D. & JONES, J. 1959. Investigation of some ancient woods. *Tappi*, 42, 913-920.
- BURTIN, P., JAY-ALLEMAND, C., CHARPENTIER, J. P. & JANIN, G. 1998. Natural wood colouring process in Juglans sp. (J-nigra, J-regia and hybrid J-nigra 23 x J-regia) depends on native phenolic compounds accumulated in the transition zone between sapwood and heartwood. *Trees-Structure and Function*, 12, 258-264.

CAI, Z., HUNT, M. O., ROSS, R. J. & SOLTIS, L. 2000. Static and vibration moduli of elasticity of salvaged and new joists. *Forest products journal*, 50, 35-40.

CAPRETTI, C., MACCHIONI, N., PIZZO, B., GALOTTA, G., GIACHI, G. & GIAMPAOLA, D. 2008. The characterization of waterlogged archaeological wood: the three Roman ships found in Naples (Italy). *Archaeometry*, 50, 855-876.

CARRILLO, F., COLOM, X., SUNOL, J. & SAURINA, J. 2004. Structural FTIR analysis and thermal characterisation of lyocell and viscose-type fibres. *European Polymer Journal*, 40, 2229-2234.

CAVALLI, A., CIBECCHINI, D., TOGNI, M. & SOUSA, H. S. 2016. A review on the mechanical properties of aged wood and salvaged timber. *Construction and Building Materials*, 114, 681-687.

CHEN, H., FERRARI, C., ANGIULI, M., YAO, J., RASPI, C. & BRAMANTI, E. 2010. Qualitative and quantitative analysis of wood samples by Fourier transform infrared spectroscopy and multivariate analysis. *Carbohydrate Polymers*, 82, 772-778.

CHINI, A. R. 2001. Deconstruction and Materials Reuse: Technology, Economic, and Policy.

CHOW, S.-Z. 1971. Infrared spectral characteristics and surface inactivation of wood at high temperatures. *Wood Science and Technology*, 5, 27-39.

CHOWDHURY, K. A., PRESTON, R. D. & WHITE, R. K. 1967. Structural Changes in Some Ancient Indian Timbers. *Proceedings of the Royal Society Series B-Biological Sciences*, 168, 148.

CHRISTENSEN, M., FROSCH, M., JENSEN, P., SCHNELL, U., SHASHOUA, Y. & NIELSEN, O. F. 2006. Waterlogged archaeological wood—chemical changes by conservation and degradation. *Journal of Raman Spectroscopy*, 37, 1171-1178.

COLOM, X. & CARRILLO, F. 2002. Crystallinity changes in lyocell and viscose-type fibres by caustic treatment. *European Polymer Journal*, 38, 2225-2230.

COLOM, X., CARRILLO, F., NOGUES, F. & GARRIGA, P. 2003. Structural analysis of photodegraded wood by means of FTIR spectroscopy. *Polymer Degradation and Stability*, 80, 543-549.

CORTI, A., MUNIYASAMY, S., VITALI, M., IMAM, S. H. & CHIPELLINI, E. 2010. Oxidation and biodegradation of polyethylene films containing pro-oxidant additives: Synergistic effects of sunlight exposure, thermal aging and fungal biodegradation. *Polymer degradation and stability*, 95, 1106-1114.

CREWS, K. & MACKENZIE, C. Development Of Grading Rules For Re-Cycled Timber Used In Structural Applications. World Conference on Timber Engineering, 2008. WCTE.

CROLL, S. & SKAJA, A. 2003. Quantitative spectroscopy to determine the effects of photodegradation on a model polyester-urethane coating. *Journal of Coatings Technology*, 75, 85-94.

CROOK, F. M., NELSON, P. F. & SHARP, D. W. 1965. An Examination of Ancient Victorian Woods. *Holzforschung*, 19, 153.

DACKERMANN, U., CREWS, K., KASAL, B., LI, J., RIGGIO, M., RINN, F. & TANNERT, T. 2014. In situ assessment of structural timber using stress-wave measurements. *Materials and structures*, 47, 787-803.

DEPPE, H.-J. & RÜHL, H. 1993. Zur Beurteilung alter Bauhölzer. *Holz als Roh-und Werkstoff*, 51, 379-383.

DING, S. H. & DUAN, L. L. 2006. Accelerated aging and aging mechanism of acrylic sealant. *Polymer degradation stability*, 91, 1010-1016.

DINWOODIE, J. 1975. Timber — a review of the structure - mechanical property relationship. *Journal of Microscopy*, 104, 3-32.

DINWOODIE, J. 2002. *Timber: its nature and behaviour*, CRC Press.

DIROL, D. & GUYONNET, R. The improvement of wood durability by retification process. The international research group on wood preservation Section 4 Report prepared for the 24 Annual Meeting, 1993. 1-11.

DONETZHUBER, A. & SWAN, B. 1965. Chemical changes of wood extractives on chip seasoning. *Svensk Papperstidning*, 68, 419-429.

DWianto, W., TANAKA, F., INOUE, M. & NORIMOTO, M. 1996. Crystallinity changes of wood by heat or steam treatment. *Wood research : bulletin of the Wood Research Institute Kyoto University*, 1996, 47-49.

ERHARDT, D., MECKLENBURG, M. F., TUMOSA, C. S. & OLSTAD, T. M. New versus old wood: differences and similarities in physical, mechanical, and chemical properties. ICOM committee for conservation, 11th triennial meeting in Edinburgh, Scotland, 1-6 September 1996: Preprints, 1996. 903-910.

ESTEVEES, B., GRACA, J. & PEREIRA, H. 2008. Extractive composition and summative chemical analysis of thermally treated eucalypt wood. *Holzforschung*, 62, 344-351.

ESTEVEES, B., MARQUES, A. V., DOMINGOS, I. & PEREIRA, H. 2007. Influence of steam heating on the properties of pine (*Pinus pinaster*) and eucalypt (*Eucalyptus globulus*) wood. *Wood Science and Technology*, 41, 193-207.

ESTEVEES, B. & PEREIRA, H. 2008. Wood modification by heat treatment: a review. *BioResources*, 4, 370-404.

EVANS, P., MICHELL, A. & SCHMALZL, K. 1992. Studies of the degradation and protection of wood surfaces. *Wood Science and Technology*, 26, 151-163.

EVANS, R. & ELIC, J. 2001. Rapid prediction of wood stiffness from microfibril angle and density. *Forest products journal*, 51.

EVANS, R., ILIC, J. & MATHESON, C. Rapid estimation of solid wood stiffness using SilviScan. Proceedings of 26th Forest Products Research Conference: Research developments and industrial applications and Wood Waste Forum, Clayton, Victoria, Australia, 19-21 June 2000, 2000. CSIRO Forestry and Forest Products, 49-50.

FAIX, O. 1991. Classification of lignins from different botanical origins by FT-IR spectroscopy. *Holzforschung-International Journal of the Biology, Chemistry, Physics and Technology of Wood*, 45, 21-28.

FAIX, O., BREMER, J., SCHMIDT, O. & TATJANA, S. J. 1991. Monitoring of chemical changes in white-rot degraded beech wood by pyrolysis—gas chromatography and Fourier-transform infrared spectroscopy. *Journal of Analytical and Applied Pyrolysis*, 21, 147-162.

FALK, R. H., DEVISSER, D., COOK, S. & STANSBURY, D. 1999. Effect of damage on the grade yield of recycled lumber. *Forest products journal*, 49, 71.

FALK, R. H. & GREEN, D. Stress grading of recycled lumber and timber. Structural engineering in the 21st century: proceedings of the 1999 Structures Congress, April 18-21, 1999, New Orleans, Louisiana. Reston, VA: American Society of Civil Engineers, 1999.: p. 650-653: ill., 1999.

FEIO, A. & MACHADO, J. 2015. In-situ assessment of timber structural members: Combining information from visual strength grading and NDT/SDT methods—A review. *Construction Building Materials*, 101, 1157-1165.

FENGEL, D. 1991. Aging and Fossilization of Wood and Its Components. *Wood Science and Technology*, 25, 153-177.

FENGEL, D. & STÖCKLHUBER, P. 1985. Vergleich der Extrakte und des Lignins aus frischem und gelagertem Kiefernholz (*Pinus sylvestris* L.). *European Journal of Wood and Wood Products*, 43, 447-450.

FENGEL, D. & WEGENER, G. 1983. *Wood: chemistry, ultrastructure, reactions*, Walter de Gruyter.

FENGEL, D. & WEGENER, G. 1984. Wood: chemistry, ultrastructure. *Reactions*, 613, 1960-1982.

FENGEL, D. & WEGENER, G. 1988. Chemische Analysen von Fichtenholz nach 17jähriger Wasserlagerung. *Holz als Roh-und Werkstoff*, 46, 7-8.

FERRAZ, A., BAEZA, J., RODRIGUEZ, J. & FREER, J. 2000. Estimating the chemical composition of biodegraded pine and eucalyptus wood by DRIFT spectroscopy and multivariate analysis. *Bioresource Technology*, 74, 201-212.

FISCHER, K. & SCHMIDT, I. 1983. Changes of lignin during outside chip storage and their causes. *Cellulose chemistry technology*, 17, 387-394.

FISHER, K. & SCHMIDT, I. 1983. Changes of lignin during outside chip storage and their causes. *Cellulose chemistry and technology*, 17, 387-394.

FOLLRICH, J., MULLER, U. & GINDL, W. 2006. Effects of thermal modification on the adhesion between spruce wood (*Picea abies* Karst.) and a thermoplastic polymer. *Holz Als Roh-Und Werkstoff*, 64, 373-376.

FORSTHUBER, B. & GRÜLL, G. 2010. The effects of HALS in the prevention of photo-degradation of acrylic clear topcoats and wooden surfaces. *Polymer degradation and stability*, 95, 746-755.

FRIDLEY, K. J., MITCHELL, J. B., HUNT, M. O. & SENFT, J. F. 1996. Effect of 85 years of service of mechanical properties of timber roof members. Part 1. Experimental observations. *Forest products journal*, 46, 72.

FUFA, S. M., JELLE, B. P. & HOVDE, P. J. 2013. Durability, reaction to fire properties, and environmental impact of treated and untreated wooden claddings. *Wood Material Science & Engineering*, 8, 175-187.

FUNAOKA, M., KAKO, T. & ABE, I. 1990. Condensation of lignin during heating of wood. *Wood Science and Technology*, 24, 277-288.

GASPAR, F., GOMES, A. & CRUZ, H. Assessment of natural and artificial ageing of glued laminated timber-Core drilling, shear and delamination tests. World Conference on Timber Engineering, Italy, 2010.

GENESTAR, C. & PALOU, J. 2006. SEM–FTIR spectroscopic evaluation of deterioration in an historic coffered ceiling. *Analytical Bioanalytical Chemistry*, 384, 987.

GERHARDS, C. 2007. Effect of moisture content and temperature on the mechanical properties of wood: an analysis of immediate effects. *Wood and fiber science*, 14, 4-36.

GIERLINGER, N., JACQUES, D., GRABNER, M., WIMMER, R., SCHWANNINGER, M., ROZENBERG, P. & PAQUES, L. E. 2004. Colour of larch heartwood and relationships to extractives and brown-rot decay resistance. *Trees-Structure and Function*, 18, 102-108.

GORING, D. & TIMELL, T. 1962. Molecular weight of native celluloses. *Tappi*, 45, 454-460.

GOROYIAS, G. & HALE, M. 2002. Heat treatment of wood strands for OSB production: Effect on the mechanical properties, water absorption and dimensional stability. *International Research Group Wood Pre*, , Section 4-Processes.

GROSSER, D., FENGEL, D. & SELMEIER, A. 1974. Untersuchungen an alten und fossilen HölzernStudies on ancient and fossil woods. *Forstwissenschaftliches Centralblatt*, 93, 332-346.

GULLER, B. 2007. The effects of thinning treatments on density, MOE, MOR and maximum crushing strength of *Pinus brutia* Ten. wood. *Annals of Forest Science*, 64, 467-475.

GULMINE, J. & AKCELRUD, L. 2006. FTIR characterization of aged XLPE. *Polymer Testing*, 25, 932-942.

GUTIERREZ, A., DEL RIO, J. C., GONZALEZ-VILA, F. J. & ROMERO, J. 1998. Variation in the composition of wood extractives from *Eucalyptus globulus* during seasoning. *Journal of Wood Chemistry and Technology*, 18, 439-446.

HANDA, T., FUKUOKA, M., YOSHIZAWA, S. & KANAMOTO, T. 1982. The effect of moisture on the dielectric relaxations in wood. *Journal of Applied Polymer Science*, 27, 439-453.

HARRINGTON, J., ASTLEY, R. & BOOKER, R. 1998. Modelling the elastic properties of softwood. *Holz als Roh-und Werkstoff*, 56, 37-41.

HARRINGTON, K., HIGGINS, H. & MICHELL, A. 1964. Infrared spectra of *Eucalyptus regnans* F. Muell. and *Pinus radiata* D. Don. *Holzforschung-International Journal of the Biology, Chemistry, Physics and Technology of Wood*, 18, 108-113.

HAVIMO, M. 2009. A literature-based study on the loss tangent of wood in connection with mechanical pulping. *Wood science and technology*, 43, 627.

HAW, J. F. & SCHULTZ, T. P. 1985. Carbon-13 CP/MAS NMR and FT-IR study of low-temperature lignin pyrolysis. *Holzforschung-International Journal of the Biology, Chemistry, Physics and Technology of Wood*, 39, 289-296.

HEDGES, J. I., COWIE, G. L., ERTEL, J. R., BARBOUR, R. J. & HATCHER, P. G. 1985. Degradation of carbohydrates and lignins in buried woods. *Geochimica et Cosmochimica Acta*, 49, 701-711.

HEMMILÄ, V., ADAMOPOULOS, S., KARLSSON, O. & KUMAR, A. 2017. Development of sustainable bio-adhesives for engineered wood panels—A Review. *Rsc Advances*, 7, 38604-38630.

HIGGINS, H., STEWART, C. & HARRINGTON, K. 1961. Infrared spectra of cellulose and related polysaccharides. *Journal of polymer science*, 51, 59-84.

HIGUCHI, T. 2012. *Biochemistry and molecular biology of wood*, Springer Science & Business Media.

HILLIS, W. & ROZSA, A. 1978. The softening temperatures of wood. *Holzforschung-International Journal of the Biology, Chemistry, Physics Technology of Wood*, 32, 68-73.

HILLIS, W. E. 1984. High-Temperature and Chemical Effects on Wood Stability .1. General-Considerations. *Wood Science and Technology*, 18, 281-293.

HIRASHIMA, Y. 2005. Strength properties of aged wood III. Static and impact bending strength properties of aged keyaki and akamatsu woods. *Mokuzai gakkaiishi*, 51, 146-152.

HOFFMANN, P. & JONES, M. A. 1990a. Structure and degradation process for waterlogged archaeological wood. ACS Publications.

HOFFMANN, P. & JONES, M. A. 1990b. Structure and degradation process for waterlogged archaeological wood. *Structure degradation process for waterlogged archaeological wood*, 35-65.

HOFFMANN, P. & PARAMESWARAN, N. 1982. Chemische und ultrastrukturelle Untersuchungen an wassergesättigten Eichenholzern aus archäologischen Funden. *Berliner Beiträge zur Archäometrie*, 7, 273-285.

HORIE, H. 2002. Strength deterioration of recycled lumber collected from demolished wooden buildings in Hokkaido. *Mokuzai Gakkaishi*, 48, 280-287.

HORIKAWA, Y., HIRANO, S., MIHASHI, A., KOBAYASHI, Y., ZHAI, S. & SUGIYAMA, J. 2019. Prediction of Lignin Contents from Infrared Spectroscopy: Chemical Digestion and Lignin/Biomass Ratios of *Cryptomeria japonica*. *Applied biochemistry and biotechnology*, 1-11.

HUANG, C. L., LINDSTROM, H., NAKADA, R. & RALSTON, J. 2003. Cell wall structure and wood properties determined by acoustics - a selective review. *Holz Als Roh-Und Werkstoff*, 61, 321-335.

HUISMAN, D., MANDERS, M., KRETSCHMAR, E., KLAASSEN, R. & LAMERSDORF, N. 2008. Burial conditions and wood degradation at archaeological sites in the Netherlands. *International biodeterioration & biodegradation*, 61, 33-44.

HUMAR, M., BUČAR, B. & POHLEVEN, F. 2006. Brown-rot decay of copper-impregnated wood. *international biodeterioration & biodegradation*, 58, 9-14.

- IYAMA, K., KASUYA, N., LAM, T. B. T., NAKANO, J. & SAKAGUCHI, H. 1988. Chemical Characterization of Ancient Buried Wood. *Holzforschung*, 42, 5-10.
- ILLSTON, J. M., DINWOODIE, J. M. & SMITH, A. A. 1979. *Concrete, timber and metals. The nature and behaviour of structural materials*, Van Nostrand Reinhold Company Ltd.
- IMAMURA, T., WATANABE, T., KUWAHARA, M. & KOSHIJIMA, T. 1994. Ester linkages between lignin and glucuronic acid in lignin-carbohydrate complexes from *Fagus crenata*. *Phytochemistry*, 37, 1165-1173.
- INOUE, M., NORIMOTO, M., TANAHASHI, M. & ROWELL, R. M. 1993. Steam or Heat Fixation of Compressed Wood. *Wood and Fiber Science*, 25, 224-235.
- JÄMSÄ, S., AHOLA, P. & VIITANIEMI, P. 2000. Long-term natural weathering of coated ThermoWood. *Pigment & resin technology*, 29, 68-74.
- JÄMSÄ, S. & VIITANIEMI, P. Heat treatment of wood–Better durability without chemicals. Proceedings of special seminar held in Antibes, France, 2001.
- JELLE, B. P. 2012. Accelerated climate ageing of building materials, components and structures in the laboratory. *Journal of Materials Science*, 47, 6475-6496.
- JELLE, B. P. & NILSEN, T.-N. 2011. Comparison of accelerated climate ageing methods of polymer building materials by attenuated total reflectance Fourier transform infrared radiation spectroscopy. *Construction and Building Materials*, 25, 2122-2132.
- JELLINEK, H. 1983. Degradation and Stabilization of Polymers. I.(Retroactive Coverage). *Elsevier Science Publishers B. V, 1 Molenwerf, P. O. Box 211, 1000 AE Amsterdam. The Netherlands, 1983.*
- KAČÍK, F., ŠMÍRA, P., KAČÍKOVÁ, D., REINPRECHT, L. & NASSWETTROVA, A. 2014. Chemical changes in fir wood from old buildings due to ageing. *Cellulose chemistry and technology*, 48, 79-88.
- KAMDEM, D., PIZZI, A. & JERMANNAUD, A. 2002. Durability of heat-treated wood. *Holz als Roh-und Werkstoff*, 60, 1-6.
- KAMDEM, D., PIZZI, A. & TRIBOULOT, M. 2000. Heat-treated timber: potentially toxic byproducts presence and extent of wood cell wall degradation. *Holz als Roh-und Werkstoff*, 58, 253-257.

KÄRKÄS, M. D., MATSUURA, B. S., MONOS, T. M., MAGALLANES, G. & STEPHENSON, C. R. 2016. Transition-metal catalyzed valorization of lignin: the key to a sustainable carbon-neutral future. *Organic & biomolecular chemistry*, 14, 1853-1914.

KAWAMOTO, H., HORIGOSHI, S. & SAKA, S. 2007. Pyrolysis reactions of various lignin model dimers. *Journal of wood science*, 53, 168-174.

KEEGSTRA, K. & RAIKHEL, N. 2001. Plant glycosyltransferases. *Current opinion in plant biology*, 4, 219-224.

KELLEY, S. S., RIALS, T. G. & GLASSER, W. G. 1987. Relaxation behaviour of the amorphous components of wood. *Journal of materials science*, 22, 617-624.

KIM, G.-H. 1998. Effect of heat treatment on the decay resistance and the bending properties of radiata pine sapwood. *Material und Organismen*, 32, 101-108.

KIM, S. & KIM, H. J. 2003. Curing behavior and viscoelastic properties of pine and wattle tannin-based adhesives studied by dynamic mechanical thermal analysis and FT-IR-ATR spectroscopy. *Journal of Adhesion Science and Technology*, 17, 1369-1383.

KIM, Y.-S., BANG, J.-W., KIM, I.-J. & CHOI, K.-N. 1990. Chemical composition of archaeological woods submerged in the seawater. *Journal of the Korean Wood Science Technology*, 18, 3-7.

KOCAEFE, D., PONCSAK, S. & BOLUK, Y. 2008. Effect of Thermal Treatment on the Chemical Composition and Mechanical Properties of Birch and Aspen. *Bioresources*, 3, 517-537.

KOHARA 1955. Studies on the permanence of wood (X). *Journal of the Japanese Forestry Society*, 37, 63-66.

KOMOROWICZ, M., WRÓBLEWSKA, H., FOJUTOWSKI, A., KROPACZ, A., NOSKOWIAK, A. & POMIAN, I. 2018. The impact of 5 years' underwater exposure in the Baltic Sea (Puck Bay) on selected properties of English oak wood samples. *International biodeterioration & biodegradation*, 131, 40-50.

KONDO, T. 1997. The assignment of IR absorption bands due to free hydroxyl groups in cellulose. *Cellulose*, 4, 281.

KORKUT, S., AKGÜL, M. & DÜNDAR, T. 2008. The effects of heat treatment on some technological properties of Scots pine (*Pinus sylvestris* L.) wood. *BioResources*, 99, 1861-1868.

KOTILAINEN, R. A., TOIVANEN, T. J. & ALEN, R. J. 2000. FTIR monitoring of chemical changes in softwood during heating. *Journal of Wood Chemistry and Technology*, 20, 307-320.

KRÁNITZ, K. 2014. *Effect of natural aging on wood*. ETH Zurich.

KRÁNITZ, K., SONDEREGGER, W., BUES, C.-T. & NIEMZ, P. 2016. Effects of aging on wood: a literature review. *Wood science technology*, 50, 7-22.

KRETSCHMANN, D. E. & GREEN, D. W. 2007. Modeling moisture content-mechanical property relationships for clear southern pine. *Wood fiber science*, 28, 320-337.

KUBOJIMA, Y., OKANO, T. & OHTA, M. 1998. Vibrational properties of Sitka spruce heat-treated in nitrogen gas. *Journal of wood science*, 44, 73.

KUBOJIMA, Y., OKANO, T. & OHTA, M. 2000. Vibrational properties of heat-treated green wood. *Journal of wood science*, 46, 63-67.

LANDEL, R. F. & NIELSEN, L. E. 1993. *Mechanical properties of polymers and composites*, CRC press.

LAVERS, G. 1967. The strength properties of timber. Forest Products Res. *Bulletin of the Association for Preservation Technolog.*

LEICHTI, R. J., MEISENZAHN, M. & PARRY, D. 2005. Structural timbers from retired Douglas-fir utility poles. *Forest products journal*, 55, 61.

LI, J. & GELLERSTEDT, G. 2008. Improved lignin properties and reactivity by modifications in the autohydrolysis process of aspen wood. *Industrial Crops and Products*, 27, 175-181.

LIANG, C. & MARCHESSAULT, R. 1959. Infrared spectra of crystalline polysaccharides. II. Native celluloses in the region from 640 to 1700 cm.⁻¹. *Journal of Polymer Science*, 39, 269-278.

LIN, C.-J., YANG, T.-H., ZHANG, D.-Z., WANG, S.-Y. & LIN, F.-C. 2007. Changes in the dynamic modulus of elasticity and bending properties of railroad ties after 20 years of service in Taiwan. *Building environment*, 42, 1250-1256.

LIU, C., WU, S., ZHANG, H. & XIAO, R. 2019. Catalytic oxidation of lignin to valuable biomass-based platform chemicals: A review. *Fuel Processing Technology*, 191, 181-201.

LU, Z., CASSIDY, B. M., DEJONG, S. A., BELLIVEAU, R. G., MYRICK, M. L. & MORGAN, S. L. 2017. Attenuated Total Reflection (ATR) Sampling in Infrared Spectroscopy of Heterogeneous Materials Requires Reproducible Pressure Control. *Applied spectroscopy*, 71, 97-104.

ŁUCEJKO, J. J., ZBOROWSKA, M., MODUGNO, F., COLOMBINI, M. P. & PRĄDZYŃSKI, W. 2012. Analytical pyrolysis vs. classical wet chemical analysis to assess the decay of archaeological waterlogged wood. *Analytical Chimica Acta*, 745, 70-77.

MACLEOD, I. T., SCULLY, A. D., GHIGGINO, K. P., RITCHIE, P. J. A., PARAVAGNA, O. M. & LEARY, B. 1995. Photodegradation at the Wood-Clearcoat Interface. *Wood Science and Technology*, 29, 183-189.

MARCHESSAULT, R. 1962. Application of infra-red spectroscopy to cellulose and wood polysaccharides. *Pure and Applied Chemistry*, 5, 107-130.

MARCHESSAULT, R. & LIANG, C. 1962. The infrared spectra of crystalline polysaccharides. VIII. Xylans. *Journal of Polymer Science*, 59, 357-378.

MATSUO, M., YOKOYAMA, M., UMEMURA, K., GRIL, J., YANO, K. & KAWAI, S. 2010. Color changes in wood during heating: kinetic analysis by applying a time-temperature superposition method. *Applied Physics a-Materials Science & Processing*, 99, 47-52.

MATSUO, M., YOKOYAMA, M., UMEMURA, K., SUGIYAMA, J., KAWAI, S., GRIL, J., KUBODERA, S., MITSUTANI, T., OZAKI, H., SAKAMOTO, M. & IMAMURA, M. 2011. Aging of wood: Analysis of color changes during natural aging and heat treatment. *Holzforschung*, 65, 361-368.

MATSUO, M., YOKOYAMA, M., UMEMURA, K., SUGIYAMA, J., KAWAI, S., GRIL, J., YANO, K. I., KUBODERA, S., MITSUTANI, T. & OZAKI, H. Evaluation of the aging wood from historical buildings as compared with the accelerated aging wood and cellulose, Analysis of color properties. Proceedings of the International conference on wooden cultural heritage, Evaluation of deterioration and management of change, 2009.

MAZELA, B., ZAKRZEWSKI, R., GRZESKOWIAK, W., COFTA, G. & BARTKOWIAK, M. Preliminary research on the biological resistance of thermally modified wood. First European Conference on Wood Modification, 2003. 113-119.

MBURU, F., DUMARÇAY, S., BOCQUET, J. F., PETRISSANS, M. & GÉRARDIN, P. 2008. Effect of chemical modifications caused by heat treatment on mechanical properties of *Grevillea robusta* wood. *Polymer degradation and stability*, 93, 401-405.

MCCARTHY, C., BIRKINSHAW, C., PEMBROKE, J. & HALE, M. 1991. Dynamic mechanical analysis as a technique for the study of fungal degradation of wood. *BioTechnology Techniques*, 5, 493-496.

MCLEAN, J. P., JIN, G., BRENNAN, M., NIEUWOUTD, M. K. & HARRIS, P. J. 2014. Using NIR and ATR-FTIR spectroscopy to rapidly detect compression wood in *Pinus radiata*. *Canadian Journal of Forest Research-Revue Canadienne De Recherche Forestiere*, 44, 820-830.

METSA-KORTELAJINEN, S., ANTIKAINEN, T. & VIITANIEMI, P. 2006. The water absorption of sapwood and heartwood of Scots pine and Norway spruce heat-treated at 170 degrees C, 190 degrees C, 210 degrees C and 230 degrees C. *Holz Als Roh-Und Werkstoff*, 64, 192-197.

MISHNAEVSKY JR, L. & QING, H. 2008. Micromechanical modelling of mechanical behaviour and strength of wood: State-of-the-art review. *Computational Materials Science*, 44, 363-370.

MISSANJO, E. & MATSUMURA, J. 2016. Wood density and mechanical properties of *Pinus kesiya* Royle ex Gordon in Malawi. *Forests*, 7, 135.

MITCHELL, P. H. 1988. Irreversible property changes of small loblolly pine specimens heated in air, nitrogen, or oxygen. *Wood and Fiber Science*, 20, 320-335.

MOHEBBY, B. 2005. Attenuated total reflection infrared spectroscopy of white-rot decayed beech wood. *International biodeterioration & biodegradation*, 55, 247-251.

MONTES, H. & CAVAILLÉ, J. 1999. Secondary dielectric relaxations in dried amorphous cellulose and dextran. *Polymer*, 40, 2649-2657.

MÜLLER, G., SCHÖPPER, C., VOS, H., KHARAZIPOUR, A. & POLLE, A. 2009. FTIR-ATR spectroscopic analyses of changes in wood properties during particle-and fibreboard production of hard-and softwood trees. *BioResources*, 4, 49-71.

NAKAJIMA, S. & MURAKAMI, T. Comparison of two structural reuse options of two-by-four salvaged lumbers. Proceedings of the “WCTE 2010-World Conference on Timber Engineering”. Riva del Garda (Italy), 2010. 20-24.

NAKAMURA, T., KAWAMOTO, H. & SAKA, S. 2008. Pyrolysis behavior of Japanese cedar wood lignin studied with various model dimers. *Journal of Analytical and Applied Pyrolysis*, 81, 173-182.

NAKAO, T., TANAKA, C. & TAKAHASHI, A. 1989. Long-term changes in degree of crystallinity of wood cellulose. *Holzforschung*, 43, 419-420.

NARAYANAMURTI, D., GHOSH, S., PRASAD, B. & GEORGE, J. 1958. Note on examination of an old timber specimen. *Holz Als Roh-und Werkstoff*, 16, 245-247.

NAUMANN, A., NAVARRO-GONZÁLEZ, M., PEDDIREDDI, S., KÜES, U. & POLLE, A. 2005. Fourier transform infrared microscopy and imaging: detection of fungi in wood. *Fungal Genetics and Biology*, 42, 829-835.

NICHOLAS, D., SHI, J. & SCHULTZ, T. 2009. Evaluation of variables that influence dynamic MOE in wood decay studies. *The Int. Res. Group on Wood Preservation*.

NILSSON, T. & DANIEL, G. 1990. Structure and the aging process of dry archaeological wood. *Structure the aging process of dry archaeological wood.*, 67-86.

NILSSON, T. & ROWELL, R. 2012. Historical wood—structure and properties. *Journal of Cultural Heritage*, 13, S5-S9.

NOGUCHI, T., OBATAYA, E. & ANDO, K. 2012. Effects of aging on the vibrational properties of wood. *Journal of Cultural Heritage*, 13, S21-S25.

NUNES, L., NOBRE, T. & RAPP, A. 2004. Thermally modified wood in choice tests with subterranean termites. *COST E37, Reinbeck*.

NUOPPONEN, M., VUORINEN, T., JÄMSÄ, S. & VIITANIEMI, P. 2003. The effects of a heat treatment on the behaviour of extractives in softwood studied by FTIR spectroscopic methods. *Wood Science and Technology*, 37, 109-115.

NUOPPONEN, M., VUORINEN, T., JÄMSÄ, S. & VIITANIEMI, P. 2005. Thermal Modifications in Softwood Studied by FT-IR and UV Resonance Raman Spectroscopies. *Journal of wood chemistry and technology*, 24, 13-26.

- OBATAYA, E., NORIMOTO, M. & TOMITA, B. 2001. Mechanical relaxation processes of wood in the low-temperature range. *Journal of applied polymer science*, 81, 3338-3347.
- OHASHI, H., MATSUMIYA, I. & YASUE, M. 1988. Fluctuation of extractives in the withering process of *Cercidiphyllum japonicum* sapwood. *Research Bulletin of the Faculty of Agriculture-Gifu University*.
- OOKA, Y., TANAHASHI, H., IZUNO, K., SUZUKI, Y. & TOKI, K. Effects of Aged Wooden Members on Seismic Performance of Old Traditional Wooden Structures. World Conference of Earthquake Engineering, 2012.
- ORMONDROYD, G. A., ALFREDSEN, G., PRABHAKARAN, R. T. D., CURLING, S. F., STEFANOWSKI, B. K., SPEAR, M. J. & GOBAKKEN, L. R. 2017. Assessment of the use of dynamic mechanical analysis to investigate initial onset of brown rot decay of Scots pine (*Pinus sylvestris* L.). *International Biodeterioration & Biodegradation*, 120, 1-5.
- OSBORNE, B. G., FEARN, T. & HINDLE, P. H. 1993. *Practical NIR spectroscopy with applications in food and beverage analysis*, Longman scientific and technical.
- PAN, D. R., TAI, D. S., CHEN, C. L. & ROBERT, D. 1990. Comparative-Studies on Chemical-Composition of Wood Components in Recent and Ancient Woods of *Bischofia-Polycarpa*. *Holzforschung*, 44, 7-16.
- PANDEY, K. K. 1999. A study of chemical structure of soft and hardwood and wood polymers by FTIR spectroscopy. *Journal of Applied Polymer Science*, 71, 1969-1975.
- PANDEY, K. K. 2005. Study of the effect of photo-irradiation on the surface chemistry of wood. *Polymer degradation and stability*, 90, 9-20.
- PANDEY, K. K. & PITMAN, A. J. 2003. FTIR studies of the changes in wood chemistry following decay by brown-rot and white-rot fungi. *International Biodeterioration & Biodegradation*, 52, 151-160.
- PANDEY, K. K. & VUORINEN, T. 2008. Comparative study of photodegradation of wood by a UV laser and a xenon light source. *Polymer degradation and stability*, 93, 2138-2146.
- PARKER, F. S. 1983. *Applications of infrared, Raman, and resonance Raman spectroscopy in biochemistry*, Springer Science & Business Media.

PASSIALIS, C. N. 1997. Physico-chemical characteristics of waterlogged archaeological wood. *Holzforschung*, 51, 111-113.

PATWARDHAN, P. R., BROWN, R. C. & SHANKS, B. H. 2011. Product distribution from the fast pyrolysis of hemicellulose. *ChemSusChem*, 4, 636-643.

PÉTRISSANS, M., GÉRARDIN, P. & SERRAJ, M. 2003. Wettability of heat-treated wood. *Holzforschung*, 57, 301-307.

PLOMION, C., LEPROVOST, G. & STOKES, A. 2001. Wood formation in trees. *Plant Physiol*, 127, 1513-23.

PONCSAK, S., KOCAEFE, D., BOUAZARA, M. & PICHETTE, A. 2006. Effect of high temperature treatment on the mechanical properties of birch (*Betula papyrifera*). *Wood Science and Technology*, 40, 647-663.

QING, H. & MISHNAEVSKY JR, L. 2009. 3D hierarchical computational model of wood as a cellular material with fibril reinforced, heterogeneous multiple layers. *Mechanics of Materials*, 41, 1034-1049.

RAMAGE, M. H., BURRIDGE, H., BUSSE-WICHER, M., FEREDAY, G., REYNOLDS, T., SHAH, D. U., WU, G., YU, L., FLEMING, P. & DENSLEY-TINGLEY, D. 2017. The wood from the trees: The use of timber in construction. *Renewable Sustainable Energy Reviews*, 68, 333-359.

RAMMER, D. R. Evaluation of recycled timber members. *Materials and construction: exploring the connection: proceedings of the Fifth ASCE Materials Engineering Congress*, May 10-12, 1999, Cincinnati, Ohio. Reston, VA: American Society of Civil Engineers, 1999.: p. 46-51: ill., 1999.

RANA, R., LANGENFELD-HEYSER, R., FINKELDEY, R. & POLLE, A. 2010. FTIR spectroscopy, chemical and histochemical characterisation of wood and lignin of five tropical timber wood species of the family of Dipterocarpaceae. *Wood Science and Technology*, 44, 225-242.

RAPP, A. O. & SAILER, M. Heat treatment of wood in Germany-state of the art. *Proceedings of the seminar on production of heat treated wood in Europe*, 2000. 2000.

REIAN, G. & JOTUN, A. Optimization of Curing Conditions for a Chemical Resistant Tank Coating with the Help of Dynamic Mechanical Analysis.

REITERER, A., SINN, G. & STANZL-TSCHEGG 2002. Fracture characteristics of different wood species under mode I loading perpendicular to the grain. *Materials Science Engineering: A*, 332, 29-36.

ROBINSON, N., EVERSLED, R. P., HIGGS, W. J., JERMAN, K. & EGLINTON, G. 1987. Proof of a pine wood origin for pitch from Tudor (Mary Rose) and Etruscan shipwrecks: application of analytical organic chemistry in archaeology. *Analyst*, 112, 637-644.

ROSELEY, A. S., ROJO, E., ANSELL, M. P. & SMEDLEY, D. 2011. Creep response of thixotropic ambient temperature cure adhesives measured by DMTA in static tension and shear. *International Journal of Adhesion & Adhesives*, 31, 575-582.

ROSS, R. J., PELLERIN, R. F., VOLNY, N., SALSIG, W. W. & FALK, R. H. 1999. Inspection of timber bridges using stress wave timing nondestructive evaluation tools: a guide for use and interpretation. (*General technical report FPL; GTR-114*): 15 p., 114.

ROWELL, R. M., IBACH, R. E., MCSWEENEY, J. & NILSSON, T. 2009. Understanding decay resistance, dimensional stability and strength changes in heat-treated and acetylated wood. *Wood material science and engineering*, 4, 14-22.

RUG, W. & SEEMANN, A. 1991. Strength of old timber: test cores from 50–400 year old timber indicates strength of old timbers corresponds to that of new. *Building research information*, 19, 31-37.

RUSCHE, H. 1973. THERMAL-DEGRADATION OF WOOD AT TEMPERATURES UP TO 200 DEGREES C. 1. STRENGTH PROPERTIES OF DRIED WOOD AFTER HEAT-TREATMENT. *Holz als Roh-und Werkstoff*, 31, 273-281.

SAITO, Y., SHIDA, S., OHTA, M., YAMAMOTO, H., TAI, T. & GOTO, O. Deterioration of rafter in historic building of fukushoji-temple. 10th World Conference on Timber Engineering, Miyazaki, 2008a.

SAITO, Y., SHIDA, S., OHTA, M., YAMAMOTO, H., TAI, T., OHMURA, W., MAKIHARA, H., NOSHIRO, S. & GOTO, O. 2008b. Deterioration character of aged timbers: Insect damage and material aging of rafters in a historic building of Fukushoji-temple [Wakayama, Japan]. *Journal of the Japan Wood Research Society*.

SANDAK, A., SANDAK, J., ZBOROWSKA, M. & PRĄDZYŃSKI, W. 2010. Near infrared spectroscopy as a tool for archaeological wood characterization. *Journal of Archaeological Science*, 37, 2093-2101.

SANDBERG, D., HALLER, P. & NAVI, P. 2013. Thermo-hydro and thermo-hydro-mechanical wood processing: An opportunity for future environmentally friendly wood products. *Wood Material Science & Engineering*, 8, 64-88.

SANTOS, J. A. 2000. Mechanical behaviour of Eucalyptus wood modified by heat. *Wood Science and Technology*, 34, 39-43.

SARKANEN, K. V. & LUDWIG, C. H. 1971. *Lignins. Occurrence, formation, structure, and reactions*.

SCANDOLA, M. & CECCORULLI, G. 1985. Viscoelastic properties of cellulose derivatives: 1. Cellulose acetate. *Polymer*, 26, 1953-1957.

SCHNABEL, W. 1981. *Polymer degradation: principles and practical applications*, Hanser Munich.

SCHNIEWIND, A. P. 1989. *Wood & Wood Based Materials*, Pergamon Press, Oxford.

SCHULTZ, T. P., TEMPLETON, M. C. & MCGINNIS, G. D. 1985. Rapid-Determination of Lignocellulose by Diffuse Reflectance Fourier-Transform Infrared Spectrometry. *Analytical Chemistry*, 57, 2867-2869.

SCHWANNINGER, M., HINTERSTOISSER, B., GIERLINGER, N., WIMMER, R. & HANGER, J. 2004. Application of Fourier transform near infrared Spectroscopy (FT-NIR) to thermally modified wood. *Holz Als Roh-Und Werkstoff*, 62, 483-485.

SCOTT, G. 1969. Degradation and Stabilization of Polymers. *European Polymer Journal*, 5, 189.

SEIFERT, K. 1960. Zur frage der cellulose-schnellbestimmung nach der acetylaceton-methode. *Das papier*, 14, 104-106.

SERNEK, M., BOONSTRA, M., PIZZI, A., DESPRES, A. & GERARDIN, P. 2008. Bonding performance of heat treated wood with structural adhesives. *Holz Als Roh-Und Werkstoff*, 66, 173-180.

SHEVCHENKO, S. M., BEATSON, R. P. & SADDLER, J. N. 1999. The nature of lignin from steam explosion/ enzymatic hydrolysis of softwood: structural features and possible uses: scientific note. *Appl Biochem Biotechnol*, 77-79, 867-76.

- SHI, J. L., KOCAEFE, D. & ZHANG, J. 2007. Mechanical behaviour of Québec wood species heat-treated using ThermoWood process. *Holz als Roh-und Werkstoff*, 65, 255-259.
- SHIDA, S. & SAITO, Y. 2007. Effects of heat treatment on brittleness of *Styrax tonkinensis* wood. *Journal of Wood Science*, 53, 181-186.
- SIESLER, H. W., OZAKI, Y., KAWATA, S. & HEISE, H. M. 2008. *Near-infrared spectroscopy: principles, instruments, applications*, John Wiley & Sons.
- SIVONEN, H., MAUNU, S. L., SUNDHOLM, F., JAMSA, S. & VIITANIEMI, P. 2002. Magnetic resonance studies of thermally modified wood. *Holzforschung*, 56, 648-654.
- SMITH, M. J. 2012. *An investigation into the strength properties of reclaimed timber joists*. Northumbria University.
- SPRAGG, R. 2011. Contact and Orientation Effects in FT-IR ATR Spectra. *Solutions for Materials Analysis*, 26.
- SQUIRRELL, J. & CLARKE, R. 1987. An investigation into the condition and conservation of the hull of the Mary Rose. Part I: assessment of the hull timbers. *Studies in conservation*, 32, 153-162.
- STACCIOLI, G. & TAMBURINI, U. 1988. Sedimentary pyrite in a buried gymnosperm. *European Journal of Wood Products*, 46, 436-436.
- STAMM, A. J. 1956. Thermal Degradation of Wood and Cellulose. *Industrial and Engineering Chemistry*, 48, 413-417.
- STARK, N. M. & MATUANA, L. 2004. Surface chemistry changes of weathered HDPE/wood-flour composites studied by XPS and FTIR spectroscopy. *Polymer degradation and stability*, 86, 1-9.
- STEINER, T. 2002. The hydrogen bond in the solid state. *Angewandte Chemie International Edition*, 41, 48-76.
- SUBRAMANIAN, R. & HOFMANN, R. 1983. Study of the kinetics of in situ polymerization in wood by dynamic mechanical measurements. *Journal of Polymer Science: Polymer Letters Edition*, 21, 105-109.

SUDIYANI, Y., IMAMURA, Y., DOI, S. & YAMAUCHI, S. 2003. Infrared spectroscopic investigations of weathering effects on the surface of tropical wood. *Journal of wood science*, 49, 0086-0092.

SUGIYAMA, M., OBATAYA, E. & NORIMOTO, M. 1998. Viscoelastic properties of the matrix substance of chemically treated wood. *Journal of Materials Science*, 33, 3505-3510.

SUN, N., DAS, S. & FRAZIER, C. E. 2007. Dynamic mechanical analysis of dry wood: Linear viscoelastic response region and effects of minor moisture changes. *Holzforschung*, 61, 28-33.

SUNDQVIST, B., KARLSSON, O. & WESTERMARK, U. 2006. Determination of formic-acid and acetic acid concentrations formed during hydrothermal treatment of birch wood and its relation to colour, strength and hardness. *Wood Science and Technology*, 40, 549-561.

SUNDQVIST, B. & MORÉN, T. 2002. The influence of wood polymers and extractives on wood colour induced by hydrothermal treatment. *European Journal of Wood Products*, 60, 375-376.

TAGER, A. 1972. *Physical chemistry of polymers*, Mir Publishers.

TAMBURINI, D., ŁUCEJKO, J. J., PIZZO, B., MOHAMMED, M. Y., SLOGGETT, R. & COLOMBINI, M. P. 2017. A critical evaluation of the degradation state of dry archaeological wood from Egypt by SEM, ATR-FTIR, wet chemical analysis and Py (HMDS)-GC-MS. *Polymer degradation and stability*, 146, 140-154.

TAMBURINI, D., ŁUCEJKO, J. J., ZBOROWSKA, M., MODUGNO, F., PRĄDZYŃSKI, W. & COLOMBINI, M. P. 2015. Archaeological wood degradation at the site of Biskupin (Poland): wet chemical analysis and evaluation of specific Py-GC/MS profiles. *Journal of Analytical and Applied Pyrolysis*, 115, 7-15.

THYGESEN, A., ODDERSHEDE, J., LILHOLT, H., THOMSEN, A. B. & STÅHL, K. 2005. On the determination of crystallinity and cellulose content in plant fibres. *Cellulose*, 12, 563.

TIEMANN, H. 1920. Effect of different methods of drying on the strength and hygroscopicity of wood. *The kiln drying of lumber*, 256-264.

- TJEERDSMA, B. F., BOONSTRA, M., PIZZI, A., TEKELY, P. & MILITZ, H. 1998. Characterisation of thermally modified wood: molecular reasons for wood performance improvement. *Holz Als Roh-Und Werkstoff*, 56, 149-153.
- TJEERDSMA, B. F. & MILITZ, H. 2005. Chemical changes in hydrothermal treated wood: FTIR analysis of combined hydrothermal and dry heat-treated wood. *Holz Als Roh-Und Werkstoff*, 63, 102-111.
- TOBOLSKY, A. & EYRING, H. 1943. Mechanical properties of polymeric materials. *Journal of Chemical Physics*, 11, 125-134.
- TOBOLSKY, A. V. & MARK, H. F. 1971. *Polymer science and materials*, John Wiley & Sons.
- TSUCHIKAWA, S. & SIESLER, H. 2003. Near-infrared spectroscopic monitoring of the diffusion process of deuterium-labeled molecules in wood. Part I: Softwood. *Applied spectroscopy*, 57, 667-674.
- TSUCHIKAWA, S., YONENOBU, H. & SIESLER, H. 2005. Near-infrared spectroscopic observation of the ageing process in archaeological wood using a deuterium exchange method. *Analyst*, 130, 379-384.
- UNSAI, O. & AYRILMIS, N. 2005. Variations in compression strength and surface roughness of heat-treated Turkish river red gum (*Eucalyptus camaldulensis*) wood. *Journal of Wood Science*, 51, 405-409.
- VAN BERGEN, P. F., POOLE, I., OGILVIE, T. M., CAPLE, C. & EVERSLED, R. P. 2000. Evidence for demethylation of syringyl moieties in archaeological wood using pyrolysis - gas chromatography/mass spectrometry. *Rapid Communications in Mass Spectrometry*, 14, 71-79.
- VAN KREVELEN, D. W. & TE NIJENHUIS, K. 2009. *Properties of polymers: their correlation with chemical structure; their numerical estimation and prediction from additive group contributions*, Elsevier.
- VARGA, D. & VAN DER ZEE, M. E. 2008. Influence of steaming on selected wood properties of four hardwood species. *Holz Als Roh-Und Werkstoff*, 66, 11-18.
- WACEK, A. V. & SCHROTH, D. 1950. The lignin-carbohydrate bond. *Papier, Darmstadt*, 4, 410-4.

WANG, X., DIVOS, F., PILON, C., BRASHAW, B. K., ROSS, R. J. & PELLERIN, R. F. 2004. Assessment of decay in standing timber using stress wave timing nondestructive evaluation tools: A guide for use and interpretation. *Gen. Tech. Rep. FPL-GTR-147*. Madison, WI: US Department of Agriculture, Forest Service, Forest Products Laboratory, 2004. 12 pages, 147.

WARD, I. M. & SWEENEY, J. 2012. *Mechanical properties of solid polymers*, John Wiley & Sons.

WATANABE, T., OHNISHI, J., YAMASAKI, Y., KAIZU, S. & KOSHIJIMA, T. 1989. Binding-site analysis of the ether linkages between lignin and hemicelluloses in lignin-carbohydrate complexes by DDQ-oxidation. *Agricultural and biological chemistry*, 53, 2233-2252.

WĘGIEL, A., BEMBENEK, M., ŁACKA, A. & MEDERSKI, P. S. 2018. Relationship between stand density and value of timber assortments: a case study for Scots pine stands in north-western Poland. *New Zealand Journal of Forestry Science*, 48, 12.

WEILAND, J. J. & GUYONNET, R. 2003. Study of chemical modifications and fungi degradation of thermally modified wood using DRIFT spectroscopy. *Holz Als Roh-Und Werkstoff*, 61, 216-220.

WETTON, R. E., MARSH, R. D. L. & VANDEVELDE, J. G. 1991. Theory and Application of Dynamic Mechanical Thermal-Analysis. *Thermochimica Acta*, 175, 1-11.

WIKBERG, H. & MAUNU, S. L. 2004. Characterisation of thermally modified hard- and softwoods by C-13 CPMAS NMR. *Carbohydrate Polymers*, 58, 461-466.

WINANDY, J. & ROWELL, R. 1984. The chemistry of wood strength. *Advances in chemistry series*.

WINANDY, J. E. & LEBOW, P. K. 1996. Kinetic models for thermal degradation of strength of fire-retardant-treated wood. *Wood and Fiber Science*.

WINANDY, J. E. & LEBOW, P. K. 2001. Modeling strength loss in wood by chemical composition. Part I. An individual component model for southern pine. *Wood and Fiber Science*, 33, 239-254.

WINDEISEN, E., STROBEL, C. & WEGENER, G. 2007. Chemical changes during the production of thermo-treated beech wood. *Wood Science and Technology*, 41, 523-536.

WOCHNOWSKI, C., ELDIN, M. S. & METEV, S. 2005. UV-laser-assisted degradation of poly (methyl methacrylate). *Polymer degradation and stability*, 89, 252-264.

XIA, Y., CHEN, T.-Y., WEN, J.-L., ZHAO, Y.-L., QIU, J. & SUN, R.-C. 2018. Multi-analysis of chemical transformations of lignin macromolecules from waterlogged archaeological wood. *International Journal of Biological Macromolecules*, 109, 407-416.

YAMAUCHI, S., SUDIYANI, Y., IMAMURA, Y. & DOI, S. 2004. Depth profiling of weathered tropical wood using Fourier transform infrared photoacoustic spectroscopy. *Journal of Wood Science*, 50, 433-438.

YANG, H. P., YAN, R., CHEN, H. P., LEE, D. H. & ZHENG, C. G. 2007. Characteristics of hemicellulose, cellulose and lignin pyrolysis. *Fuel*, 86, 1781-1788.

YANG, J. L. & EVANS, R. 2003. Prediction of MOE of eucalypt wood from microfibril angle and density. *Holz als Roh- und Werkstoff*, 61, 449-452.

YILDIZ, S., GEZER, E. D. & YILDIZ, U. C. 2006. Mechanical and chemical behavior of spruce wood modified by heat. *Building and Environment*, 41, 1762-1766.

YOKOYAMA, M., GRIL, J., MATSUO, M., YANO, H., SUGIYAMA, J., CLAIR, B., KUBODERA, S., MISTUTANI, T., SAKAMOTO, M., OZAKI, H., IMAMURA, M. & KAWAI, S. 2009. Mechanical characteristics of aged Hinoki wood from Japanese historical buildings. *Comptes Rendus Physique*, 10, 601-611.

YONENOBU, H. & TSUCHIKAWA, S. 2003. Near-infrared spectroscopic comparison of antique and modern wood. *Applied spectroscopy*, 57, 1451-1453.

ZAMAN, A., ALEN, R. & KOTILAINEN, R. 2000. Thermal behavior of scots pine (*Pinus sylvestris*) and silver birch (*Betula pendula*) at 200-230 degrees C. *Wood and Fiber Science*, 32, 138-143.

ZHOU, X., LI, W., MABON, R. & BROADBELT, L. J. 2016. A Critical Review on Hemicellulose Pyrolysis. *Energy Technology*.

ZOIA, L., SALANTI, A. & ORLANDI, M. 2015. Chemical characterization of archaeological wood: Softwood Vasa and hardwood Riksapplet case studies. *Journal of Cultural Heritage*, 16, 428-437.

Appendix I C₁₄ Identification Report



BETA ANALYTIC INC.

DR. M.A. TAMERS and MR. D.G. HOOD

4985 S.W. 74 COURT
 MIAMI, FLORIDA, USA 33155
 PH: 305-667-5167 FAX:305-663-0964
 beta@radiocarbon.com

REPORT OF RADIOCARBON DATING ANALYSES

Mr. Qiushi Peng

Report Date: 7/3/2015

University of Bath

Material Received: 6/25/2015

Sample Data	Measured Radiocarbon Age	d13C	Conventional Radiocarbon Age(*)
Beta - 413712 SAMPLE : Sample-1 ANALYSIS : AMS-Standard delivery MATERIAL/PRETREATMENT : (wood): acid/alkali/acid 2 SIGMA CALIBRATION : Cal AD 1305 to 1365 (Cal BP 645 to 585) and Cal AD 1385 to 1420 (Cal BP 565 to 530)	580 +/- 30 BP	-25.7 ‰	570 +/- 30 BP

Dates are reported as RCYBP (radiocarbon years before present, "present" = AD 1950). By international convention, the modern reference standard was 95% the ¹⁴C activity of the National Institute of Standards and Technology (NIST) Oxalic Acid (SRM 4990C) and calculated using the Libby ¹⁴C half-life (5568 years). Quoted errors represent 1 relative standard deviation statistics (68% probability) counting errors based on the combined measurements of the sample, background, and modern reference standards. Measured ¹³C/¹²C ratios (delta ¹³C) were calculated relative to the PDB-1 standard.

The Conventional Radiocarbon Age represents the Measured Radiocarbon Age corrected for isotopic fractionation, calculated using the delta ¹³C. On rare occasion where the Conventional Radiocarbon Age was calculated using an assumed delta ¹³C, the ratio and the Conventional Radiocarbon Age will be followed by ***. The Conventional Radiocarbon Age is not calendar calibrated. When available, the Calendar Calibrated result is calculated from the Conventional Radiocarbon Age and is listed as the "Two Sigma Calibrated Result" for each sample.

CALIBRATION OF RADIOCARBON AGE TO CALENDAR YEARS

(Variables: C13/C12 = -25.7 ‰; lab. mult = 1)

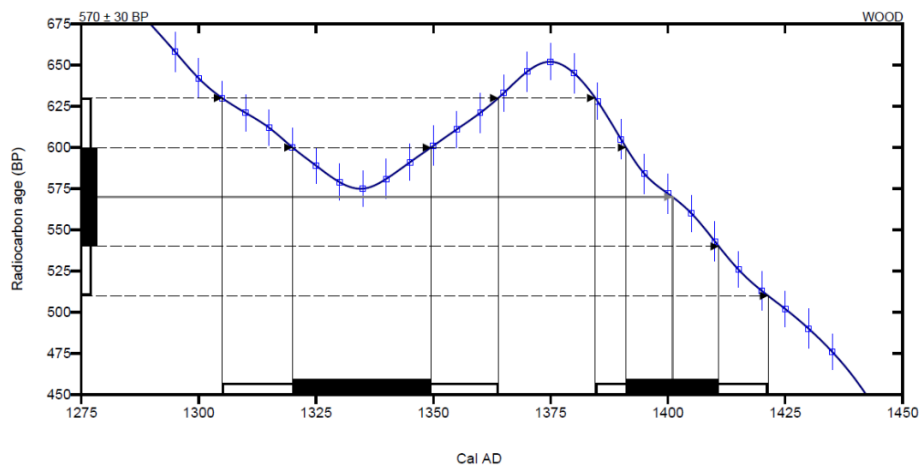
Laboratory number **Beta-413712**

Conventional radiocarbon age **570 ± 30 BP**

Calibrated Result (95% Probability) **Cal AD 1305 to 1365 (Cal BP 645 to 585)**
Cal AD 1385 to 1420 (Cal BP 565 to 530)

Intercept of radiocarbon age with calibration curve **Cal AD 1400 (Cal BP 550)**

Calibrated Result (68% Probability) **Cal AD 1320 to 1350 (Cal BP 630 to 600)**
Cal AD 1390 to 1410 (Cal BP 560 to 540)



Database used
INTCAL13

References

Mathematics used for calibration scenario

A Simplified Approach to Calibrating C14 Dates, Talma, A. S., Vogel, J. C., 1993, Radiocarbon 35(2):317-322

References to INTCAL13 database

Reimer PJ et al. IntCal13 and Marine13 radiocarbon age calibration curves 0–50,000 years cal BP. Radiocarbon 55(4):1869–1887, 2013.

Beta Analytic Radiocarbon Dating Laboratory

4985 S.W. 74th Court, Miami, Florida 33155 • Tel: (305)667-5167 • Fax: (305)663-0964 • Email: beta@radiocarbon.com

Appendix II Regression Models

Bending MOR Nonlinear Curve Fitting by Origin

MOR (σ_1) regression model Curve Fitting by Origin Pro

Nonlinear Curve Fit (NewFunction10 (User)) (15/06/2019 17:00:41)

Notes

Description	Nonlinear Curve Fit
User Name	pqshe
Operation Time	15/06/2019 17:00:41
Iteration Algorithm	Levenberg Marquardt
Model	NewFunction10 (User)
Number of Parameters	2
Number of Derived Parameters	0
Number of Datasets	1
Equation	$a \cdot x^1 \cdot (\ln(x^2) + b)$
Report Status	New Analysis Report
Data Filter	No

Input Data

Dep/Indep	Data	Range	Weight Type
x1 Indep	[alloldneweach]"all oldnew each"IA	[1*:637*]	No Weighting
B x2 Indep	[alloldneweach]"all oldnew each"IC	[1*:637*]	No Weighting
y Dep	[alloldneweach]"all oldnew each"IB	[1*:637*]	Statistical

Parameters

	Value	Standard Error	t-Value	Prob> t	Dependency
B a	22.85425	0.53783	42.49374	8.11695E-188	0.96446
b	6.71716	0.15168	44.28459	2.47369E-196	0.96446

Reduced Chi-sqr = 0.720446493025

COD(R²) = 0.81768863540181

Iterations Performed = 20

Total Iterations in Session = 20

Fit converged. Chi-Sqr tolerance value of 1E-9 was reached.

Standard Error was scaled with square root of reduced Chi-Sqr.

Statistics

	B
Number of Points	637
Degrees of Freedom	635
Reduced Chi-Sqr	0.72045
Residual Sum of Squares	457.48352
R-Square (COD)	0.81769
Adj. R-Square	0.8174
Fit Status	Succeeded(100)

Fit Status Code :

100 : Fit converged. Chi-Sqr tolerance value of 1E-9 was reached

Summary

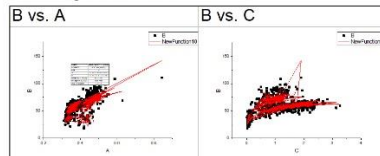
	a		b		Statistics	
	Value	Standard Error	Value	Standard Error	Reduced Chi-Sqr	Adj. R-Square
B	22.85425	0.53783	6.71716	0.15168	0.72045	0.8174

ANOVA

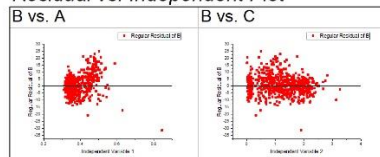
	DF	Sum of Squares	Mean Square	F Value	Prob>F
Regression	2	36606.01124	18303.00562	25405.0867	0
Residual	635	457.48352	0.72045		
Uncorrected Total	637	37063.49476			
Corrected Total	636	2509.35274			

At the 0.05 level, the fitting function is significantly better than the function y=0.

Fitted Curves Plot



Residual vs. Independent Plot



MOR (σ_2) regression model Curve Fitting by Origin Pro

Nonlinear Curve Fit (NewFunction10 (User)) (15/06/2019 17:06:32)

Notes

Description	Nonlinear Curve Fit
User Name	pqshe
Operation Time	15/06/2019 17:06:32
Iteration Algorithm	Levenberg Marquardt
Model	NewFunction10 (User)
Number of Parameters	2
Number of Derived Parameters	0
Number of Datasets	1
Equation	$a*x1*(\ln(x2)+b)$
Report Status	New Analysis Report
Data Filter	No

Input Data

	Dep/Indep	Data	Range	Weight Type
x1	Indep	[alloldneweac1]"all oldnew each"!A	[1*:637*]	No Weighting
B x2	Indep	[alloldneweac1]"all oldnew each"!D	[1*:637*]	No Weighting
y	Dep	[alloldneweac1]"all oldnew each"!B	[1*:637*]	Statistical

Parameters

	Value	Standard Error	t-Value	Prob> t	Dependency
B a	24.75646	0.61681	40.13615	2.43128E-176	0.96551
b	6.70748	0.14817	45.26824	6.1661E-201	0.96551

Reduced Chi-sqr = 0.782937173343
 COD(R²) = 0.80187516234902
 Iterations Performed = 27
 Total Iterations in Session = 27

Fit converged. Chi-Sqr tolerance value of 1E-9 was reached.
 Standard Error was scaled with square root of reduced Chi-Sqr.

Statistics

	B
Number of Points	637
Degrees of Freedom	635
Reduced Chi-Sqr	0.78294
Residual Sum of Squares	497.16511
R-Square (COD)	0.80188
Adj. R-Square	0.80156
Fit Status	Succeeded(100)

Fit Status Code :
 100 : Fit converged. Chi-Sqr tolerance value of 1E-9 was reached.

Summary

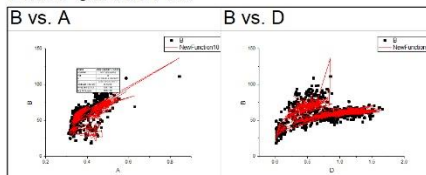
	a		b		Statistics	
	Value	Standard Error	Value	Standard Error	Reduced Chi-Sqr	Adj. R-Square
B	24.75646	0.61681	6.70748	0.14817	0.78294	0.80156

ANOVA

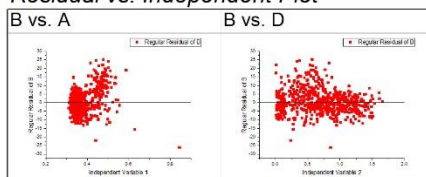
		DF	Sum of Squares	Mean Square	F Value	Prob>F
B	Regression	2	36566.32965	18283.16483	23352.02038	0
	Residual	635	497.16511	0.78294		
	Uncorrected Total	637	37063.49476			
	Corrected Total	636	2509.35274			

At the 0.05 level, the fitting function is significantly better than the function y=0.

Fitted Curves Plot



Residual vs. Independent Plot



MOR (σ_3) regression model Curve Fitting by Origin Pro

Nonlinear Curve Fit (NewFunction10 (User)) (15/06/2019 17:11:07)

Notes

Description	Nonlinear Curve Fit
User Name	pqshe
Operation Time	15/06/2019 17:11:07
Iteration Algorithm	Levenberg Marquardt
Model	NewFunction10 (User)
Number of Parameters	2
Number of Derived Parameters	0
Number of Datasets	1
Equation	$a*x1*(\ln(x2)+b)$
Report Status	New Analysis Report
Data Filter	No

Input Data

Dep/Indep	Data	Range	Weight Type
x1 Indep	[alloldneweac2]"all oldnew each"!A	[1*:637*]	No Weighting
B x2 Indep	[alloldneweac2]"all oldnew each"!E	[1*:637*]	No Weighting
y Dep	[alloldneweac2]"all oldnew each"!B	[1*:637*]	Statistical

Parameters

	Value	Standard Error	t-Value	Prob> t	Dependency
B a	23.84291	0.5578	42.74418	5.10467E-189	0.96436
b	5.90796	0.14455	40.87195	5.91314E-180	0.96436

Reduced Chi-sqr = 0.714199906615
 COD(R^2) = 0.81926935472442
 Iterations Performed = 20
 Total Iterations in Session = 20

Fit converged. Chi-Sqr tolerance value of 1E-9 was reached.
 Standard Error was scaled with square root of reduced Chi-Sqr.

Statistics

	B
Number of Points	637
Degrees of Freedom	635
Reduced Chi-Sqr	0.7142
Residual Sum of Squares	453.51694
R-Square (COD)	0.81927
Adj. R-Square	0.81898
Fit Status	Succeeded(100)

Fit Status Code :
 100 : Fit converged. Chi-Sqr tolerance value of 1E-9 was reached

Summary

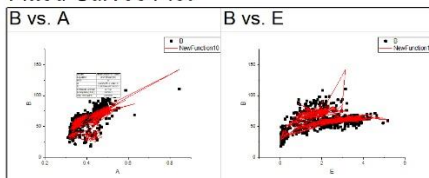
	a		b		Statistics	
	Value	Standard Error	Value	Standard Error	Reduced Chi-Sqr	Adj. R-Square
B	23.84291	0.5578	5.90796	0.14455	0.7142	0.81898

ANOVA

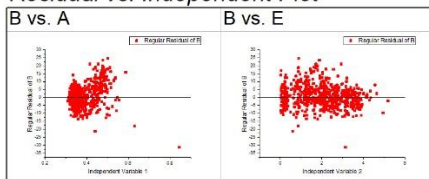
	DF	Sum of Squares	Mean Square	F Value	Prob>F
Regression	2	36609.97782	18304.98891	25630.06343	0
Residual	635	453.51694	0.7142		
Uncorrected Total	637	37063.49476			
Corrected Total	636	2509.35274			

At the 0.05 level, the fitting function is significantly better than the function y=0.

Fitted Curves Plot



Residual vs. Independent Plot



MOR (σ_4) regression model Curve Fitting by Origin Pro

Nonlinear Curve Fit (NewFunction10 (User)) (15/06/2019 17:12:19)

Notes

Description	Nonlinear Curve Fit
User Name	pqshe
Operation Time	15/06/2019 17:12:19
Iteration Algorithm	Levenberg Marquardt
Model	NewFunction10 (User)
Number of Parameters	2
Number of Derived Parameters	0
Number of Datasets	1
Equation	$a*x1*(\ln(x2)+b)$
Report Status	New Analysis Report
Data Filter	No

Input Data

	Dep/Indep	Data	Range	Weight Type
x1	Indep	[alloldneweac3]"all oldnew each"!A	[1*.637*]	No Weighting
B x2	Indep	[alloldneweac3]"all oldnew each"!F	[1*.637*]	No Weighting
y	Dep	[alloldneweac3]"all oldnew each"!B	[1*.637*]	Statistical

Parameters

		Value	Standard Error	t-Value	Prob> t	Dependency
B	a	25.43515	0.601	42.32129	5.47859E-187	0.96453
	b	5.55012	0.13684	40.55897	2.02091E-178	0.96453

Reduced Chi-sqr = 0.724789977431
 COD(R^2) = 0.81658950232703
 Iterations Performed = 21
 Total Iterations in Session = 21

Fit converged. Chi-Sqr tolerance value of 1E-9 was reached.

Standard Error was scaled with square root of reduced Chi-Sqr.

Statistics

		B
Number of Points		637
Degrees of Freedom		635
Reduced Chi-Sqr		0.72479
Residual Sum of Squares		460.24164
R-Square (COD)		0.81659
Adj. R-Square		0.8163
Fit Status	Succeeded(100)	

Fit Status Code :
 100 : Fit converged. Chi-Sqr tolerance value of 1E-9 was reached.

Summary

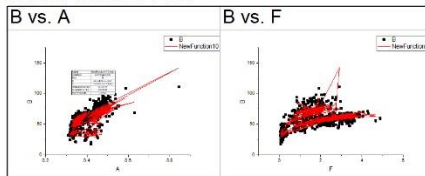
		a		b		Statistics	
	Value	Standard Error	Value	Standard Error	Reduced Chi-Sqr	Adj. R-Square	
B	25.43515	0.601	5.55012	0.13684	0.72479	0.8163	

ANOVA

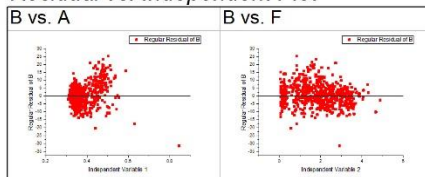
		DF	Sum of Squares	Mean Square	F Value	Prob>F
B	Regression	2	36603.25312	18301.62656	25250.9377	0
	Residual	635	460.24164	0.72479		
	Uncorrected Total	637	37063.49476			
	Corrected Total	636	2509.35274			

At the 0.05 level, the fitting function is significantly better than the function y=0.

Fitted Curves Plot



Residual vs. Independent Plot



MOR (σ_5) regression model Curve Fitting by Origin Pro

Nonlinear Curve Fit (NewFunction10 (User)) (15/06/2019 17:13:33)

Notes

Description	Nonlinear Curve Fit
User Name	pqshe
Operation Time	15/06/2019 17:13:33
Iteration Algorithm	Levenberg Marquardt
Model	NewFunction10 (User)
Number of Parameters	2
Number of Derived Parameters	0
Number of Datasets	1
Equation	$a \times x1 \times (\ln(x2) + b)$
Report Status	New Analysis Report
Data Filter	No

Input Data

	Dep/Indep	Data	Range	Weight Type
x1	Indep	[alloldneweac4]"all oldnew each"!A	[1*:637*]	No Weighting
B x2	Indep	[alloldneweac4]"all oldnew each"!G	[1*:637*]	No Weighting
y	Dep	[alloldneweac4]"all oldnew each"!B	[1*:637*]	Statistical

Parameters

	Value	Standard Error	t-Value	Prob> t	Dependency
B a	25.8844	0.6443	40.17416	1.57909E-176	0.96549
B b	5.90611	0.14158	41.71506	4.64145E-184	0.96549

Reduced Chi-sqr = 0.781874322892
 COD(R^2) = 0.80214412016607
 Iterations Performed = 21
 Total Iterations in Session = 21

Fit converged. Chi-Sqr tolerance value of 1E-9 was reached.
 Standard Error was scaled with square root of reduced Chi-Sqr.

Statistics

		B
Number of Points		637
Degrees of Freedom		635
Reduced Chi-Sqr		0.78187
Residual Sum of Squares		496.4902
R-Square (COD)		0.80214
Adj. R-Square		0.80183
Fit Status		Succeeded(100)

Fit Status Code :
 100 : Fit converged. Chi-Sqr tolerance value of 1E-9 was reached

Summary

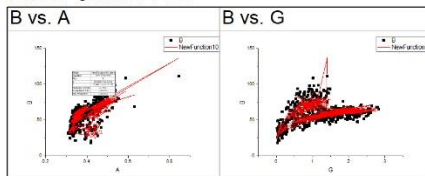
		a		b		Statistics	
	Value	Standard Error	Value	Standard Error	Reduced Chi-Sqr	Adj. R-Square	
B	25.8844	0.6443	5.90611	0.14158	0.78187	0.80183	

ANOVA

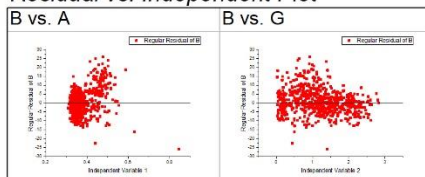
		DF	Sum of Squares	Mean Square	F Value	Prob>F
B	Regression	2	36567.00456	18283.50228	23384.19583	0
	Residual	635	496.4902	0.78187		
	Uncorrected Total	637	37063.49476			
	Corrected Total	636	2509.35274			

At the 0.05 level, the fitting function is significantly better than the function y=0.

Fitted Curves Plot



Residual vs. Independent Plot



MOR (σ_6) regression model Curve Fitting by Origin Pro

Nonlinear Curve Fit (NewFunction10 (User)) (15/06/2019 17:15:07)

Notes

Description	Nonlinear Curve Fit
User Name	pqshe
Operation Time	15/06/2019 17:15:07
Iteration Algorithm	Levenberg Marquardt
Model	NewFunction10 (User)
Number of Parameters	2
Number of Derived Parameters	0
Number of Datasets	1
Equation	$a \cdot x_1 \cdot (\ln(x_2) + b)$
Report Status	New Analysis Report
Data Filter	No

Input Data

	Dep/Indep	Data	Range	Weight Type
x1	Indep	[alloldneweac5]"all oldnew each"!A	[1*:637*]	No Weighting
B x2	Indep	[alloldneweac5]"all oldnew each"!H	[1*:637*]	No Weighting
y	Dep	[alloldneweac5]"all oldnew each"!B	[1*:637*]	Statistical

Parameters

	Value	Standard Error	t-Value	Prob> t	Dependency
B a	27.8036	0.70087	39.6704	4.88028E-174	0.96573
b	5.54231	0.13347	41.5258	3.84439E-183	0.96573

Reduced Chi-sqr = 0.796112956104
 COD(R²) = 0.7985409870034
 Iterations Performed = 22
 Total Iterations in Session = 22

Fit converged. Chi-Sqr tolerance value of 1E-9 was reached.
 Standard Error was scaled with square root of reduced Chi-Sqr.

Statistics

	B
Number of Points	637
Degrees of Freedom	635
Reduced Chi-Sqr	0.79611
Residual Sum of Squares	505.53173
R-Square (COD)	0.79854
Adj. R-Square	0.79822
Fit Status	Succeeded(100)

Fit Status Code :
 100 : Fit converged. Chi-Sqr tolerance value of 1E-9 was reached

Summary

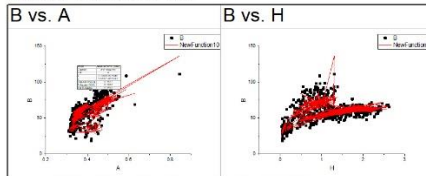
	a		b		Statistics	
	Value	Standard Error	Value	Standard Error	Reduced Chi-Sqr	Adj. R-Square
B	27.8036	0.70087	5.54231	0.13347	0.79611	0.79822

ANOVA

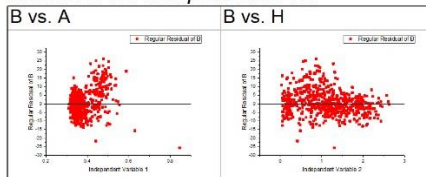
	DF	Sum of Squares	Mean Square	F Value	Prob>F
Regression	2	36557.96303	18278.98152	22960.28645	0
Residual	635	505.53173	0.79611		
Uncorrected Total	637	37063.49476			
Corrected Total	636	2509.35274			

At the 0.05 level, the fitting function is significantly better than the function y=0.

Fitted Curves Plot



Residual vs. Independent Plot



Bending MOR Multiple Regression Analysis by SPSS

Regression

Model Summary^a

Model	R	R Square	Adjusted R Square	Std. Error of the Estimate	Durbin-Watson
1	.706 ^a	.498	.497	10.19744095	
2	.806 ^b	.649	.648	8.53039095	
3	.867 ^c	.752	.750	7.18269401	
4	.897 ^d	.805	.803	6.37654417	
5	.903 ^e	.815	.814	6.20663349	
6	.905 ^f	.819	.817	6.14669176	1.786

a. Predictors: (Constant), Peak1054

b. Predictors: (Constant), Peak1054, Peak1366

c. Predictors: (Constant), Peak1054, Peak1366, density

d. Predictors: (Constant), Peak1054, Peak1366, density, Peak1456

e. Predictors: (Constant), Peak1054, Peak1366, density, Peak1456, Peak1318

f. Predictors: (Constant), Peak1054, Peak1366, density, Peak1456, Peak1318, Peak1421

j. Dependent Variable: MOR

ANOVA^a

Model		Sum of Squares	df	Mean Square	F	Sig.
1	Regression	65476.290	1	65476.290	629.654	.000 ^b
	Residual	66032.254	635	103.988		
	Total	131508.544	636			
2	Regression	85373.905	2	42686.953	586.621	.000 ^c
	Residual	46134.639	634	72.768		
	Total	131508.544	636			
3	Regression	98851.382	3	32950.461	638.685	.000 ^d
	Residual	32657.162	633	51.591		
	Total	131508.544	636			
4	Regression	105811.225	4	26452.806	650.580	.000 ^e
	Residual	25697.319	632	40.660		
	Total	131508.544	636			
5	Regression	107200.973	5	21440.195	556.566	.000 ^f

	Residual	24307.571	631	38.522		
	Total	131508.544	636			
6	Regression	107705.998	6	17951.000	475.123	.000 ^g
	Residual	23802.546	630	37.782		
	Total	131508.544	636			

a. Dependent Variable: MOR

b. Predictors: (Constant), Peak1054

c. Predictors: (Constant), Peak1054, Peak1366

d. Predictors: (Constant), Peak1054, Peak1366, density

e. Predictors: (Constant), Peak1054, Peak1366, density, Peak1456

f. Predictors: (Constant), Peak1054, Peak1366, density, Peak1456, Peak1318

g. Predictors: (Constant), Peak1054, Peak1366, density, Peak1456, Peak1318, Peak1421

Coefficients^a

Model		Unstandardized Coefficients		Standardized Coefficients	t	Sig.	95.0% Confidence Interval for B		Correlations			Collinearity Statistics
		B	Std. Error	Beta			Lower Bound	Upper Bound	Zero-order	Partial	Part	Tolerance
1	(Constant)	99.691	1.703		58.547	.000	96.347	103.034				
	Peak1054	-.251	.010	-.706	25.093	.000	-.270	-.231	-.706	-.706	-.706	1.000
2	(Constant)	67.156	2.429		27.648	.000	62.387	71.926				
	Peak1054	-.191	.009	-.538	20.984	.000	-.209	-.173	-.706	-.640	-.494	.843
	Peak1366	.039	.002	.424	16.536	.000	.034	.043	.637	.549	.389	.843
3	(Constant)	-10.642	5.230		-2.035	.042	-20.912	-.372				
	Peak1054	-.047	.012	-.133	-4.015	.000	-.070	-.024	-.706	-.158	-.080	.359
	Peak1366	.048	.002	.521	23.274	.000	.044	.052	.637	.679	.461	.781
	density	127.251	7.873	.495	16.163	.000	111.791	142.712	.659	.540	.320	.419
4	(Constant)	-2.867	4.681		-.612	.540	-12.058	6.325				
	Peak1054	-.046	.010	-.129	-4.381	.000	-.066	-.025	-.706	-.172	-.077	.359
	Peak1366	.082	.003	.893	25.763	.000	.075	.088	.637	.716	.453	.258
	density	116.615	7.037	.453	16.573	.000	102.797	130.433	.659	.550	.291	.413
	Peak1456	-.067	.005	-.433	13.083	.000	-.077	-.057	.354	-.462	-.230	.282
5	(Constant)	-16.319	5.077		-3.214	.001	-26.288	-6.349				
	Peak1054	-.025	.011	-.071	-2.341	.020	-.046	-.004	-.706	-.093	-.040	.322
	Peak1366	.038	.008	.411	4.718	.000	.022	.053	.637	.185	.081	.039
	density	138.407	7.751	.538	17.857	.000	123.187	153.627	.659	.579	.306	.323

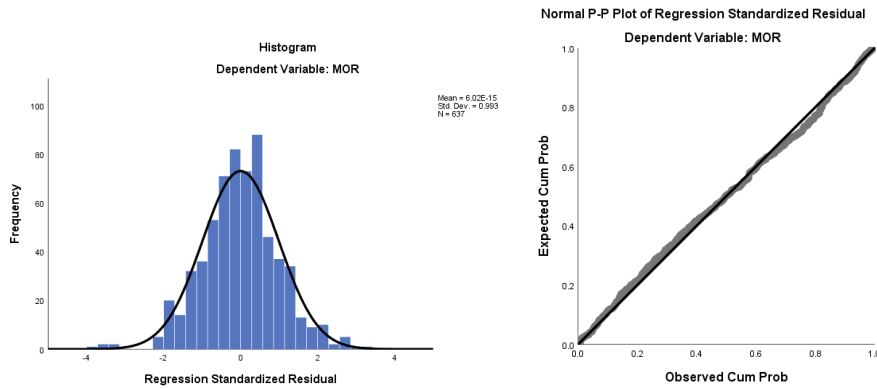
Peak1456	-.054	.005	-.350	-9.971	.000	-.065	-.044	.354	-.369	-.171	.238
Peak1318	.053	.009	.441	6.006	.000	.036	.071	.619	.233	.103	.054
(Constant)	-4.916	5.917		-.831	.406	-16.534	6.703				
Peak1054	-.039	.011	-.111	-3.479	.001	-.062	-.017	-.706	-.137	-.059	.284
Peak1366	.045	.008	.489	5.505	.000	.029	.061	.637	.214	.093	.036
6 density	137.258	7.682	.533	17.867	.000	122.172	152.344	.659	.580	.303	.322
Peak1456	-.054	.005	-.348	10.019	.000	-.065	-.044	.354	-.371	-.170	.238
Peak1318	.059	.009	.489	6.615	.000	.042	.077	.619	.255	.112	.053
Peak1421	-.032	.009	-.158	-3.656	.000	-.050	-.015	.642	-.144	-.062	.154

h. Predictors in the Model: (Constant), Peak1054, Peak1366, density, Peak1456, Peak1318, Peak1421, Peak1110

i. Predictors in the Model: (Constant), Peak1054, Peak1366, density, Peak1456, Peak1318, Peak1421, Peak1110, Peak1025

j. Predictors in the Model: (Constant), Peak1054, Peak1366, density, Peak1456, Peak1318, Peak1421, Peak1110, Peak1025, Peak1204

Charts



Bending MOE Multiple Regression Analysis by SPSS

Regression

Model Summary ^h						
Model	R	R Square	Adjusted R Square	Std. Error of the Estimate	Durbin-Watson	
1	.742 ^a	.550	.549	634.71297496		
2	.758 ^b	.575	.574	617.14997975		
3	.769 ^c	.591	.589	606.13115830		
4	.783 ^d	.614	.611	589.29624207		
5	.792 ^e	.628	.625	578.82145606		
6	.797 ^f	.635	.632	573.69803838		
7	.801 ^g	.642	.638	568.81835710	1.868	

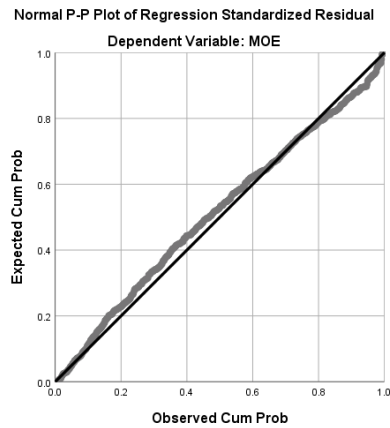
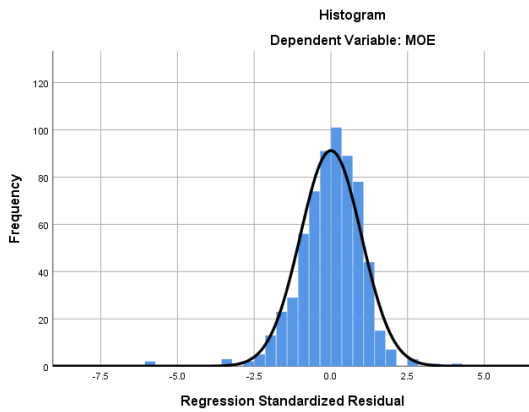
- a. Predictors: (Constant), density
- b. Predictors: (Constant), density, Peak1025
- c. Predictors: (Constant), density, Peak1025, Peak1054
- d. Predictors: (Constant), density, Peak1025, Peak1054, Peak1226
- e. Predictors: (Constant), density, Peak1025, Peak1054, Peak1226, Peak895
- f. Predictors: (Constant), density, Peak1025, Peak1054, Peak1226, Peak895, Peak1456
- g. Predictors: (Constant), density, Peak1025, Peak1054, Peak1226, Peak895, Peak1456, Peak1507
- h. Dependent Variable: MOE

Coefficients^a

Model		Unstandardized Coefficients		Standardized Coefficients			95.0% Confidence Interval for B
		B	Std. Error	Beta	t	Sig.	Lower Bound
1	(Constant)	631.868	174.352		3.624	.000	289.491
	density	12542.374	450.332	.742	27.851	.000	11658.054
2	(Constant)	-3959.171	767.123		-5.161	.000	-5465.581
	density	10683.255	532.463	.632	20.064	.000	9637.650
	Peak1025	.483	.079	.193	6.136	.000	.329
3	(Constant)	-5687.283	831.113		-6.843	.000	-7319.355
	density	12971.181	699.465	.767	18.544	.000	11597.629
	Peak1025	.495	.077	.198	6.399	.000	.343
	Peak1054	4.352	.884	.186	4.925	.000	2.617
4	(Constant)	-9724.941	1041.889		-9.334	.000	-11770.924
	density	14556.960	727.450	.861	20.011	.000	13128.449
	Peak1025	.652	.079	.260	8.203	.000	.496
	Peak1054	8.180	1.062	.350	7.706	.000	6.096
	Peak1226	3.031	.494	.194	6.139	.000	2.061
5	(Constant)	-10514.662	1035.945		-10.150	.000	-12548.979
	density	13362.807	754.820	.790	17.703	.000	11880.543
	Peak1025	.687	.078	.274	8.761	.000	.533
	Peak1054	7.862	1.045	.337	7.525	.000	5.810
	Peak1226	3.142	.486	.201	6.472	.000	2.189
	Peak895	1.042	.212	.132	4.907	.000	.625
6	(Constant)	-10814.056	1030.312		-10.496	.000	-12837.319
	density	13349.065	748.149	.789	17.843	.000	11879.896
	Peak1025	.709	.078	.283	9.096	.000	.556
	Peak1054	7.908	1.036	.339	7.636	.000	5.874
	Peak1226	4.396	.599	.281	7.336	.000	3.219

Peak895	1.066	.211		.135	5.061	.000	.652
Peak1456	-1.173	.334		-.115	-3.510	.000	-1.830
7 (Constant)	-11641.870	1049.459			-11.093	.000	-13702.738
density	13750.990	750.914		.813	18.312	.000	12276.388
Peak1025	.749	.078		.299	9.584	.000	.595
Peak1054	7.956	1.027		.341	7.748	.000	5.939
Peak1226	2.807	.752		.179	3.731	.000	1.330
Peak895	1.173	.211		.148	5.554	.000	.758
Peak1456	-2.533	.516		-.248	-4.913	.000	-3.546
Peak1507	4.556	1.323		.238	3.443	.001	1.958

Charts



Storage Moduli of Peak γ Multiple Regression Analysis by SPSS

Regression

Model Summary^d

Model	R	R Square	Adjusted R Square	Std. Error of the Estimate	Durbin-Watson
1	.728 ^a	.529	.525	1.133562491E+009	
2	.762 ^b	.581	.574	1.073883306E+009	
3	.781 ^c	.611	.600	1.040104561E+009	1.820

a. Predictors: (Constant), density

b. Predictors: (Constant), density, p1025

c. Predictors: (Constant), density, p1025, p1318

d. Dependent Variable: @1111storageM

ANOVA^a

Model	Sum of Squares	df	Mean Square	F	Sig.
-------	----------------	----	-------------	---	------

1	Regression	170566924628522430000.000	1	170566924628522430000.000	132.741	.000 ^b
	Residual	151625742776031050000.000	118	1284963921830771710.000		
	Total	322192667404553500000.000	119			
2	Regression	187265300930212600000.000	2	93632650465106300000.000	81.192	.000 ^c
	Residual	134927366474340880000.000	117	1153225354481545980.000		
	Total	322192667404553500000.000	119			
3	Regression	196701837603942100000.000	3	65567279201314040000.000	60.608	.000 ^d
	Residual	125490829800611380000.000	116	1081817498281132540.000		
	Total	322192667404553500000.000	119			

a. Dependent Variable: @1111storageM

b. Predictors: (Constant), density

c. Predictors: (Constant), density, p1025

d. Predictors: (Constant), density, p1025, p1318

Coefficients^a

Model	Unstandardized Coefficients		Standardized Coefficients		t	Sig.
	B	Std. Error	Beta			
1 (Constant)	847188543.899	673078936.922			1.259	.211
	density	18595711664.469	1614027243.957	.728	11.521	.000
2 (Constant)	-8801156649.781	2614502036.534			-3.366	.001
	density	13934500451.459	1959210986.580	.545	7.112	.000
	p1025	1040794.323	273517.352	.292	3.805	.000
3 (Constant)	-9316273883.271	2538262794.097			-3.670	.000
	density	13965915655.331	1897614281.562	.546	7.360	.000
	p1025	979872.670	265715.779	.275	3.688	.000
	p1318	2783218.591	942362.513	.172	2.953	.004

Coefficients^a

Model	95.0% Confidence Interval for B		Correlations			
	Lower Bound	Upper Bound	Zero-order	Partial	Part	
1 (Constant)	-485690996.457	2180068084.255				
	density	15399498303.691	21791925025.246	.728	.728	.728
2 (Constant)	-13979040929.787	-3623272369.776				
	density	10054385757.773	17814615145.146	.728	.549	.426
	p1025	499107.539	1582481.107	.633	.332	.228
3 (Constant)	-14343623174.333	-4288924592.208				
	density	10207451466.633	17724379844.029	.728	.564	.426
	p1025	453589.089	1506156.252	.633	.324	.214

p1318	916750.894	4649686.287	.228	.264	.171
-------	------------	-------------	------	------	------

Coefficients^a

Collinearity Statistics

Model		Tolerance	VIF
1 (Constant)			
	density	1.000	1.000
2 (Constant)			
	density	.609	1.642
	p1025	.609	1.642
3 (Constant)			
	density	.609	1.642
	p1025	.605	1.652
	p1318	.991	1.009

a. Dependent Variable: @1111storageM

Coefficient Correlations^a

Model		density	p1025	p1318	
1	Correlations	density	1.000		
	Covariances	density	2605083944234178600.000		
2	Correlations	density	1.000	-.625	
		p1025	-.625	1.000	
	Covariances	density	3838507689937590300.000	-335045381524014.900	
		p1025	-335045381524014.800	74811742104.408	
3	Correlations	density	1.000	-.624	.006
		p1025	-.624	1.000	-.078
		p1318	.006	-.078	1.000
	Covariances	density	3600939961587065900.000	314518738410119.250	-10023711741008.482
		p1025	-314518738410119.250	70604875266.750	-19438393259.184
		p1318	10023711741008.482	-19438393259.184	888047105430.496

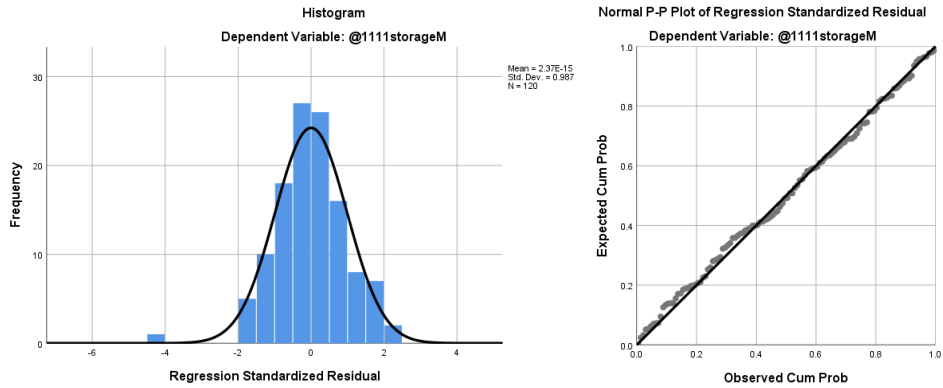
a. Dependent Variable: @1111storageM

Residuals Statistics^a

	Minimum	Maximum	Mean	Std. Deviation	N
Predicted Value	6.22658150E+009	1.24249139E+010	8.50974658E+009	1.285673605E+009	120
Residual	-4.460239360E+009	2.301244928E+009	2.559026082E-006	1.026910312E+009	120
Std. Predicted Value	-1.776	3.045	.000	1.000	120
Std. Residual	-4.288	2.213	.000	.987	120

a. Dependent Variable: @1111storageM

Charts



Loss Moduli of Peak γ of Tan δ Multiple Regression Analysis by SPSS

Regression

Variables Entered/Removed^a

Model	Variables Entered	Variables Removed	Method
1	p1025		Stepwise (Criteria: Probability-of-F-to-enter <= .050, Probability-of-F-to-remove >= .100).
2	density		Stepwise (Criteria: Probability-of-F-to-enter <= .050, Probability-of-F-to-remove >= .100).

a. Dependent Variable: @11111LossM

Model Summary^c

Model	R	R Square	Adjusted R Square	Std. Error of the Estimate	Durbin-Watson
1	.559 ^a	.312	.306	5.893509712E+007	
2	.619 ^b	.383	.373	5.604475744E+007	2.174

a. Predictors: (Constant), p1025

b. Predictors: (Constant), p1025, density

c. Dependent Variable: @11111LossM

ANOVA^a

Model		Sum of Squares	df	Mean Square	F	Sig.
1	Regression	185924758166868416.000	1	185924758166868416.000	53.529	.000 ^b
	Residual	409854789339418690.000	118	3473345672367955.000		
	Total	595779547506287100.000	119			
2	Regression	228280811629283904.000	2	114140405814641952.000	36.339	.000 ^c
	Residual	367498735877003200.000	117	3141014836555583.000		
	Total	595779547506287100.000	119			

a. Dependent Variable: @11111LossM

b. Predictors: (Constant), p1025

c. Predictors: (Constant), p1025, density

Coefficients^a

Model		Unstandardized Coefficients		Standardized Coefficients	t	Sig.
		B	Std. Error	Beta		
1	(Constant)	-474073399.994	130330497.227		-3.637	.000
	p1025	85711.221	11715.021	.559	7.316	.000
2	(Constant)	-264495003.985	136447909.818		-1.938	.055
	p1025	52937.702	14274.562	.345	3.709	.000
	density	375475721.382	102249009.668	.342	3.672	.000

Coefficients^a

Model		95.0% Confidence Interval for B		Correlations		
		Lower Bound	Upper Bound	Zero-order	Partial	Part
1	(Constant)	-732163266.888	-215983533.101			
	p1025	62512.290	108910.152	.559	.559	.559
2	(Constant)	-534722939.329	5732931.359			
	p1025	24667.680	81207.724	.559	.324	.269
	density	172976915.717	577974527.047	.557	.321	.267

Coefficients^a

Collinearity Statistics

Model	Tolerance	VIF	
1	(Constant)		
	p1025	1.000	1.000
2	(Constant)		
	p1025	.609	1.642
	density	.609	1.642

a. Dependent Variable: @11111LossM

Coefficient Correlations^a

Model		p1025	density
1	Correlations	p1025	1.000
	Covariances	p1025	137241718.747
2	Correlations	p1025	1.000
		density	-.625
		density	1.000

Covariances	p1025	203763116.190	-912555824580.769
	density	-912555824580.769	10454859978123732.000

a. Dependent Variable: @11111LossM

Collinearity Diagnostics^a

Model	Dimension	Eigenvalue	Condition Index	Variance Proportions		
				(Constant)	p1025	density
1	1	1.999	1.000	.00	.00	
	2	.001	48.429	1.00	1.00	
2	1	2.986	1.000	.00	.00	.00
	2	.014	14.746	.03	.01	.69
	3	.001	70.635	.97	.99	.31

a. Dependent Variable: @11111LossM

Casewise Diagnostics^a

Case Number	Std. Residual	@11111LossM	Predicted Value	Residual
118	-3.941	2.700000E+008	4.90891541E+008	-2.208915405E+008

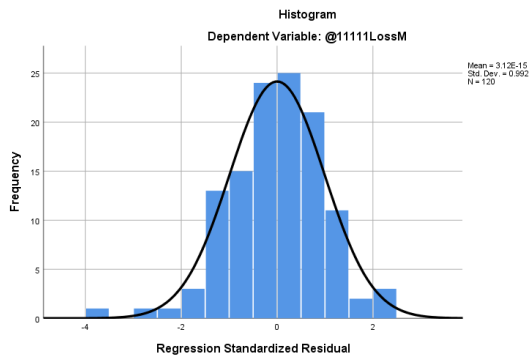
a. Dependent Variable: @11111LossM

Residuals Statistics^a

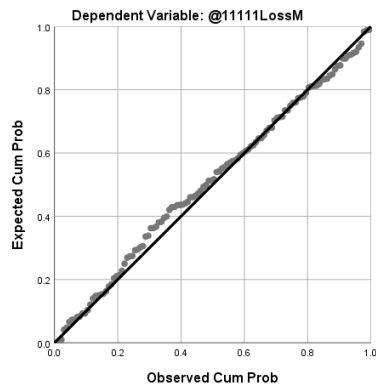
	Minimum	Maximum	Mean	Std. Deviation	N
Predicted Value	4.18845792E+008	5.79375424E+008	4.78657657E+008	4.379870030E+007	120
Residual	-2.208915360E+008	1.301088800E+008	1.753369967E-007	5.557179744E+007	120
Std. Predicted Value	-1.366	2.300	.000	1.000	120
Std. Residual	-3.941	2.322	.000	.992	120

a. Dependent Variable: @11111LossM

Charts



Normal P-P Plot of Regression Standardized Residual



Storage Moduli of Peak β of Tan δ Multiple Regression Analysis by SPSS

Regression

Variables Entered/Removed^a

Model	Variables Entered	Variables Removed	Method
1	density	.	Stepwise (Criteria: Probability-of-F-to-enter \leq .050, Probability-of-F-to-remove \geq .100).
2	p1025	.	Stepwise (Criteria: Probability-of-F-to-enter \leq .050, Probability-of-F-to-remove \geq .100).

a. Dependent Variable: @2222storageM

Model Summary^c

Model	R	R Square	Adjusted R Square	Std. Error of the Estimate	Durbin-Watson
1	.693 ^a	.480	.475	766565299.804	
2	.720 ^b	.519	.510	740440083.539	1.959

a. Predictors: (Constant), density

b. Predictors: (Constant), density, p1025

c. Dependent Variable: @2222storageM

ANOVA^a

Model		Sum of Squares	df	Mean Square	F	Sig.
1	Regression	63933425873324070000.000	1	63933425873324070000.000	108.800	.000 ^b
	Residual	69339438345979520000.000	118	587622358864233220.000		
	Total	133272864219303600000.000	119			
2	Regression	69127436693951790000.000	2	34563718346975896000.000	63.044	.000 ^c
	Residual	64145427525351800000.000	117	548251517310699140.000		
	Total	133272864219303600000.000	119			

a. Dependent Variable: @2222storageM

b. Predictors: (Constant), density

c. Predictors: (Constant), density, p1025

Coefficients^a

Model		Unstandardized Coefficients		Standardized Coefficients		
		B	Std. Error	Beta	t	Sig.
1	(Constant)	1339760650.939	455165869.552		2.943	.004
	density	11384904250.261	1091476903.638	.693	10.431	.000
2	(Constant)	-4041290696.200	1802693175.211		-2.242	.027
	density	8785264998.808	1350871494.822	.534	6.503	.000
	p1025	580469.250	188589.589	.253	3.078	.003

Coefficients^a

Model		95.0% Confidence Interval for B		Correlations		
		Lower Bound	Upper Bound	Zero-order	Partial	Part
1 (Constant)		438408310.650	2241112991.228			
	density	9223482827.264	13546325673.258	.693	.693	.693
2 (Constant)		-7611430066.208	-471151326.191			
	density	6109934790.759	11460595206.856	.693	.515	.417
	p1025	206977.451	953961.048	.587	.274	.197

Coefficients^a

Collinearity Statistics

Model	Tolerance	VIF	
1 (Constant)			
	density	1.000	1.000
2 (Constant)			
	density	.609	1.642
	p1025	.609	1.642

a. Dependent Variable: @2222storageM

Coefficient Correlations^a

Model		density	p1025
1	Correlations	density	1.000
	Covariances	density	1191321831175765760.000
2	Correlations	density	1.000
		p1025	-.625
	Covariances	density	-159282952004696.500
		p1025	35566033093.192

a. Dependent Variable: @2222storageM

Collinearity Diagnostics^a

Model	Dimension	Eigenvalue	Condition Index	Variance Proportions		
				(Constant)	density	p1025
1	1	1.988	1.000	.01	.01	
	2	.012	12.932	.99	.99	
2	1	2.986	1.000	.00	.00	.00
	2	.014	14.746	.03	.69	.01
	3	.001	70.635	.97	.31	.99

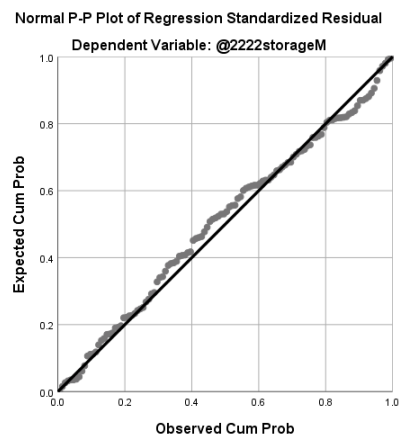
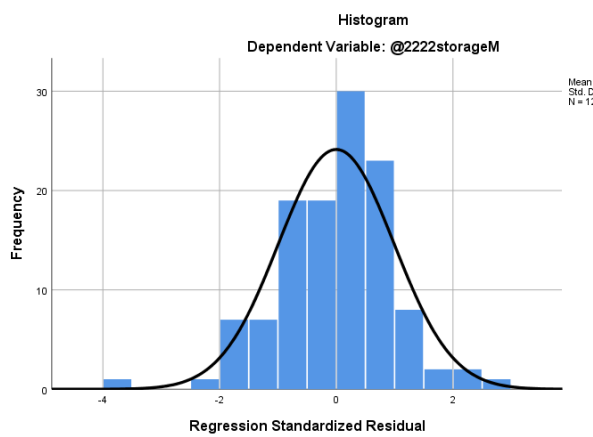
a. Dependent Variable: @2222storageM

Residuals Statistics^a

	Minimum	Maximum	Mean	Std. Deviation	N
Predicted Value	5097365504.00	8500041728.00	6031029858.49	762169816.616	120
Residual	-2851695616.000	1961107712.000	.000	734191532.296	120
Std. Predicted Value	-1.225	3.239	.000	1.000	120
Std. Residual	-3.851	2.649	.000	.992	120

a. Dependent Variable: @2222storageM

Charts



Loss Moduli of Peak β of Tan δ Multiple Regression Analysis by SPSS

Regression

Model Summary^f

Model	R	R Square	Adjusted R Square	Std. Error of the Estimate	Durbin-Watson
1	.757 ^a	.574	.570	50829128.6065	
2	.795 ^b	.632	.626	47429766.8902	
3	.807 ^c	.652	.643	46323409.9255	
4	.815 ^d	.665	.653	45669352.1442	
5	.826 ^e	.682	.668	44689079.0389	1.550

a. Predictors: (Constant), density

b. Predictors: (Constant), density, p1025

c. Predictors: (Constant), density, p1025, p1335

d. Predictors: (Constant), density, p1025, p1335, p1154

e. Predictors: (Constant), density, p1025, p1335, p1154, peak895

f. Dependent Variable: @2222LossM

ANOVA^a

Model		Sum of Squares	df	Mean Square	F	Sig.
1	Regression	410167399056559870.000	1	410167399056559870.000	158.758	.000 ^b
	Residual	304864837157896190.000	118	2583600314897425.500		
	Total	715032236214456060.000	119			
2	Regression	451831050104942080.000	2	225915525052471040.000	100.426	.000 ^c
	Residual	263201186109513952.000	117	2249582787260803.000		
	Total	715032236214456060.000	119			
3	Regression	466112672587425470.000	3	155370890862475168.000	72.405	.000 ^d
	Residual	248919563627030592.000	116	2145858307129574.000		
	Total	715032236214456060.000	119			
4	Regression	475177917808415620.000	4	118794479452103904.000	56.957	.000 ^e
	Residual	239854318406040448.000	115	2085689725269917.000		
	Total	715032236214456060.000	119			
5	Regression	487361264685166850.000	5	97472252937033376.000	48.807	.000 ^f
	Residual	227670971529289216.000	114	1997113785344642.200		
	Total	715032236214456060.000	119			

a. Dependent Variable: @2222LossM

b. Predictors: (Constant), density

c. Predictors: (Constant), density, p1025

d. Predictors: (Constant), density, p1025, p1335

e. Predictors: (Constant), density, p1025, p1335, p1154

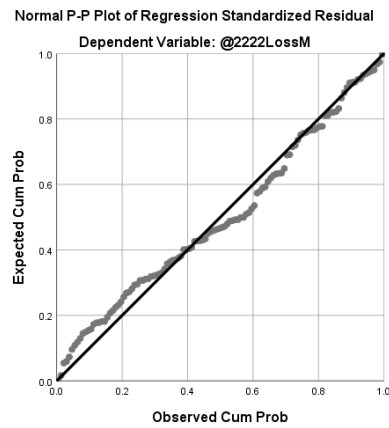
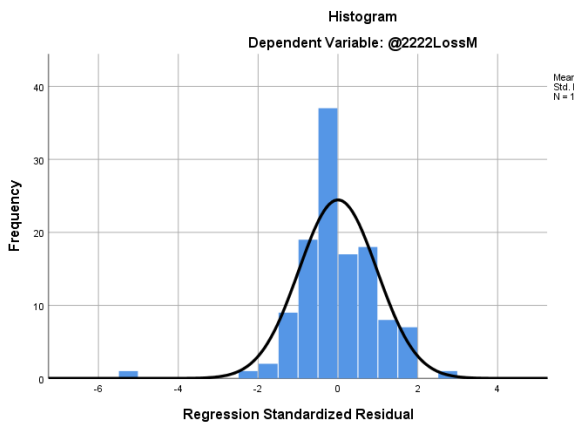
f. Predictors: (Constant), density, p1025, p1335, p1154, peak895

Coefficients^a

Model		Unstandardized Coefficients		Standardized Coefficients	t	Sig.
		B	Std. Error	Beta		
1	(Constant)	-54440172.757	30180970.267		-1.804	.074
	density	911897370.658	72373247.159	.757	12.600	.000
2	(Constant)	-536381726.825	115473647.329		-4.645	.000
	density	679066628.107	86531674.233	.564	7.848	.000
	p1025	51988.400	12080.330	.309	4.304	.000
3	(Constant)	-568822111.243	113478943.142		-5.013	.000
	density	640510359.354	85824519.428	.532	7.463	.000
	p1025	57943.098	12022.201	.345	4.820	.000
	p1335	-180582.544	69998.303	-.144	-2.580	.011
4	(Constant)	-386600618.856	141971727.885		-2.723	.007
	density	622411825.720	85056904.169	.517	7.318	.000

	p1025	52743.916	12111.976	.314	4.355	.000
	p1335	-186797.959	69074.338	-.149	-2.704	.008
	p1154	-182452.900	87515.674	-.120	-2.085	.039
5	(Constant)	-	141725259.541		-3.216	.002
	density	565004658.791	86415559.365	.469	6.538	.000
	p1025	56967.607	11974.729	.339	4.757	.000
	p1335	-150450.466	69175.137	-.120	-2.175	.032
	p1154	-225070.615	87358.192	-.148	-2.576	.011
	peak895	82797.555	33522.439	.142	2.470	.015

Charts



Temperature of Peak β of Tan δ Multiple Regression Analysis by SPSS

Regression

Variables Entered/Removed^a

Model	Variables Entered	Variables Removed	Method
1	density		Stepwise (Criteria: Probability-of-F-to-enter <= .050, Probability-of-F-to-remove >= .100).
2	moisture		Stepwise (Criteria: Probability-of-F-to-enter <= .050, Probability-of-F-to-remove >= .100).

a. Dependent Variable: @2222temperature

Model Summary^c

Model	R	R Square	Adjusted R Square	Std. Error of the Estimate	Durbin-Watson
1	.547 ^a	.299	.293	11.5811	

2	.572 ^b	.327	.316	11.3920	1.572
---	-------------------	------	------	---------	-------

a. Predictors: (Constant), density

b. Predictors: (Constant), density, moisture

c. Dependent Variable: @2222temperature

ANOVA^a

Model		Sum of Squares	df	Mean Square	F	Sig.
1	Regression	6748.007	1	6748.007	50.313	.000 ^b
	Residual	15826.271	118	134.121		
	Total	22574.279	119			
2	Regression	7390.265	2	3695.133	28.473	.000 ^c
	Residual	15184.014	117	129.778		
	Total	22574.279	119			

a. Dependent Variable: @2222temperature

b. Predictors: (Constant), density

c. Predictors: (Constant), density, moisture

Coefficients^a

Model		Unstandardized Coefficients		Standardized Coefficients	t	Sig.
		B	Std. Error	Beta		
1	(Constant)	14.940	6.877		2.173	.032
	density	116.964	16.490	.547	7.093	.000
2	(Constant)	31.464	10.046		3.132	.002
	density	112.455	16.347	.526	6.879	.000
	moisture	-1.671	.751	-.170	-2.225	.028

Coefficients^a

Model		95.0% Confidence Interval for B		Correlations		
		Lower Bound	Upper Bound	Zero-order	Partial	Part
1	(Constant)	1.323	28.558			
	density	84.310	149.618	.547	.547	.547
2	(Constant)	11.568	51.360			
	density	80.081	144.829	.547	.537	.522
	moisture	-3.159	-.183	-.235	-.201	-.169

Coefficients^a

Collinearity Statistics

Model		Tolerance	VIF
1	(Constant)		

density	1.000	1.000
2 (Constant)		
density	.985	1.016
moisture	.985	1.016

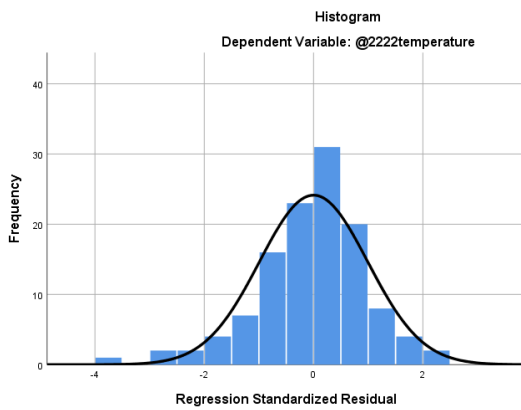
a. Dependent Variable: @2222temperature

Residuals Statistics^a

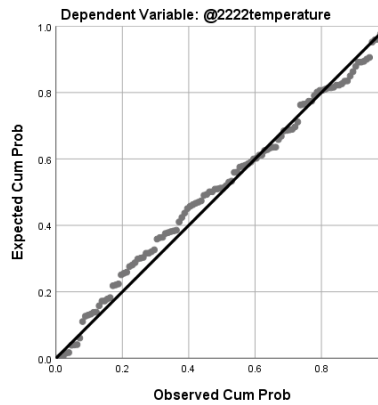
	Minimum	Maximum	Mean	Std. Deviation	N
Predicted Value	52.047	96.806	63.137	7.8805	120
Residual	-43.3084	25.2275	.0000	11.2959	120
Std. Predicted Value	-1.407	4.272	.000	1.000	120
Std. Residual	-3.802	2.214	.000	.992	120

a. Dependent Variable: @2222temperature

Charts



Normal P-P Plot of Regression Standardized Residual



Peak area Changes in Air Treatment Multiple Regression Analysis by SPSS

Peak 895 Regression

Model Summary^b

Model	R	R Square	Adjusted R Square	Std. Error of the Estimate	Durbin-Watson
1	.670 ^a	.449	.357	.056150074553	.871

a. Predictors: (Constant), period, temp

b. Dependent Variable: p895_A

ANOVA^a

Model		Sum of Squares	df	Mean Square	F	Sig.
1	Regression	.031	2	.015	4.885	.028 ^b

Residual	.038	12	.003		
Total	.069	14			

a. Dependent Variable: p895_A

b. Predictors: (Constant), period, temp

Coefficients^a

Model	Unstandardized Coefficients		Standardized Coefficients	t	Sig.
	B	Std. Error	Beta		
1 (Constant)	.309	.083		3.714	.003
temp	-.001	.000	-.649	-3.030	.010
period	-.002	.003	-.165	-.768	.457

Residuals Statistics^a

	Minimum	Maximum	Mean	Std. Deviation	N
Predicted Value	-.00696007069	.13213315606	.06258654587	.046906934921	15
Residual	-.094131737947	.067260988057	.000000000000	.051984867625	15
Std. Predicted Value	-1.483	1.483	.000	1.000	15
Std. Residual	-1.676	1.198	.000	.926	15

a. Dependent Variable: p895_A

Peak 1054 Regression

Model Summary^b

Model	R	R Square	Adjusted R Square	Std. Error of the Estimate	Durbin-Watson
1	.841 ^a	.707	.658	.118545132552	.306

a. Predictors: (Constant), period, temp

b. Dependent Variable: p1054_A

ANOVA^a

Model		Sum of Squares	df	Mean Square	F	Sig.
1	Regression	.407	2	.204	14.490	.001 ^b
	Residual	.169	12	.014		
	Total	.576	14			

a. Dependent Variable: p1054_A

b. Predictors: (Constant), period, temp

Coefficients^a

Model	Unstandardized Coefficients		Standardized Coefficients	t	Sig.
	B	Std. Error	Beta		
1 (Constant)	-.561	.176		-3.191	.008
temp	.005	.001	.812	5.199	.000

period	.008	.005	.218	1.395	.188
--------	------	------	------	-------	------

Residuals Statistics^a

	Minimum	Maximum	Mean	Std. Deviation	N
Predicted Value	.08407731354	.59464001656	.33935866993	.170554234726	15
Residual	-.170070290565	.139958143234	.000000000000	.109751466447	15
Std. Predicted Value	-1.497	1.497	.000	1.000	15
Std. Residual	-1.435	1.181	.000	.926	15

a. Dependent Variable: p1054_A

Peak 1110 Regression

Model Summary^b

Model	R	R Square	Adjusted R Square	Std. Error of the Estimate	Durbin-Watson
1	.876 ^a	.767	.729	.030513885244	.704

a. Predictors: (Constant), period, temp

b. Dependent Variable: p1110_A

ANOVA^a

Model		Sum of Squares	df	Mean Square	F	Sig.
1	Regression	.037	2	.018	19.784	.000 ^b
	Residual	.011	12	.001		
	Total	.048	14			

a. Dependent Variable: p1110_A

b. Predictors: (Constant), period, temp

Coefficients^a

Model		Unstandardized Coefficients		Standardized Coefficients		t	Sig.
		B	Std. Error	Beta			
1	(Constant)	.139	.045			3.072	.010
	temp	-.001	.000	-.852		-6.121	.000
	period	-.002	.001	-.202		-1.449	.173

Residuals Statistics^a

	Minimum	Maximum	Mean	Std. Deviation	N
Predicted Value	-.20474010706	-.05431405827	-.12952707947	.051298814298	15
Residual	-.039650134742	.043053593487	.000000000000	.028250368281	15
Std. Predicted Value	-1.466	1.466	.000	1.000	15
Std. Residual	-1.299	1.411	.000	.926	15

a. Dependent Variable: p1110_A

Peak 1154 Regression

Model Summary^b

Model	R	R Square	Adjusted R Square	Std. Error of the Estimate	Durbin-Watson
-------	---	----------	-------------------	----------------------------	---------------

1	.941 ^a	.885	.866	.026857274711	.666
---	-------------------	------	------	---------------	------

a. Predictors: (Constant), period, temp

b. Dependent Variable: p1154_A

ANOVA^a

Model		Sum of Squares	df	Mean Square	F	Sig.
1	Regression	.067	2	.033	46.249	.000 ^b
	Residual	.009	12	.001		
	Total	.075	14			

a. Dependent Variable: p1154_A

b. Predictors: (Constant), period, temp

Coefficients^a

Model		Unstandardized Coefficients		Standardized Coefficients	t	Sig.
		B	Std. Error	Beta		
1	(Constant)	.450	.040		11.288	.000
	temp	-.002	.000	-.938	-9.593	.000
	period	-.001	.001	-.067	-.690	.503

Residuals Statistics^a

	Minimum	Maximum	Mean	Std. Deviation	N
Predicted Value	.02201529406	.19848756492	.11025143280	.069034217979	15
Residual	-.021557267755	.044145401567	.000000000000	.024865004753	15
Std. Predicted Value	-1.278	1.278	.000	1.000	15
Std. Residual	-.803	1.644	.000	.926	15

a. Dependent Variable: p1154_A

Peak 1204 Regression

Model Summary^b

Model	R	R Square	Adjusted R Square	Std. Error of the Estimate	Durbin-Watson
1	.706 ^a	.499	.415	.027172221170	.856

a. Predictors: (Constant), period, temp

b. Dependent Variable: p1204_A

ANOVA^a

Model		Sum of Squares	df	Mean Square	F	Sig.
1	Regression	.009	2	.004	5.973	.016 ^b
	Residual	.009	12	.001		
	Total	.018	14			

a. Dependent Variable: p1204_A

b. Predictors: (Constant), period, temp

Coefficients^a

Model		Unstandardized Coefficients		Standardized Coefficients		t	Sig.
		B	Std. Error	Beta			
1	(Constant)	-.196	.040			-4.860	.000
	temp	.001	.000	.578		2.827	.015
	period	.002	.001	.406		1.989	.070

Residuals Statistics^a

	Minimum	Maximum	Mean	Std. Deviation	N
Predicted Value	-.10329042375	-.01524754893	-.05926898587	.025099715860	15
Residual	-.045188955963	.029495453462	.000000000000	.025156588515	15
Std. Predicted Value	-1.754	1.754	.000	1.000	15
Std. Residual	-1.663	1.086	.000	.926	15

a. Dependent Variable: p1204_A

Peak 1226 Regression

Model Summary^b

Model	R	R Square	Adjusted R Square	Std. Error of the Estimate	Durbin-Watson
1	.904 ^a	.817	.787	.070696706481	.524

a. Predictors: (Constant), period, temp

b. Dependent Variable: p1226_A

ANOVA^a

Model		Sum of Squares	df	Mean Square	F	Sig.
1	Regression	.268	2	.134	26.797	.000 ^b
	Residual	.060	12	.005		
	Total	.328	14			

a. Dependent Variable: p1226_A

b. Predictors: (Constant), period, temp

Coefficients^a

Model		Unstandardized Coefficients		Standardized Coefficients		t	Sig.
		B	Std. Error	Beta			
1	(Constant)	.496	.105			4.728	.000
	temp	-.004	.001	-.890		-7.210	.000
	period	-.004	.003	-.156		-1.266	.230

Residuals Statistics^a

	Minimum	Maximum	Mean	Std. Deviation	N
Predicted Value	-.40820080042	-.02044950426	-.21432515127	.138321426657	15
Residual	-.088338777423	.098637059331	.000000000000	.065452431847	15
Std. Predicted Value	-1.402	1.402	.000	1.000	15

Std. Residual	-1.250	1.395	.000	.926	15
---------------	--------	-------	------	------	----

a. Dependent Variable: p1226_A

Peak 1262 Regression

Model Summary^b

Model	R	R Square	Adjusted R Square	Std. Error of the Estimate	Durbin-Watson
1	.909 ^a	.826	.797	.029239929326	.401

a. Predictors: (Constant), period, temp

b. Dependent Variable: p1262_A

ANOVA^a

Model		Sum of Squares	df	Mean Square	F	Sig.
1	Regression	.049	2	.024	28.483	.000 ^b
	Residual	.010	12	.001		
	Total	.059	14			

a. Dependent Variable: p1262_A

b. Predictors: (Constant), period, temp

Coefficients^a

Model		Unstandardized Coefficients		Standardized Coefficients		Sig.
		B	Std. Error	Beta	t	
1	(Constant)	.245	.043		5.639	.000
	temp	-.002	.000	-.903	-7.497	.000
	period	-.001	.001	-.105	-.874	.399

Residuals Statistics^a

	Minimum	Maximum	Mean	Std. Deviation	N
Predicted Value	-.13003617525	.02726318873	-.05138649080	.058982603054	15
Residual	-.033971920609	.038677740842	.000000000000	.027070914286	15
Std. Predicted Value	-1.333	1.333	.000	1.000	15
Std. Residual	-1.162	1.323	.000	.926	15

a. Dependent Variable: p1262_A

Peak 1318 Regression

Model Summary^b

Model	R	R Square	Adjusted R Square	Std. Error of the Estimate	Durbin-Watson
1	.932 ^a	.869	.847	.110385361907	.260

a. Predictors: (Constant), period, temp

b. Dependent Variable: p1318_A

ANOVA^a

Model		Sum of Squares	df	Mean Square	F	Sig.
1	Regression	.967	2	.484	39.688	.000 ^b
	Residual	.146	12	.012		
	Total	1.113	14			

a. Dependent Variable: p1318_A

b. Predictors: (Constant), period, temp

Coefficients^a

Model		Unstandardized Coefficients		Standardized Coefficients	t	Sig.
		B	Std. Error	Beta		
1	(Constant)	1.203	.164		7.345	.000
	temp	-.008	.001	-.905	-8.648	.000
	period	-.011	.005	-.224	-2.142	.053

Residuals Statistics^a

	Minimum	Maximum	Mean	Std. Deviation	N
Predicted Value	-.56588166952	.21056066453	-.17766049387	.262841395149	15
Residual	-.118633300066	.158773809671	.000000000000	.102196986775	15
Std. Predicted Value	-1.477	1.477	.000	1.000	15
Std. Residual	-1.075	1.438	.000	.926	15

a. Dependent Variable: p1318_A

Peak 1335 Regression

Model Summary^b

Model	R	R Square	Adjusted R Square	Std. Error of the Estimate	Durbin-Watson
1	.914 ^a	.836	.808	.095497991279	1.784

a. Predictors: (Constant), period, temp

b. Dependent Variable: p1335_A

ANOVA^a

Model		Sum of Squares	df	Mean Square	F	Sig.
1	Regression	.556	2	.278	30.482	.000 ^b
	Residual	.109	12	.009		
	Total	.665	14			

a. Dependent Variable: p1335_A

b. Predictors: (Constant), period, temp

Coefficients^a

Model		Unstandardized Coefficients		Standardized Coefficients	t	Sig.
		B	Std. Error	Beta		
1	(Constant)	-.861	.142		-6.082	.000
	temp	.006	.001	.913	7.802	.000
	period	.001	.004	.035	.296	.773

Residuals Statistics^a

	Minimum	Maximum	Mean	Std. Deviation	N
Predicted Value	-.14429496229	.34757208824	.10163856227	.199281032563	15
Residual	-.124846786261	.194242209196	.000000000000	.088413959814	15
Std. Predicted Value	-1.234	1.234	.000	1.000	15
Std. Residual	-1.307	2.034	.000	.926	15

a. Dependent Variable: p1335_A

Peak 1366 Regression

Model Summary^b

Model	R	R Square	Adjusted R Square	Std. Error of the Estimate	Durbin-Watson
1	.926 ^a	.858	.835	.112324563267	.382

a. Predictors: (Constant), period, temp

b. Dependent Variable: p1366_A

ANOVA^a

Model		Sum of Squares	df	Mean Square	F	Sig.
1	Regression	.918	2	.459	36.370	.000 ^b
	Residual	.151	12	.013		
	Total	1.069	14			

a. Dependent Variable: p1366_A

b. Predictors: (Constant), period, temp

Coefficients^a

Model		Unstandardized Coefficients		Standardized Coefficients	t	Sig.
		B	Std. Error	Beta		
1	(Constant)	1.220	.167		7.323	.000
	temp	-.007	.001	-.897	-8.261	.000
	period	-.011	.005	-.230	-2.121	.055

Residuals Statistics^a

	Minimum	Maximum	Mean	Std. Deviation	N
--	---------	---------	------	----------------	---

Predicted Value	-.50799721479	.25281241536	-.12759240140	.256034582481	15
Residual	-.113768123090	.153173759580	.000000000000	.103992338371	15
Std. Predicted Value	-1.486	1.486	.000	1.000	15
Std. Residual	-1.013	1.364	.000	.926	15

a. Dependent Variable: p1366_A

Peak 1421 Regression

Model Summary^b

Model	R	R Square	Adjusted R Square	Std. Error of the Estimate	Durbin-Watson
1	.879 ^a	.772	.734	.071910556964	.325

a. Predictors: (Constant), period, temp

b. Dependent Variable: p1421_A

ANOVA^a

Model		Sum of Squares	df	Mean Square	F	Sig.
1	Regression	.211	2	.105	20.365	.000 ^b
	Residual	.062	12	.005		
	Total	.273	14			

a. Dependent Variable: p1421_A

b. Predictors: (Constant), period, temp

Coefficients^a

Model		Unstandardized Coefficients		Standardized Coefficients	t	Sig.
		B	Std. Error	Beta		
1	(Constant)	.448	.107		4.202	.001
	temp	-.004	.001	-.850	-6.170	.000
	period	-.005	.003	-.224	-1.629	.129

Residuals Statistics^a

	Minimum	Maximum	Mean	Std. Deviation	N
Predicted Value	-.38170626760	-.01551206596	-.19860917293	.122653747782	15
Residual	-.087876163423	.104911342263	.000000000000	.066576239023	15
Std. Predicted Value	-1.493	1.493	.000	1.000	15
Std. Residual	-1.222	1.459	.000	.926	15

a. Dependent Variable: p1421_A

Peak 1456 Regression

Model Summary^b

Model	R	R Square	Adjusted R Square	Std. Error of the Estimate	Durbin-Watson
1	.952 ^a	.906	.890	.075713759181	.694

a. Predictors: (Constant), period, temp

b. Dependent Variable: p1456_A

ANOVA^a

Model		Sum of Squares	df	Mean Square	F	Sig.
1	Regression	.664	2	.332	57.904	.000 ^b
	Residual	.069	12	.006		
	Total	.733	14			

a. Dependent Variable: p1456_A

b. Predictors: (Constant), period, temp

Coefficients^a

Model		Unstandardized Coefficients		Standardized Coefficients	t	Sig.
		B	Std. Error	Beta		
1	(Constant)	.958	.112		8.530	.000
	temp	-.006	.001	-.915	-10.349	.000
	period	-.010	.003	-.261	-2.949	.012

Residuals Statistics^a

	Minimum	Maximum	Mean	Std. Deviation	N
Predicted Value	-.52565300465	.13300365210	-.19632469073	.217760660243	15
Residual	-.104087769985	.128650605679	.000000000000	.070097320079	15
Std. Predicted Value	-1.512	1.512	.000	1.000	15
Std. Residual	-1.375	1.699	.000	.926	15

a. Dependent Variable: p1456_A

Peak 1507 Regression

Model Summary^b

Model	R	R Square	Adjusted R Square	Std. Error of the Estimate	Durbin-Watson
1	.897 ^a	.805	.773	.091839296506	.574

a. Predictors: (Constant), period, temp

b. Dependent Variable: p1507_A

ANOVA^a

Model		Sum of Squares	df	Mean Square	F	Sig.
1	Regression	.419	2	.209	24.816	.000 ^b
	Residual	.101	12	.008		
	Total	.520	14			

a. Dependent Variable: p1507_A

b. Predictors: (Constant), period, temp

Coefficients^a

Model		Unstandardized Coefficients		Standardized Coefficients		t	Sig.
		B	Std. Error	Beta			
1	(Constant)	.754	.136			5.537	.000
	temp	-.005	.001	-.887		-6.966	.000
	period	-.004	.004	-.134		-1.055	.312

Residuals Statistics^a

	Minimum	Maximum	Mean	Std. Deviation	N
Predicted Value	-.36336803436	.11196826398	-.12569989087	.172921530957	15
Residual	-.119476653636	.114676721394	.000000000000	.085026666654	15
Std. Predicted Value	-1.374	1.374	.000	1.000	15
Std. Residual	-1.301	1.249	.000	.926	15

a. Dependent Variable: p1507_A

Peak 1595 Regression

Model Summary^b

Model	R	R Square	Adjusted R Square	Std. Error of the Estimate	Durbin-Watson
1	.924 ^a	.854	.830	.356636452330	.298

a. Predictors: (Constant), period, temp

b. Dependent Variable: p1595_A

ANOVA^a

Model		Sum of Squares	df	Mean Square	F	Sig.
1	Regression	8.927	2	4.463	35.093	.000 ^b
	Residual	1.526	12	.127		
	Total	10.453	14			

a. Dependent Variable: p1595_A

b. Predictors: (Constant), period, temp

Coefficients^a

Model		Unstandardized Coefficients		Standardized Coefficients		t	Sig.
		B	Std. Error	Beta			
1	(Constant)	-3.483	.529			-6.585	.000
	temp	.023	.003	.886		8.036	.000
	period	.039	.016	.261		2.368	.036

Residuals Statistics^a

	Minimum	Maximum	Mean	Std. Deviation	N
Predicted Value	-.45589902997	1.97342824936	.75876460547	.798522102520	15
Residual	-.520910859108	.484907001257	.000000000000	.330181195878	15
Std. Predicted Value	-1.521	1.521	.000	1.000	15

Std. Residual	-1.461	1.360	.000	.926	15
---------------	--------	-------	------	------	----

a. Dependent Variable: p1595_A

Peak 1642 Regression

Model Summary^b

Model	R	R Square	Adjusted R Square	Std. Error of the Estimate	Durbin-Watson
1	.865 ^a	.749	.707	.033855461573	.492

a. Predictors: (Constant), period, temp

b. Dependent Variable: p1642_A

ANOVA^a

Model		Sum of Squares	df	Mean Square	F	Sig.
1	Regression	.041	2	.020	17.884	.000 ^b
	Residual	.014	12	.001		
	Total	.055	14			

a. Dependent Variable: p1642_A

b. Predictors: (Constant), period, temp

Coefficients^a

Model		Unstandardized Coefficients		Standardized Coefficients	t	Sig.
		B	Std. Error	Beta		
1	(Constant)	.191	.050		3.809	.002
	temp	-.002	.000	-.824	-5.695	.000
	period	-.003	.002	-.264	-1.828	.093

Residuals Statistics^a

	Minimum	Maximum	Mean	Std. Deviation	N
Predicted Value	-.18134118617	-.01421576831	-.09777847860	.054114991483	15
Residual	-.050078988075	.046744126827	.000000000000	.031344066811	15
Std. Predicted Value	-1.544	1.544	.000	1.000	15
Std. Residual	-1.479	1.381	.000	.926	15

a. Dependent Variable: p1642_A

Peak 1730 Regression

Model Summary^b

Model	R	R Square	Adjusted R Square	Std. Error of the Estimate	Durbin-Watson
1	.848 ^a	.720	.673	.644171824480	.237

a. Predictors: (Constant), period, temp

b. Dependent Variable: p1730_A

ANOVA^a

Model	Sum of Squares	df	Mean Square	F	Sig.
-------	----------------	----	-------------	---	------

1	Regression	12.780	2	6.390	15.399	.000 ^b
	Residual	4.979	12	.415		
	Total	17.759	14			

a. Dependent Variable: p1730_A

b. Predictors: (Constant), period, temp

Coefficients^a

Model		Unstandardized Coefficients		Standardized Coefficients		t	Sig.
		B	Std. Error	Beta			
1	(Constant)	-4.809	.955			-5.034	.000
	temp	.027	.005	.800		5.232	.000
	period	.054	.029	.283		1.850	.089

Residuals Statistics^a

	Minimum	Maximum	Mean	Std. Deviation	N
Predicted Value	-1.17683219910	1.82515799999	.32416289007	.955427164433	15
Residual	-.905765056610	.809890568256	.000000000000	.596387222810	15
Std. Predicted Value	-1.571	1.571	.000	1.000	15
Std. Residual	-1.406	1.257	.000	.926	15

a. Dependent Variable: p1730_A

Peak area Changes in Vacuum Treatment Multiple Regression Analysis by SPSS

Peak 895Regression

Model Summary^b

Model	R	R Square	Adjusted R Square	Std. Error of the Estimate	Durbin-Watson
1	.572 ^a	.327	.214	.106336205032	.465

a. Predictors: (Constant), period, temp

b. Dependent Variable: p895

ANOVA^a

Model		Sum of Squares	df	Mean Square	F	Sig.
1	Regression	.066	2	.033	2.911	.093 ^b
	Residual	.136	12	.011		
	Total	.202	14			

a. Dependent Variable: p895

b. Predictors: (Constant), period, temp

Coefficients^a

Model		Unstandardized Coefficients		Standardized Coefficients		t	Sig.
		B	Std. Error	Beta			
1	(Constant)	.226	.158			1.435	.177

temp	-.002	.001	-.527	-2.225	.046
period	.005	.005	.221	.934	.369

a. Dependent Variable: p895

Residuals Statistics^a

	Minimum	Maximum	Mean	Std. Deviation	N
Predicted Value	-.11148623377	.11063919216	-.00042352033	.068568034124	15
Residual	-.132889434695	.194035410881	.000000000000	.098448195952	15
Std. Predicted Value	-1.620	1.620	.000	1.000	15
Std. Residual	-1.250	1.825	.000	.926	15

a. Dependent Variable: p895

Peak 1025 Regression

Model Summary^b

Model	R	R Square	Adjusted R Square	Std. Error of the Estimate	Durbin-Watson
1	.568 ^a	.322	.209	.007086954910	2.506

a. Predictors: (Constant), period, temp

b. Dependent Variable: p1025

ANOVA^a

Model		Sum of Squares	df	Mean Square	F	Sig.
1	Regression	.000	2	.000	2.853	.097 ^b
	Residual	.001	12	.000		
	Total	.001	14			

a. Dependent Variable: p1025

b. Predictors: (Constant), period, temp

Coefficients^a

Model		Unstandardized Coefficients		Standardized Coefficients	t	Sig.
		B	Std. Error	Beta		
1	(Constant)	.009	.011		.835	.420
	temp	.000	.000	-.567	-2.386	.034
	period	3.894E-5	.000	.029	.120	.906

Residuals Statistics^a

	Minimum	Maximum	Mean	Std. Deviation	N
Predicted Value	-.01764542237	-.00632857950	-.01198700093	.004524726035	15
Residual	-.011354804970	.009918206371	.000000000000	.006561245302	15
Std. Predicted Value	-1.251	1.251	.000	1.000	15
Std. Residual	-1.602	1.400	.000	.926	15

a. Dependent Variable: p1025

Peak 1054 Regression

Model Summary^b

Model	R	R Square	Adjusted R Square	Std. Error of the Estimate	Durbin-Watson
1	.555 ^a	.308	.193	.074421527303	.589

a. Predictors: (Constant), period, temp

b. Dependent Variable: p1054

ANOVA^a

Model		Sum of Squares	df	Mean Square	F	Sig.
1	Regression	.030	2	.015	2.675	.109 ^b
	Residual	.066	12	.006		
	Total	.096	14			

a. Dependent Variable: p1054

b. Predictors: (Constant), period, temp

Coefficients^a

Model		Unstandardized Coefficients		Standardized Coefficients		t	Sig.
		B	Std. Error	Beta			
1	(Constant)	-.073	.110			-.665	.519
	temp	.001	.001	.457		1.903	.081
	period	.004	.003	.316		1.316	.213

Residuals Statistics^a

	Minimum	Maximum	Mean	Std. Deviation	N
Predicted Value	.09670008719	.25775450468	.17722730133	.046008835516	15
Residual	-.131377682090	.112124785781	.000000000000	.068900945833	15
Std. Predicted Value	-1.750	1.750	.000	1.000	15
Std. Residual	-1.765	1.507	.000	.926	15

a. Dependent Variable: p1054

Peak 1110 Regression

Model Summary^b

Model	R	R Square	Adjusted R Square	Std. Error of the Estimate	Durbin-Watson
1	.673 ^a	.452	.361	.016803722367	2.013

a. Predictors: (Constant), period, temp

b. Dependent Variable: p1110

ANOVA^a

Model		Sum of Squares	df	Mean Square	F	Sig.
1	Regression	.003	2	.001	4.955	.027 ^b
	Residual	.003	12	.000		
	Total	.006	14			

a. Dependent Variable: p1110

b. Predictors: (Constant), period, temp

Coefficients^a

Model		Unstandardized Coefficients		Standardized Coefficients	t	Sig.
		B	Std. Error	Beta		
1	(Constant)	-.109	.025		-4.367	.001
	temp	.000	.000	.669	3.130	.009
	period	.000	.001	-.072	-.337	.742

Residuals Statistics^a

	Minimum	Maximum	Mean	Std. Deviation	N
Predicted Value	-.06515327841	-.02775163576	-.04645245793	.014137701722	15
Residual	-.018551502377	.038294386119	.000000000000	.015557223919	15
Std. Predicted Value	-1.323	1.323	.000	1.000	15
Std. Residual	-1.104	2.279	.000	.926	15

a. Dependent Variable: p1110

Peak 1154 Regression

Model Summary^b

Model	R	R Square	Adjusted R Square	Std. Error of the Estimate	Durbin-Watson
1	.767 ^a	.588	.519	.041030543843	.915

a. Predictors: (Constant), period, temp

b. Dependent Variable: p1154

ANOVA^a

Model		Sum of Squares	df	Mean Square	F	Sig.
1	Regression	.029	2	.014	8.558	.005 ^b
	Residual	.020	12	.002		
	Total	.049	14			

a. Dependent Variable: p1154

b. Predictors: (Constant), period, temp

Coefficients^a

Model		Unstandardized Coefficients		Standardized Coefficients	t	Sig.
		B	Std. Error	Beta		
1	(Constant)	.277	.061		4.557	.001
	temp	-.001	.000	-.751	-4.054	.002
	period	.002	.002	.152	.823	.427

Residuals Statistics^a

	Minimum	Maximum	Mean	Std. Deviation	N
Predicted Value	.02659853175	.15646274388	.09153063747	.045366604428	15
Residual	-.050990678370	.090406112373	.000000000000	.037986902194	15
Std. Predicted Value	-1.431	1.431	.000	1.000	15
Std. Residual	-1.243	2.203	.000	.926	15

a. Dependent Variable: p1154

Peak 1204 Regression

Model Summary^b

Model	R	R Square	Adjusted R Square	Std. Error of the Estimate	Durbin-Watson
1	.924 ^a	.853	.828	.030614970490	1.824

a. Predictors: (Constant), period, temp

b. Dependent Variable: p1204

ANOVA^a

Model		Sum of Squares	df	Mean Square	F	Sig.
1	Regression	.065	2	.033	34.777	.000 ^b
	Residual	.011	12	.001		
	Total	.076	14			

a. Dependent Variable: p1204

b. Predictors: (Constant), period, temp

Coefficients^a

Model		Unstandardized Coefficients		Standardized Coefficients		t	Sig.
		B	Std. Error	Beta			
1	(Constant)	-.310	.045			-6.829	.000
	temp	.002	.000	.923		8.338	.000
	period	.000	.001	-.019		-.170	.868

Residuals Statistics^a

	Minimum	Maximum	Mean	Std. Deviation	N
Predicted Value	-.07363096625	.09162077308	-.00899490573	.068238612498	15
Residual	-.058225173503	.041541121900	.000000000000	.028343955033	15
Std. Predicted Value	-1.211	1.211	.000	1.000	15
Std. Residual	-1.902	1.357	.000	.926	15

a. Dependent Variable: p1204

Peak 1226 Regression

Model Summary^b

Model	R	R Square	Adjusted R Square	Std. Error of the Estimate	Durbin-Watson
-------	---	----------	-------------------	----------------------------	---------------

1	.695 ^a	.483	.397	.039581811111	.902
---	-------------------	------	------	---------------	------

a. Predictors: (Constant), period, temp

b. Dependent Variable: p1226

ANOVA^a

Model		Sum of Squares	df	Mean Square	F	Sig.
1	Regression	.018	2	.009	5.600	.019 ^b
	Residual	.019	12	.002		
	Total	.036	14			

a. Dependent Variable: p1226

b. Predictors: (Constant), period, temp

Coefficients^a

Model		Unstandardized Coefficients		Standardized Coefficients	t	Sig.
		B	Std. Error	Beta		
1	(Constant)	.090	.059		1.534	.151
	temp	-.001	.000	-.602	-2.900	.013
	period	-.003	.002	-.347	-1.671	.121

Residuals Statistics^a

	Minimum	Maximum	Mean	Std. Deviation	N
Predicted Value	-.16385829449	-.04296753928	-.10341291507	.035403847735	15
Residual	-.076135732234	.080607205629	.000000000000	.036645636312	15
Std. Predicted Value	-1.707	1.707	.000	1.000	15
Std. Residual	-1.924	2.036	.000	.926	15

a. Dependent Variable: p1226

Peak 1262 Regression

Model Summary^b

Model	R	R Square	Adjusted R Square	Std. Error of the Estimate	Durbin-Watson
1	.738 ^a	.545	.469	.020802163026	.786

a. Predictors: (Constant), period, temp

b. Dependent Variable: p1262

ANOVA^a

Model		Sum of Squares	df	Mean Square	F	Sig.
1	Regression	.006	2	.003	7.178	.009 ^b
	Residual	.005	12	.000		
	Total	.011	14			

a. Dependent Variable: p1262

b. Predictors: (Constant), period, temp

Coefficients^a

Model	Unstandardized Coefficients	Standardized Coefficients	t	Sig.
-------	-----------------------------	---------------------------	---	------

		B	Std. Error	Beta		
1	(Constant)	.086	.031		2.798	.016
	temp	-.001	.000	-.654	-3.360	.006
	period	-.002	.001	-.341	-1.752	.105

Residuals Statistics^a

	Minimum	Maximum	Mean	Std. Deviation	N
Predicted Value	-.06409113854	.00672719022	-.02868197233	.021065543964	15
Residual	-.037579432130	.038419764489	.000000000000	.019259060649	15
Std. Predicted Value	-1.681	1.681	.000	1.000	15
Std. Residual	-1.807	1.847	.000	.926	15

a. Dependent Variable: p1262

Peak 1318 Regression

Model Summary^b

Model	R	R Square	Adjusted R Square	Std. Error of the Estimate	Durbin-Watson
1	.963 ^a	.928	.916	.036080634268	.481

a. Predictors: (Constant), period, temp

b. Dependent Variable: p1318

ANOVA^a

Model		Sum of Squares	df	Mean Square	F	Sig.
1	Regression	.201	2	.100	77.062	.000 ^b
	Residual	.016	12	.001		
	Total	.216	14			

a. Dependent Variable: p1318

b. Predictors: (Constant), period, temp

Coefficients^a

Model		Unstandardized Coefficients		Standardized Coefficients		t	Sig.
		B	Std. Error	Beta			
1	(Constant)	.566	.054			10.575	.000
	temp	-.004	.000	-.953		-12.278	.000
	period	-.003	.002	-.143		-1.838	.091

Residuals Statistics^a

	Minimum	Maximum	Mean	Std. Deviation	N
Predicted Value	-.20716759562	.12144514173	-.04286122993	.119713996664	15
Residual	-.055915892124	.043493527919	.000000000000	.033404176418	15
Std. Predicted Value	-1.372	1.372	.000	1.000	15
Std. Residual	-1.550	1.205	.000	.926	15

a. Dependent Variable: p1318

Peak 1335 Regression

Model Summary^b

Model	R	R Square	Adjusted R Square	Std. Error of the Estimate	Durbin-Watson
1	.906 ^a	.820	.790	.049866593208	1.678

a. Predictors: (Constant), period, temp

b. Dependent Variable: p1335

ANOVA^a

Model		Sum of Squares	df	Mean Square	F	Sig.
1	Regression	.136	2	.068	27.353	.000 ^b
	Residual	.030	12	.002		
	Total	.166	14			

a. Dependent Variable: p1335

b. Predictors: (Constant), period, temp

Coefficients^a

Model		Unstandardized Coefficients		Standardized Coefficients		t	Sig.
		B	Std. Error	Beta			
1	(Constant)	-.477	.074			-6.446	.000
	temp	.003	.000	.902		7.371	.000
	period	.001	.002	.075		.614	.550

Residuals Statistics^a

	Minimum	Maximum	Mean	Std. Deviation	N
Predicted Value	-.11690136045	.13793130219	.01051497060	.098573538533	15
Residual	-.075294494629	.068827085197	.000000000000	.046167494299	15
Std. Predicted Value	-1.293	1.293	.000	1.000	15
Std. Residual	-1.510	1.380	.000	.926	15

a. Dependent Variable: p1335

Peak 1366 Regression

Model Summary^b

Model	R	R Square	Adjusted R Square	Std. Error of the Estimate	Durbin-Watson
1	.974 ^a	.949	.940	.029356342023	1.523

a. Predictors: (Constant), period, temp

b. Dependent Variable: p1366

ANOVA^a

Model		Sum of Squares	df	Mean Square	F	Sig.
-------	--	----------------	----	-------------	---	------

1	Regression	.191	2	.095	110.803	.000 ^b
	Residual	.010	12	.001		
	Total	.201	14			

a. Dependent Variable: p1366

b. Predictors: (Constant), period, temp

Coefficients^a

Model		Unstandardized Coefficients		Standardized Coefficients	t	Sig.
		B	Std. Error	Beta		
1	(Constant)	.529	.044		12.157	.000
	temp	-.003	.000	-.952	-14.557	.000
	period	-.004	.001	-.204	-3.112	.009

Residuals Statistics^a

	Minimum	Maximum	Mean	Std. Deviation	N
Predicted Value	-.24645674229	.09055002034	-.07795336060	.116796136467	15
Residual	-.052215896547	.054586123675	.000000000000	.027178691500	15
Std. Predicted Value	-1.443	1.443	.000	1.000	15
Std. Residual	-1.779	1.859	.000	.926	15

a. Dependent Variable: p1366

Peak 1421 Regression

Model Summary^b

Model	R	R Square	Adjusted R Square	Std. Error of the Estimate	Durbin-Watson
1	.935 ^a	.874	.853	.021094661240	.708

a. Predictors: (Constant), period, temp

b. Dependent Variable: p1421

ANOVA^a

Model		Sum of Squares	df	Mean Square	F	Sig.
1	Regression	.037	2	.018	41.495	.000 ^b
	Residual	.005	12	.000		
	Total	.042	14			

a. Dependent Variable: p1421

b. Predictors: (Constant), period, temp

Coefficients^a

Model		Unstandardized Coefficients		Standardized Coefficients	t	Sig.
		B	Std. Error	Beta		
1	(Constant)	.122	.031		3.899	.002
	temp	-.001	.000	-.904	-8.808	.000

period		-0.002	.001		-.238	-2.324	.038
--------	--	--------	------	--	-------	--------	------

Residuals Statistics^a

	Minimum	Maximum	Mean	Std. Deviation	N
Predicted Value	-.22552023828	-.07219632715	-.14885828367	.051359562826	15
Residual	-.040627852082	.036256358027	.000000000000	.019529861374	15
Std. Predicted Value	-1.493	1.493	.000	1.000	15
Std. Residual	-1.926	1.719	.000	.926	15

a. Dependent Variable: p1421

Peak 1456 Regression

Model Summary^b

Model	R	R Square	Adjusted R Square	Std. Error of the Estimate	Durbin-Watson
1	.919 ^a	.845	.819	.037964531786	1.411

a. Predictors: (Constant), period, temp

b. Dependent Variable: p1456

ANOVA^a

Model		Sum of Squares	df	Mean Square	F	Sig.
1	Regression	.094	2	.047	32.689	.000 ^b
	Residual	.017	12	.001		
	Total	.112	14			

a. Dependent Variable: p1456

b. Predictors: (Constant), period, temp

Coefficients^a

Model		Unstandardized Coefficients		Standardized Coefficients		t	Sig.
		B	Std. Error	Beta			
1	(Constant)	.287	.056			5.100	.000
	temp	-.002	.000		-.844	-7.427	.000
	period	-.006	.002		-.363	-3.197	.008

Residuals Statistics^a

	Minimum	Maximum	Mean	Std. Deviation	N
Predicted Value	-.29160448909	-.02464209311	-.15812328733	.082040861582	15
Residual	-.048475556076	.082367874682	.000000000000	.035148326606	15
Std. Predicted Value	-1.627	1.627	.000	1.000	15
Std. Residual	-1.277	2.170	.000	.926	15

a. Dependent Variable: p1456

Peak 1507 Regression

Model Summary^b

Model	R	R Square	Adjusted R Square	Std. Error of the Estimate	Durbin-Watson
1	.602 ^a	.362	.255	.036810197043	1.099

a. Predictors: (Constant), period, temp

b. Dependent Variable: p1507

ANOVA^a

Model		Sum of Squares	df	Mean Square	F	Sig.
1	Regression	.009	2	.005	3.402	.068 ^b
	Residual	.016	12	.001		
	Total	.025	14			

a. Dependent Variable: p1507

b. Predictors: (Constant), period, temp

Coefficients^a

Model		Unstandardized Coefficients		Standardized Coefficients	t	Sig.
		B	Std. Error	Beta		
1	(Constant)	.073	.055		1.333	.207
	temp	-7.620E-5	.000	-.060	-.262	.798
	period	-.004	.002	-.598	-2.595	.023

Residuals Statistics^a

	Minimum	Maximum	Mean	Std. Deviation	N
Predicted Value	-.04713065550	.02872879989	-.00920092820	.025660546527	15
Residual	-.064686059952	.064052022994	.000000000000	.034079620299	15
Std. Predicted Value	-1.478	1.478	.000	1.000	15
Std. Residual	-1.757	1.740	.000	.926	15

a. Dependent Variable: p1507

Peak 1595 Regression

Model Summary^b

Model	R	R Square	Adjusted R Square	Std. Error of the Estimate	Durbin-Watson
1	.929 ^a	.863	.840	.181167779796	.403

a. Predictors: (Constant), period, temp

b. Dependent Variable: p1595

ANOVA^a

Model		Sum of Squares	df	Mean Square	F	Sig.
1	Regression	2.474	2	1.237	37.689	.000 ^b
	Residual	.394	12	.033		
	Total	2.868	14			

a. Dependent Variable: p1595

b. Predictors: (Constant), period, temp

Coefficients^a

Model		Unstandardized Coefficients		Standardized Coefficients	t	Sig.
		B	Std. Error	Beta		
1	(Constant)	-1.794	.269		-6.677	.000
	temp	.012	.001	.901	8.421	.000
	period	.017	.008	.226	2.114	.056

Residuals Statistics^a

	Minimum	Maximum	Mean	Std. Deviation	N
Predicted Value	-.20697799325	1.03758788109	.41530491827	.420374748295	15
Residual	-.188831865788	.280879139900	.000000000000	.167728771966	15
Std. Predicted Value	-1.480	1.480	.000	1.000	15
Std. Residual	-1.042	1.550	.000	.926	15

a. Dependent Variable: p1595

Peak 1642 Regression

Model Summary^b

Model	R	R Square	Adjusted R Square	Std. Error of the Estimate	Durbin-Watson
1	.912 ^a	.832	.804	.023473459909	1.392

a. Predictors: (Constant), period, temp

b. Dependent Variable: p1642

ANOVA^a

Model		Sum of Squares	df	Mean Square	F	Sig.
1	Regression	.033	2	.016	29.751	.000 ^b
	Residual	.007	12	.001		
	Total	.039	14			

a. Dependent Variable: p1642

b. Predictors: (Constant), period, temp

Coefficients^a

Model		Unstandardized Coefficients		Standardized Coefficients	t	Sig.
		B	Std. Error	Beta		
1	(Constant)	.164	.035		4.722	.000
	temp	-.001	.000	-.897	-7.583	.000
	period	-.002	.001	-.167	-1.412	.183

Residuals Statistics^a

	Minimum	Maximum	Mean	Std. Deviation	N
Predicted Value	-.15334643424	-.01656093821	-.08495368573	.048392773004	15

Residual	-.035215944052	.049713898450	.000000000000	.021732200995	15
Std. Predicted Value	-1.413	1.413	.000	1.000	15
Std. Residual	-1.500	2.118	.000	.926	15

a. Dependent Variable: p1642

Peak 1730 Regression

Model Summary^b

Model	R	R Square	Adjusted R Square	Std. Error of the Estimate	Durbin-Watson
1	.940 ^a	.884	.865	.101742378179	.491

a. Predictors: (Constant), period, temp

b. Dependent Variable: p1730

ANOVA^a

Model		Sum of Squares	df	Mean Square	F	Sig.
1	Regression	.948	2	.474	45.768	.000 ^b
	Residual	.124	12	.010		
	Total	1.072	14			

a. Dependent Variable: p1730

b. Predictors: (Constant), period, temp

Coefficients^a

Model		Unstandardized Coefficients		Standardized Coefficients		t	Sig.
		B	Std. Error	Beta			
1	(Constant)	-1.475	.151			-9.776	.000
	temp	.008	.001	.938		9.542	.000
	period	.003	.005	.069		.704	.495

Residuals Statistics^a

	Minimum	Maximum	Mean	Std. Deviation	N
Predicted Value	-.52825087309	.13799774647	-.19512657433	.260155899940	15
Residual	-.181039199233	.153854832053	.000000000000	.094195138716	15
Std. Predicted Value	-1.280	1.280	.000	1.000	15
Std. Residual	-1.779	1.512	.000	.926	15

a. Dependent Variable: p1730

Treated in Air

Nonlinear Curve Fit (NewFunction13 (User)) (03/08/2019 15:01:04)

Parameters

		Value	Standard Error	t-Value	Prob> t	Dependency
y	a	120	38.59475	3.10923	0.00903	0.9599
	b	35.6621	21.57732	1.65276	0.12428	0.9599

Reduced Chi-sqr = 0.0916860129157

COD(R²) = 0.97408102898519

Iterations Performed = 12

Total Iterations in Session = 12

Fit converged. Chi-Sqr tolerance value of 1E-9 was reached.

Standard Error was scaled with square root of reduced Chi-Sqr.

Statistics

	y
Number of Points	14
Degrees of Freedom	12
Reduced Chi-Sqr	0.09169
Residual Sum of Squares	1.10023
R-Square (COD)	0.97408
Adj. R-Square	0.97192
Fit Status	Succeeded(100)

Fit Status Code :

100 : Fit converged. Chi-Sqr tolerance value of 1E-9 was reached

Summary

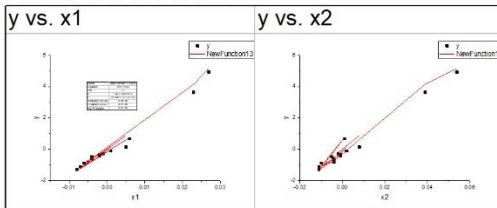
	a		b		Statistics	
	Value	Standard Error	Value	Standard Error	Reduced Chi-Sqr	Adj. R-Square
y	120	38.59475	35.6621	21.57732	0.09169	0.97192

ANOVA

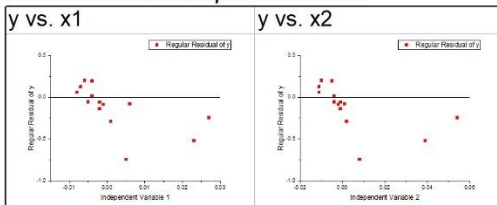
		DF	Sum of Squares	Mean Square	F Value	Prob>F
y	Regression	2	42.03928	21.01964	229.25677	2.75204E-10
	Residual	12	1.10023	0.09169		
	Uncorrected Total	14	43.13951			
	Corrected Total	13	42.44891			

At the 0.05 level, the fitting function is significantly better than the function y=0.

Fitted Curves Plot



Residual vs. Independent Plot



Treated in Vacuum

Nonlinear Curve Fit (NewFunction13 (User)) (03/08/2019 15:08:42)

Parameters

		Value	Standard Error	t-Value	Prob> t	Dependency
y	a	165.07811	22.11189	7.46558	1.25264E-5	0.7249
	b	8	17.37505	0.46043	0.65418	0.7249

Reduced Chi-sqr = 0.0343001586542

COD(R^2) = 0.94655141905888

Iterations Performed = 6

Total Iterations in Session = 6

Fit converged. Chi-Sqr tolerance value of 1E-9 was reached.

Standard Error was scaled with square root of reduced Chi-Sqr.

Statistics

	y
Number of Points	13
Degrees of Freedom	11
Reduced Chi-Sqr	0.0343
Residual Sum of Squares	0.3773
R-Square (COD)	0.94655
Adj. R-Square	0.94169
Fit Status	Succeeded(100)

Fit Status Code :

100 : Fit converged. Chi-Sqr tolerance value of 1E-9 was reached.

Summary

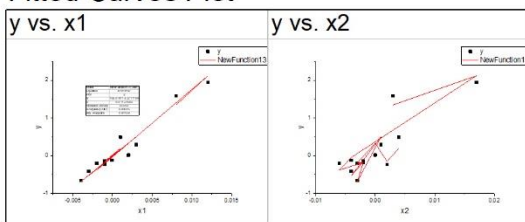
	a		b		Statistics	
	Value	Standard Error	Value	Standard Error	Reduced Chi-Sqr	Adj. R-Square
y	165.07811	22.11189	8	17.37505	0.0343	0.94169

ANOVA

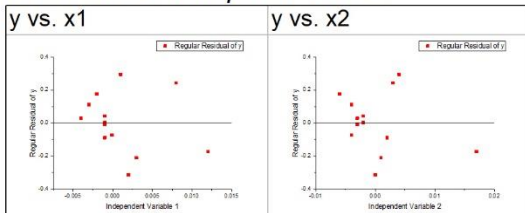
		DF	Sum of Squares	Mean Square	F Value	Prob>F
y	Regression	2	7.04967	3.52484	102.76442	7.62646E-8
	Residual	11	0.3773	0.0343		
	Uncorrected Total	13	7.42697			
	Corrected Total	12	7.05915			

At the 0.05 level, the fitting function is significantly better than the function y=0.

Fitted Curves Plot



Residual vs. Independent Plot



Treated in Air and Vacuum

Nonlinear Curve Fit (NewFunction14 (User)) (03/08/2019 15:14:02)

Parameters

	Value	Standard Error	t-Value	Prob> t	Dependency
a	137.2649	77.65528	1.76762	0.10757	0.97848
b	29.75643	34.2544	0.86869	0.40538	0.96543
c	152.25664	106.87026	1.42469	0.1847	0.93161
d	8	43.94634	0.18204	0.85919	0.75028

Reduced Chi-sqr = 0.19918346477
 COD(R²) = 0.97498841968793
 Iterations Performed = 8
 Total Iterations in Session = 8

Fit converged. Chi-Sqr tolerance value of 1E-9 was reached.
 Standard Error was scaled with square root of reduced Chi-Sqr.

Statistics

	y
Number of Points	14
Degrees of Freedom	10
Reduced Chi-Sqr	0.19918
Residual Sum of Squares	1.99183
R-Square (COD)	0.97499
Adj. R-Square	0.96748
Fit Status	Succeeded(100)

Fit Status Code :
 100 : Fit converged. Chi-Sqr tolerance value of 1E-9 was reached.

Summary

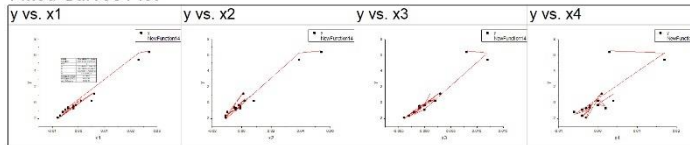
	a		b		c		d		Statistics	
	Value	Standard Error	Value	Standard Error	Value	Standard Error	Value	Standard Error	Reduced Chi-Sqr	Adj. R-Square
y	137.2649	77.65528	29.75643	34.2544	152.25664	106.87026	8	43.94634	0.19918	0.96748

ANOVA

		DF	Sum of Squares	Mean Square	F Value	Prob>F
y	Regression	4	79.58234	19.89558	99.88572	5.10183E-8
	Residual	10	1.99183	0.19918		
	Uncorrected Total	14	81.57417			
	Corrected Total	13	79.6365			

At the 0.05 level, the fitting function is significantly better than the function y=0.

Fitted Curves Plot



Residual vs. Independent Plot

